COMPUTATION OF SET-UP, LONGSHORE CURRENTS, RUN-UP AND OVERTOPPING DUE TO WIND-GENERATED WAVES

J. A. BATTJES

STELLINGEN

I

De in dit proefschrift gegeven berekening van het snelheidsprofiel van een brandingsstroom, aangedreven door onregelmatige golven, is uit te breiden met de turbulente horizontale uitwisseling van hoeveelheid beweging. Er mag echter verwacht worden dat het effect hiervan gering zal zijn.

II

De door Longuet-Higgins en Stewart gegeven definitie van de "radiation stress" in staande golven bevat de over de diepte geïntegreerde drukverhoging overeenkomend met de door de golven teweeggebrachte verandering van de over de tijd gemiddelde waterstand. Dit is niet logisch, en ook niet consistent met de door deze schrijvers gegeven definitie en toepassingen van de "radiation stress" in lopende golven.
(M.S. Longuet-Higgins en R.W. Stewart, Deep-Sea Research, 11, 1964, p. 529-562).

III

In Nederland moeten betere mogelijkheden worden gerealiseerd voor het verrichten van metingen in de natuur ten behoeve van fundamenteel onderzoek van de beweging van water en zand bij stranden.

IV

Voor een wetenschappelijk verantwoorde vaststelling van ontwerpcriteria voor zeedijken is destructief onderzoek van prototypen onontbeerlijk.

V

Publicaties van resultaten van waterloopkundige proeven op schaal dienen in ieder geval de model-waarden te bevatten, en niet slechts de tot het prototype omgerekende waarden.

VI

De modelwetten die door Yalin en Russell zijn afgeleid voor het op verkleinde schaal nabootsen van sediment transport door golven zijn niet geschikt voor praktische toepassing, in tegenstelling tot wat door deze auteurs wordt gesuggereerd.
(S. Yalin en R.C.H. Russell, Proc. 8th Conf. Coastal Eng., Mexico, 1962, p. 151-167).

VII

Volgens de conventionele opvatting vindt de energie overdracht in trochoïdale zwaartekrachtsgolven uitsluitend plaats door advectie van potentiële energie. Er is echter een alternatieve benadering mogelijk, waarin de energie overdracht geheel bestaat uit het vermogen geleverd door de druk. Beide opvattingen hebben recht van bestaan.

VIII

Het feit dat de groepssnelheid van zwaartekrachtsgolven op diep water de helft is van de fasesnelheid wordt veelal "uitgelegd" door gebruik te maken van het feit dat de potentiële energie de helft is van de totale, en door te stellen dat de potentiële energie met de golfvorm zou mee bewegen. Deze uitleg geeft een fundamenteel verkeerd beeld van het mechanisme van de energie overdracht in golven; het is slechts bij toeval dat hij voor de genoemde categorie tot een numeriek juist resultaat leidt.

IX

In beschouwingen over zandtransport door golven langs een kust wordt veel gebruik gemaakt van een grootheid die men pleegt te noemen "the longshore component of the energy flux per unit length of shoreline"; dit is een onbestaanbaar begrip.

X

Het onderwijs in de mechanica van golven is bij uitstek geschikt om een bijdrage te leveren tot de verwezenlijking van de derde doelstelling van het wetenschappelijk onderwijs, n.l. het bevorderen van het inzicht in de samenhang der wetenschappen.
(Wet op het Wetenschappelijk Onderwijs, art. 1).

XI

Het is een misvatting te menen dat alle universitaire studenten lid moeten kunnen zijn van een vakgroep volgens de Wet Universitaire Bestuurshervorming 1970.

XII

Medische specialisten die hun beroep uitoefenen in ziekenhuizen doen dit veelal als vrije ondernemers, en niet in dienstverband. Aan deze situatie, die meer in het persoonlijk belang is van de specialisten dan in dat van de patiënten of van de Nederlandse gezondheidszorg in het algemeen, dient zo spoedig mogelijk een einde te worden gemaakt.

XIII

Het zou tot de gewone omgangsvormen moeten behoren dat men in een gesloten ruimte niet rookt dan na zich ervan te hebben overtuigd dat hiertegen bij eventueel overige aanwezigen geen bezwaar bestaat.

J.A. Battjes
maart 1974

CONTENTS OF CHAPTERS 1 THROUGH 9

	PAGE
1 INTRODUCTION	1
2 CHARACTERISTIC FEATURES OF REGULAR WAVES ON PLANE SLOPES	4
2.1 Introduction	4
2.2 Phenomenological description	5
2.3 Characteristics of surf	8
2.3.1 Breaking criterion	9
2.3.2 Breaker types	16
2.3.3 Breaker height-to-depth ratio	20
2.3.4 Set-up, run-up and run-down	21
2.3.5 Reflection and absorption	22
2.3.6 General comments regarding the parameter ξ	26
2.4 Implications for further work	30
3 EQUATIONS OF MOTION	32
3.1 Introduction	32
3.2 Irrotational wave motion	33
3.2.1 Basic equations	33
3.2.2 Progressive waves in water of constant depth	35
3.2.3 Progressive waves in water of variable depth	38
3.3 Equations of motion for a weak current in the presence of waves	42
3.3.1 Introduction	42
3.3.2 Conservation of mass	43
3.3.3 Conservation of vertical momentum	44
3.3.4 Conservation of horizontal momentum	45
3.3.5 Steady, irrotational mean flow	49
3.3.6 Steady, uniform mean flow	55
3.4 Set-up and longshore currents due to regular waves	56
3.4.1 Set-up	57
3.4.2 Longshore currents	58
4 PROBABILISTIC DESCRIPTION OF WIND WAVES	65
4.1 Introduction	65
4.2 Stochastic processes in one dimension	65
4.2.1 General concepts	65
4.2.2 Gaussian processes	72

4.3 Wind waves considered as a quasi-stationary Gaussian process 76

4.3.1 General considerations 76
4.3.2 An explicit representation 78
4.3.3 Transformation of the spectrum due to shoaling, refraction and dissipation 81

4.4 Statistical properties of wind waves at a fixed point 83

4.4.1 Introduction 83
4.4.2 Distribution of instantaneous values 83
4.4.3 Average interval between level crossings 84
4.4.4 Distribution of zero-crossing intervals 84
4.4.5 Distribution of intervals between maxima 86
4.4.6 Distribution of the heights of the maxima 86
4.4.7 Distribution of the zero-crossing wave heights 90
4.4.8 Distribution of the largest wave height in a record 95

4.5 Empirical data for wind-driven waves 96

4.5.1 Directional spectra 97
4.5.2 Frequency spectra 100
4.5.3 Distribution of wave periods 103
4.5.4 Joint distribution of wave heights and wave periods 104

5 RADIATION STRESSES 106

5.1 Introduction 106

5.2 Radiation stresses expressed in terms of the two-dimensional energy spectrum 107

5.2.1 General formulation 107
5.2.2 Effects of short-crestedness on the radiation stresses 110

5.3 Radiation stresses in the surf zone 119

5.3.1 Introduction 119
5.3.2 The equilibrium range of shallow-water wave spectra proposed by Ijima, Matsuo and Koga 122
5.3.3 Radiation stresses in irregular, breaking waves 125

6 SET-UP AND LONGSHORE CURRENTS 136

6.1 Introduction 136

6.2 Supplementary equations 136

6.2.1 Shoaling and refraction 136
6.2.2 Set-up 139
6.2.3 Longshore current velocity 141

6.3 Numerical evaluation 145

6.3.1 Boundary conditions 145
6.3.2 Presentation and discussion of results 147

6.4 Comparison with empirical data 152

6.4.1 Purpose and scope 152
6.4.2 Field data 152
6.4.3 Laboratory measurements 154

7 RUN-UP 163

7.1 Introduction 163

7.2 Run-up of periodic waves breaking on a slope 165

7.3 A check of the applicability of Hunt's formula to irregular waves 167

7.4 Run-up distributions of breaking waves with arbitrary joint distribution of $\underline{H}$ and $\underline{L}_0$ 170

7.4.1 Analytical solution 170
7.4.2 Graphical solution for discrete data 173

7.5 Run-up distributions of breaking waves with a bivariate Rayleigh distribution of $\underline{H}$ and $\underline{L}_0$ 174

7.5.1 Probability density and distribution function 174
7.5.2 Special values 179
7.5.3 Maximum run-up 183

7.6 Steepness distribution 185

7.7 Comparison with empirical data 190

8 OVERTOPPING 195

8.1 Introduction 195

8.2 Overtopping due to periodic waves breaking on a slope 195

8.2.1 Relation between run-up and overtopping 195
8.2.2 Empirical data 199

8.3 Overtopping due to random waves breaking on a slope 200

8.3.1 Distribution of overtopped volume 200
8.3.2 Mean discharge 203
8.3.3 Comparison with empirical data 206

9 SUMMARY AND CONCLUSIONS 209

1 INTRODUCTION

The impingement of wind-generated water waves on seashores is a phenomenon which is of great interest, not only because of the aesthetic, sportive and other pleasures which may be derived from it, but also from the professional viewpoint of coastal engineers, who often have reason to consider the power released by the waves on the shores with some concern. The latter is particularly true if the sea is bordered by a beach of sand or gravel, or by a man-made dike or seawall.

Beaches can serve functions in the recreational sphere as well as in the context of flood protection; both functions generally demand that beach stability should satisfy certain minimum requirements. Similarly, the structural integrity of dikes or seawalls should be maintained if these structures are to perform satisfactorily.

The stability of beaches and dikes can be affected by a number of factors. In many cases the effects of wind-generated waves are relatively important or even predominant, and it is fitting that this is reflected in the pertinent research which is carried out.

Past investigations have partly been aimed at the effects of a given, stable beach or structure on an incident wave train. The results obtained from such studies can serve as boundary conditions for subsequent investigations of the response of beach or dike to the waves, or they may be of interest in other contexts, regardless of the effects on stability. The subjects have included wave-induced longshore currents and changes in mean water level ("set-up") on beaches as well as run-up and overtopping on dikes. These are of importance in various engineering applications.

The majority of the investigations up to the present have been restricted to regular waves; this is a major drawback since the results should be applied to wind-generated waves, which are essentially irregular.

This thesis deals with the problems of calculating the effects mentioned above, taking the random character of the waves into account.

The solutions to these problems are not trivial, since wave breaking is almost invariably involved in the processes of wind-wave motion on beaches or dikes. Wave breaking is a highly nonlinear phenomenon, the details of which are not well understood. An approach based on the details of the water motion in the breakers is therefore not (yet) practicable. The approach used in the following utilizes empirical knowledge of the gross characteristics of periodic breaking waves, and represents an attempt to use this knowledge in a formulation in which moreover those elements are incorporated which are deemed essential to a description of irregular waves. Non-breaking waves are not considered extensively since these are not nearly as common as are breaking waves on beaches or on sea-dikes exposed to wind-generated waves.

The main body of this thesis has been divided into two parts. Part I, "Phenomenological, hydrodynamic and probabilistic description of waves", contains basic information which is necessary for the computational models outlined in Part II, "Computation of set-up, longshore currents, run-up and overtopping".

Part I is made up as follows. In chapter 2 a description is given of the characteristic features of waves incident on a plane slope, as functions of the wave steepness and the slope angle. The primary purpose of this chapter is to provide an integral view of the total subject matter, so that the elements into which it can be divided can be seen in a proper perspective. Chapter 3 summarizes the necessary hydrodynamics; it includes a résumé of the theory of sinusoidal progressive waves, as well as equations for the effects of waves on a mean flow, with a summary of previous calculations of set-up and longshore current velocities due to periodic waves. The stochastic aspects of wind-generated waves are reviewed in chapter 4.

Part II consists of the chapters 5 through 9. In chapter 5 the effects of the irregularity of the waves on the radiation stresses are considered, both outside the surf zone, where the waves are treated as a linear superposition of independent sinusoidal spectral components, and inside the surf zone, where the nonlinearities of the

breaking process cannot be ignored. The results of chapter 5 are applied in chapter 6 for the calculations of the set-up and longshore currents induced by irregular waves. In these chapters the bottom slope is assumed to be gentle. The run-up and overtopping of irregular waves on relatively steep slopes is considered in the chapters 7 and 8. A summary of the results is given in chapter 9.

Following part II, three appendices provide auxiliary information. In Appendix 1, various properties of the bivariate Rayleigh probability density function are given. Appendix 2 contains a list of symbols, while the references are listed in Appendix 3.

2 CHARACTERISTIC FEATURES OF REGULAR WAVES ON PLANE SLOPES

2.1 Introduction

The purpose of this chapter is to provide necessary general background information as a preliminary to the more detailed analyses in following chapters. To this end the major features of the propagation of waves onto a slope will be mentioned in broad terms. A situation will be considered with the simplest possible geometry and boundary conditions compatible with this end, i.e. a rigid, plane, impermeable slope extending to deep water or to water of constant depth from which periodic, long-crested waves are approaching. The wave crests are in general assumed to be parallel to the depth contours. Oblique incidence is mentioned only briefly.

The motion will be assumed to be determined wholly by the slope angle α (fig. 2.1), the still water depth d and the incident wave height H at the toe of the slope, the wave period T, the acceleration of gravity g, the viscosity μ and the mass density ρ of the water; g, μ and ρ are assumed to be constants. Effects of surface tension and compressibility are ignored.

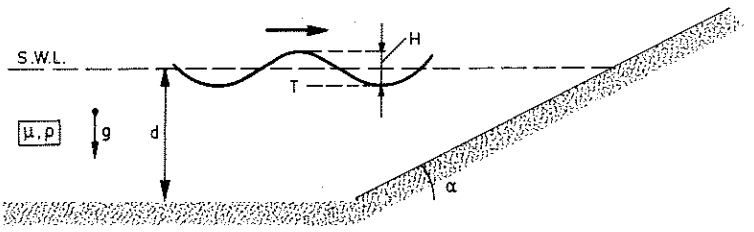

Fig. 2.1 - Definition sketch

Let X be any dimensionless dependent variable, then

$$X = f(\alpha, \frac{H}{gT^2}, \frac{d}{gT^2}, Re), \qquad (2.1.1)$$

in which Re is a typical Reynolds number. An equivalent formulation is

$$X = f(\alpha, \frac{H}{L_0}, \frac{d}{L_0}, Re) \qquad (2.1.2)$$

in which

$$L_0 = \frac{gT^2}{2\pi}, \qquad (2.1.3)$$

i.e. the deep-water wavelength of small-amplitude sinusoidal, long-crested gravity surface waves with period T. The ratio H/L_0 is a wave steepness, if we define this parameter in a generalized sense as the ratio of a wave height to a wave length. Various steepnesses will be used in the following; the precise definition will in each case be given in the context.

2.2 Phenomenological description

In this section the major flow regimes which can be established by regular waves incident on a plane slope will be considered as functions of the independent parameters in the right-hand side of (2.1.2). We shall be mainly concerned with the changes brought about by variations in slope angle and wave steepness. The relative depth d/L_0 is of far smaller influence, particularly if the waves are breaking on the slope [1-3], while the Reynolds number is assumed to be larger than some minimum value above which variations in its actual value do not significantly affect the resultant motion. At first only the variation of the flow with the slope angle α will be considered. Thus, until further notice it is assumed that the incident wave parameters are kept constant.

For sufficiently large α the waves do not break and there is almost complete reflection, unless the incident (progressive) waves are only marginally stable. The resultant motion is highly organized and can be described by deterministic analytical theories appropriate for standing waves. The amplitude of the vertical motion

of the waterline (intersection of water surface and slope facing) is of the same order of magnitude as the incident wave height; it increases with decreasing slope angle. Due to nonlinearities both the mean position of the waterline and the position midway between the maximum and minimum elevation are above the still water level (S.W.L.).

For values of α decreasing below some critical limit, which is dealt with in par. 2.3.1, the waves are no longer stable and breaking sets in. This is accompanied by aeration of the water and the irreversible transformation of organized wave energy into turbulent energy, which greatly increases the total rate of energy dissipation. The reflection diminishes as a result, and the motion approaches that of a progressive wave.

The amplitude of the vertical motion of the waterline reaches a maximum for slope angles for which the transition occurs from nonbreaking to breaking. It decreases with decreasing α below this transition value. The mean elevation of the waterline above still water level also decreases, but at a lower rate, so that it increases relative to the variable part of the run-up.

The character of the breakers also varies with the slope angle. The major distinction is between plunging and spilling breakers. This is described in some detail in par. 2.3.2. In plunging breakers the wave profile and the particle motions vary drastically within relatively short distances and time intervals. These variations are much more gradual in spilling breakers, which can occur on gentle slopes only.

The flow in breaking waves is highly complex and does not lend itself to a detailed deterministic treatment. However, provided the overall properties vary only gradually, the relationships between various flow parameters can in a first approximation be assumed to be the same as for stable waves in water of constant depth. This approach is restricted to gentle slopes, and particularly to spilling breakers; it cannot reasonably be applied in the area of rapid wave deformation occurring in plunging breakers.

Outside the breaker zone the dissipation of energy occurs mainly in the laminar or turbulent boundary layers at the bottom and at the free surface, and to a smaller extent in the remaining parts of the water. This consumes generally only a minor portion of the incident wave power, the bulk of which is dissipated in the surf zone. However, for very low values of α all of the incident wave power is dissipated gradually, so that wave breaking does not occur.

So far the properties of the oscillatory flow have been emphasized. However, the mean flow is also of interest. This is affected by the oscillatory motions, which give rise to a change in the time-averaged flux of momentum. These additional fluxes have been called radiation stresses [4], and appear as surface stresses in the equations of motion for the mean flow. One of their effects is a slight depression of the mean water level in shoaling waves outside the breaker zone and a set-up inside the breaker zone. Another effect is the generation of a mean longshore current in the surf zone by obliquely incident waves.

In the preceding description the slope angle was the only independent variable which was varied. We shall next consider the effects of varying H/L_0. Low values of this parameter give rise to non-breaking, almost sinusoidal standing waves. With increasing values of H/L_0 (at constant α) a sequence of flow regimes is established which in the main correspond to those described above for decreasing values of α (at constant H/L_0). An illustration of this is afforded by the fact that for a considerable range of values of α and H/L_0 a number of flow parameters appears to be a function of the similarity parameter ξ only, defined by

$$\xi = \frac{\tan \alpha}{\sqrt{H/L_0}} \, . \qquad (2.2.1)$$

Thus, insofar as this is true, the slope angle and the wave steepness need not be known separately for the determination of these parameters. A paramount example is the breaking criterion given by

Iribarren and Nogales [5], which is expressed in terms of ξ only. In section 2.3 special attention will be paid to this criterion, and to the rôle and interpretation of the parameter ξ in general, because of its relevance to this study.

Several of the phenomena mentioned above are amenable to approximative calculations. This holds particularly for non-breaking waves, which can be described by means of deterministic analytical theories. Most of these imply an irrotational oscillatory main flow with laminar or turbulent boundary layers at the bottom and at the free surface, with a superimposed weak rotational mean velocity field. On gentle slopes the local effects of the bottom slope can be neglected, so that locally constant-depth-solutions can be applied. These are connected in such a manner that the wave frequency is conserved and that the energy balance, integrated vertically and over one wave period, is fulfilled. In this manner the main cumulative effects of the bottom slope are accounted for.

The regimes mentioned above can be broadly divided into three categories:

(a) non-breaking, standing waves;

(b) breaking, progressive waves;

(c) non-breaking, progressive waves (on very mild slopes).

Not all of these are of equal relevance to this study, which is aimed primarily at waves breaking on beaches or dikes, as has been pointed out in the Introduction. Cases (a) and (c) are therefore excluded from further consideration. Additional information concerning case (b) is given in the following section.

2.3 Characteristics of surf

The purpose of this section is to provide some of the details omitted from the rather general and mainly qualitative considerations of section 2.2, insofar as these details are related to waves

breaking on a slope. Many characteristic properties of the surf appear to be governed by the parameter ξ defined by (2.2.1), which may therefore be called the surf-similarity parameter. Its rôle will receive special attention in the following pages. The importance of ξ has also been noted by Bowen et al [6], though with a more restricted scope than is given here, and without an attempt at interpretation.

2.3.1 Breaking criterion

We shall in this paragraph discuss three criteria for the occurrence of wave breaking on a slope.

Iribarren and Nogales [5] have given an expression for the condition at which the transition occurs between non-breaking and breaking of waves approaching a slope which is plane in the neighbourhood of the still-water line. They use the shallow-water trochoidal theory for uniform, progressive waves. According to this theory, progressive waves are at the limit of stability if their amplitude ($\frac{1}{2}H$) equals the mean depth (d). Thus, denoting the condition of incipient breaking by the index "c",

$$\tfrac{1}{2}H_c = d_c \ . \tag{2.3.1}$$

The depth d_c at which this would occur is equated by Iribarren and Nogales to the mean undisturbed depth in the one-quarter wavelength adjacent to the still-water line (see fig. 2.2), or

$$d_c = \frac{1}{2}(\tfrac{1}{4} L_c \tan \alpha_c) = \frac{1}{8} L_c \tan \alpha_c . \tag{2.3.2}$$

The wavelength L_c is calculated as $T_c \sqrt{gd_c}$, so that

$$d_c = \frac{1}{8} T_c \sqrt{gd_c} \tan \alpha_c \ . \tag{2.3.3}$$

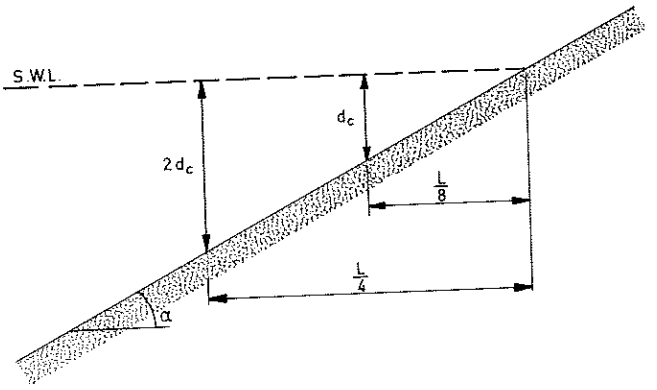

Fig. 2.2 - Breaking depth according to Iribarren and Nogales.

Elimination of d_c between (2.3.1) and (2.3.3) gives

$$(T\sqrt{g/H}\,\tan\alpha)_c = 4\sqrt{2} \tag{2.3.4}$$

or, substituting (2.1.3) and rearranging,

$$\xi_c = \left(\frac{\tan\alpha}{\sqrt{H/L_0}}\right)_c = \frac{4}{\sqrt{\pi}} \approx 2.3 \ . \tag{2.3.5}$$

Laboratory experiments by Iribarren and Nogales and others [1,7] have confirmed the validity of (2.3.5), with the proviso that $\xi \approx 2.3$ corresponds to a regime about halfway between complete reflection and complete breaking. This quantitative agreement is considered to be fortuitous because one can raise valid objections against the derivation on several scores. These pertain to the numerical estimates used by Iribarren and Nogales, rather than to the approach as such. For instance, the limiting height for waves in shallow water is given by (2.3.1) as twice the depth, which is unrealistic. A height-to-depth ratio of order one seems more reasonable. Also,

the wave height at incipient breaking is the height of a standing wave, i.e. roughly twice the height of the incident wave, instead of one times this height, as implied by Iribarren and Nogales. Thus, instead of (2.3.1) it is preferred to write

$$2H_c = d_c \ , \qquad (2.3.6)$$

in which H_c is the height of the incident wave for conditions of incipient breaking. Furthermore, the depth d_c is equated by Iribarren and Nogales to the depth at one-eighth wavelength from the still-water line. It seems to be more logical to choose the depth at one-half wavelength distance, since that location corresponds to the first antinode seaward from the shore (see fig. 2.3). This gives, instead of (2.3.2),

$$d_c = \frac{1}{2} L_c \tan \alpha_c \ . \qquad (2.3.7)$$

Lastly, the length $L_c/4$ in (2.3.2) is calculated by Iribarren and Nogales on the basis of the phase speed corresponding to the mean

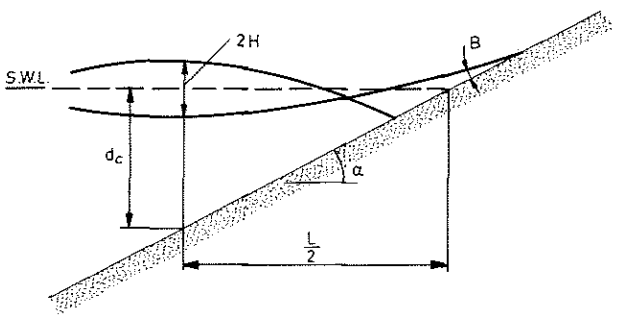

Fig. 2.3 - Breaking depth at location of antinode.

depth (d_c) in the interval considered, whereas it is more accurate to base it on the harmonic mean of the phase speed in this interval. This follows from the fact that it is the phase difference $\Delta\psi$ across

the interval which is the determining factor. It is given by

$$\Delta\psi = \int k(x)dx = \omega \int \frac{dx}{c(x)} , \qquad (2.3.8)$$

in which k is the wave number, ω is the angular frequency ($2\pi/T$) and x is a horizontal coordinate perpendicular to the still-water line. Putting $c = \sqrt{gd}$ and $x = d \cot \alpha_c$, integrating from $d = 0$ to $d = d_c$, and equating the result to π (in view of eq. 2.3.7) gives

$$\Delta\psi = 2\omega_c \cot \alpha_c \sqrt{d_c/g} = \pi . \qquad (2.3.9)$$

After some rearrangement this can be written as

$$d_c = \frac{1}{4} T_c \sqrt{gd_c} \tan \alpha_c , \qquad (2.3.10)$$

which replaces (2.3.3). Elimination of d_c between (2.3.6) and (2.3.10) gives (2.3.5). The fact that this result is exactly the same as that originally given by Iribarren and Nogales is considered to be significant only insofar as the original result had been confirmed empirically. The agreement between the calculated results merely shows how certain variations in a set of numerical factors can just compensate for each other in the end. This, together with the fact that the factors used by Iribarren and Nogales are considered to be not quite realistic, seems to justify the statement that it may have been accidental that the result they obtained is as good as it is now known to be.

The preceding derivations suggest a physical interpretation of the parameter ξ, at least if wave breaking occurs ($\xi < \xi_c$). Consider the local steepness of the breaking waves. Their celerity is proportional to $(gd)^{\frac{1}{2}}$, their wavelength to $T(gd)^{\frac{1}{2}}$, and their steepness to $H/(T(gd)^{\frac{1}{2}})$, or to $(H/gT^2)^{\frac{1}{2}}$, since H/d is of order one for waves breaking in shallow water. Thus, the parameter ξ, given by

$$\xi \equiv \frac{\tan \alpha}{\sqrt{H/L_0}} = \frac{1}{\sqrt{2\pi}} \frac{\tan \alpha}{\sqrt{H/gT^2}} , \qquad (2.3.11)$$

is roughly proportional to the ratio of the tangent of the slope angle (the slope "steepness") to the local steepness of the breaking wave. The criterion for breaking given by Iribarren and Nogales can therefore be said to imply that incipient breaking corresponds to a critical value of this ratio.

Munk and Wimbush [8] give a different derivation of a breaking criterion than Iribarren and Nogales, though the result is very similar. They argue that the downslope component of the particle acceleration cannot exceed g sin α, and that breaking sets in if this limit value is attained. An expression for the critical condition is obtained by equating the maximum downslope acceleration in harmonic motion with frequency $\omega = 2\pi/T$, and with vertical amplitude A (at the slope), to g sin α:

$$\left(\frac{\omega^2 A}{\sin \alpha}\right)_c = g \sin \alpha_c . \qquad (2.3.12)$$

In their discussion of this equation, Munk and Wimbush implicitly equate A to the amplitude of the incident (progressive) wave. However, it seems to be more logical to set it approximately equal to the height H of the incident wave, since we are dealing with the limiting conditions for the existence of a standing wave. On this understanding, and with substitution of (2.1.3), eq. (2.3.12) can be transformed into

$$\left(\frac{\sin \alpha}{\sqrt{H/L_0}}\right)_c = \sqrt{2\pi} \approx 2.5 . \qquad (2.3.13)$$

It can be seen that the criteria (2.3.5) and (2.3.13) are roughly equal, except on very steep slopes. It may be wondered to which extent the derivations have a common base, although they are quite different when considered superficially. It has already been remark-

ed that the criterion given by Iribarren and Nogales corresponds to a critical value of the ratio of the slope angle to a local wave steepness. This is closely related to the criterion adopted by Munk and Wimbush, for the occurrence of a maximum downslope acceleration equal to g sin α implies a zero pressure gradient parallel to the slope facing, which means that the maximum water surface slope equals the structure slope (or, that the angle B indicated in fig. 2.3 is zero). Thus, whereas Iribarren and Nogales implicitly relate the structure slope to a wave steepness (height-length ratio), Munk and Wimbush relate it to a local surface slope. The correspondence between the two is obvious.

The kinematical criterion B = 0 has been used previously by Miche [9], who applies it to his linear, potential-flow solution for periodic, standing waves on a plane slope extending to deep water. The resulting breaking criterion is

$$\left(\frac{H_0}{L_0}\right)_c = \frac{\sin^2 \alpha}{\pi} \sqrt{\frac{2\alpha}{\pi}} \quad \text{for} \quad \alpha \leq \frac{\pi}{4} , \qquad (2.3.14)$$

in which H_0 is the height of the incident waves at deep water. This equation contains an additional factor proportional to $\sqrt{\alpha}$, compared to (2.3.13). This is due to the fact that Miche takes account of the calculated ratio between amplitude at the slope and incident wave height:

$$\frac{A}{H_0} = \sqrt{\frac{\pi}{2\alpha}} \quad . \qquad (2.3.15)$$

Empirical data indicate that Miche's equation (2.3.14) is valid as a criterion for the onset of breaking [7]. It differs in this respect from (2.3.5) and (2.3.13), which more nearly correspond to conditions halfway between just-not-breaking and "complete" breaking.

It has been noted above that the basis for Miche's criterion (B = 0) is equivalent to the one used by Munk and Wimbush (maximum downslope acceleration cannot exceed g sin α). Interestingly enough,

if the critical incident wave steepness given by (2.3.14) is substituted in Miche's equations for the wave motion, then it appears that the maximum downslope acceleration would be 2g sin α. The discrepancy is due to the approximations in the linear theory, which is inadequate for a good description of waves at the limit of stability.

The preceding criteria for the incipient breaking of standing waves on a slope are to be distinguished from criteria for the limit of stability of waves propagating without change of shape in water of constant depth. This limit is generally supposed to be attained if the particle speed at the crest equals the phase speed. Miche [7] has given the following result for periodic waves:

$$\left(\frac{H}{L}\right)_{max} = 0.14 \tanh \frac{2\pi d}{L} , \qquad (2.3.16)$$

which in shallow water reduces to

$$\left(\frac{H}{d}\right)_{max} = 0.14 \times 2\pi \approx 0.88 , \qquad (2.3.17)$$

while the limiting height of a solitary wave is given by McCowan [10] as

$$\left(\frac{H}{d}\right)_{max} = 0.78 . \qquad (2.3.18)$$

Theoretically, these equations cannot be expected to indicate whether waves advancing and deforming on a slope will break, but it turns out that they are in fair agreement with measured H/d-values at the breakpoint of periodic, spilling breakers (see paragraph 2.3.3). The fact that this is true even for the theoretical solitary-wave result is fortuitous, since it has been shown that solitary waves breaking on slopes have a H/d-ratio at breaking considerably in excess of 0.78, even on slopes as gentle as 1 : 50 [11].

2.3.2 Breaker types

So far the parameter ξ has been considered only in the context of a breaking criterion, that is, as an aid in answering the question whether wave breaking will occur. However, it also gives an indication of how the waves break. The main types are surging, collapsing, plunging and spilling breakers [12 - 14]. These occur in the order of increasing wave steepness and/or decreasing slope angle. They are illustrated in fig. 2.4.

A wave which surges up and down the slope with minor air entrainment, at the base only, is said to be a surging breaker [14]. With increasing steepness of the incident waves the front face of a surging wave advancing on the slope gradually steepens. It may become vertical and lose its stability over the lower portion, after which the wave collapses. The so-called collapsing breaker was introduced as a separate type by Galvin [14]. In previous breaker classifications [12, 13] it was included in the category of surging breakers, which were then more broadly defined. However, in the more restricted definition proposed by Galvin, as well as in a photograph presented by him [15], the surging breakers are so much like standing waves that it seems hardly justified to call them "breakers".

In plunging breakers the crest becomes strongly asymmetric; it curls over, enclosing an air pocket, after which it impinges on the trough water ahead. It imparts some forward momentum to this trough water, entraining air and generating turbulence in the process. The water motion in the impact area is not at all wave-like in appearance. However, some distance shoreward from this area a travelling bore is formed, carrying the relatively small wave momentum and energy which is left after the plunge. With increasing wave steepness and for decreasing slope angle the crest of a plunging breaker becomes less asymmetric, and the forward-projected jet of water from the crest becomes less and less pronounced. Its point of impact moves closer to the point of detachment, i.e. it moves from the trough to the sloping face of the breaker; the violence of the impact thereby

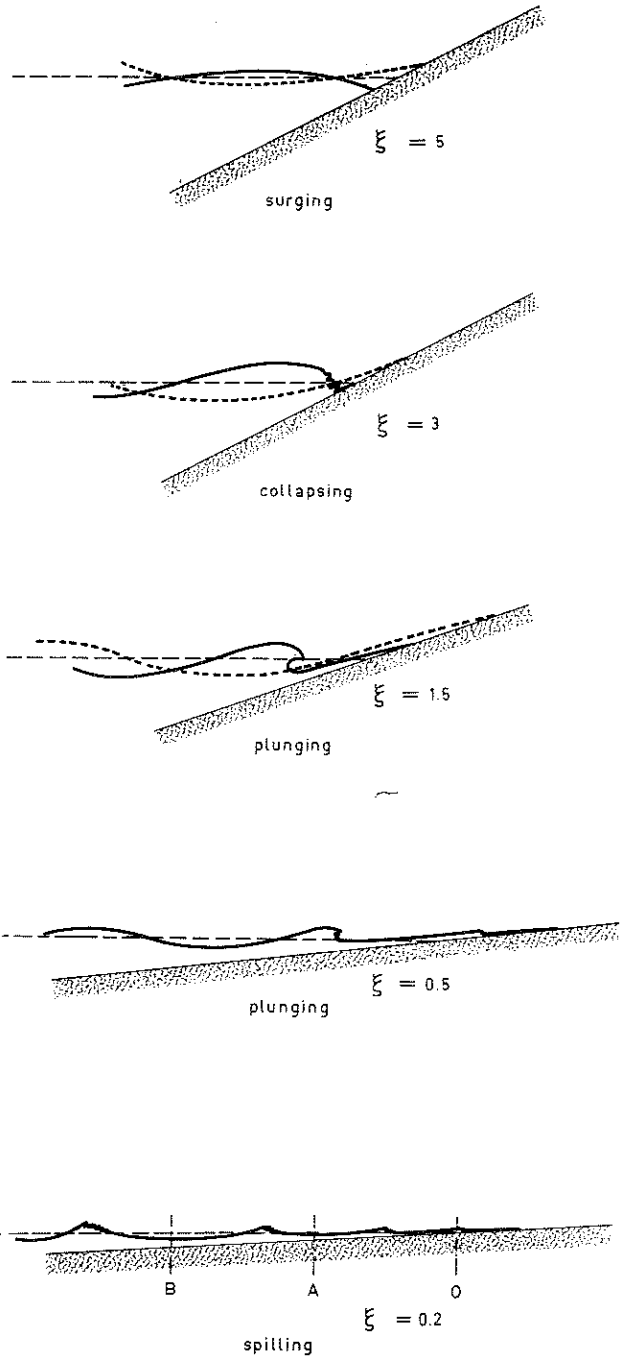

Fig. 2.4 - Breaker types as a function of ξ.

decreases. The enclosed air pocket diminishes in size, and for sufficiently steep waves and gentle slopes the air pocket and the jet of water emanating from the crest are no longer identifiable. One then speaks of spilling breakers. The wave form as a whole in these breakers is fairly stable, since the zone of instability is confined to the crest region. The wave-energy dissipation takes place much more gradually than in plunging breakers.

It is clear from the preceding description that there is a gradual transition from one breaker type to another. It would therefore be meaningless to try to pinpoint precise combinations of H/L_0 and α delineating regions in which one or another of the breaker types occurs. The values mentioned in what follows should be considered as indicating the order of magnitude only of the values in the transition ranges.

Galvin [14] has presented criteria regarding breaker types in terms of an "offshore parameter" $H_0/(L_0 \tan^2\alpha)$, in which H_0 is a deep-water wave height calculated from the motion of the generator bulkhead and the water depth, and an "inshore parameter" $H_b/(gT^2 \tan\alpha)$. The index "b" refers to values at the break point, which generally is taken to be the most seaward location where some point of the wave front is vertical, or, if this does not occur, the location where foam first appears at the crest.

Galvin's offshore parameter can be written as ξ_0^{-2}, in which the index "0" refers to deep water (wave height). Converting the critical values of the offshore parameter given by Galvin to values of ξ_0 gives

$$\begin{aligned} &\text{surging or collapsing} && \text{if} && \xi_0 > 3.3 \\ &\text{plunging} && \text{if} && 0.5 < \xi_0 < 3.3 \\ &\text{spilling} && \text{if} && \xi_0 < 0.5 \end{aligned} \qquad (2.3.19)$$

These results are based on experiments on slopes of 1 : 5, 1 : 10 and 1 : 20.

The inshore parameter used by Galvin, $H_b/(gT^2 \tan\alpha)$, is not equivalent to the parameter ξ_b used here. However, a re-analysis of Galvin's data in terms of $\xi_b = (H_b/L_0)^{-\frac{1}{2}} \tan\alpha$ showed that the class-

ification of breakers as plunging or spilling could be performed equally well with ξ_b as with Galvin's inshore parameter. The results are given in fig. 2.5. The following approximate transition values may be noted:

$$\begin{array}{lll} \text{surging or collapsing} & \text{if} & \xi_b > 2.0 \\ \text{plunging} & \text{if} & 0.4 < \xi_b < 2.0 \\ \text{spilling} & \text{if} & \xi_b < 0.4 \end{array} \qquad (2.3.20)$$

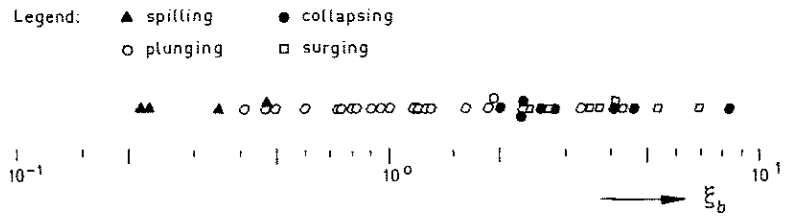

Fig. 2.5 - Breaker type classification based on Galvin's data [14].

The possibility of using a parameter equivalent to ξ_b as a breaker type discriminator has also been noted by Galvin in a recent review of breaker characteristics [15].

Fig. 2.4 gives some fairly typical profiles across the surf zone for a number of values of ξ. The incident wave steepness has been chosen fairly large in all cases for better legibility of the figure. The variation of ξ has been obtained mainly by varying the slope angle. Inspection of the figure shows that not only the form of a breaking wave varies with ξ, but the distance of the break point from the mean water line as well. This distance, expressed in wavelengths, is estimated at roughly $(d_b \cot\alpha)/(\frac{1}{2}T\sqrt{gd_b}) \approx 0.8\,\xi_b^{-1}$, where we have put $H_b \approx d_b$. Observations by the author on slopes between 1 : 3 and 1 : 25, with ξ-values from 0.15 to 1.9, have indicated that this estimate is qualitatively correct, but that it is roughly 20% too high. With spilling breakers there are

at least two breaking or broken waves in the surf zone simultaneously. This number ranges from zero to two for plunging breakers. Collapsing breakers occur almost at the instantaneous water's edge, so that there is at most one of these present at any one time. Reference should be made in this connection to Kemp [16], who points out that the total phase difference across the surf zone is indicative of the type of wave motion, and of the corresponding equilibrium profile of sand or shingle beaches.

2.3.3 Breaker height-to-depth ratio

The ratio of wave height to water depth at breaking is an important parameter of the surf zone; it is here denoted by the symbol γ_b:

$$\gamma_b = \frac{H_b}{d_b} \qquad (2.3.21)$$

The depth d_b is here defined as the still-water depth at the break point.

Values of γ_b generally range between 0.7 and 1.2. Bowen et al [6] suggest that γ_b may be a function of ξ_0 only. The data presented by them are given in fig. 2.6. In addition, data have been plotted from Iversen [12], from Goda [17], and from unpublished results gathered for this study. It can be observed that the results from Bowen et al [6] form a separate group, outside the range of the others. The reason for this is not knowm. The other points in fig. 2.6 show a weak trend with ξ_0. For values of ξ_0 less than about 0.2, in the range of spilling breakers, they are scattered about a value of $\gamma_b \approx 0.8$, while there is a slow increase with ξ_0 for higher values. According to Galvin [14], depth-to-height ratios at breaking (γ_b^{-1}) of 1.2, 0.9 and 0.8 are typical for spilling, plunging and collapsing breakers. The first two of these values are consistent with the results presented in fig. 2.6.

The scatter in the results may partly be due to the fact that for this purpose the independent variables H/L_0 and α cannot ade-

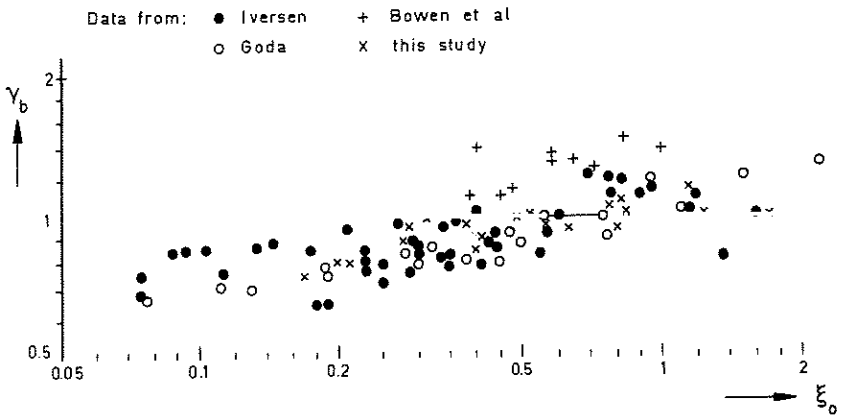

Fig. 2.6 - Breaker height-to-depth ratio.

quately be combined in the single parameter ξ. However, even values presented by various authors for the same values of α and H/L_0 show considerable scatter. This is undoubtedly to some extent due to the difficulties and ambiguities inherent in defining (experimentally) and measuring breaker characteristics. Another factor contributing to the scatter may be the occurrence of parasitic higher-harmonic free waves which are often inadvertently generated along with the intended wave train. The secondary waves affect the breaking process in a manner depending on the phase difference with the primary wave, which in turn depends (among others) on the distance from the wave generator. This distance is not commonly introduced as an independent variable, so that any effects which it may have on the results can appear as unexplained scatter.

2.3.4 Set-up, run-up and run-down

The subjects of set-up and run-up will receive extensive treatment in the chapters 3, 6 and 7. For this reason they will only briefly be mentioned here.

The set-up is defined as the wave-induced height of the mean level of the water surface above the undisturbed water level. Theoretical and experimental results [6, 18] indicate that the gradient

of the set-up in the surf zone on gently sloping beaches is proportional to the beach slope; the coefficient of proportionality is a function of γ, the average height-depth ratio of the waves in the surf zone. The maximum set-up is calculated from this in par. 3.4.1. It is roughly equal to $0.3\ \gamma\ H_b$.

The run-up height R is defined as the maximum elevation of the waterline above the undisturbed water level. It is generally determined empirically. A simple and reliable empirical formula for the run-up height of waves breaking on a smooth slope has been given by Hunt [1]. It can be written as

$$\frac{R}{H} = \xi \qquad \text{for } 0.1 < \xi < 2.3 \ . \qquad (2.3.22)$$

An investigation by Battjes and Roos [19] of some details of the run-up of breaking waves on dike slopes (1 : 3, 1 : 5, 1 : 7), such as the mean velocity of advance, particle velocities, layer thickness and so on, has shown that many of these parameters are functions of ξ only if normalized in terms of the incident wave characteristics.

Measurements of the run-down height (minimum elevation of the waterline above the undisturbed water level) are very scarce, and, if available, not very accurate since run-down is rather ill-defined experimentally. An analysis of the measurements by Battjes and Roos [19], supplemented with unpublished data gathered for this study, indicates that in the experimental range ($\cot \alpha$ = 3,5,7,10; $0.02 < H/L_0 < 0.09$; $0.3 < \xi < 1.9$) the ratio of run-down height to run-up height is roughly equal to $(1 - 0.4\ \xi)$. In other words, the ratio of the variable part of the vertical motion of the waterline to the maximum elevation (above S.W.L.) is approximately $0.4\ \xi$. It has a maximum value of about 1 for waves in the transition from non-breaking to breaking, and decreases with decreasing ξ. For very small ξ the set-up constitutes the greater part of the run-up height.

2.3.5 Reflection and absorption

The relative amount of wave energy that can be reflected off a

slope is intimately dependent on the breaking processes and the attendant energy dissipation. Because of this, and in view of the fact that these processes appear to be governed to such a large extent by the parameter ξ, it is natural to try to relate the reflection coefficient to ξ. The reflection coefficient r is defined as the ratio of the amplitude of the reflected wave to the amplitude of the incident wave. The estimation of r on a slope generally takes place according to a procedure given by Miche [7]. The theoretical reflection coefficient is set equal to 1 for non-breaking waves. For breaking waves Miche assumes that the reflected wave height equals the maximum height possible for a non-breaking wave of the given period on the given slope; in other words, only the energy corresponding to the height in excess of the critical height is assumed to be dissipated. This gives

$$r_{th} = \frac{(H_0/L_0)_c}{H_0/L_0} \qquad \text{if this is less than 1}$$
$$= 1 \qquad \text{otherwise,} \tag{2.3.23}$$

in which $(H_0/L_0)_c$ is the critical steepness for the onset of breaking, according to Miche's formula (2.3.14). The index "th" refers to "theoretical". The actual reflection coefficient will be smaller than r_{th} due to effects of viscosity, roughness, and permeability. Miche recommends a multiplication factor of 0.8 for smooth slopes.

Miche's assumption regarding the reflection coefficient can be expressed in terms of ξ and Iribarren and Nogales' breaking criterion. Substitution of (2.2.1) into (2.3.23) gives

$$r_{th} = (\xi/\xi_c')^2 \qquad \text{if this is less than 1}$$
$$= 1 \qquad \text{otherwise,} \tag{2.3.24}$$

in which ξ_c' is the critical value of ξ for the <u>onset</u> of breaking, as distinguished from ξ_c, the value given by Iribarren and Nogales

for the condition halfway between the onset of breaking and complete breaking ($\xi_c \approx 2.3$). According to Hunt [1], the reflection coefficient corresponding to $\xi = 2.3$ is about 0.5, so that (2.3.24) becomes

$$r \approx 0.1\ \xi^2 \qquad \text{if this is less than 1}$$
$$= 1 \qquad \text{otherwise.} \tag{2.3.25}$$

An extensive series of measurements of the reflection coefficient of plane slopes has recently been presented by Moraes [20]. His results for slopes with tan α = 0.10, 0.15, 0.20 and 0.30 are given in fig. 2.7.

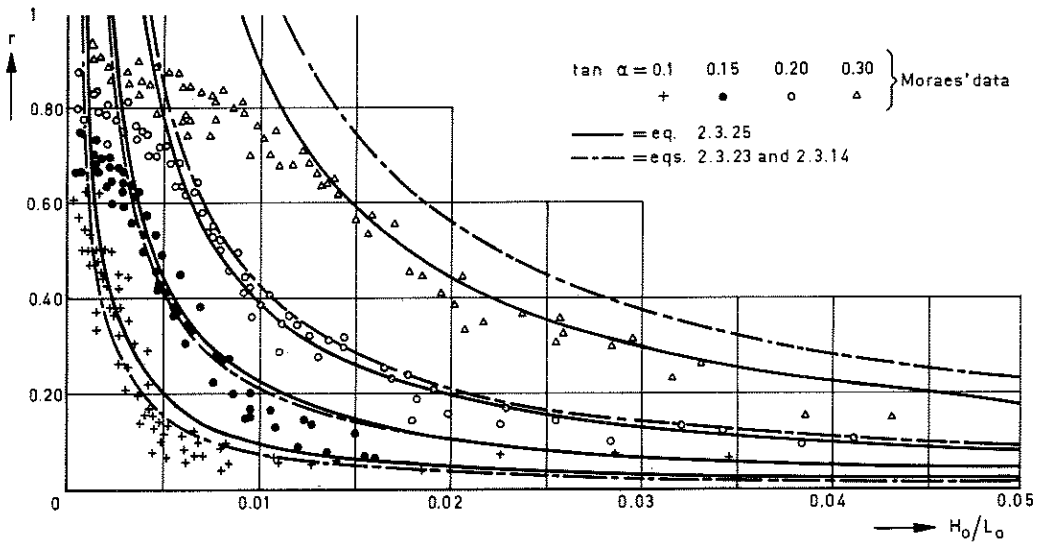

Fig. 2.7 - Reflection coefficient vs wave steepness, for various slope angles.

Also shown are the curves according to (2.3.25), and to (2.3.23) combined with (2.3.14). These equations give almost identical re-

sults for the three smallest values of tan α. Only for tan α = 0.3 do they differ significantly. Eq. (2.3.25) gives the best agreement with the experimental data. Applying the reduction of 20% to Miche's theoretical reflection coefficients would improve the agreement of his formula with the data for the 0.3 slope, but would worsen it for the others.

A replotting of Moraes' data [1] in terms of r vs ξ is presented in fig. 2.8. The experimental points for the four slopes more or less

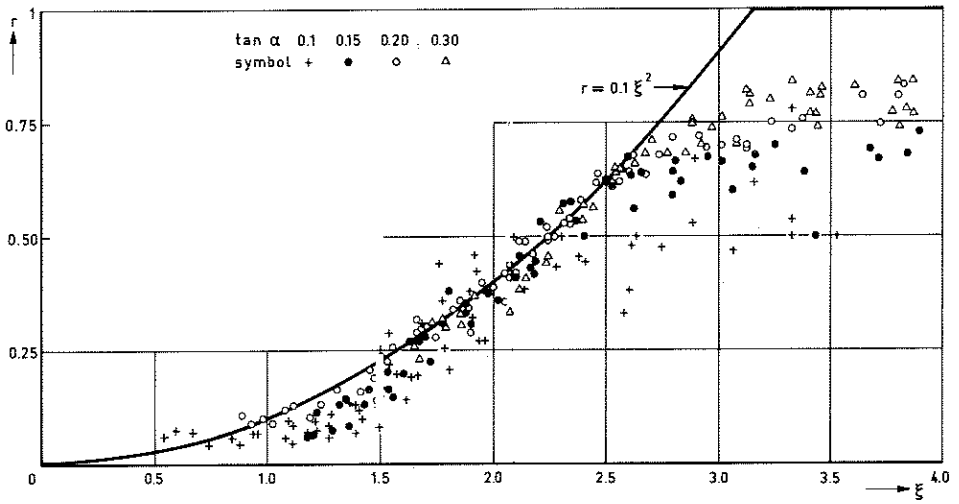

Fig. 2.8 - Reflection coefficient vs ξ.

coincide with each other and with the curve representing eq. (2.3.25) for $\xi < 2.5$, i.e. as long as the waves break. For $\xi \gtrsim 2.5$ they diverge, gentler slopes giving less reflection than steeper slopes (at the same value of ξ).

---

[1] The author is indebted to Dr. Moraes for providing the original data in tabulated form.

2.3.6 General comments regarding the parameter ξ.

In the preceding paragraphs examples have been given of a number of characteristic surf parameters for the determination of which it is not necessary to specify both α and H/L_0, but only the combination $\tan\alpha/(H/L_0)^{\frac{1}{2}}$. It may be useful to summarize them here: a breaking criterion, the breaker type, the breaker height-to-depth ratio, the number of waves in the surf zone, the reflection coefficient (therefore also the discrimination between progressive waves and standing waves), and the relative importance of set-up and run-up. They have been collected in Table 2.1. Characteristic values of ξ are given in the upper row of the table. Each of the following rows indicates how one of the parameters just mentioned varies with ξ.

The recognition of the possibility that several properties can roughly be expressed as functions of ξ alone contributes to a more unified understanding of the phenomena involved. Such understanding would be deepened by further insight in the nature of the parameter ξ itself. One interpretation has already been mentioned in paragraph 2.3.1, page 13, where it was observed that ξ is approximately proportional to the ratio of the tangent of the slope angle to the shallow-water wave steepness. In paragraph 2.3.2, ξ^{-1} was seen to be approximately proportional to the number of wavelengths within the surf zone. This is in essence equivalent to saying that ξ is approximately proportional to the relative depth change across one wavelength in the surf zone. This interpretation is obviously relevant to the dynamics of the breaking waves, particularly with regard to their rate of deformation. It makes it plausible that ξ is of importance, but it does not prove that ξ serves as the sole determining factor for the (suitably normalized) parameters of the surf. Indeed, there are valid arguments which throw doubt on this possibility of full similarity. In this regard it is useful to consider two situations of different slope angle and wave steepness as a prototype and a distorted scale model thereof. It is well known [21] that Froudian model-prototype similarity can be obtained even

ξ	$\approx$ 0.1	0.5	1.0	2.0	3.0	4.0	5.0
	breaking						no breaking
	spilling		plunging		collapsing/surging		
H_b/d_b	$\approx$ 0.8		1.0	1.1	1.2		
N*)	6-7	2-3	1-2	0-1	0-1		
r	10^{-3}	10^{-2}	10^{-1}	4×10^{-1}	8×10^{-1}		
	absorption						reflection
	progressive wave						standing wave
	set-up predominant			run-up predominant			

*) number of waves in surf zone

Table 2.1

in distorted models, provided the assumption of hydrostatic pressure distribution is valid both in the prototype and in the model. Pertinent scale ratios (λ) are given in Table 2.2, expressed in terms of the horizontal and vertical geometrical scales and the scale of the gravitational acceleration (unity).

Variable	Symbol	Scale ratio
horizontal length	ℓ	λ_ℓ
depth	d	λ_d
gravity acceleration	g	$\lambda_g = 1$
bottom slope	$\tan\alpha$	$\lambda_{\tan\alpha} = \lambda_d \lambda_\ell^{-1}$
wave height	H	$\lambda_H = \lambda_d$
wave length	L	$\lambda_L = \lambda_\ell$
wave celerity	$c \sim (gd)^{\frac{1}{2}}$	$\lambda_c = \lambda_d^{\frac{1}{2}}$
wave period	$T = L/c$	$\lambda_T = \lambda_\ell \lambda_d^{-\frac{1}{2}}$

Table 2.2 - Scale ratios for a distorted long-wave model.

Since ξ is defined as

$$\xi = \left(\frac{gT^2}{2\pi H}\right)^{\frac{1}{2}} \tan\alpha \ , \qquad (2.3.26)$$

its scale ratio is

$$\lambda_\xi = \lambda_T \lambda_H^{-\frac{1}{2}} \lambda_{\tan\alpha} \ , \qquad (2.3.27)$$

which becomes, using the values given in Table 2.2,

$$\lambda_\xi = (\lambda_\ell \lambda_d^{-\frac{1}{2}})(\lambda_d^{-\frac{1}{2}})(\lambda_d \lambda_\ell^{-1}) = 1 \ . \qquad (2.3.28)$$

In other words, a distorted long-wave model which is dynamically similar to its prototype necessarily has the same ξ as this prototype. Conversely, a distorted wave-model with the same value of ξ as its prototype is similar to this prototype if the pressure distribution in both is hydrostatic. This is not the case in breaking or near-breaking waves in shallow water, where some effects of the vertical accelerations must be taken into account due to the fact that the surface curvature is locally strong. Thus, the existence of similarity of the surf in distorted models is not proved, and must be doubted to the extent that deviations from the long-wave approximations have a significant effect. Such effects are certain to be of importance for the details of the local flow patterns, but this is not necessarily the case for overall properties of the surf. (One example of this is the total phase change across the surf zone; the phase speed in shallow water is only weakly affected by curvature of the streamlines.) The final check on this must of course be obtained empirically. In this regard it appears justified to draw the conclusion from the data presented in the preceding paragraphs that the factor ξ is a good indicator of many overall properties of the surf zone, and may indeed be given the name of "surf-similarity parameter".

It should be noted that in the arguments presented above two situations were compared with different slope and different wave steepness, but with the same ξ. Thus, the similarity referred to above pertains to two different surf zones as a whole. It might also be wondered whether similarity would exist within a surf zone. Thus, considering the lowermost sketch in fig. 2.4, is the surf in sector OA dynamically similar to the surf in OB? Such similarity would require equality of the parameters ξ for the two sectors. But $\xi_A > \xi_B$, since the two sectors have the parameters α and L_0 in common, while $H_A < H_B$. In other words, the surf zone possesses no self-similarity. This has recently also been noted by Longuet-Higgins [22].

2.4 Implications for further work

We shall conclude this chapter with a few remarks concerning the calculations of properties of waves breaking on a slope. Ideally, a unified approach would be developed which is valid for all values of ξ in the range of breaking waves. However, the differences in the flow regimes associated with small and moderate values of ξ have so far rendered this impossible.

Various local properties of waves propagating on a slope can in a first approximation be mutually related by applying results derived for waves which propagate without change of shape. This approach is evidently valid only if the wave characteristics vary gradually, i.e. for small values of ξ, which implies a gentle slope and spilling breakers. For small ξ the variable part of the elevation of the waterline above S.W.L. (the difference between run-up and run-down) is insignificant compared with the steady part (the set-up). The latter is approximately proportional to γH_b; the wave period influences this only through its effect on γ and on H_b/H.

If ξ is not small, but of order unity, then the situation is quite different: we have plunging breakers, in which the flow varies rapidly; a steady-wave approximation is inapplicable. The variable part of the elevation of the waterline above S.W.L. is predominant compared to the set-up, and is strongly influenced by the wave period (R is proportional to T in Hunt's formula).

In view of the differences mentioned above it is natural to give separate treatment in the calculation of irregular-wave properties to cases of small ξ and to cases in which ξ is of order unity ($\xi \gg 1$ implies non-breaking waves; these are not considered here). The chapters 5 and 6 deal with the first of these, giving calculations of the radiation stresses and of the set-up and longshore currents due to irregular waves on gently sloping beaches, respectively. The cases in which ξ is of order one are considered in the chapters 7 and 8, which deal with run-up and overtopping of irregular waves on dikes. The calculations therein are based on

empirical results for regular waves. The values of ξ corresponding to the limits of validity of the respective approaches cannot be given beforehand; they should be determined empirically.

A final remark regarding the relation between ξ and α seems in order. Small values of ξ imply small values of α, since H/L_0 cannot exceed an upper limit which is of order 10^{-1}. Thus, spilling breakers ($\xi < 0.4$ approximately) can occur only on slopes less than about 1 : 10, such as are typical for sand beaches. They cannot occur on slopes which are typical for sea dikes, which are generally steeper than 1 : 10. On the other hand, the lower bound of H/L_0 is formally zero, so that moderate or large values of ξ do not necessarily imply moderate or large values of tan α. However, if we restrict ourselves to wave steepnesses greater than one percent, say (common values in exposed locations), then the slope should be steeper than about 1 : 15 for plunging to occur.

3 EQUATIONS OF MOTION

3.1 Introduction

The purpose of this chapter is to summarize some results from analytical theories for periodic progressive gravity surface waves, and to formulate conservation equations for a steady flow acted upon by gradually varying waves.

We consider gravity waves on the surface of water, which is assumed to be a Newtonian fluid with constant viscosity and constant mass density, subject to gravity as the only volume force. The air-water interface is assumed to be subjected to a constant normal stress only, the atmospheric pressure. The value of this constant pressure plays no part in the problems to be considered here, and is set equal to zero. The scale of the waves is considered to be small enough to permit effects of the rotation and curvature of the earth to be neglected, while on the other hand we assume that the Reynolds number of the flow is large and that the effects of surface tension are negligible. The fact that the Reynolds number is large does not justify the conclusion that all viscous effects can be neglected, if only because energy dissipation should be possible. It does imply, however, that throughout most of the flow region the viscosity terms in the equations of motion are quite small relative to the other terms.

It can be shown [23,24] that under the conditions mentioned above vorticity cannot be generated in the interior of the water but at the boundaries only, from where it spreads to the interior. However, in wave motions the vorticity generated at the boundaries is mainly oscillatory in nature; the steady component is relatively weak. If the wave Reynolds number is large the oscillatory vorticity remains restricted to thin regions adjacent to the boundaries, while only the steady component can penetrate the whole fluid, given enough time. But, since the steady vorticity is relatively weak it can be neglected in a first approximation of the wave dynamics. Thus, outside the boundary layers the oscillatory flow can be considered to be irrota-

tional. At first only this part of the flow will be dealt with; particular emphasis will thereby be placed on periodic progressive waves. The effects of gradually varying waves on a weak mean flow will be considered in the sections 3.3 and 3.4.

3.2 Irrotational wave motion

3.2.1 Basic equations

A résumé of the governing equations is given below. The following notation is used: t is time; $\vec{x} = (x,y,z)$ is the coordinate vector; the x- and y-axes are horizontal, while z is measured positive upwards from the undisturbed water level; the equation of the free surface is $z = \zeta(x,y,t)$; the undisturbed depth is d; the particle velocity is $\vec{u} = (u,v,w)$; the velocity potential is ϕ, and p is the fluid pressure.

The velocity u, given by

$$\vec{u} = \nabla\phi \quad , \tag{3.2.1}$$

must have zero divergence because of the assumed incompressibility of the fluid, so

$$\nabla^2\phi = 0 \quad . \tag{3.2.2}$$

This is the Laplace equation. Since this is of the elliptic type we must specify boundary conditions on ϕ and/or its normal derivative at the whole surface enclosing the domain in which a solution of (3.2.2) is sought. The normal component of the particle velocity relative to a fixed or moving boundary should vanish. This gives

$$\frac{\partial\phi}{\partial n} = 0 \qquad \text{at } z = -d \tag{3.2.3}$$

and

$$\frac{\partial\zeta}{\partial t} + \frac{\partial\zeta}{\partial x}\frac{\partial\phi}{\partial x} + \frac{\partial\zeta}{\partial y}\frac{\partial\phi}{\partial y} = \frac{\partial\phi}{\partial z} \quad \text{at } z = \zeta \quad . \tag{3.2.4}$$

The kinematic boundary conditions at the bottom (3.2.3) and at the free surface (3.2.4) hold rather generally. They must be supplemented with boundary conditions at surfaces enclosing the solution domain laterally. These depend on the applications being considered. In some cases only conditions of spatial periodicity and symmetry need be given. Initial conditions will in general have to be specified as well. This is not necessary when a solution is sought which is periodic in time.

The momentum equation for irrotational flow can be integrated once with respect to the space variables, yielding the Bernoulli equation for unsteady flow:

$$\frac{\partial \phi}{\partial t} + \frac{p}{\rho} + gz + \tfrac{1}{2}|\nabla\phi|^2 = f(t) \quad . \tag{3.2.5}$$

The function of time appearing in the right-hand side can be chosen arbitrarily, and will be set equal to zero for convenience. The condition of zero pressure at the free surface can then be written as

$$\frac{\partial \phi}{\partial t} + g\zeta + \tfrac{1}{2}|\nabla\phi|^2 = 0 \qquad \text{at } z = \zeta \tag{3.2.6}$$

The problem of finding a solution to the preceding equations is greatly complicated by the fact that the boundary conditions at the free surface contain nonlinear terms, and that they are specified at a surface which itself is an unknown function of space and time. Stokes [25] gave a formal procedure to arrive at approximate solutions. His method involves a Taylor series expansion about the mean water level for the free surface conditions, while all of the dependent variables are expressed as a series in powers of a small parameter, say σ, which is of the order of the wave slope. For instance, the velocity potential is written as

$$\phi = \phi_0 + \sigma\phi_1 + \sigma^2\phi_2 + \ldots\ldots\ldots \sigma^n\phi_n + O(\sigma^{n+1}) \quad . \tag{3.2.7}$$

The convergence of the series is rapid, provided the wave slope is sufficiently small. A method of successive approximations can then be applied.

Terms in series such as (3.2.7) which are proportional to σ^k are said to be k^{th}-order terms. We refer to an m^{th}-order quantity if the first non-zero term in its power series is of m^{th} order. An approximate solution which is arrived at by retaining only the terms of order n or less is called an n^{th}-order solution or an n^{th}-order approximation.

The first-order approximations to (3.2.4), (3.2.5) and (3.2.6) are

$$\frac{\partial \zeta}{\partial t} = \frac{\partial \phi}{\partial z} \qquad \text{at } z = 0 \quad , \tag{3.2.8}$$

$$\frac{\partial \phi}{\partial t} + \frac{p}{\rho} + gz = 0 \quad , \tag{3.2.9}$$

and

$$\frac{\partial \phi}{\partial t} + g\zeta = 0 \qquad \text{at } z = 0 \quad . \tag{3.2.10}$$

Up to the first order the equations appear to be linear; they possess solutions which are harmonic in time. Linear superposition of such elementary solutions permits the analysis of more complicated motions.

3.2.2 Progressive waves in water of constant depth

In this paragraph we shall summarize the linear solution for a long-crested sinusoidal progressive wave in water of constant depth. The wave amplitude is denoted as a; the angular frequency is ω. The wave number is $\vec{k} = (k_x, k_y, 0)$, with absolute magnitude $|\vec{k}| = k$; $\vec{e}$ is a unit vector in the direction of propagation: $\vec{e} = \vec{k}/k$. Other symbols will be defined where they first appear. Expressions are given for a number of zero- and first-order quantities as well as for the mean value of some second-order quantities; the latter can readily be found from the first-order results.

Phase: $$\chi = \vec{k}.\vec{x} - \omega t \quad . \tag{3.2.11}$$

Surface profile: $$\zeta = a \cos \chi \quad . \tag{3.2.12}$$

Velocity potential: $$\phi = \frac{\omega a}{k} \frac{\cosh k(d + z)}{\sinh kd} \sin \chi \quad . \tag{3.2.13}$$

Dispersion equation: $$\omega^2 = gk \tanh kd \quad . \tag{3.2.14}$$

Phase speed: $$c = \frac{\omega}{k} = \frac{g}{\omega} \tanh kd \quad . \tag{3.2.15}$$

Horizontal particle velocity:

$$(u,v) = \omega a \frac{\cosh k(d + z)}{\sinh kd} \cos \chi (e_x, e_y) \quad . \tag{3.2.16}$$

Vertical particle velocity:

$$w = \omega a \frac{\sinh k(d + z)}{\sinh kd} \sin \chi \quad . \tag{3.2.17}$$

Pressure fluctuation:

$$\Delta p = p + \rho g z = \rho g a \frac{\cosh k(d + z)}{\cosh kd} \cos \chi . \tag{3.2.18}$$

Mean potential energy per unit area:

$$E_p = \frac{1}{4} \rho g a^2 \quad . \tag{3.2.19}$$

Mean kinetic energy per unit area:

$$E_k = \frac{1}{4} \rho g a^2 \quad . \tag{3.2.20}$$

Mean total energy per unit area:

$$E = \frac{1}{2} \rho g a^2 \quad . \tag{3.2.21}$$

Mean energy transfer per unit time per unit length:

$$\vec{P} = Enc\vec{e} = P\,\vec{e} \qquad (3.2.22)$$

in which

$$n = \frac{1}{2} + \frac{kd}{\sinh 2\,kd} \quad . \qquad (3.2.23)$$

Mean momentum per unit area, or mean mass flux per unit length:

$$\vec{M} = \frac{E}{c}\vec{e} \quad . \qquad (3.2.24)$$

The preceding equations give the first non-zero terms in the power series assumed for the respective parameters. Additional terms can be found by carrying the solution to higher orders of approximation. These will give only relatively small corrections if the wave steepness is small and the wavelength/depth ratio is not very large. The Stokes series becomes divergent if the latter condition is not fulfilled. However, even if this occurs it does not necessarily imply that all of the results from the lowest approximation, summarized in the equations (3.2.11) through (3.2.24), are unrealistic. It only means that higher-order approximations of some or all of the dependent variables are poorer than those of lower order. The use of low-order Stokes approximations has in fact proved quite seccessful in the applications to be considered here, even in very shallow water [6], particularly regarding predictions depending on the waves only through their mean second-order properties such as energy, energy flux, momentum flux etc. For this reason these approximations will also be employed here. An alternative might have been to use a cnoidal wave theory, which is a nonlinear shallow-water theory for periodic, progressive waves. This alternative has not been adopted because the cnoidal theory has the practical disadvantage of yielding equations which are far less tractable than those resulting from the Stokes theory.

3.2.3 Progressive waves in water of variable depth

Consider temporally periodic, long-crested, progressive waves in water of variable depth. There are a number of factors contributing to a modification of these waves as they propagate. A change in depth causes changes in phase speed and wavelength and in the velocity of energy transfer (i.e., the ratio of energy transfer per unit time to energy density), which in turn give rise to variations in amplitude. Refraction occurs if the phase velocity varies along the wave crests. This causes a variation of the separation between orthogonals to the wave crests, which leads to additional changes in wave amplitude, since the average energy flux is directed along the orthogonals. The variability of the amplitude in turn affects the phase speed and the energy transfer [26,27]. However, these effects are very weak in gradual refraction. They are important only if there are other factors involved, such as the occurrence of caustics, or the presence of obstacles about which the waves diffract. Since such circumstances will not be considered here, we shall neglect the effects of the amplitude variations on the wave propagation. This is tantamount to considering the waves to be locally homogeneous. In other words, the local wave parameters are assumed to be interrelated by the equations (3.2.11) through (3.2.24). The problem is hereby reduced to the geometrical-optics problem of determining the ray paths in an inhomogeneous medium in which the velocity of propagation is known, and to the calculation of the amplitudes from a simple energy balance. We will in the following give a brief summary of this approach.

The water surface elevation is written as

$$\zeta(x,y,t) = a(x,y)\ \cos\{\omega t - \psi(x,y)\} \quad . \qquad (3.2.25)$$

The local wave-number vector is $\nabla\psi$. On the basis of the above mentioned assumptions we have

$$|\nabla\psi(x,y)| = k(x,y) \quad , \qquad (3.2.26)$$

where k(x,y) is the positive real root of

$$\omega^2 = gk(x,y)\ \tanh\{k(x,y)d(x,y)\} \quad . \tag{3.2.27}$$

Eq. (3.2.26) is the two-dimensional eiconal equation of geometrical optics. It is a nonlinear first-order partial differential equation. If ψ and $\nabla\psi$ are given at some point (x,y) then there is a uniquely determined curve (a characteristic) in the x-y-ψ space passing through the point (x,y,ψ), along which the values of $\nabla\psi$ are determined in accordance with (3.2.26). The projection of the characteristic on the x-y plane is a wave ray or orthogonal. The differential equations for the ray, the characteristic curve and for $\nabla\psi$ are

$$\frac{ds}{k} = \frac{dx}{\psi_{,x}} = \frac{dy}{\psi_{,y}} = \frac{d\psi}{k^2} = \frac{d\psi_{,x}}{kk_{,x}} = \frac{d\psi_{,y}}{kk_{,y}} \quad , \tag{3.2.28}$$

in which $\psi_{,x} \equiv \frac{\partial\psi}{\partial x}$, etc., and s is a coordinate along the ray [28]. The family of characteristics passing through the points on a curve along which ψ and $\nabla\psi$ are given generates a solution surface, provided the given curve is not itself a characteristic.

Once a solution of ψ has been determined in a given problem, the amplitudes can be calculated from the time-averaged energy balance

$$\nabla\cdot\vec{P} + \varepsilon_t = 0 \quad , \tag{3.2.29}$$

in which ε_t is the mean dissipation of energy per unit area per unit time. It depends on the local values of the wave amplitude, water depth, bottom roughness etc., as well as on some constant parameters such as the wave frequency and the viscosity.

By applying Gauss'divergence theorem, (3.2.29) can be transformed into

$$\frac{\partial(P\delta b)}{\partial s} + \varepsilon_t\delta b = 0 \quad , \tag{3.2.30}$$

in which $P = |\vec{P}|$ and $\delta b(s)$ is the perpendicular distance between two ad-

jacent wave rays. This equation can be solved for P by finite difference methods if the dependence of ε_t on the local wave properties is specified. If a turbulent boundary layer develops at the bottom then it can be assumed that the rate of energy dissipation in this layer, denoted by ε_f, can be written as

$$\varepsilon_f = C_f \rho \overline{|\nabla\psi|_B^3} = \frac{4}{3\pi} C_f \rho \left(\frac{\omega a}{\sinh kd}\right)^3 \quad , \tag{3.2.31}$$

in which C_f is a coefficient which is of order 10^{-2} [29], and the index B refers to the value of the indexed variable at the bottom. Outside the surf zone we can usually neglect the other contributions to the energy dissipation, in which case $\varepsilon_t \approx \varepsilon_f$.

If the energy dissipation can be totally neglected then (3.2.30) reduces to

$$\frac{\partial(P\delta b)}{\partial s} = 0 \quad , \tag{3.2.32}$$

which gives

$$\frac{a_2}{a_1} = \left(\frac{n_1 c_1 \delta b_1}{n_2 c_2 \delta b_2}\right)^{\frac{1}{2}} \quad , \tag{3.2.33}$$

where the indices 1 and 2 refer to the values of the variables at two different positions along the ray. The parameter $(n_1 c_1 / n_2 c_2)^{\frac{1}{2}}$ is a so-called shoaling coefficient; it expresses the effects on the amplitude brought about by changes in depth. Similarly, the parameter $(\delta b_1 / \delta b_2)^{\frac{1}{2}}$ is referred to as a refraction coefficient.

The preceding equations are simplified if the depth contours are straight and parallel, say in the y-direction, and if the time-mean properties of the incident waves are independent of y. In that case the time-independent and the time-mean wave properties everywhere are independent of y. In particular,

$$\frac{\partial k_x}{\partial y} = 0 \quad \text{and} \quad \frac{\partial k_y}{\partial y} = 0 \quad . \tag{3.2.34}$$

But

$$\frac{\partial k_x}{\partial y} = \frac{\partial k_y}{\partial x} \tag{3.2.35}$$

since $\vec{k} = \nabla\psi$. Thus k_y is a constant. Introducing the direction of propagation with respect to the x-axis, θ, we have

$$k_y = k \sin\theta = \text{constant} \quad , \tag{3.2.36}$$

or, since ω is constant,

$$\frac{\sin\theta}{\omega/k} = \frac{\sin\theta}{c} = \text{constant} \quad , \tag{3.2.37}$$

which is Snell's law.

The energy balance (3.2.29) reduces to

$$\frac{dP_x}{dx} + \varepsilon_t = 0 \quad , \tag{3.2.38}$$

which for negligible energy dissipation becomes

$$\frac{dP_x}{dx} = \frac{d}{dx}(Enc \cos\theta) = 0 \tag{3.2.39}$$

or

$$\frac{H_2}{H_1} = \frac{a_2}{a_1} = \left(\frac{n_1 c_1 \cos\theta_1}{n_2 c_2 \cos\theta_2}\right)^{\frac{1}{2}} \quad . \tag{3.2.40}$$

The ratio $\cos\theta_1/\cos\theta_2$ is equal to $\delta b_1/\delta b_2$ in the situation considered here, i.e. straight, parallel depth contours. It therefore equals the square of the refraction coefficient from point 1 to point 2.

3.3 Equations of motion for a weak current in the presence of waves

3.3.1 Introduction

In this section we hall be dealing with situations in which the bottom slope is small, and where gradually varying progressive waves are superimposed on a weak, nearly horizontal mean flow. Most of what follows in the paragraphs 3.3.1 through 3.3.4 has been adapted from Phillips [30].

Both the waves and the mean flow are permitted to vary horizontally and in time on a length-scale and a time-scale which are large compared with a typical wavelength and wave period. The local conservation equations can then be averaged over a time interval which is large compared with a typical wave period, but which is short in relation to the time scale of the gradual variations. Averages to be used in the following will be so defined, and be indicated by an overbar. Fluctuations about these averages will be denoted by a prime. The slow variation horizontally permits us to consider the waves locally as if they were horizontally homogeneous. The restriction to weak, nearly horizontal mean flows allows us to deal with these flows only in a vertically-averaged sense, and to ignore their effects on the waves.

We shall continually have to distinguish the horizontal motion from the vertical one. It is therefore convenient to introduce separate notations for the horizontal coordinates, the horizontal velocities, and so on. We will use the Cartesian tensor notation for these variables, with x_i representing the horizontal coordinates and q_i the horizontal velocities ($i=1,2$). The total velocity vector is therefore $\vec{u} = (\vec{q},w)$. The mean elevation of the free surface above the plane $z = 0$, $\bar{\zeta}$, was constant and equal to zero in the preceding section. It must now be permitted to vary because of the variation of all the mean flow properties. The equation of the bottom is $z = -d(x_1,x_2)$. The instantaneous depth therefore is $d + \zeta$; its mean value $d + \bar{\zeta}$ is written as D.

In the following paragraphs conservation equations will be given for a fixed control volume. The instantaneous equations will in general be presented first, after which time-mean values will be taken. These

should be separated into the contributions of the mean current and those of the unsteady flow, since the calculations are aimed at the effects of the waves on the mean current. Before such separation can be carried out the terms of both categories should be properly defined. For fixed points which are always submerged the velocity of the mean current is simply defined as $\overline{q}_i$. However, this definition is not suitable for points which are submerged only part of the time, i.e. for points at an elevation between the wave troughs and the wave crests. This can be most easily seen for waves propagating in one direction, say the x_1-direction, and for which $\overline{q}_i = 0$ in all points below the wave troughs. It is justified to say that in this situation there is no mean horizontal current. Yet the time-mean horizontal velocity in fixed points between the troughs and the crests is then not zero, for, considering a point above the mean water level, q_1 is either positive (if the point is submerged) or zero (if the water level drops below it). These non-zero mean velocities should in this case be wholly ascribed to the wave motion. They can be seen to arise as a consequence of the positive correlation between ζ' and q_i'. The result is a net wave-induced mass transport, which, in the Eulerian frame which has been adopted, is wholly confined to the region between the wave crests and the wave troughs. The situation is slightly more complex if $\overline{q}_i \neq 0$ below the troughs, for in that case the mean current also contributes to $\overline{q}_i$ above the troughs. The mean current velocity in this region can then by definition be determined from an extrapolation from below.

It is assumed in the following that only the organized wave motions contribute significantly to the unsteady velocity field, which can then be expressed in terms of the external wave parameters. This is in contrast to cases in which turbulence is relatively important. Such cases are not considered here.

3.3.2 Conservation of mass

Consider a control volume of unit horizontal area, extending vertically from the bottom to a height above the free surface. The

equation expressing the balance of mass for this control volume reads

$$\frac{\partial}{\partial t} \int_{-d}^{\zeta} \rho \, dz + \frac{\partial}{\partial x_i} \int_{-d}^{\zeta} \rho \, q_i \, dz = 0 \quad , \qquad (3.3.1)$$

or, after averaging,

$$\frac{\partial \rho D}{\partial t} + \frac{\partial M_i}{\partial x_i} = 0 \quad , \qquad (3.3.2)$$

in which M_i is the time-mean mass flux per unit width:

$$M_i = \overline{\int_{-d}^{\zeta} \rho q_i \, dz} \quad . \qquad (3.3.3)$$

M_i consists of a part due to the mean current, designated by a superscript "c" and defined by

$$M_i^c = \int_{-d}^{\overline{\zeta}} \rho \overline{q_i} \, dz = \rho D \tilde{U}_i \quad , \qquad (3.3.4)$$

in which $\tilde{U}_i$ is the vertically-averaged mean current velocity, and a part due to the waves, designated by a superscript "w" and defined by

$$M_i^w = \overline{\int_{-d}^{\zeta} \rho q_i' \, dz} = \overline{\int_{\overline{\zeta}}^{\zeta} \rho q_i' \, dz} \quad . \qquad (3.3.5)$$

3.3.3 Conservation of vertical momentum

Consider a control volume with unit horizontal area, extending vertically from an arbitrary level between the bottom and the free surface to a level above this surface. The balance of vertical momentum for this control volume is, neglecting stresses due to molecular viscosity,

$$\frac{\partial}{\partial t} \int_{z}^{\zeta} \rho w \, dz^* + \frac{\partial}{\partial x_i} \int_{z}^{\zeta} \rho q_i w \, dz^* - \rho w(z)^2 - p(z) + \rho g(\zeta - z) = 0 \quad . \qquad (3.3.6)$$

Taking the time-mean value gives

$$\frac{\partial}{\partial t}\int_z^{\zeta} \rho w \, dz^* + \frac{\partial}{\partial x_i}\int_z^{\zeta} \rho q_i \, w \, dz^* - \overline{\rho w(z)^2} - \overline{p(z)} + \rho g(\bar{\zeta} - z) = 0 \quad . \tag{3.3.7}$$

We have restricted ourselves to nearly horizontal, slowly varying mean flows. This implies that the first term of (3.3.7) can be neglected. The second term vanishes identically in a wave field which is horizontally homogeneous; the restriction to gradually varying progressive waves permits this term to be neglected. Reference is made to Dorrestein [31], who shows that in typical cases of waves on beaches the errors involved in these approximations are quite small. Eq. (3.3.7) then reduces to

$$\overline{p(z)} = \rho g(\bar{\zeta} - z) - \overline{\rho w(z)^2} \quad , \tag{3.3.8}$$

which shows that the mean pressure is less than the hydrostatic value by an amount $\rho w(z)^2$ [31]. At a rigid horizontal bottom the vertical velocity vanishes, in which case

$$\bar{p}_B = \rho g(\bar{\zeta} + d) = \rho g D \quad . \tag{3.3.9}$$

The index B refers to the value of the indexed variable at $z = -d$. At gently sloping bottoms w^2 is quite small, being only of the order of the bottom slope squared times a second-order quantity, and any effects which it may have on $\bar{p}_B$ will be neglected.

3.3.4 Conservation of horizontal momentum

Consider a control volume of unit horizontal area, extending vertically from the bottom to a height above the free surface. The balance of horizontal momentum for this control volume is, neglecting lateral shear stresses,

$$\frac{\partial}{\partial t}\int_{-d}^{\zeta}\rho q_i\,dz + \frac{\partial}{\partial x_j}\int_{-d}^{\zeta}(\rho q_i q_j + p\,\delta_{ij})dz + \tau_i - p_B\frac{\partial d}{\partial x_i} = 0 \quad , \tag{3.3.10}$$

in which δ_{ij} is the Kronecker delta, defined by

$$\begin{aligned}\delta_{ij} &= 1 \text{ if } i = j \\ &= 0 \text{ if } i \neq j \quad ,\end{aligned} \tag{3.3.11}$$

and τ_i is the horizontal component of the shear force per unit horizontal area exerted by the water on the bottom, which for gently sloping bottoms is very nearly equal to the tangential stress at the bottom. Taking the average of (3.3.10) and substituting (3.3.3) and (3.3.9) gives

$$\frac{\partial M_i}{\partial t} + \frac{\partial}{\partial x_j}\overline{\int_{-d}^{\zeta}(\rho q_i q_j + p\,\delta_{ij})dz} + \overline{\tau}_i - \rho g D\frac{\partial d}{\partial x_i} = 0 \quad . \tag{3.3.12}$$

This equation will be transformed into a momentum balance for a mean flow with depth D and mass flux M_i; these quantities define a mean velocity U_i as

$$U_i = \frac{M_i}{\rho D} = \frac{M_i^c + M_i^w}{\rho D} = \hat{U}_i + \frac{M_i^w}{\rho D} \quad . \tag{3.3.13}$$

This parameter should be distinguished from $\hat{U}_i$, which is the vertically-averaged mean current velocity, and also from the time-mean value of the instantaneous vertically-averaged horizontal velocity.

The contributions of the mean value and of the fluctuations of the horizontal velocity to the integral in (3.3.12) are separated as follows:

$$\overline{\int_{-d}^{\zeta}\rho q_i q_j\,dz} = \int_{-d}^{\zeta}\rho(\overline{q}_i\overline{q}_j + \overline{q}_i q_j' + q_i'\overline{q}_j + q_i' q_j')\,dz$$

$$\approx \rho D \tilde{U}_i \tilde{U}_j + \tilde{U}_i M_j^w + M_i^w \tilde{U}_j + \overline{\int_{-d}^{\zeta} \rho q_i' q_j' \, dz}$$

$$= U_j M_i - \frac{M_i^w M_j^w}{\rho D} + \overline{\int_{-d}^{\zeta} q_i' q_j' \, dz} \quad . \tag{3.3.14}$$

The last term in (3.3.12) can be rewritten as

$$\rho g D \frac{\partial d}{\partial x_i} = \frac{\partial}{\partial x_i} \left(\tfrac{1}{2} \rho g D^2 \right) - \rho g D \frac{\partial \bar{\zeta}}{\partial x_i} \quad . \tag{3.3.15}$$

Substitution of (3.3.14) and (3.3.15) into (3.3.12) gives the momentum balance for the mean flow in the form

$$\frac{\partial M_i}{\partial t} + \frac{\partial}{\partial x_j} (U_j M_i + S_{ij}) + \bar{\tau}_i + \rho g D \frac{\partial \bar{\zeta}}{\partial x_i} = 0 \quad , \tag{3.3.16}$$

in which the quantity S_{ij}, defined by

$$S_{ij} = \int_{-d}^{\zeta} (\rho q_i' q_j' + p \delta_{ij}) dz - \tfrac{1}{2} \rho g D^2 \delta_{ij} - \frac{M_i^w M_j^w}{\rho D} \quad , \tag{3.3.17}$$

represents the contribution of the unsteady flow to the mean horizontal flux of horizontal momentum. It appears as a stress (force per unit length) in the vertically integrated equation of motion of the mean flow. It has already been pointed out that the contribution of the turbulence to S_{ij} will be neglected. The contribution of the waves to S_{ij} has been called "radiation stress" by Longuet-Higgins and Stewart who developed the concept and gave many of its applications [4,18,32-35]. It has been introduced independently by Dorrestein [36] and Ludgren [37]; these authors deal with two-dimensional motion only.

An expression for the radiation stresses in progressive waves to the second order of approximation can be given as follows [34]. The wave momentum M_i^w is of second order, so that $M_i^w M_j^w / (\rho D)$ need not be taken into account. The integral in (3.3.17) can be divided into four parts:

$$\int_{-d}^{\overline{\zeta}} \rho \overline{q_i' q_j'} \, dz + \overline{\int_{\overline{\zeta}}^{\zeta} \rho q_i' q_j' \, dz} + \int_{-d}^{\overline{\zeta}} \overline{p} \, \delta_{ij} \, dz + \overline{\int_{\overline{\zeta}}^{\zeta} p \, \delta_{ij} \, dz} \quad . \tag{3.3.18}$$

The second and fourth integral in (3.3.18) have an interval of integration equal to $\zeta - \overline{\zeta} = \zeta'$, which is of first order in the wave amplitude. The second integral can therefore be neglected, since the integrand is of second order, while the fourth can be evaluated to second order by using a hydrostatic pressure distribution on the interval of integration. Eq. (3.3.8) for the mean pressure is substituted in the third integral in (3.3.18). (The validity of the result is thereby restricted to quasi-steady and quasi-homogeneous waves, for which (3.3.8) is applicable.) Eq. (3.3.17) then becomes

$$S_{ij} = \int_{-d}^{\overline{\zeta}} \rho (\overline{q_i' q_j'} - \overline{w^2} \, \delta_{ij}) dz + \tfrac{1}{2} \rho g \overline{\zeta'^2} \, \delta_{ij} \quad . \tag{3.3.19}$$

The quantities q_i', w and ζ', which are of first order, appear in (3.3.19) in product form only. It is therefore sufficient to use the respective first-order approximations for these variables for the evaluation of S_{ij} to the second order of approximation. We shall give the result for a long-crested, progressive sinusoidal wave, to which the equations (3.2.11) through (3.2.24) are applicable, provided the still-water depth d used in these equations is replaced by the mean water depth $D = d + \overline{\zeta}$. Substitution of (3.2.12), (3.2.16) and (3.2.17) into (3.3.19) and integration gives

$$S_{ij} = \{ n e_i e_j + (n - \tfrac{1}{2}) \delta_{ij} \} E \quad , \tag{3.3.20}$$

in which n is given by (3.2.23). If the direction of propagation with respect to the x_1-axis is θ then

$$S_{11} = (n \cos^2 \theta + n - \tfrac{1}{2}) E \quad , \tag{3.3.21}$$

$$S_{12} = S_{21} = (n \sin \theta \cos \theta) E \quad , \tag{3.3.22}$$

and

$$S_{22} = (n \sin^2\theta + n - \tfrac{1}{2})E \quad . \tag{3.3.23}$$

The largest principal stress, which has a magnitude of $(2n - \frac{1}{2})E$, acts across a plane perpendicular to the direction of propagation. The smallest principal stress has a magnitude of $(n - \frac{1}{2})E$ and acts across a plane perpendicular to the wave crests.

3.3.5 Steady, irrotational mean flow

If the flow is irrotational and steady (after averaging over the waves, as described in paragraph 3.3.1) then (3.3.2) and (3.3.16) reduce to

$$\frac{\partial M_i}{\partial x_i} = 0 \tag{3.3.24}$$

and

$$\frac{\partial}{\partial x_j}(U_j M_i) + \frac{\partial}{\partial x_j} S_{ij} + \rho g D \frac{\partial \bar{\zeta}}{\partial x_i} = 0 \quad . \tag{3.3.25}$$

For the waves to drive a mean current, there should be an imbalance between the divergence of the radiation stresses on the one hand, and the horizontal pressure gradient associated with the wave-induced changes in mean water level (wave set-up) on the other hand. However, such imbalance is impossible in steady irrotational flows, as has been pointed out by Bowen [38], who notes that a second-order interaction of two sets of waves in a conservative field produces an effect equivalent to a fluctuating pressure field at the surface [33], and that the radiation stress in periodic waves is the steady component of the second-order self-interaction of the waves. Thus, a steady distribution of radiation stress in irrotational waves is equivalent to a steady distribution of normal pressures at the water surface, and should give rise to (spatial) variations in the surface elevation only, without driving a mean current. The same conclusion is given by

Longuet-Higgins [22], who states "if there were no dissipation at all, there would be no current. This is as we might expect, since without dissipation it is impossible to generate vorticity in a fluid initially irrotational; and without vorticity we expect no current*, since the fluid at infinity is at rest. ..... Thus, even if the wave amplitude were to vary in an arbitrary manner along the coastline, due perhaps to refraction by uneven bottom contours, still no currents would be generated unless there were some dissipation by breaking; the stress gradients would simply be balanced by a wave set-up or set-down. A special case of this general result was discovered by Bowen (1969), but it is possible also to give a general proof." Longuet-Higgins refers for this proof to some of his unpublished lecture notes. From a logical point of view it is of course not necessary to give a proof in addition to the arguments just quoted. But it may nevertheless be instructive to give a proof expressed explicitly in terms of the equations of motion. This will be done in the following, based on the geometrical-optics approximation of irrotational waves in water of gradually varying depth. It is not known to the author whether this is of the same generality as the unpublised proof referred to by Longuet-Higgins. However, before presenting our proof we should first complete the quotation given above. At the point marked * the following footnote is added [22]: "This expectation derives from a neglect of the Stokes velocity, which however is negligible for all but extremely small beach slopes (see Longuet-Higgins 1970b, Appendix 2)." The reference given in this footnote is Longuet-Higgins' paper on longshore currents [39], in which it is shown that the ratio of the longshore component of the wave-induced Lagrangian mass transport velocity to the velocity of the wave-driven longshore current in the surf zone is negligible for ordinary beach slopes. Although this is true it does not, in the author's opinion, warrant the neglect of the Stokes velocity (i.e., the wave-induced Lagrangian mean velocity) in the present context, for it concerns a ratio of two velocities in a situation in which dissipation occurs, and in which the waves drive a rotational mean current. The magnitude of this ratio does not appear to be relevant to the question of the

negligibility of the Stokes velocity in the framework of non-dissipative, irrotational flows. And within this framework it would be inconsistent to neglect the Stokes velocity in relation to the wave-driven mean current velocity, since the latter is expected to be zero. It is therefore preferred to say only that in steady, irrotational flow the waves do not drive a mean current as defined in paragraph 3.3.1, i.e. a mean Eulerian velocity field which is non-zero below the wave troughs.

We shall now present a proof of the following equality:

$$\frac{\partial}{\partial x_j} S_{ij} + \rho g D \frac{\partial \overline{\zeta}}{\partial x_i} = 0 \quad . \tag{3.3.26}$$

This proof will not be given for completely arbitrary irrotational gravity waves, but only for the kind of waves considered in this thesis, i.e. progressive waves of gradually varying amplitude and wavelength in water of gradually varying depth, in which horizontal inhomogeneities of the average properties have a negligible influence on the local wave dynamics. In other words, the geometrical-optics approximations are used. Let the water surface elevation above its mean value be given, to first order, by

$$\zeta'(x_1,x_2,t) = a(x_1,x_2) \cos \{\omega t - \psi(x_1,x_2)\} . \tag{3.3.27}$$

Locally the equations (3.2.11) through (3.2.24) hold, provided d is replaced by D, while

$$|\nabla\psi| \equiv (\frac{\partial \psi}{\partial x_i} \frac{\partial \psi}{\partial x_i})^{\frac{1}{2}} = k \quad , \tag{3.3.28}$$

(see eq. 3.2.26), so that

$$e_i \equiv |\nabla\psi|^{-1} \frac{\partial \psi}{\partial x_i} = k^{-1} \frac{\partial \psi}{\partial x_i} \quad . \tag{3.3.29}$$

The local radiation stresses are given by (3.3.20), i.e. by

$$S_{ij} = n\,E\,e_i e_j + (n - \tfrac{1}{2})E\,\delta_{ij} \quad . \tag{3.3.30}$$

The elevation of the mean water level above the undisturbed value, $\overline{\zeta}$, still needs to be defined independently of (3.3.26). It can be expressed directly in terms of local flow parameters by means of the Bernoulli equation for unsteady flow, eq. (3.2.5). Longuet-Higgins and Stewart [35] take the average of this equation at the elevation $z = 0$, and supplement this with the time-averaged balance of vertical momentum between $z = 0$ and $z = \zeta$, to arrive at the result

$$\overline{\zeta} = \text{const} - \frac{1}{2g}\,(\overline{q^2} - \overline{w^2})_{z\,=\,0} \quad , \tag{3.3.31}$$

in which q is the magnitude of the horizontal velocity vector. This result follows also from Bernoulli's equation by taking its average value at $z = \zeta$, taking account of the fact that the mean value of $\frac{\partial \phi}{\partial t}$ at the variable elevation $z = \zeta(t)$ is not zero, even in periodic waves, but is given, to second order, by

$$\overline{\left.\frac{\partial \phi}{\partial t}\right|_{z\,=\,\overline{\zeta}\,+\,\zeta'}} \approx \overline{\left.\frac{\partial \phi}{\partial t}\right|_{z\,=\,\overline{\zeta}} + \zeta' \frac{\partial}{\partial z}\frac{\partial \phi}{\partial t}\Big|_{z\,=\,\overline{\zeta}}} = \overline{\zeta' \frac{\partial}{\partial t}\frac{\partial \phi}{\partial z}\Big|_{z\,=\,\overline{\zeta}}} \approx \overline{\zeta' \frac{\partial}{\partial t}\frac{\partial \zeta'}{\partial t}}$$

$$= \overline{\frac{\partial}{\partial t}\left(\zeta' \frac{\partial \zeta'}{\partial t}\right) - \left(\frac{\partial \zeta'}{\partial t}\right)^2} = -\overline{\left(\frac{\partial \zeta'}{\partial t}\right)^2} \approx -\left.\overline{w^2}\right|_{z\,=\,\overline{\zeta}} \approx -\left.\overline{w^2}\right|_{z\,=\,0} \quad . \tag{3.3.32}$$

Substitution of (3.2.16), (3.2.17) and (3.2.14) into (3.3.31) gives

$$\overline{\zeta} = -\frac{ka^2}{2\sinh 2kD} \quad , \tag{3.3.33}$$

where $\overline{\zeta}$ has been chosen to be zero in deep water. Eq. (3.3.33) is due to Longuet-Higgins and Stewart [34] and Lundgren [37].

From (3.3.29) and (3.3.30) we have

$$\frac{\partial}{\partial x_j} S_{ij} = \frac{\partial}{\partial x_j} (n\, k^{-2} E \frac{\partial \psi}{\partial x_i} \frac{\partial \psi}{\partial x_j}) + \frac{\partial}{\partial x_j} \{ (n - \tfrac{1}{2}) E \delta_{ij} \}$$

$$= \frac{\partial \psi}{\partial x_i} \{ \frac{\partial}{\partial x_j} (n\, k^{-2} E \frac{\partial \psi}{\partial x_j}) \} + n\, k^{-2} E \frac{\partial \psi}{\partial x_j} \frac{\partial}{\partial x_j} (\frac{\partial \psi}{\partial x_i}) + \frac{\partial}{\partial x_i} \{ (n - \tfrac{1}{2}) E \}. \qquad (3.3.34)$$

Utilizing (3.2.15), (3.2.22), (3.2.29) and (3.3.29), the first term in the right-hand side of (3.3.34) can be written as

$$\omega^{-1} k e_i \{ \frac{\partial}{\partial x_j} (n \frac{\omega}{k} E e_j) \} = \frac{e_i}{c} \frac{\partial P_j}{\partial x_j} = - \frac{\epsilon_t}{c} e_i \quad , \qquad (3.3.35)$$

in which ϵ_t is the power dissipated per unit area, which is zero on the present assumptions. The second term of the right-hand side of (3.3.34) can be written as

$$n\, k^{-2} E \frac{\partial \psi}{\partial x_j} \frac{\partial}{\partial x_i} (\frac{\partial \psi}{\partial x_j}) = \tfrac{1}{2} n\, k^{-2} \quad E \frac{\partial}{\partial x_i} (\frac{\partial \psi}{\partial x_j} \frac{\partial \psi}{\partial x_j}) =$$

$$= \tfrac{1}{2} n\, k^{-2} E \frac{\partial k^2}{\partial x_i} = n\, k^{-1} E \frac{\partial k}{\partial x_i} \quad , \qquad (3.3.36)$$

where use has been made of (3.3.28). Substitution of the dispersion equation (3.2.27) and of the definition of n given by (3.2.23) gives after some manipulations

$$n\, k^{-1} \frac{\partial k}{\partial x_i} = - \frac{k}{\sinh 2kD} \frac{\partial D}{\partial x_i} \quad . \qquad (3.3.37)$$

Finally, the factor $(n - \frac{1}{2})$ in the third term of the right-hand side of (3.3.34) equals kD/sinh 2kD, as can be seen from (3.2.23), so that

$$\frac{\partial}{\partial x_j} S_{ij} = - \frac{kE}{\sinh 2kD} \frac{\partial D}{\partial x_i} + \frac{\partial}{\partial x_i} \frac{kD\, E}{\sinh 2kD} = D \frac{\partial}{\partial x_i} \frac{kE}{\sinh 2kD} \qquad (3.3.38)$$

Substitution of $E = \frac{1}{2}\rho g a^2$ and of (3.3.33) gives

$$\frac{\partial}{\partial x_j} S_{ij} = D \frac{\partial}{\partial x_i} \frac{k \frac{1}{2}\rho g a^2}{\sinh 2k\bar{D}} = - \rho g D \frac{\partial \bar{\zeta}}{\partial x_i} \quad , \qquad (3.3.39)$$

which proves (3.3.26).

If the waves being considered approach a shore from deep water which is otherwise at rest, and if they break on a beach, then the flow is approximately irrotational and non-dissipative outside the surf-zone, and highly rotational and dissipative inside this zone. The wave-driven current is then confined to a relatively narrow region along the shore. The surf zone can be considered as a boundary layer bordering on the flow in deeper water. This similarity is more than superficial, for the mechanism generating a longshore current in the surf zone is in various respects similar to the mechanism generating a mass transport current in the bottom boundary layer under a progressive wave. In the latter case a boundary layer develops because of the no-slip condition at the bottom; in our situation the analogous condition is the vanishing of the wave height (thus, also the momentum flux) at the shore due to breaking. The mass transport current in the bottom boundary layer under a progressive wave arises as a consequence of an in-phase relationship between velocity components parallel and normal to the bottom, causing a net downward flux of horizontal momentum, equivalent to a net shear stress exerted by the waves on the bottom. The in-phase normal velocity components in turn are due to phase differences within the boundary layer in the longitudinal direction, which are a consequence of the progressive character of the waves. The analogy in our situation is given by the phase differences in the longshore direction, which exist if the waves come in obliquely. Associated herewith are velocity fluctuations in the direction parallel to the shore. These are in phase with the velocity fluctuations perpendicular to the shore, so that there is a net shoreward flux of longshore momentum: the radiation shear stress.

3.3.6 Steady, uniform mean flow

Consider the quasi-two-dimensional situation of an impermeable beach with straight depth contours, parallel to the x_2-axis (see fig. 3.1), and obliquely incident waves which are uniform in the

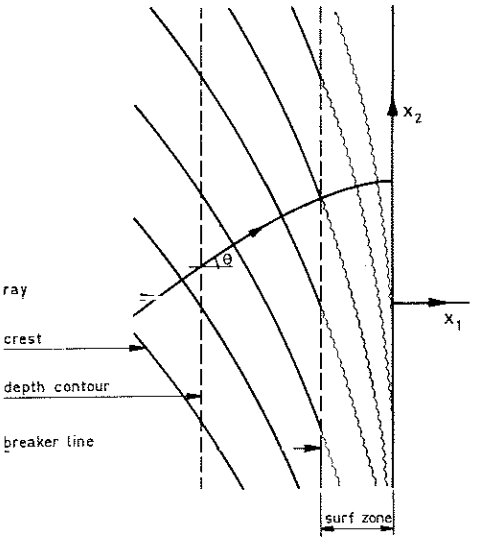

Fig. 3.1 - Plan view of beach (definition sketch)

x_2-direction, apart from phase differences. All time-independent or time-mean quantities are assumed to be independent of x_2. The mean mass balance (3.3.24) then reduces to

$$\frac{dM_1}{dx_1} = 0 \qquad (3.3.40)$$

or

$$M_1 = \text{constant} = 0 \quad , \qquad (3.3.41)$$

so that, in view of (3.3.13),

$$\hat{U}_1 = - \frac{M_1^W}{\rho D} \tag{3.3.42}$$

The momentum balance for the steady and uniform mean flow is obtained from (3.3.16) by equating the acceleration terms to zero. The bottom shear stress $\overline{\tau}_i$ is retained, and (3.3.26) is not used, since the flow is not assumed to be everywhere irrotational. It follows that

$$\frac{\partial}{\partial x_j} S_{ij} + \overline{\tau}_i + \rho g D \frac{\partial \overline{\zeta}}{\partial x_i} = 0 \quad . \tag{3.3.43}$$

This expresses a static balance between the driving force due to the divergence of the radiation stresses, the bottom friction, and the vertically integrated pressure gradient due to the mean tilt of the free surface. Writing the two components of (3.3.43) explicitly, and utilizing the fact that mean properties are independent of x_2, gives

$$\frac{dS_{11}}{dx_1} + \overline{\tau}_1 + \rho g D \frac{d\overline{\zeta}}{dx_1} = 0 \tag{3.3.44}$$

for the momentum balance in the x_1-direction, and

$$\frac{dS_{21}}{dx_1} + \overline{\tau}_2 = 0 \tag{3.3.45}$$

in the x_2-direction. According to (3.3.42) the mean current in the direction perpendicular to the shore only compensates for the wave-induced onshore mass flux. This means that it is weak relative to the oscillatory particle velocities. For this reason $\overline{\tau}_1$ will be neglected in (3.3.44), which then reduces to

$$\frac{dS_{11}}{dx_1} + \rho g D \frac{d\overline{\zeta}}{dx_1} = 0 \quad . \tag{3.3.46}$$

3.4 Set-up and longshore currents due to regular waves

The preceding equations have been used by various authors for

calculations of the set-up of the mean water level and the longshore current velocities induced by regular waves. Some results will be summarized here for future reference. The same situation is considered as in the previous paragraph, viz. a quasi-steady and quasi-two-dimensional flow, uniform in x_2 (see fig. 3.1). The waves are assumed to be periodic. The bottom slope is supposed to be small, so that the waves break on the beach with negligible reflection.

3.4.1 Set-up

Outside the surf zone the flow is considered to be irrotational; the wave-induced change in mean water level is then given by (3.3.33).

Inside the breaker zone the energy dissipation must be taken into account. A semi-empirical similarity approach to this problem was given by Longuet-Higgins and Stewart [34], who postulated that after breaking the wave height H would decay in constant proportion to the undisturbed depth. This was modified by Bowen et al [6] who assumed that H would be proportional to the mean total depth, including the effect of the set-up. They put

$$H = \gamma\ (d + \bar{\zeta}) = \gamma D \qquad (3.4.1)$$

in the breaker zone. This assumption is reasonable for spilling breakers, which propagate with relatively minor changes in shape. It is furthermore assumed that within the surf zone the shallow-water approximations to the wave equations apply. In particular, it is assumed that n = 1 (eq. 3.2.23), so that, for perpendicular incidence,

$$S_{11} = \frac{3}{2} E = \frac{3}{16} \rho g H^2 \quad , \qquad (3.4.2)$$

as follows from (3.3.21), or

$$S_{11} = \frac{3}{16} \rho g \gamma^2 (d + \bar{\zeta})^2 \quad . \qquad (3.4.3)$$

Substitution of this expression in (3.3.46) gives

$$\frac{d\bar{\zeta}}{dx_1} = - \frac{\frac{3}{8}\gamma^2}{1 + \frac{3}{8}\gamma^2} \frac{dd}{dx_1} \qquad (3.4.4)$$

[6]. It can be seen that there is a set-up in the surf zone, with a gradient proportional to the local bottom slope. Experiments by Bowen et al [6] have confirmed the validity of (3.3.33) and (3.4.4).

The total rise of the mean water level in the surf zone can be calculated by integrating (3.4.4) from the breakpoint to the point of maximum set-up. This gives

$$\bar{\zeta}_{max} - \bar{\zeta}_b = \frac{\frac{3}{8}\gamma^2}{1 + \frac{3}{8}\gamma^2} (\bar{\zeta}_{max} + d_b) \qquad (3.4.5)$$

or

$$\bar{\zeta}_{max} = \bar{\zeta}_b + \frac{3}{8}\gamma^2 D_b \quad , \qquad (3.4.6)$$

in which $\bar{\zeta}_b$ is the set-up at the breaker line, which is estimated from (3.3.33) as

$$\bar{\zeta}_b \approx - \frac{1}{4} \frac{a_b^2}{D_b} = - \frac{1}{16} \frac{H_b^2}{D_b} \quad . \qquad (3.4.7)$$

With the substitution of $H_b = \gamma D_b$ we find

$$\bar{\zeta}_{max} = \frac{5}{16} \gamma H_b \approx 0.3 \gamma H_b \quad . \qquad (3.4.8)$$

3.4.2 Longshore currents

A review of longshore current theories was given by Galvin in 1967 [40]. He correctly concluded that the theories then available were not in satisfactory agreement with experimental data. All of the theories developed until 1967 involve averaging over the width of the surfzone in a very early stage of the development. This not only leads to a loss of information regarding the velocity variation with

distance offshore, but it may also give erroneous results for the average velocity. Furthermore, some of the earlier theories include unknown coefficients introduced ad hoc. The theories involving a momentum balance generally assume a bottom friction proportional to the square of the longshore current velocity, independent of the oscillatory velocities due to the waves. More recent theories [39,41-43] have given improvements on these points. We shall deal with these theories only. Their purpose is the prediction of the vertically-averaged mean current velocity in the longshore direction, $\tilde{U}_2$. This will for brevity be called the longshore current velocity, denoted as V. The term "longshore current profile" shall refer to the variation of V with the distance offshore.

The driving force for the longshore current is supplied by the gradient of the radiation shear stress. This is given by

$$\frac{dS_{12}}{dx_1} = \frac{d}{dx_1}(E\, n \sin\theta \cos\theta) = \frac{\sin\theta}{c}\frac{dP_1}{dx_1} = -\frac{\sin\theta_0}{c_0}\varepsilon_t \quad , \quad (3.4.9)$$

where use has been made of Snell's law and of the energy balance (3.2.29) with $\frac{\partial P_2}{\partial x_2} = 0$ [39]. ε_t is the mean rate of energy dissipation per unit area, which will be set equal to zero outside the surfzone. If follows that in this approximation the longshore thrust exerted by the incident waves across vertical planes parallel to the depth contours is independent of the distance offshore, and therefore equal to the value which it has in deep water. This result was first proved by Bowen [41], in the manner just described. (It follows also directly from (3.3.26), equating the x_2-derivatives to zero.)

Inside the surf zone the approximation (3.4.1) for the wave height is assumed to hold. Furthermore, breaking generally takes place in shallow water, so that $c \overset{\sim}{\sim} (gD)^{\frac{1}{2}}$, $n \overset{\sim}{\sim} 1$ and $\cos\theta \overset{\sim}{\sim} 1$. With these approximations, (3.4.9) becomes

$$\frac{dS_{12}}{dx_1} = \frac{\sin\theta_0}{c_0}\frac{d}{dx_1}\left(\frac{1}{8}\rho g \gamma^2 D^2 \sqrt{gD}\right) = -\frac{5}{16}\gamma^2 m_D \rho (gD)^{3/2}\frac{\sin\theta_0}{c_0} \quad , \quad (3.4.10)$$

in which m_D is the mean-depth gradient,

$$m_D = - \frac{dD}{dx_1} = - \frac{d(d + \bar{\zeta})}{dx_1} \quad , \tag{3.4.11}$$

which can be expressed in terms of the bottom slope by means of (3.4.4).

The longshore current was assumed to be unaccelerated. Thus, there should be a balance between driving forces and resistive forces. In the simplest form of the theory the shear stress at the bottom is the only resistance, as in (3.3.45). More refined models take lateral shear stresses into account, due to turbulent exchange of horizontal momentum, which is generally assumed to be expressible as a gradient-type diffusion. These two types of resistive forces play very different rôles in the dynamics of the littoral zone. This can be seen most easily from the momentum balance of the whole nearshore water mass between the waterline and a point seaward of the surf zone, where the turbulent momentum exchange is negligible. The longshore thrust exerted by the incident waves on this mass must in the steady, uniform flow regime be balanced by the integrated longshore bottom shear stress $\int \bar{\tau}_2 \, dx_1$. The internal shear stresses do not appear in this overall balance. The order of magnitude of the longshore current velocity is therefore mainly determined by the longshore bottom shear stress, while the lateral stresses only redistribute this velocity in the direction normal to the shore. Their effects will at first be neglected. The mean bottom stress can then be determined from (3.3.45). It should next be expressed in terms of V.

Bowen [41] assumes $\bar{\tau}_2$ to be proportional to V, with a coefficient of proportionality which is constant in the surf zone. This assumption does not seem to be justifiable inasmuch as the flow in the bottom boundary layer is ordinarily turbulent, due to the relatively strong wave-induced oscillatory velocities. This has been taken into account by Thornton [42], and shortly after him, though apparently independently, by Longuet-Higgins [39] and Bakker [43]. These authors use a quadratic relationship between the instantaneous shear stress and the instantaneous velocity outside the bottom boundary layer. The time-

mean value of the longshore shear stress can then be written as

$$\bar{\tau}_2 = C_f \, \rho \overline{q_2 \, |\vec{q}|} \quad . \tag{3.4.12}$$

The longshore current velocity is generally small compared with the maximum oscillatory particle velocity, and is directed roughly perpendicular to it. This means that the absolute magnitude of the resultant velocity in a first approximation can be equated to the oscillatory particle velocity. Assuming a sinusoidal variation of this velocity in time, with an amplitude $\hat{q}'$, gives

$$\bar{\tau}_2 \approx C_f \, \rho \, \overline{(\bar{q}_2 + \hat{q}_2' \sin \omega t) \, | \, \hat{q}' \sin \omega t \, |} = \frac{2}{\pi} C_f \, \rho \hat{q}' \, \bar{q}_2 \quad , \tag{3.4.13}$$

in which, in shallow water,

$$\hat{q}' = \frac{\omega a}{\sinh kD} \approx \frac{\omega a}{kD} = \tfrac{1}{2} \frac{H}{D} \, c \approx \tfrac{1}{2} \gamma \sqrt{gD} \quad , \tag{3.4.14}$$

as follows from (3.2.16). Thornton and Longuet-Higgins implicitly include the coefficient of proportionality between $\bar{q}_2$ and the vertically-averaged mean velocity V in the coefficient C_f, which gives

$$\bar{\tau}_2 = \frac{2}{\pi} C_f \, \rho \hat{q}' \, V \quad . \tag{3.4.15}$$

Thornton uses a semi-empirical expression for C_f in terms of bottom roughness and total particle excursion, obtained by Jonsson [44] for a wave boundary layer with zero mean flow, in the presence of artificial roughness. Thornton's procedure can be seen to imply that Jonsson's results still hold even in the case of a superimposed mean flow, and that the value of $\bar{q}_2$ just outside the (relatively thin) wave boundary layer is equal to the vertically-averaged mean flow velocity V. Longuet-Higgins bases his estimate of C_f on empirical data for steady, unidirectional flow past a flat plate of finite length. The finite length of the plate limits the boundary layer growth, just as the finite duration of flow-in-one-direction does under oscillatory waves. The plate length can

then be compared to the total particle excursion just outside the boundary layer. Bakker arrives at (3.4.15), and at an expression for C_f, on the basis of Bijker's results concerning the mean bottom shear stress due to a combination of waves and current [45], by considering the limiting case of a relatively weak current perpendicular to the direction of wave propagation. This limiting case is in itself appropriate in the present problem, but it is not consistent with the assumptions originally made by Bijker in his derivations, which in effect imply a relatively strong current. This is reflected in Bakker's result, according to which C_f would be determined by the ratio of bottom roughness to mean water depth. The latter is not a relevant parameter for the boundary layer flow if this is mainly governed by the oscillatory wave motion. However, in a more recent publication [46] Bakker calculates the turbulent shear stress in the wave boundary layer and arrives at results comparable to Jonsson's.

Because of the uncertainties in the values predicted by either of the methods described, it is preferred not to assign a priori values to C_f, but to deal with it as a coefficient to be determined empirically. An analysis of available data by Longuet-Higgins [39] indicates that its order of magnitude should be 0.01. This agrees with empirical results obtained by Bretschneider and Reid [29] from measurements involving wave energy dissipation, referred to in par. 3.2.3.

It may be of interest to point out that a formula similar to (3.4.15) has already been given in 1927 by Mazure [47] in an analysis of tidal motion in the presence of a net (river) discharge. In this case the current is directed against the direction of wave propagation, rather than perpendicular to it. The change in absolute magnitude of the instantaneous total velocity is then of first order in the mean velocity, which gives a factor $4/\pi$ instead of $2/\pi$ in the right-hand side of (3.4.15). The same result has been given by Bowden [48]. The equation for the mean bottom shear stress so obtained is used in the prediction of storm surges at sea [49].

Substitution of (3.4.10), (3.4.14) and (3.4.15) into (3.3.45)

gives the following result for the longshore current velocity inside the surfzone:

$$V = \frac{5\pi}{16} \frac{\gamma^m D}{C_f} \frac{\sin \theta_0}{c_0} gD \quad , \tag{3.4.16}$$

or, equivalently,

$$V = \frac{5\pi}{16} \frac{\gamma^m D}{C_f} \sin \theta_b \sqrt{\frac{g}{D_b}} D \quad . \tag{3.4.17}$$

This equation has been given, in essentially the form shown here, by Thornton, Longuet-Higgins and Bakker. Outside the surf zone the longshore current velocity is zero, to the present approximation. The total longshore current profile is shown graphically in fig. 3.2, for a beach with a constant bottom slope. The velocity at the theoretical

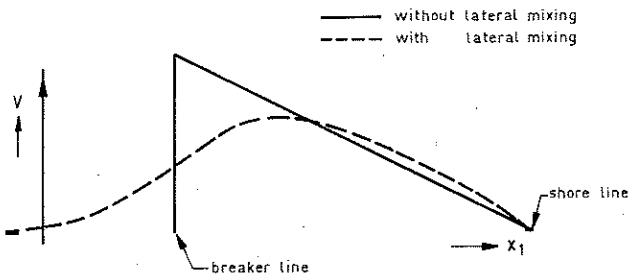

Fig. 3.2 - Calculated longshore current profiles due to periodic waves on a plane beach [39, 41 - 43].

breaker line is discontinuous, due to the fact that the wave energy dissipation was implicitly assumed to be discontinuous, and that lateral mixing was neglected. As noted previously, some form of lateral mixing can be taken into account [39, 41 - 42]. This will of course smoothen the calculated profile, particularly near the breaker line. However, it need not have much effect on the calculated values away from the breaker line, especially on beaches of gentle

slope, where the longshore current varies only slowly with distance offshore. It should also be remembered that the theoretical results mentioned here are for periodic waves only, and that the calculated discontinuity is ultimately due to the fact that all the waves are assumed to break at the same distance from the shore. This is obviously not the case for random waves, to be dealt with in the following chapters. The variability in breaker position of these waves gives rise to a smooth longshore current profile, quite apart from the effects of lateral friction due to turbulence. These effects should therefore be much less in random waves than in periodic waves.

4 PROBABILISTIC DESCRIPTION OF WIND WAVES

4.1 Introduction

Randomness is one of the characteristic properties of wind-generated water waves. Realistic descriptions of these waves should therefore be not just hydrodynamical in nature but probabilistic as well. In this chapter a summary will be given of methods and results which will be used for this purpose in the remaining chapters.

In section 4.2 elementary concepts from the theory of stochastic processes in one dimension will be introduced. Following this, the sea surface in the presence of wind waves will in section 4.3 be described as a Gaussian process in space and time. The statistical properties of wind waves at a fixed point are dealt with in section 4.4. Empirical data pertaining specifically to wind-driven waves are presented in section 4.5.

It may be noted that a distinction is made between wind-driven waves ("sea") and wind waves in general. The first term refers to those waves which are still acted upon by the wind field generating them. Their properties depend on the local wind field. The term wind waves refers to waves generated by wind, regardless of whether they are still wind-driven or have already to some extent transformed into swell, or whether they consist of a mixture of wind-driven waves and swell.

4.2 Stochastic processes in one dimension

4.2.1 General concepts

The purpose of this section is to introduce some concepts related to stochastic processes. Such processes can be considered at an abstract level, in which one deals with non-physical entities using deductive formalisms based on the axioms of probability theory [50,51], or from a more applied point of view, when one has to deal with physical realities having certain observable frequencies of

occurrence which are assumed to converge to limit values if the number of observations would be increased indefinitely [52, 53]. The supposed limits are equated to probabilities of the events being considered. Once the probabilities have been so assigned they can be used for deductive reasoning, using the methods of probability theory. We shall introduce various concepts which are of use for the description of stochastic processes from this applied point of view.

Consider a series of experiments in which a certain dependent (real) variable z varies with one independent variable, which for convenience will be taken to be the time. We shall assume that the values of z are affected by a large number of uncontrollable small factors which cannot be described in detail and which vary on repetition of the experiment. We thus obtain a series of different time functions ${}^{k}z(t)$, k = 1, 2, ..., which can be regarded as realizations of a stochastic process [52,53]. The infinite collection of time functions which are actually obtained, or which could conceivably have been obtained from repetitions of the experiment, is called the ensemble.

A description of the process should aim at the properties which are common to the various realizations, rather than at the erratic differences between them. These common properties can be found from ensemble-averages. For an arbitrary function h of the values of z at times t_i (i = 1,2, ...,n) the ensemble average is defined as

$$< h > = \lim_{N\to\infty} \frac{1}{N} \sum_{k=1}^{N} h \{{}^{k}z(t_1), \ldots\ldots\ldots, {}^{k}z(t_n)\} \quad . \qquad (4.2.1)$$

Of fundamental importance for the description of the process is the function defined by

$$\begin{aligned} {}^{k}U &= 1 \quad \text{if} \quad \{{}^{k}z(t_1) \leq z_1, \ldots\ldots\ldots, {}^{k}z(t_n) \leq z_n\} \qquad (4.2.2) \\ &= 0 \quad \text{otherwise} \end{aligned}$$

The ensemble average of this function equals the fraction of the total number of realizations in which the event described by the expression

in the brackets occurs. It represents the joint probability function of the stochastic variables $\underline{z}_{t_i}$, i = 1, 2, ..., n. (Stochastic variables are underscored.) Regarded as a function of the z_i this is called the distribution function F:

$$< U > = \Pr \{\underline{z}_{t_1} \leq z_1, \ldots\ldots, \underline{z}_{t_n} \leq z_n\} = F(z_1,\ldots,z_n;t_1,\ldots,t_n) \tag{4.2.3}$$

The explicit expression of the dependence of F on the parameters $(t_1,\ldots, t_n)$ will be omitted in the following.

The mathematical expectation of a function $h(\underline{z}_{t_1},\ldots. \underline{z}_{t_n})$ is defined in terms of the distribution function as

$$E\{h(\underline{z}_{t_1},\ldots\ldots,\underline{z}_{t_n})\} = \int_{-\infty}^{\infty}\ldots\ldots\int_{-\infty}^{\infty} h(z_1,\ldots\ldots,z_n)\,dF(z_1,\ldots\ldots,z_n). \tag{4.2.4}$$

It follows from the definitions given that the mathematical expectation of a quantity is equal to its ensemble average. Furthermore, since the stochastic process is described in terms of ensemble averages, it is specified if the joint distribution function of the variables $\underline{z}_{t_i}$, i = 1, 2, ..., n, is known for an arbitrary number n of arbitrary instants t_i, within the interval of definition of the process.

The n-th partial derivative of F with respect to the z_i is

$$\frac{\partial^n F(z_1,\ldots\ldots,z_n)}{\partial z_1 \ldots\ldots\ldots \partial z_n} = f(z_1, \ldots\ldots, z_n) \quad . \tag{4.2.5}$$

It is the joint probability density function (abbreviated as p.d.f.) of the stochastic variables $(\underline{z}_{t_1},\ldots\ldots,\underline{z}_{t_n})$. It is allowed to contain Dirac delta functions*) [54]. The expectation of h given by (4.2.4) can

---

*) The term "function" is used here instead of the more correct designation "distribution" in order to avoid confusion with probability distributions and distribution functions.

be expressed in terms of the p.d.f. as

$$E\{h(\underline{z}_{t_1},\ldots\ldots,\underline{z}_{t_n})\} = \int_{-\infty}^{\infty}\ldots\int_{-\infty}^{\infty} h(z_1,\ldots\ldots z_n) f(z_1,\ldots\ldots z_n)\,dz_1\ldots\ldots dz_n \tag{4.2.6}$$

The first-order moments of the joint p.d.f. are equal to the mean or expected values of the $\underline{z}_{t_i}$:

$$\mu(t_i) = E\{\underline{z}_{t_i}\} = \int_{-\infty}^{\infty}\ldots\int_{-\infty}^{\infty} z_i\, f(z_1,\ldots\ldots z_n)\,dz_1\ldots\ldots dz_n = \int_{-\infty}^{\infty} z_i\, f(z_i)\,dz_i, \tag{4.2.7}$$

in which

$$f(z_i) = \int_{-\infty}^{\infty}\ldots\ldots\int_{-\infty}^{\infty}\int_{-\infty}^{\infty}\ldots\ldots\int_{-\infty}^{\infty} f(z_1,\ldots\ldots z_n)\,dz_1\ldots\ldots dz_{i-1}\,dz_{i+1}\ldots\ldots dz_n \tag{4.2.8}$$

is the marginal p.d.f. of $\underline{z}_{t_i}$.

The second-order moments of the joint p.d.f. about the mean values $\{\mu(t_1),\ldots\ldots\mu(t_n)\}$, denoted by $C(t_i,t_j)$, are defined by

$$C(t_i,t_j) = E\{(\underline{z}_{t_i} - \mu(t_i))(\underline{z}_{t_j} - \mu(t_j))\} \quad . \tag{4.2.9}$$

They are of major importance as quantitative measures of the variability of $\underline{z}$ at certain times t_i, and of the degree to which the variability of $\underline{z}$ at time t_i is related to the variability of $\underline{z}$ at time t_j. They are called the covariances of the stochastic variables $(\underline{z}_{t_i},\underline{z}_{t_j})$. For i = j they are called the variances of the variables $\underline{z}_{t_i}$, for brevity written as σ_i^2. The standard deviation of $\underline{z}_{t_i}$ is $\sigma_i (\geq 0)$.

A stochastic process $\{\underline{z}_t\}$ is said to be stationary if

$$Pr\{\underline{z}_{t_1} \leq z_1,\ldots\ldots,\underline{z}_{t_n} \leq z_n\} = Pr\{\underline{z}_{t_1+\tau} \leq z_1,\ldots\ldots,\underline{z}_{t_n+\tau} \leq z_n\} \tag{4.2.10}$$

for arbitrary τ, n and $t_i (i = 1,2,.....,n)$. It follows from this definition that in stationary processes the mathematical expectation of an arbitrary function h of $\underline{z}_{t_i}$ $(i = 1,2,.....,n)$ does not depend on the n values of the times t_i but only on their (n - 1) differences. Thus, the expected value and the variance of $\underline{z}_t$ are constant:

$$\mu(t_i) = E\{\underline{z}_{t_i}\} = \text{const} = \mu \qquad (4.2.11)$$

and

$$\sigma_i^2 = E\{(\underline{z}_{t_i} - \mu(t_i))^2\} = \text{const} = \sigma^2 \quad , \qquad (4.2.12)$$

while the covariances $C(t_i,t_j)$ depend on the time difference $t_i - t_j$ only:

$$C(t_i,t_j) = E\{(\underline{z}_{t_i} - \mu)(\underline{z}_{t_j} - \mu)\} = C(t_i - t_j) \quad , \qquad (4.2.13)$$

or, writing $t_i - t_j = \tau$,

$$E\{(\underline{z}_t - \mu)(\underline{z}_{t+\tau} - \mu)\} = C(\tau) \quad . \qquad (4.2.14)$$

$C(\tau)$ is the auto-covariance function of the stationary stochastic process $\{\underline{z}_t\}$. Its Fourier transform, which may include delta functions, is a non-negative function called the spectral density $\tilde{S}(\omega)$ of the process $\{\underline{z}_t\}$, often referred to as the power spectrum or the energy spectrum:

$$\tilde{S}(\omega) = \frac{1}{2\pi} \int_{-\infty}^{\infty} C(\tau) e^{-i\omega\tau} \, d\tau \quad . \qquad (4.2.15)$$

The inverse relation is

$$C(\tau) = \int_{-\infty}^{\infty} \tilde{S}(\omega) e^{i\omega\tau} \, d\omega \quad . \qquad (4.2.16)$$

The variance of $\{\underline{z}_t\}$ is given by

$$\sigma^2 = C(0) = \int_{-\infty}^{\infty} \tilde{S}(\omega)\, d\omega \quad , \tag{4.2.17}$$

which suggests that $\tilde{S}(\omega)$ should be interpreted as the contribution to the variance of $\{\underline{z}_t\}$ per unit of frequency.

The process $\{\underline{z}_t\}$ was assumed to be real and stationary. It follows that the auto-covariance function $C(\tau)$ is even and real, so that (4.2.15) can be written as

$$\tilde{S}(\omega) = \frac{1}{2\pi} \int_{-\infty}^{\infty} C(\tau) \cos \omega\tau \quad d\tau = \frac{1}{\pi} \int_{0}^{\infty} C(\tau) \cos \omega\tau \, d\tau \quad , \tag{4.2.18}$$

so that $\tilde{S}(\omega)$ is also even and real. Eq. (4.2.16) can therefore be written as

$$C(\tau) = \int_{-\infty}^{\infty} \tilde{S}(\omega) \cos \omega\tau \, d\omega = 2 \int_{0}^{\infty} \tilde{S}(\omega) \cos \omega\tau \, d\omega \quad . \tag{4.2.19}$$

Since $\tilde{S}(\omega)$ is even, we can restrict its interval of definition to non-negative frequencies, and define

$$S(\omega) = 2\tilde{S}(\omega) \quad \text{for} \quad \omega \geq 0 \quad . \tag{4.2.20}$$

This gives the so-called Wiener-Khinchine relations:

$$S(\omega) = \frac{2}{\pi} \int_{0}^{\infty} C(\tau) \cos \omega\tau \, d\tau \tag{4.2.21}$$

$$C(\tau) = \int_{0}^{\infty} S(\omega) \cos \omega\tau \, d\omega \quad . \tag{4.2.22}$$

The spectral density function is a particularly useful tool if linear transformations are applied to a stochastic process [52, 53]. Consider a linear, time-invariant system, not necessarily a physical system. It may, for example, also represent a mathematical operator. Let the response of this system to an input $Re\{e^{i\omega t}\}$ be given by

$Re\{H(\omega)e^{i\omega t}\}$; $H(\omega)$ is the frequency response function. If a stochastic process $\{\underline{u}_t\}$, with spectral density $S_{uu}(\omega)$, acts as an input to this system, then the spectral density of the output process $\{\underline{v}_t\}$ is given by

$$S_{vv}(\omega) = |H(\omega)|^2 S_{uu}(\omega) \quad . \tag{4.2.23}$$

In particular, if the system acts as an ideal band-pass filter, specified by

$$\begin{aligned} |H(\omega)| \quad &= 1 \text{ for } \omega_1 \leq \omega \leq \omega_2 \\ &= 0 \text{ otherwise,} \end{aligned} \tag{4.2.24}$$

then the variance of the filtered process is

$$\sigma_v^2 = \int_{\omega_1}^{\omega_2} S_{uu}(\omega)d\omega \tag{4.2.25}$$

as compared to

$$\sigma_u^2 = \int_0^{\infty} S_{uu}(\omega)d\omega \tag{4.2.26}$$

for the unfiltered process. This permits the interpretation of the spectral density as the contribution to the variance per unit of frequency of spectral components.

In stationary processes $\{\underline{z}_t\}$ it is often useful to consider averages of functions of ${}^k z(t)$ with respect to time in individual realizations. For an arbitrary function this time average is defined as

$$\lim_{T\to\infty} \frac{1}{2T} \int_{-T}^{T} h\{{}^k z(t), {}^k z(t+\tau_1), \ldots\ldots, {}^k z(t+\tau_{n-1})\}\, dt \quad .$$

Time averages can in general depend on the particular realization in which they have been determined. Stationary processes for which this is not the case are called ergodic. Time-averaging of arbitrary func-

tions of $^{k}z(t)$ in such processes yields the same results as ensemble-averaging.

4.2.2 Gaussian processes

An important class of stochastic processes are those which can be regarded as the result of a superposition of a large number of stochastically independent components. In many such cases the central limit theorem can be applied. This theorem states that under certain not very restrictive conditions the sum of a large number of stochastically independent variables is approximately Gaussian distributed [51].

Consider n stochastic variables $\underline{z}_i$ (i = 1,.....n) with mean values $\mu_i = E\{\underline{z}_i\}$ and covariances $C_{ij} = E\{(\underline{z}_i - \mu_i)(\underline{z}_j - \mu_j)\}$. They are said to be jointly Gaussian distributed if their p.d.f. is given by

$$f(z_1,.....,z_n) = (2\pi)^{-\frac{n}{2}} ||C||^{-\frac{1}{2}} \exp\{-\tfrac{1}{2} ||C||^{-1} \sum_{i=1}^{n} \sum_{j=1}^{n} |C_{ij}| (z_i - \mu_i)(z_j - \mu_j)\} \quad , \tag{4.2.27}$$

[51], in which $|C_{ij}|$ is the cofactor of C_{ij} in the determinant $||C||$ of the covariance matrix (C_{ij}). For n = 1 (4.2.27) reduces to

$$f(z_1) = (2\pi)^{-\frac{1}{2}} \sigma_1^{-1} \exp\{-\tfrac{1}{2}(\frac{z_1 - \mu_1}{\sigma_1})^2\} \quad , \tag{4.2.28}$$

in which

$$\sigma_1^{\,2} = C_{11} \quad , \tag{4.2.29}$$

the variance of $\underline{z}_1$.

A stochastic process $\{\underline{z}_t\}$ is said to be Gaussian if the joint p.d.f. of the variables $\underline{z}_{t_i}$ is of the form (4.2.27) for an arbitrary number n of arbitrary instants t_i (i = 1,...., n). Rice [55] shows that the (weak) conditions which are sufficient for the applicability

of the central limit theorem are fulfilled in processes which have a finite spectral density and which result from the superposition of independent components. In other words, such processes are Gaussian. They are completely specified by the mean values $\mu(t_i)$ and the auto-covariances $C(t_i,t_j)$. Stationary Gaussian processes are therefore completely specified by the mean value μ and the auto-covariance function $C(\tau)$, or, in view of (4.2.22), by μ and the spectral density function $S(\omega)$. The value of the mean, μ, is generally of no importance for the description of the process. It will assumed to be zero in the following.

It can be shown that stationary Gaussian processes are ergodic if and only if the spectral density is finite for every frequency [50]. This condition, which means that there shall be no finite contribution to the variance at discrete frequencies, is fulfilled in the applications to be considered in the following chapters. A consequence of the ergodicity is that the probability of an "event", interpreted as the relative frequency of occurrence in the ensemble, is equal in value to the fraction of time during which the event occurs in any one realization. The two interpretations will be used interchangeably in what follows.

An important property of Gaussian processes is that they remain Gaussian under a linear transformation. This follows from the following theorem [56]. If the stochastic variables $\underline{z}_i$ ($i = 1,.....,n$) are jointly Gaussian in n dimensions, then the variables $\underline{Z}_j$ obtained as linear combinations of the $\underline{z}_i$ according to

$$\underline{Z}_j = \sum_{i=1}^{n} A_{ij}\, \underline{z}_i \quad , \quad j = 1,2,.....,m \quad , \qquad (4.2.30)$$

for arbitrary constants A_{ij}, are jointly Gaussian in m dimensions. The output of a linear system can be regarded as (the limit of) a weighted sum of values of the input at different times [52,53]. Thus, the response of a linear system to a Gaussian process is again a Gaussian process. It is fully specified by its spectrum, which for stationary processes can be found simply by application of (4.2.23).

Although we only need to know the spectral density function of a stationary Gaussian process in order to determine its statistical properties, it may be advantageous to have an explicit representation of the process as a random function of time. Many representations are possible, in view of the wide range of applicability of the central limit theorem. A model which has found many applications is the random phase model due to Rice [55]:

$$\underline{z}_t = \sum_{j=1}^{n} a_j \cos(\omega_j t + \underline{\psi}_j) \quad (\omega_j > 0) \quad . \tag{4.2.31}$$

The phases $\underline{\psi}_j$ are independent random variables, each with a uniform p.d. of $(2\pi)^{-1}$ on the interval $(-\pi,\pi)$. This makes the process (4.2.31) a stationary one, because the addition of a constant time lag τ to t merely changes the point of zero phase. This is of no consequence for the ensemble averages, since the integrations over the phases are still carried out over an interval of length 2π, with equal weight being given to all the phases on that interval. A similar argument applies to time averages, provided that there is no zero-frequency term, as indicated in (4.2.31). The process given by (4.2.31) is therefore also ergodic.

The expected value of $\underline{z}_t$ is zero. The auto-covariance function is

$$C(\tau) = \sum_{j=1}^{n} \tfrac{1}{2} a_j^2 \cos \omega_j \tau \quad , \tag{4.2.32}$$

the variance is

$$C(0) = \sigma^2 = \sum_{j=1}^{n} \tfrac{1}{2} a_j^2 \quad , \tag{4.2.33}$$

and the spectrum is

$$S(\omega) = \sum_{j=1}^{n} \tfrac{1}{2} a_j^2 \, \delta(\omega - \omega_j) \quad , \tag{4.2.34}$$

in which δ is the Dirac delta function. The spectrum is discrete since the variance consists of finite contributions at discrete frequencies. In order to obtain a continuous spectrum we should take

the limit of the preceding expressions for $n \to \infty$, such that each infinitesimally narrow frequency interval $(\omega, \omega + d\omega)$ contains an uncountably infinite number of spectral components which together contribute to the total variance of $\{\underline{z}_t\}$ in proportion to $d\omega$:

$$\lim_{\substack{n\to\infty \\ \max(\omega_{j+1} - \omega_j) \to 0}} \sum_{\omega_j=\omega}^{\omega+d\omega} \tfrac{1}{2} a_j^2 = S(\omega)d\omega \quad . \tag{4.2.35}$$

In this case the central limit theorem is applicable, so that the process given by (4.2.31) is Gaussian after passage to the limit.

In the representation mentioned above the process $\{\underline{z}_t\}$ is expressed as the sum of an uncountably infinite number of spectral components of different frequencies. This results in an oscillatory but nonperiodic appearance of the realizations $z(t)$. The structure of these realizations is wholly governed by the shape of the variance density spectrum. If this is narrow, which means that the spectral density is significant only in a relatively narrow frequency band, then the realizations resemble amplitude-modulated sine curves. The realizations of broad-spectrum processes are less regular because of the superposition of sinusoids of widely different frequencies but of appreciable variance content.

The statistical properties of ergodic Gaussian processes have been the subject of extensive studies [55, 57 - 59], which have yielded numerous useful results. Some of these will be mentioned in section 4.4, together with empirical data for wind waves. However, before turning to these details we shall first consider the quantitative description of wind waves from a more general point of view in the following section.

4.3 Wind waves considered as a quasi-stationary Gaussian process

4.3.1 General considerations

The sea surface in the presence of wind waves is a random, moving surface; it is a stochastic process in three dimensions: two space dimensions in addition to time. If we are interested not only in the surface itself but also in sub-surface phenomena associated with the wind waves, then we have to consider three independent space variables and time. Although the preceding section dealt with random processes in one dimension only, many of the concepts mentioned there are quite general, and apply directly to multidimensional processes.

The elevation of the sea surface above a horizontal datum plane is denoted as $\underline{\zeta}$, which is a function of location $\vec{x} = (x,y)$ and time t. The stochastic process $\{\underline{\zeta}(\vec{x},t)\}$ can be described through the joint distribution functions of the variables $\underline{\zeta}(\vec{x}_i,t_i)$, $i = 1, 2,\ldots,n$, for arbitrary n and arbitrary values of $\vec{x}_i$ and t_i. As before, the process is stationary if these distribution functions are invariant under the addition of an arbitrary constant time lag to the instants t_i. If these distribution functions are invariant under the addition of an arbitrary constant (horizontal) vector to the $\vec{x}_i$, then the wave field is said to be horizontally homogeneous.

For a consideration of local properties, sea waves can often be described as quasi-stationary and quasi-homogeneous, since variations of mean wave properties in time and space generally take place on scales which are large compared to typical wave periods and wavelengths. If $\{\underline{\zeta}(\vec{x},t)\}$ is a stationary and homogeneous process then its mean value is a constant, which will be assumed to be zero, while its auto-covariance function is a function of time- and space-differences only:

$$E\{\underline{\zeta}(\vec{x},t)\ \underline{\zeta}(\vec{x}+\vec{r},\ t+\tau)\} = C(\vec{r},\tau) \quad . \qquad (4.3.1)$$

The three-dimensional Fourier transform of $C(\vec{r},\tau)$ gives the spectral density in wavenumber-frequency spave [30]. Reduced forms of this

three-dimensional spectral density function are obtained by integrating it either over the frequencies, which gives the two-dimensional wavenumber spectrum, or over the wavenumbers, which gives the one-dimensional frequency spectrum. The first of these resolves the variance of $\underline{\zeta}(\vec{x};\ t = \text{constant})$ into the contributions of a continuum of long-crested sinusoidal spectral components in space. The latter resolves the variance of $\underline{\zeta}(t;\ \vec{x} = \text{constant})$ into the contributions of a continuum of sinusoidal spectral components in time.

The variance of $\underline{\zeta}$ is, apart from a constant factor $\frac{1}{2}\rho g$, equal to the average gravitational potential energy of the waves per unit horizontal area. For this reason the various variance density spectra are frequently referred to as energy density spectra, or simply as energy spectra.

Important simplifications are obtained by assuming that the waves behave linearly. This implies that the spectral components are hydrodynamically independent of each other. The linear dispersion equation (3.2.14) then applies to individual spectral components, making the absolute value of the wavenumber a known function of the wave frequency, so that the number of independent dimensions of the spectral density function in effect is reduced to two. Instead of having to deal with a three-dimensional wavenumber-frequency spectrum it is sufficient to deal with the spectrum as a function of two wavenumber-components (k_x,k_y), or as a function of the absolute value of the wavenumber and the direction of propagation (k,θ), or as a function of the frequency and direction (ω,θ). We shall use the latter form, written as $G(\omega,\theta)$.

A consequence of the assumed hydrodynamical independence of the spectral components is that they can be also stochastically independent. This is commonly the case for wind waves, even for those generated in a single wind field, because such fields are usually so large that they can be sub-divided into many areas in which the processes of wave generation are mutually independent.

The assumption that the sea surface can be regarded as the result of a superposition of an uncountably infinite number of spectral components which are stochastically independent is sufficient for the

applicability of the central limit theorem. Under these circumstances the wave field can be considered to be Gaussian, and completely described by its two-dimensional spectral density function. Needless to say, this is only approximately the case for real waves, which are not exactly linear. It turns out however that for many applications the approximation is quite good (see section 4.4).

4.3.2 An explicit representation

A representation of the sea surface as a stationary Gaussian process in space and time can be obtained by a straightforward generalization of the one-dimensional Rice representation [60]:

$$\underline{\zeta}(x,y,t) = \sum_{j=1}^{n} \sum_{\ell=1}^{m} a_{j\ell} \cos(\omega_j t - k_j x \cos\theta_\ell - k_j y \sin\theta_\ell - \underline{\psi}_{j\ell}) \quad . \tag{4.3.2}$$

The phases are independent random variables, each with a uniform p.d. of $(2\pi)^{-1}$ on the interval $(-\pi,\pi)$. The wave frequency and wavenumber are related according to the dispersion relation

$$\omega_j^2 = g k_j \tanh k_j d \quad . \tag{4.3.3}$$

The spectrum of the process described by (4.3.2) is discrete, which is not realistic for wind waves. In order to obtain a continuous spectrum we should consider the limit of (4.3.2) for $n\to\infty$, $\max|\omega_{j+1} - \omega_j| \to 0$, $m\to\infty$ and $\max|\theta_{\ell+1} - \theta_\ell| \to 0$, such that the spectral components with angular frequencies in the infinitesimal interval $(\omega, \omega + d\omega)$ and with directions of propagation in the infinitesimal interval $(\theta, \theta + d\theta)$ contribute to the total variance of $\underline{\zeta}$ in proportion to $d\omega d\theta$:

$$\sum_{\omega_j=\omega}^{\omega+d\omega} \sum_{\theta_\ell=\theta}^{\theta+d\theta} \tfrac{1}{2} a_{j\ell}^2 \to G(\omega,\theta) d\omega d\theta \quad . \tag{4.3.4}$$

The total variance of $\underline{\zeta}$ is then given by

$$\sigma^2 = \int_0^{\infty} \int_{-\pi}^{\pi} G(\omega,\theta)\,d\omega\,d\theta \quad . \tag{4.3.5}$$

If the surface elevation is considered as a function of time, at a fixed point (x,y), then the phase term $(k_j x \cos\theta_\ell + k_j y \sin\theta_\ell)$ in (4.3.2) is a constant, say $\alpha_{j\ell}$, for each pair (j,ℓ):

$$\underline{\zeta}_t = \sum_{j=1}^{n} \sum_{\ell=1}^{m} a_{j\ell} \cos(\omega_j t - \alpha_{j\ell} - \underline{\psi}_{j\ell}) \quad . \tag{4.3.6}$$

This expression can be put into in a form similar to the representation (4.2.31) for a one-dimensional process as follows. Eq. (4.3.6) can be written as

$$\underline{\zeta}_t = Re \sum_{j=1}^{n} e^{i\omega_j t} \sum_{\ell=1}^{m} a_{j\ell}\, e^{-i(\alpha_{j\ell} + \underline{\psi}_{j\ell})} = Re \sum_{j=1}^{n} \underline{b}_j\, e^{i\omega_j t} \quad , \tag{4.3.7}$$

in which

$$\underline{b}_j = \sum_{\ell=1}^{m} a_{j\ell}\, e^{-i(\alpha_{j\ell} + \underline{\psi}_{j\ell})} \quad . \tag{4.3.8}$$

Define

$$\underline{B}_j = |\underline{b}_j| \quad , \quad \underline{\beta}_j = \arg(\underline{b}_j) \quad , \tag{4.3.9}$$

then (4.3.7) becomes

$$\underline{\zeta}_t = \sum_{j=1}^{n} \underline{B}_j \cos(\omega_j t + \underline{\beta}_j) \quad . \tag{4.3.10}$$

It follows from (4.3.8) and from the given p.d.f. of $\underline{\psi}_{j\ell}$ that the phases $\underline{\beta}_j$ are mutually independent, each with a uniform p.d. of $(2\pi)^{-1}$ on the interval $(-\pi,\pi)$, while the random amplitudes $\underline{B}_j$ (which in the limit for $m\to\infty$ are Rayleigh-distributed [61]) have mean-square values

$$E\{\underline{B}_j^2\} = \sum_{\ell=1}^{m} a_{j\ell}^2 \quad . \tag{4.3.11}$$

With this information the auto-covariance function and the spectral density function of $\{\underline{\zeta}_t\}$ can be derived in a straightforward manner from (4.3.10), with the result

$$C(\tau) = \sum_{j=1}^{n} E\{\tfrac{1}{2} \underline{B}_j^2\} \cos \omega_j \tau \qquad (4.3.12)$$

and

$$S(\omega) = \sum_{j=1}^{n} E\{\tfrac{1}{2} \underline{B}_j^2\} \delta(\omega - \omega_j) = \sum_{j=1}^{n} \left(\sum_{\ell=1}^{m} \tfrac{1}{2} a_{j\ell}^2 \right) \delta(\omega - \omega_j) \quad . \qquad (4.3.13)$$

Thus, the contribution to the variance of $\underline{\zeta}_t$ at $\omega = \omega_j$ equals $\sum_{\ell=1}^{m} \tfrac{1}{2} a_{j\ell}^2$, which is the sum, over all the directions of propagation, of the variances of the components with $\omega = \omega_j$. It follows that in the limit when the frequencies ω_j and the directions of propagation θ_ℓ are densely distributed in $(0,\infty)$ and $(-\pi,\pi)$, respectively, the spectral density $S(\omega)$ can be obtained from the two-dimensional spectrum $G(\omega,\theta)$ by integration over θ:

$$S(\omega) = \int_{-\pi}^{\pi} G(\omega,\theta) d\theta \quad . \qquad (4.3.14)$$

The two-dimensional spectrum $G(\omega,\theta)$ can therefore conveniently be factorized into the one-dimensional frequency spectrum $S(\omega)$, the integral of which yields the variance of $\underline{\zeta}$, and a directional spectrum $D(\theta;\omega)$ which has unit area, or

$$G(\omega,\theta) = S(\omega)\, D(\theta;\omega) \quad , \qquad (4.3.15)$$

in which

$$\int_{-\pi}^{\pi} D(\theta;\omega) d\theta = 1 \qquad (4.3.16)$$

for all ω.

The representation of the sea surface as a quasi-stationary and quasi-homogeneous Gaussian process has many realistic features [62,63]. The superposition of spectral components of different frequencies and wavelengths results in an oscillatory but non-periodic behaviour of the surface in time and in space, while the fact that these components have different directions of propagation causes short-crestedness. Both properties are clearly present in wind waves. A quantitative test of the agreement between the Gaussian model and real waves can obviously be made only on those items for which quantitative theoretical and empirical results are available or obtainable. Many theoretical results concerning the statistical properties of the waves considered as a random moving surface have been derived by Longuet-Higgins. However, no empirical data are available for most of these. The situation is quite different in the simpler case of the variation of the elevation of the water surface with time at a fixed point, of which many measurements have been made, analysed and compared with theoretical predictions. A number of these will be presented in section 4.4. We shall pay no attention to the statistical geometry of the sea surface, since the equations presented in chapter 3, which are to be used in the chapters 5 and 6, are based exclusively on mass- and momentum balances for a fixed control volume of infinitesimal horizontal extent. The waves appear in these equations only in their time-averaged properties at fixed points. These properties can in a first approximation be calculated from the two-dimensional energy spectrum, without having to go into the details of the surface geometry.

4.3.3 Transformation of the spectrum due to shoaling, refraction and dissipation

It has been observed in the introduction of this section that statistical wave properties generally vary relatively slowly in time and space, so that for a description of the local properties the field can be considered to be stationary and homogeneous. However, it may be necessary to take account of the variations of the local properties if the waves are considered on a larger scale. This is in fact the case

in the problems to be dealt with in following chapters, in which predictions have to be made concerning the wave motion in the nearshore region, for a given topography and given wave properties offshore. In such cases the spectral density is considered as a slowly varying function of space and time. Its transformation can be calculated from an energy balance, assuming the geometrical-optics approximation to be applicable. The formulation is simplest in terms of the two-dimensional wave-number spectrum $G'(\vec{k})$, which is related to $G(\omega,\theta)$ according to

$$G'(\vec{k}) \equiv G'(k_x,k_y) = G(\omega,\theta)\,\frac{\partial(\omega,\theta)}{\partial(k_x,k_y)} = k^{-1}\,\frac{\partial\omega}{\partial k}\,G(\omega,\theta) = \omega^{-1}\,cc_g\,G(\omega,\theta) \qquad (4.3.17)$$

in which

$$c_g = \frac{\partial\omega}{\partial k} = nc \quad . \qquad (4.3.18)$$

Longuet-Higgins [64] has shown that in the statistically steady state the spectral density $G'(\vec{k})$ is constant along wave rays, if there is no generation or dissipation. This can also be written as

$$\frac{\partial}{\partial s}\{\,cc_g\,G(\omega,\theta)\} = 0 \quad , \qquad (4.3.19)$$

in which s is a coordinate along the wave ray traced by the spectral component (ω,θ). More generally, it can be shown [30] that

$$\frac{d}{dt}\,G'(\vec{k};\vec{x},t) \equiv \left(\frac{\partial}{\partial t} + \vec{c}_g\,.\,\nabla\right) G'(\vec{k};\vec{x},t) = Q(\vec{k};\vec{x},t) \quad , \qquad (4.3.20)$$

in which Q is a source function, which may contain terms representing energy transfer between wind and waves, wave-wave interactions, energy dissipation, etc. Collins [65] describes procedures for the integration of (4.3.20) in which several of these possible source terms are taken into account. If Q = 0 then the spectral density in wave-

number space is constant, following a wave group.

4.4 Statistical properties of wind waves at a fixed point

4.4.1 Introduction

In this section we shall summarize theoretical and empirical results concerning a number of statistical properties of wind waves at a fixed point which will be used in subsequent chapters. Particular attention will be paid to the distributions of crest heights and wave heights.

The theoretical results to be mentioned in the following have been derived from the assumed model of a stationary Gaussian process with zero mean, except where otherwise stated. These results will simply be referred to as "theoretical" in order to avoid repeated use of the more complete description. Similarly, the term "empirical" will be used to refer to results based on the analyses of wind wave records.

The theoretical results are conveniently expressed in terms of the moments of the spectrum of $\underset{\sim}{\zeta}_t$ about $\omega = 0$:

$$m_j = \int_0^\infty \omega^j \, S(\omega) d\omega \qquad (4.4.1)$$

The moments are assumed to exist up to all orders required. The zeroth moment equals the variance of $\underset{\sim}{\zeta}$:

$$\sigma^2 = \int_0^\infty S(\omega) d\omega = m_0 \quad . \qquad (4.4.2)$$

4.4.2 Distribution of instantaneous values

The theoretically predicted Gaussian distribution of instantaneous values of the water surface elevation, or of variables which linearly depend thereon, has been reasonably verified empirically, both in the univariate case [66] and in the multivariate case [67]. Needless to say, the assumption that the elevations at various times are jointly Gaussian distributed is also checked indirectly through the theoretical

results to be mentioned in the following paragraphs, which are without exception based on this assumption.

Though the Gaussian function is a good first approximation to the measured surface elevation distribution, it is no more than that. Detailed analyses of wave records by Kinsman [68] brought small but systematic differences to light, in the sense that high positive elevations had a greater p.d. than the best-fit Gaussian curve, while the opposite was true for negative elevations of large absolute value, resulting in a positive skewness. Similar deviations from the Gaussian distribution were found by Koelé and de Bruyn [69] and by Collins [70]. These deviations are due to the nonlinear character of the waves, which causes the crests to be narrower than the troughs, and at a greater distance from the mean water level. Longuet-Higgins [71,72] has considered theoretically the perturbations on the Gaussian p.d.f. due to the nonlinear coupling between the spectral components. His results are in very close agreement with Kinsman's and Collins' data.

4.4.3 Average interval between level crossings

Consider the time intervals τ_η between successive crossings of a level η by a realization $\zeta(t)$. Rice [55] has derived the following theoretical result for their average value:

$$E\{\tau_\eta\} = \pi \left(\frac{m_0}{m_2}\right)^{\frac{1}{2}} \exp\left(\frac{\eta^2}{2m_0}\right) . \qquad (4.4.3)$$

4.4.4 Distribution of zero-crossing intervals

An important special case of (4.4.3) is obtained by putting $\eta = 0$, resulting in an expression for the average interval between successive zero-crossings:

$$E\{\tau_0\} = \pi \left(\frac{m_0}{m_2}\right)^{\frac{1}{2}} . \qquad (4.4.4)$$

In later applications the time interval between successive zero-

upcrossings will be considered, denoted by $\underline{T}$ (see fig. 4.1). This quantity will for brevity be referred to as "zero-crossing period",

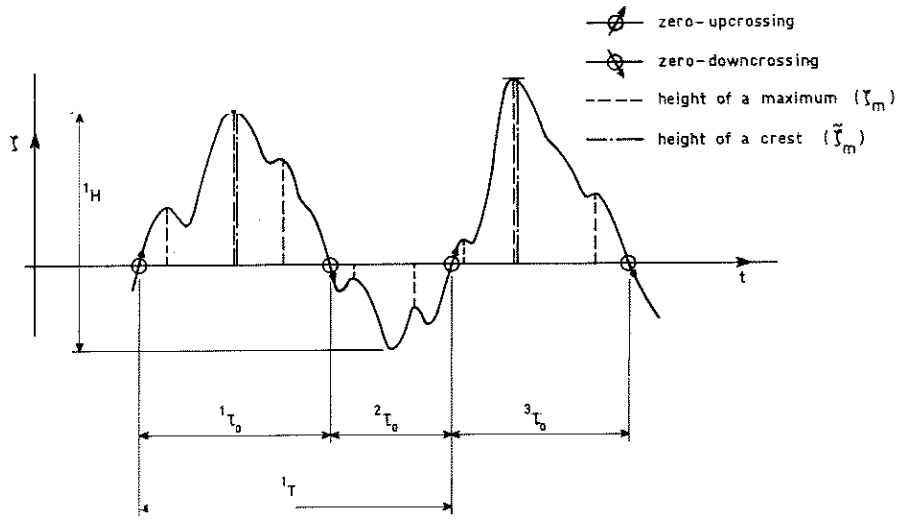

Fig. 4.1 - Definition sketch

or simply as "period". Its theoretical mean value is

$$\overline{T} = E\{\underline{T}\} = 2\, E\{\underline{\tau}_0\} = 2\pi \left(\frac{m_0}{m_2}\right)^{\frac{1}{2}} \quad . \tag{4.4.5}$$

Empirical data are in general in agreement with this relationship [70,73].

The calculation of the p.d.f. of $\underline{\tau}_0$ or of $\underline{T}$ poses a formidable theoretical problem. A first approximation was given by Rice [55]. Further contributions are due to McFadden [74,75] and Ehrenfeld et al [76] and in particular to Longuet-Higgins [77-79]. The p.d.f. depends in a complicated manner on the spectrum. It has to be calculated numerically. Some results obtained from numerical simulation of Gaussian processes with various spectral shapes have been given by Goda [80].

4.4.5 Distribution of intervals between maxima

A maximum of $\zeta(t)$ corresponds to a downward zero-crossing of $\zeta'(t) = \frac{d\zeta(t)}{dt}$. The distribution of the time intervals between maxima of $\underline{\zeta}(t)$, denoted as $\underline{T}_m$, can therefore be calculated using the theoretical results pertaining to the distribution of zero-crossing intervals, referred to in the preceding paragraph. These results should then be applied to the process $\{\underline{\zeta}'(t)\}$, of which the spectral density is $\omega^2 S(\omega)$. It follows in particular that the average time interval between maxima can theoretically be calculated from (4.4.5), provided the zeroth and second moment of $\{\underline{\zeta}'(t)\}$ are used. This gives

$$\overline{T}_m = E\{\underline{T}_m\} = 2\pi \left(\frac{m_2}{m_4}\right)^{\frac{1}{2}} \quad , \tag{4.4.6}$$

a result which is due to Rice [55].

4.4.6 Distribution of the heights of the maxima

Rice [55] has derived the theoretical probability distribution of the heights of the maxima. His result has been elaborated by Cartwright and Longuet-Higgins [58].

It is convenient to normalize the process $\{\underline{\zeta}(t)\}$ so that it will have a standard deviation of unity. We therefore define

$$\underline{\xi}(t) = \frac{\underline{\zeta}(t)}{\sqrt{m_0}} \quad . \tag{4.4.7}$$

The value of $\underline{\xi}(t)$ at a maximum is denoted by $\underline{\xi}_m$ (see fig. 4.1). The theoretical expressions for the p.d.f. and the probability of exceedance of $\underline{\xi}_m$, written as $f(\eta)$ and $Q(\eta)$, are

$$f(\eta) = (2\pi)^{-\frac{1}{2}} \left[(1-\nu^2)^{\frac{1}{2}} e^{-\frac{1}{2}\frac{\eta^2}{1-\nu^2}} + \nu\eta e^{-\frac{1}{2}\eta^2} \int_{-\infty}^{\nu\eta/(1-\nu^2)^{\frac{1}{2}}} e^{-\frac{1}{2}v^2} dv \right] \tag{4.4.8}$$

and

$$Q(\eta) = (2\pi)^{-\frac{1}{2}} \left[\int_{\eta/(1-\nu^2)^{\frac{1}{2}}}^{\infty} e^{-\frac{1}{2}v^2}\, dv + \nu e^{-\frac{1}{2}\eta^2} \int_{-\infty}^{\nu\eta/(1-\nu^2)^{\frac{1}{2}}} e^{-\frac{1}{2}v^2}\, dv \right] \tag{4.4.9}$$

in which

$$\nu = \frac{m_2}{(m_0\, m_4)^{\frac{1}{2}}} \quad . \tag{4.4.10}$$

The parameter ν is related as follows to the widely used parameter ε introduced by Cartwright and Longuet-Higgins [58]:

$$\nu^2 + \varepsilon^2 = 1 \quad . \tag{4.4.11}$$

The reason for using ν instead of ε is that the term $(1 - \varepsilon^2)^{\frac{1}{2}}$, which is ν, occurs much more frequently in what follows than ε itself.

Substitution of (4.4.5) and (4.4.6) in (4.4.10) gives

$$\nu = \frac{\overline{T}_m}{\overline{T}} = \frac{N}{N_m} \quad , \tag{4.4.12}$$

in which N and N_m are the number of upward zero-crossings and of maxima in a long time interval. It follows that for continuous processes $\nu \leq 1$. The lower bound on ν is theoretically zero [58]. This case is of no practical importance, however, as it would imply that there are infinitely more maxima that zero-crossings. It will be included here only for the sake of completeness. Thus we have

$$0 \leq \nu \leq 1 \quad , \tag{4.4.13}$$

which can also be inferred directly from the definition of ν given in (4.4.10). The value of ν is wholly determined by the shape of the spectral density function. A spectrum is said to be narrow if the moments about the mean frequency

$$\overline{\omega} = m_1/m_0 \tag{4.4.14}$$

are small compared with the moments about $\omega = 0$. In this case $m_j \approx (\bar{\omega})^j m_0$, so that $\nu = 1$. The realizations then have the appearance of a slowly-amplitude-modulated sine curve with a well-defined envelope. There are no positive minima or negative maxima, so $\nu = N/N_m \approx 1$. For $\nu = 1$ the eqs. (4.4.8) and (4.4.9) reduce to

$$\begin{aligned} f(\eta) &= 0 && \text{for} \quad \eta \leq 0 \\ &= \eta e^{-\frac{1}{2}\eta^2} && \text{for} \quad \eta \geq 0 \end{aligned} \tag{4.4.15}$$

and

$$\begin{aligned} Q(\eta) &= 1 && \text{for} \quad \eta \leq 0 \\ &= e^{-\frac{1}{2}\eta^2} && \text{for} \quad \eta \geq 0 \ . \end{aligned} \tag{4.4.16}$$

These equations describe the Rayleigh-distribution [61]. Eq. (4.4.16) follows also from (4.4.3) and from the fact that there are no positive minima if $\nu = 1$, so that in this case the number of upcrossings of a given positive level equals the number of maxima above that level.

With increasing spectral width, ν diminishes in value. The corresponding realizations are less regular in appearance, having more extremes than zero-crossings. In other words, the proportion of negative maxima (and of positive minima) increases [58]. It is equal to $1-Q(0)$, which, from (4.4.9), equals $\frac{1}{2}(1 - \nu)$. In the extreme case $\nu = 0$ the distribution of $\underset{\sim}{\xi}_m$ reduces to the Gaussian form.

The parameter $(-\nu)$ can be shown to be equal to the coefficient of linear correlation between $\underset{\sim}{\zeta}(t)$ and its second derivative, or, roughly speaking, between the elevation and the curvature. The importance of this correlation coefficient for the statistical properties of a stationary random process was already pointed out in 1921 by Taylor in his pioneering paper on the diffusion by continuous movements [81], in which he also introduced the auto-covariancefunction.

The expression (4.4.9) for the probability of exceedance of $\underset{\sim}{\xi}_m$ with arbitrary ν is somewhat unwieldy for analytical work. However, with increasing values of $\nu\eta/(1-\nu^2)^{\frac{1}{2}}$ the integrals occurring in (4.4.9) converge rapidly to 0 and to $(2\pi)^{\frac{1}{2}}$ respectively, in which case

$$Q(\eta) \approx \nu \, e^{-\frac{1}{2}\eta^2} \tag{4.4.17}$$

[55, 58], or, substituting (4.4.12),

$$Q(\eta) \approx \frac{N}{N_m} e^{-\frac{1}{2}\eta^2} \quad . \tag{4.4.18}$$

The errors in this approximation are small even for moderate values of $\nu\eta/(1-\nu^2)^{\frac{1}{2}}$. For example, for $\nu = 0.7$, which is a common value for wind-driven waves, the relative error is less than 0.02 for $\eta > 1$, i.e. for all the maxima higher than (only) one standard deviation above the mean level. The error diminishes rapidly with increasing values of η and/or ν.

Eq. (4.4.18) can be interpreted as follows. $Q(\eta)N_m/N$, which is the ratio of the expected number of maxima with a height in excess of η (>0) to the expected number of zero-upcrossings, is nearly equal to $\exp(-\frac{1}{2}\eta^2)$, which is of the same form as the probability of exceedance of the Rayleigh distribution. This theoretical result is relevant to the practice of considering not every maximum in a record but only the highest maximum in each interval between a zero-upcrossing and the next zero-downcrossing. This subclass of all the maxima will for brevity be referred to as crest height, denoted by $\underset{\sim}{\zeta}_m$, (see fig. 4.1), and by $\underset{\sim}{\tilde{\xi}}_m$ in normalized form. It follows from the definition of the crest heights that they are positive, and equal in number to the upward zero-crossings. Their theoretical distribution is not known except for the case of a narrow spectrum ($\nu = 1$), when it is of the Rayleigh type. The following arguments show that the Rayleigh distribution applies approximately for other values of ν as well, provided $\nu\eta/(1-\nu^2)^{\frac{1}{2}}$ is not small.

The probability of occurrence of more than one maximum above η on an interval between a zero-upcrossing and the next zero-downcrossing diminishes with increasing η. This implies that for moderate and large

values of η the expected number of occurrences of $\{\tilde{\underline{\xi}}_m > \eta\}$ is approximately equal to (but never larger than) the expected number of occurrences of $\{\underline{\xi}_m > \eta\}$. If we divide both by the expected number of zero-crossings we obtain

$$\tilde{Q}(\eta) \overset{\text{def}}{=} \Pr\{\tilde{\underline{\xi}}_m > \eta\} \approx \frac{N_m}{N} Q(\eta) \quad . \tag{4.4.19}$$

Substitution of (4.4.18) gives

$$\tilde{Q}(\eta) \approx e^{-\frac{1}{2}\eta^2} \quad . \tag{4.4.20}$$

The errors in (4.4.18) and (4.4.19) are of opposite sign, and they diminish rapidly with increasing η and/or ν. Thus, the conclusion is that theoretically, for sufficiently large values of $\nu\eta/(1-\nu^2)^{\frac{1}{2}}$, the crest heights are approximately Rayleigh distributed. This is in agreement with data presented by Koelé and de Bruyn [69]. The equivalent of the crest height based on the trough depth was also found to be Rayleigh distributed, though it was systematically smaller. This is to be expected if nonlinear effects play a measurable rôle. The same trend is shown by data given by Collins [70]. In this case there was good agreement with the Rayleigh distribution only in the upper 80% ($Q > 0.2$). The effects of nonlinearities on the p.d.f. of the heights of all the maxima (not just the highest maxima between successive zero-crossings) is dealt with by Longuet-Higgins [72].

4.4.7 Distribution of zero-crossing wave heights

Consider $\zeta(t)$ on a time interval between two successive zero-upcrossings. The height of the highest maximum on this interval above the height of the lowest minimum on the same interval is called a zero-crossing wave height, or simply wave height, denoted by H (see fig. 4.1). The zero-crossing wave height is used extensively in the analysis of wind wave records, particularly in civil engineering applications.

The distribution of $\underline{H}$ is known theoretically only in the case of a narrow spectrum, $\nu = 1$, when it is of the Rayleigh type. The

applicability of the Rayleigh distribution to the heights of sea waves seems to have been first suggested by Barber [82]. Longuet-Higgins [57] gave an outline of the arguments underlying the assumption of a Gaussian model for the wave motion, and the conditions for the spectrum to be narrow, as well as numerous relationships between characteristic parameters of the Rayleigh distribution and of the distribution of the largest wave height in a finite sample.

The Rayleigh distribution for $\underline{H}$ can be written as

$$\begin{aligned} F(H) &= 0 && \text{for } H < 0 \\ &= 1 - e^{-\frac{\pi}{4}(H/\overline{H})^2} && \text{for } H \geq 0 \end{aligned} \qquad (4.4.21)$$

in which

$$\overline{H} = E\{\underline{H}\} \quad . \qquad (4.4.22)$$

The root-mean-square wave height (H_{rms}) is related to the standard deviation of $\underline{\zeta}(t)$ and to $\overline{H}$ as follows:

$$H_{rms} \overset{\text{def}}{=} (E\{\underline{H}^2\})^{\frac{1}{2}} = 2\sqrt{2}\sqrt{m_0} = \frac{2}{\sqrt{\pi}}\overline{H} \quad . \qquad (4.4.23)$$

The so-called significant wave height, which is defined as the mean value of the highest one-third fraction of the heights, is given by

$$H_{1/3} \approx 1.41\ H_{rms} \approx 4\sqrt{m_0} \quad . \qquad (4.4.24)$$

Empirical data on wave height distributions have been collected and analysed by a score of investigators. The earliest systematic efforts in this direction preceded the theoretical developments. Based on the data available at the time, most of which had been obtained with pressure recorders, Longuet-Higgins [57] concludes "In examples quoted above, the discrepancy between theory and observation is in all cases less than 8%, and in some cases it is smaller still. In view of the somewhat strict assumptions made in deriving the theoretical probability-distribution, this agreement is surprisingly close; and it may indicate that the probability-distribution does not depend very critically upon the narrowness of the wave

spectrum." The wealth of data gathered since then, both with pressure meters and with surface sensors, in swell as well as in wind-driven waves, gives strong support to Longuet-Higgins' last-mentioned statement, and confirms the applicability of the Rayleigh distribution for wave heights in general [69, 83-87]. This is particularly noteworthy because in many of the measurements the spectrum was far from narrow, and probably much wider than the spectra of the pressure records on which Longuet-Higgins' conclusions were based. For example, in most of the cases analysed by Koelé and de Bruyn [69] the value of ν^2 (also of ε^2) was between 0.4 and 0.6. Even so these authors could state "we have seen that the distributions of $\underline{H}$ and $\underset{\sim}{\zeta}_m$ are independent of the width of the energy spectrum (expressed in terms of ε). The distributions f(H) and f(η) correspond to a great extent with the formula of the Rayleigh distribution". Similarly, Goodknight and Russell [84], after analysing wave records taken in the Gulf of Mexico during hurricanes, conclude "The agreement of the theoretical and experimental values suggest that, for practical purposes, the particular statistics studied for waves generated by a distant hurricane may be approximated by a Rayleigh distribution. The results of these tests are in agreement with other work in this field. It should be emphasized that these data were collected during severe oceanographic conditions (maximum wave heights to 20 ft in a 33-ft water depth), and the data were measured with a surface sensing instrument."

The goodness-of-fit of the Rayleigh distribution to deep-water wave height data can be judged from Table 4.1, adapted from Titov [87], in which average values derived from "a large number of wave recordings taken in different seas and oceans under a large variety of meteorological conditions" are compared to values obtained from (4.4.21).

100 F($H/\overline{H}$)	1	10	20	30	40	50	60	70	80
$H/\overline{H}$, measured	0.10	0.37	0.54	0.69	0.81	0.93	1.05	1.21	1.38
$H/\overline{H}$, eq.(4.4.21)	0.11	0.37	0.53	0.67	0.81	0.94	1.08	1.24	1.43

$100\ F(H/\overline{H})$	90	95	97	98	99
$H/\overline{H}$, measured	1.69	1.91	2.10	2.28	2.52
H/H, eq.(4.4.21)	1.71	1.95	2.11	2.23	2.42

Table 4.1

The table illustrates the fact that the Rayleigh distribution gives an excellent description of the short-term wave height variability. This is in strong contrast with the dictum "The basic law of the seaway is the apparent lack of any law", which, interestingly enough, is due to Rayleigh himself [30]. (Rayleigh derived the distribution named after him for the intensity of sound consisting of a large number of components of the same frequency in random phases [61]. It took almost 70 years before it was realized that under certain circumstances a similar model applied to wind waves.)

The empirical fact that the zero-crossing wave heights are to a good approximation Rayleigh distributed, even if the waves are definitely nonlinear and do not possess a narrow spectrum, calls for an explanation. The nonlinearity of the waves gives rise to higher crests, but also to higher troughs. The wave height is only slightly affected by this since it is measured from crest to trough. The fact that the spectral width appears to have no measurable influence on the distribution of $\underline{H}$ can probably be explained with reference to the crest heights, which were shown theoretically and empirically to be approximately Rayleigh distributed. The only additional assumption required is that the crest height, defined as the largest maximum between successive zero-crossings, is strongly correlated with the immediately following largest trough depth between successive zero-crossings. This assumption is rejected by Jahns and Wheeler [88], who point out that for a wide spectrum a relatively high crest is on the average followed by a not-so-deep trough. This would be the case for a purely Gaussian process, quite apart from hydrodynamical nonlinearities. The use of a Rayleigh distribution for $\underline{H}$ would therefore, according to these authors, result in an overestimation of the probability of exceedance for the relatively high waves, if the spectrum is not narrow.

It is difficult to establish empirically whether the effect mentioned above is real in wind waves, because to do so would require long-lasting records in stationary conditions in order to obtain statistically significant results at the low levels of probability under consideration. This applies also to the effects of wave breaking. This phenomenon occurs so infrequently in deep water that it does not have an appreciable influence on the measured distributions for the short sample lengths which are commonly used (typically 100 to 200 waves). Svasek [86] reports that "The wave recordings of limited duration, e.g. 30 min., at some stations in the shallow part of the North Sea show only small deviations of the extreme values of wave heights from the Rayleigh distribution." The wave heights at the exceedance probability level of 0.5% were found to be "almost never" more than 15% greater or 10% smaller than the corresponding heights obtained from the Rayleigh distribution. In this regard it is also pertinent to note that theoretical predictions concerning the largest crest height in a finite sample have been well verified empirically, as shown by Cartwright [59], who states "one may justifiably suspect that non-linearities might become important for the largest waves considered in a theory of extreme values. But the satisfactory results of measurements shown ... confirm that the assumed representation still holds good well into the tail of the probability distribution." The data on which this conclusion is based were obtained with a shipborne wave recorder. The data derived from surface sensors at a fixed point should under the same conditions have a wider spectrum as well as stronger nonlinearities. Yet also for such measurements there is agreement with predictions concerning the largest wave height, based on an assumed Rayleigh distribution for the individual wave heights [73, 84]. This was the case even in hurricane waves, where the theory is put to a severe test. The inevitable conclusion is that the short-term probability distribution of wave heights is not significantly affected by wave breaking, at least in deep water. The situation in this regard is of course quite different in shallow water where the larger wave heights may be of the same order of magnitude as the water depth. This case will be considered in chapter 5.

4.4.8 Distribution of the largest wave height in a record

The distribution function of the largest wave height in a finite sample has been derived by Longuet-Higgins [57]. Consider an ensemble of records, each containing N wave heights. If the records contain at least a few wave groups, then the N realizations of the wave height $\underline{H}$ in each record can be considered as N independent random samples from a universe of wave heights. The probability that the height $\underline{H}$ shall not exceed a value H is given by F(H). The probability that all of the N heights in a record shall not exceed H is then given by $\{F(H)\}^N$. It is equal to the probability that the maximum wave height in the record, denoted by $\underline{H}_{max}$, shall not exceed H:

$$F_N(H) \equiv \Pr\{\underline{H}_{max} \leq H\} = \{F(H)\}^N \quad . \tag{4.4.25}$$

Expressed in terms of the probability of exceedance of $\underline{H}$,

$$Q(H) = 1 - F(H) \quad , \tag{4.4.26}$$

(4.4.25) becomes

$$F_N(H) = \{1 - Q(H)\}^N \quad . \tag{4.4.27}$$

For large N, $F_N(H)$ is vanishingly small unless Q(H) is of order N^{-1}. Therefore only relatively large values of H are of interest. Eq. (4.4.27) then approximates to

$$F_N(H) = e^{-NQ(H)} \quad . \tag{4.4.28}$$

Substitution of the Rayleigh distribution for $\underline{H}$ gives

$$F_N(H) = e^{-Ne^{-\frac{\pi}{4}(H/\overline{H})^2}} \quad . \tag{4.4.29}$$

The expected value of $\underset{\sim}{H}_{max}$ has been calculated from this distribution function by Longuet-Higgins [57], with the result

$$E\{\underset{\sim}{H}_{max}\} \approx \frac{2}{\sqrt{\pi}} \overline{H} \{(\ell n\ N)^{\frac{1}{2}} + 0.29(\ell n\ N)^{-\frac{1}{2}}\} \quad , \qquad (4.4.30)$$

which is valid for N > 20 approximately. Empirical data are in good agreement with this theory [57, 73, 84].

The distribution of the largest maximum ($\underset{\sim}{\xi}_{m_{max}}$) has been considered by Cartwright [59], who uses the approximate form of the probability of exceedance of $\underset{\sim}{\xi}_m$ given by (4.4.18), which, apart from the constant factor N/N_m, equals the probability of exceedance according to the Rayleigh distribution. The resulting distribution function of $\underset{\sim}{\xi}_{m_{max}}$ is therefore equal to the one derived by Longuet-Higgins for $\frac{1}{2}\underset{\sim}{H}_{max}$, provided the number of maxima (N_m) is replaced by the number of upward zero-crossings (N).

4.5 Empirical data for wind-driven waves

It will be assumed in the applications to be given in the following chapters that the incident waves at some point offshore are known in terms of parameters such as the two-dimensional spectrum and the joint distribution of zero-crossing wave heights and -periods. No specific functions will be postulated à priori for these parameters, with the exception of the marginal distribution of the wave heights, which can be assumed to be of the Rayleigh type without great loss of generality. Both the two-dimensional spectrum and the distribution of the wave periods can vary between wide limits so that no generally applicable functions can be given. They could almost be chosen at will if quantitative evaluations would be required. However, it is preferred to choose somewhat realistic conditions for the cases to be worked out analytically or numerically. These conditions will be chosen to correspond to wind-driven waves in a more or less stationary and homogeneous wind field. It is for this purpose that some empirical data concerning wind-driven waves are presented in this section.

4.5.1 Directional spectra

Directional spectra are difficult to measure, and detailed data are correspondingly scarce. We shall present some of the results.

The directional spectrum $D(\theta;\omega)$ is defined by the eqs. (4.3.14) and (4.3.15). The angle θ will be measured from the mean direction of propagation. The parameters appearing in the analytical expressions for $D(\theta;\omega)$ to be presented do not depend on θ; they may depend on ω. The coefficients are determined so as to agree with

$$\int_{-\pi}^{\pi} D(\theta;\omega)d\theta = 1 \qquad (4.5.1)$$

for all ω.

St.Denis and Pierson [89] propose the equation

$$D_1(\theta;\omega) = D_1(\theta) = \frac{2}{\pi}\cos^2\theta \quad \text{for} \quad |\theta| \leq \frac{\pi}{2} \qquad (4.5.2)$$
$$= 0 \qquad \text{otherwise.}$$

This result seems to have been inferred from observed angular spreading of swell.

Titov [87] presents a result which in appearance is very similar to (4.5.2), but it applies to a differently defined quantity. He considers what could properly be described as a marginal directional spectral density,

$$D'(\theta) = \int_0^{\infty} G(\omega,\theta)d\omega \quad , \qquad (4.5.3)$$

as opposed to the conditional density defined by (4.3.14-15). Titov states that in the open sea $D'(\theta)$ varies as $\cos^2\theta$. This is based on stereophotographs of the sea surface. The result given by Titov is of course implied by (4.5.2), but the reverse is not necessarily true. However, it does give indirect support to the validity of (4.5.2), at least in the frequency band which contributes most to the variance.

Various authors have proposed an equation similar to (4.5.2) but with different exponents:

$$D_2(\theta;\omega) = B_2(\cos\theta)^m \quad \text{for} \quad |\theta| \leq \frac{\pi}{2}$$
$$= 0 \quad \text{otherwise.} \tag{4.5.4}$$

In view of (4.5.1), the coefficient B_2 is given by

$$B_2 = \{I(m)\}^{-1} \quad , \tag{4.5.5}$$

in which

$$I(m) = \int_{-\frac{\pi}{2}}^{\frac{\pi}{2}} (\cos\theta)^m \, d\theta = \sqrt{\pi}\,\frac{\Gamma(\frac{1}{2}m + \frac{1}{2})}{\Gamma(\frac{1}{2}m + 1)} \quad , \; (m > -1) \quad , \tag{4.5.6}$$

where $\Gamma(.)$ is the gamma function [90], defined by

$$\Gamma(x) = \int_0^\infty t^{x-1} e^{-t} \, dt \qquad \text{for } x > 0$$
$$\Gamma(x+1) = x\,\Gamma(x) \quad \text{for } x \neq 0,-1,-2,.... \tag{4.5.7}$$

Two useful particular cases of (4.5.7) are

$$\Gamma(1) = 1 \tag{4.5.8}$$

and

$$\Gamma(\tfrac{1}{2}) = \sqrt{\pi} \quad . \tag{4.5.9}$$

The International Ship Structures Congress Committee on Environmental Conditions [91] recommends (4.5.4) with m = 4, but some of its data represented swell, which of course has a narrower angular distribution of the energy than wind-driven waves. Moreover, its choice for the exponent m was deliberately on the high side because this was considered to be the safe side for the applications envisaged. The distribution measured by Barber [92] is approximately proportional to

$\cos^4\theta$ [93], but "it is not expected that (this result) will apply to open water", where the distribution can be expected to be broader, "because the fetch in the wind direction was much greater than elsewhere". It appears then that if (4.5.4) is used as a representation of the directional spectrum of wind-driven waves, the exponent m should be nearer to 2 than to 4.

The data available at the time when (4.5.2) was proposed (1953) did not permit to formulate a variation of D with ω. Later investigations have shown that the width of the angular energy distribution increases with increasing frequency. The first clear evidence of this came from the analysis of stereophotographs of the sea surface in a project named SWOP [93], which provided the basis for the equation

$$\begin{aligned} D_3(\theta;\omega) &= \frac{1}{\pi}\,(A_0 + A_2\cos^2\theta + A_4\cos^4\theta) && \text{for } |\theta| \leq \tfrac{\pi}{2} \\ &= 0 && \text{otherwise,} \end{aligned} \qquad (4.5.10)$$

in which

$$\begin{aligned} A_0 &= \tfrac{1}{2}\,(1 - C) \quad , \\ A_2 &= 1 - 0.92\,C \quad , \\ A_4 &= 2.56\,C \quad , \end{aligned} \qquad (4.5.11)$$

where

$$C = \exp\{-\tfrac{1}{2}(\frac{\omega W}{g})^4\} \quad , \qquad (4.5.12)$$

and W is the mean wind speed at anemometer height (15 ft above sea level). The peak of the frequency spectrum was at $\omega = \hat{\omega} \approx 0.85\ g/W$. The distribution (4.5.10-12) is wider than (4.5.2) at high frequencies, and narrower at low frequencies. Cote et al [93] state that this "would appear to give more realistic swell forecasts than previously used formulas" (i.e., than eq. 4.5.2).

Longuet-Higgins et al [94] have fitted the following function to their data, which had been obtained with a pitch and-roll buoy:

$$D_4(\theta;\omega) = B_4 \ (\cos \tfrac{1}{2}\theta)^{2s} \quad , \tag{4.5.13}$$

with

$$B_4 = \{2I(2s)\}^{-1} = \frac{1}{2\sqrt{\pi}} \frac{\Gamma(s+1)}{\Gamma(s+\frac{1}{2})} \quad . \tag{4.5.14}$$

The exponent s is in general a decreasing function of ω; this is qualitatively in agreement with (4.5.10-12).

Krylov et al [95] have proposed a directional spectrum as in (4.5.4), with

$$m \underset{\sim}{\propto} 2\hat{\omega}/\omega \quad . \tag{4.5.15}$$

This distribution broadens with increasing frequency; it agrees with (4.5.2) at the peak of the frequency spectrum. The fact that (4.5.4) would apply with m inversely proportional to ω has also been noted by St.Denis [96], based on the data of Longuet-Higgins et al [94].

4.5.2 Frequency spectra

The first empirical formula for a one-dimensional spectrum of fully developed wind waves on deep water has been given by Neumann [97]. It can be written as

$$S(\omega) = 0.025 \ g^2 \ \omega^{-6} \exp\{-2(\frac{\omega W}{g})^{-2}\} \quad , \tag{4.5.16}$$

in which W is the average wind velocity at 7.5m above sea level. The coefficient 0.025 has the dimension $[s^{-1}]$. The Neumann spectrum is mainly based on visual wave observations. Strekalov [98] proposes a spectrum similar to Neumann's, that is to say, with the same exponents of ω.

Pierson and Moskowitz [99] have given the following spectrum for fully developed waves in deep water:

$$S(\omega) = \beta_1 \, g^2 \, \omega^{-5} \exp \{- \beta_2 (\frac{\omega W}{g})^{-4}\} \qquad (4.5.17)$$

with

$$\beta_1 = 8.10^{-3} \quad , \quad \beta_2 = 0.74 \quad . \qquad (4.5.18)$$

W is the mean wind velocity at 19.5m above sea level. The Pierson-Moskowitz spectrum is based on measurements made in the North Atlantic Ocean with a ship-borne wave recorder. A spectrum similar to (4.5.17) has been given by Davidan [100], based on measurements in the Barents Sea and in the Atlantic.

It may be seen that for high frequencies the spectral density in the Pierson-Moskowitz spectrum is proportional to $g^2 \, \omega^{-5}$, with a dimensionless coefficient of proportionality. That this should be so had been inferred on dimensional grounds by Phillips [101]. He argued that breaking limits the wave growth, and that consequently there should be a range of frequencies in the spectrum of wind-driven waves in which the spectral density has reached a saturation value. This range is called the equilibrium range. The equilibrium spectral density, denoted as $S_e(\omega)$, should be independent of the wind velocity, duration, fetch, etc., and be wholly determined by the frequency and the gravitational acceleration g. (Effects of finite depth and of surface tension and viscosity are not considered.) On dimensional grounds the equilibrium spectrum should then be given by

$$S_e(\omega) = \beta \, g^2 \, \omega^{-5} \quad , \qquad (4.5.19)$$

in which β is a dimensionless constant. However, it has been found that the coefficient β is not actually a constant but that it decreases with increasing values of the dimensionless fetch F, defined by

$$F^* = \frac{gF}{W^2} \quad , \qquad (4.5.20)$$

in which F is the (dimensional) fetch and W is the mean wind velocity. Strekalov et al [102] report measured β-values from approximately 1.4×10^{-2} at $F^* = 10^2$, to 0.6×10^{-2} at $F^* = 4 \times 10^4$.

In the examples to be given later we shall mainly use the Pierson-Moskowitz spectrum, because this is dimensionally homogeneous. While this spectrum was determined from fully developed waves, it turns out [73,91] that for many practical purposes the spectra of developing waves in simple wind fields can be considered similar to it. One then writes

$$S(\omega) = \beta\, g^2\, \omega^{-5} \exp\left\{-\frac{5}{4}\left(\frac{\hat{\omega}}{\omega}\right)^4\right\} \quad , \tag{4.5.21}$$

in which β and $\hat{\omega}$ vary with the stage of the wave growth ($\hat{\omega}$ is the frequency at which $S(\omega)$ attains its maximum). The significant wave height $H_{1/3}$ and the mean zero-crossing period $\bar{T}$ can be expressed in terms of β and $\hat{\omega}$ (or vica versa) by means of (4.4.24) and (4.4.5), which gives

$$H_{1/3} = 4\sqrt{m_0} = 4\sqrt{\frac{\beta}{5}}\, g\hat{\omega}^{-2} \tag{4.5.22}$$

and

$$\bar{T} = 2\pi\sqrt{m_0/m_2} = 2\pi\left(\frac{4}{5\pi}\right)^{\frac{1}{4}} \hat{\omega}^{-1} \quad . \tag{4.5.23}$$

If we define a wave steepness $\tilde{\delta}$ by

$$\tilde{\delta} = H_{1/3}/\tilde{L}_0 \quad , \tag{4.5.24}$$

in which $\tilde{L}_0$ is a wavelength defined by

$$\tilde{L}_0 = \frac{g\bar{T}^2}{2\pi} \quad , \tag{4.5.25}$$

then

$$\tilde{\delta} = \frac{2}{\pi g}\frac{m_2}{\sqrt{m_0}} = \sqrt{\beta/\pi} \quad . \tag{4.5.26}$$

Corresponding to the above-mentioned range of β from 1.4×10^{-2} to 0.6×10^{-2} we find $\tilde{\delta}$ in the range from 0.067 to 0.044; the wave steepness is a decreasing function of the dimensionless fetch F^*.

4.5.3 Distribution of wave periods

It has been noted in paragraph 4.4.4 that the shape of the p.d.f. of the wave period $\underline{T}$ (the time interval between successive zero-up-crossings) varies with the shape of the energy spectrum. Energy spectra of wind-driven waves are to a fair degree similar. It is therefore not unreasonable to expect the same of the corresponding p.d.f. of $\underline{T}$. Bretschneider [83] finds that $\underline{T}^2$ is approximately Rayleigh-distributed. The distribution function of $\underline{T}$ can then be written as

$$F(T) = 1 - e^{-\Gamma^4(\frac{5}{4})(T/\overline{T})^4} = 1 - e^{-0.675(T/\overline{T})^4} \qquad (4.5.27)$$

This distribution is also given by Titov [87], who presents results obtained by Vilenskii and Glukhovskii from the same data as were used for Table 4.1. A comparison of average values of these data with values obtained from (4.5.27) is given in Table 4.2. It can be seen that

$100\ F(T/\overline{T})$	1	10	20	30	40	50	60	70	80	90	95	97	98	99
$T/\overline{T}$, measured	0.44	0.66	0.76	0.85	0.93	1.00	1.07	1.15	1.23	1.37	1.47	1.52	1.57	1.65
$T/\overline{T}$, eq. 4.5.27	0.35	0.62	0.76	0.85	0.93	1.00	1.07	1.15	1.24	1.35	1.45	1.52	1.55	1.61

Table 4.2

(4.5.27) gives a very good fit indeed to the averaged data points.

Goda [80] made numerical simulations of stationary Gaussian processes with various spectra, including a Pierson-Moskowitz spectrum, as well as spectra which were much narrower or broader. The

width of F(T) was found to vary qualitatively in the same way as the width of S(ω). It is interesting to note that the calculated distribution corresponds to (4.5.27) only for the process with a Pierson-Moskowitz type spectrum.

4.5.4 Joint distribution of wave heights and periods

An empirical expression for the joint p.d. of $\underline{H}$ and $\underline{T}$ for fully developed waves has been given by Bretschneider [83]. He considered the coefficient of linear correlation of $\underline{H}$ and $\underline{T}^2$, defined by

$$\lambda = \frac{\mathrm{cov}(\underline{H},\underline{T}^2)}{\sigma_H \, \sigma_{T^2}} \quad , \qquad (4.5.28)$$

in which the numerator represents the covariance of $\underline{H}$ and $\underline{T}^2$, while σ_H and σ_{T^2} are the standard deviations of $\underline{H}$ and $\underline{T}^2$. Bretschneider found that λ varied in a systematic manner with the wave "age" (ratio of phase speed to wind speed), therefore also with the dimensionless fetch or duration of the wind, in the sense that λ tended to high values in a young sea and to zero in a fully developed sea. The joint p.d.f. of $\underline{H}$ and $\underline{T}^2$ in the latter case is given by Bretschneider as the product of the marginal p.d. functions. Thus, he implicitly assumes that f(H,T) is such that zero correlation implies stochastic independence. For cases of nonzero correlation Bretschneider does not give an explicit expression for f(H,T). He states "The joint distribution of wave heights and lengths (or wave heights and periods) in general is difficult to describe completely for all conditions of correlation. ... The fact that both marginal distributions are of the same type is of some help. The bivariate asymptotic problem of joint distribution for the Rayleigh type (or a modified Rayleigh type) distribution has yet to be solved." Lacking an explicit expression for f(H,T) for arbitrary λ, Bretschneider assumed that the mutual regressions of $\underline{H}$ and $\underline{T}^2$ on each other would be linear, in order to be able to proceed. However, the bivariate Rayleigh distribution had already been defined as the joint distribution of the values (say $\underline{x}$ and $\underline{y}$) of the envelope of a narrow-band Gaussian process at two different times. It has been derived by Uhlenbeck

[103] and again by Rice [55]. The p.d.f. is

$$f(x,y) = \frac{\pi^2}{4} \frac{xy}{(\mu_x \mu_y)^2 (1-\kappa^2)} \exp\{ - \frac{\pi}{4} \frac{(x/\mu_x)^2 + (y/\mu_y)^2}{1 - \kappa^2} \}$$

$$I_0 \{ \frac{\pi \kappa}{2(1-\kappa^2)} \frac{xy}{\mu_x \mu_y} \} \quad \text{for } x \geq 0,\ y \geq 0$$

$$= 0 \text{ otherwise} \quad , \qquad (4.5.29)$$

in which $\mu_x = E\{\underline{x}\}$ and $\mu_y = E\{\underline{y}\}$, and κ^2 is the coefficient of linear correlation of $\underline{x}^2$ and $\underline{y}^2$. Further details related to the bivariate Rayleigh distribution are given in Appendix 1. We shall here only remark that without supporting data it cannot be regarded as established that the joint p.d. of $\underline{H}$ and $\underline{T}^2$ in wind-driven waves would be of the form (4.5.29), even if both marginal distributions would be perfectly of the Rayleigh type, because an infinite number of bivariate distributions can exist for a given pair of marginal distributions [104]. Thus, any use which we make of (4.5.29) as the joint p.d. of $\underline{H}$ and $\underline{T}^2$ is of a tentative nature.

5 RADIATION STRESSES

5.1 Introduction

The calculation of wave-induced longshore current velocities and changes in mean water level requires the specification of the radiation stresses as a function of location in the nearshore region, in terms of the wave properties offshore. The problem of obtaining such specifications for wind-generated waves will be dealt with in this chapter. We shall seek only approximations of lowest order. For the radiation stresses these are the second-order approximations, which can be found from a first-order wave solution. The radiation stresses can then be expressed in terms of the two-dimensional energy spectrum of the surface elevation. Outside the surf zone this spectrum can be evaluated from the given deep-water waves and the topography, using available methods of refraction computations. These methods are based on linear potential flow theory, possibly corrected for a relatively weak energy dissipation in the boundary layers. They are not applicable within the surf zone because of strong non-linearities and because of the rapid transformation of organized wave motion into turbulent motion. The estimation of the radiation stresses in the offshore region and in the surf zone will therefore be considered separately, in the sections 5.2 and 5.3 respectively.

The radiation stresses are defined as the momentum fluxes induced by the waves, averaged over a certain time interval. For a definition of this interval it is necessary to distinguish various time scales. The incident waves themselves have a characteristic period, while their overall properties may vary on a much longer time scale. The latter is supposed to be so large that the corresponding rate of change has no significant dynamic effect on the water mass in the surf zone. In other words, it is assumed that the incident waves can be considered to be statistically stationary, as far as the dynamics of the surf zone are concerned. However, there is still another time scale; nonlinear self-interactions of the incident waves give rise to motions with characteristic periods corresponding to the difference-frequencies

existing in the incident wave spectrum. These relatively slow and weak motions are appreciable only, if at all, in the surf zone ("surf beat"). Our aim is to calculate the steady part (zero-frequency component) of these motions. The fluctuating part will be averaged out. This is considered permissible because the surf beat is far weaker than the incident waves (ratio of energies per unit area is of order 10^{-2}), so that its effect on the steady part of the surf "beat" is negligible compared with that of the breaking waves. The time-averages to be used throughout the following will therefore be based on an averaging interval which is long compared with the characteristic period of the surf beat, while it should be short compared with the time scale of the variations of the statistical parameters of the incident waves.

5.2 Radiation stresses expressed in terms of the two-dimensional energy spectrum

5.2.1 General formulation

The radiation stresses in a statistically stationary and homogeneous wave field are given, to second order, by (3.3.19). Since we are at first dealing with waves in a fixed point, without a mean flow, we can temporarily omit the primes on the fluctuating quantities, and choose $\overline{\zeta} = 0$, in which case

$$S_{ij} = \int_{-d}^{0} \rho(\overline{q_i q_j} - \overline{w^2}\delta_{ij})dz + \tfrac{1}{2}\rho g\overline{\zeta^2}\delta_{ij} \quad . \qquad (5.2.1)$$

We shall represent the wave field as in paragraph 4.3.2:

$$\underline{\zeta}(x_1,x_2,t) = \sum_{\ell}\sum_{m} a_{\ell m} \cos \underline{\Psi}_{\ell m} \qquad (5.2.2)$$

with

$$\underline{\Psi}_{\ell m} = \omega_\ell t - k_\ell x_1 \cos\theta_m - k_\ell x_2 \sin\theta_m - \underline{\psi}_{\ell m}. \qquad (5.2.3)$$

The notation has been changed slightly by using x_i (i = 1,2) instead of (x,y). As in paragraph 4.3.2, the limit of (5.2.2) should be considered in which the frequencies and the directions of propagation of the spectral components are continuously distributed, and in which the spectral density $G(\omega,\theta)$ is everywhere finite.

The restriction to horizontal homogeneity precludes standing waves from the considerations. The spectral density function should therefore satisfy the relation

$$G(\omega,\theta)\ G(\omega,\ \theta + \pi) = 0 \qquad (5.2.4)$$

for all (ω,θ). A sufficient condition for (5.2.4), though not a necessary one, is that the directional spectral density is zero in a continuous interval of π radians. The empirical spectra (4.5.2), (4.5.4) and (4.5.10) satisfy this condition.

The mean products of the velocity components appearing in (5.2.1) can be expressed in terms of the two-dimensional spectrum of $\underline{\zeta}$ by applying the results from the linear theory of long-crested sinusoidal progressive waves (eqs. 3.2.16-17) to individual spectral components. This gives

$$\overline{q_i q_j} = \int_0^{\infty} \int_{-\pi}^{\pi} \{\omega \frac{\cosh k(d + z)}{\sinh kd}\}^2 e_i e_j\ G(\omega,\theta)\, d\omega\ d\theta\ , \qquad (5.2.5)$$

in which

$$(e_1,\ e_2) = (\cos\theta,\ \sin\theta)\ , \qquad (5.2.6)$$

and

$$\overline{w^2} = \int_0^{\infty} \int_{-\pi}^{\pi} \{\omega \frac{\sinh k(d + z)}{\sinh kd}\}^2 G(\omega,\theta) d\omega\ d\theta$$

$$= \int_0^{\infty} \{\omega \frac{\sinh k(d + z)}{\sinh kd}\}^2 S(\omega) d\omega\ . \qquad (5.2.7)$$

It can be seen from (5.2.7) that the mean square vertical velocity depends on $G(\omega,\theta)$ only through the frequency spectrum $S(\omega)$; it is independent of the directional energy spectrum. The same holds for the mean square modulus of the horizontal velocity vector:

$$\overline{q^2} = \overline{q_i q_i} = \int_0^\infty \int_{-\pi}^{\pi} \{\omega \frac{\cosh k(d+z)}{\sinh kd}\}^2 (\cos^2\theta + \sin^2\theta)\, G(\omega,\theta)\, d\omega\, d\theta$$

$$= \int_0^\infty \{\omega \frac{\cosh k(d+z)}{\sinh kd}\}^2 S(\omega) d\omega \quad . \tag{5.2.8}$$

Substitution of (5.2.5) and (5.2.7) into (5.2.4) gives

$$S_{ij} = \rho \int_{-d}^{0} \int_0^\infty \int_{-\pi}^{\pi} \omega^2 \{ \frac{\cosh^2 k(d+z)}{\sinh^2 kd} e_i e_j -$$

$$- \frac{\sinh^2 k(d+z)}{\sinh^2 kd} \delta_{ij} \} G(\omega,\theta) dz\, d\omega\, d\theta +$$

$$+ \tfrac{1}{2} \rho g \overline{\zeta^2} \delta_{ij} \quad . \tag{5.2.9}$$

Performing the integration with respect to z, and substituting

$$\overline{\zeta^2} = \int_0^\infty \int_{-\pi}^{\pi} G(\omega,\theta) d\omega\, d\theta = \int_0^\infty S(\omega) d\omega = \frac{E}{\rho g} \quad , \tag{5.2.10}$$

gives

$$S_{ij} = \rho g \int_0^\infty \int_{-\pi}^{\pi} \{n\, e_i e_j + (n - \tfrac{1}{2})\delta_{ij}\} G(\omega,\theta) d\omega\, d\theta \quad , \tag{5.2.11}$$

where n is given by (3.2.23). Eq. (5.2.11) could have been written down at once, in view of (3.3.20) and the definition of $G(\omega,\theta)$. It was preferred to give a more detailed derivation because some of the intermediate results will be needed in what follows. Eq. 5.2.11 will be written in abbreviated form as

$$S_{ij} = E\{\overline{\overline{n\, e_i e_j}} + (\overline{\overline{n}} - \tfrac{1}{2})\delta_{ij}\} \quad , \tag{5.2.12}$$

in which the double overbar denotes an average over frequency and direction of propagation, weighted with the spectral density:

$$\overline{\overline{f(\omega,\theta)}} \overset{\text{def}}{=} \frac{\int_0^\infty \int_{-\pi}^{\pi} f(\omega,\theta)G(\omega,\theta)d\omega\, d\theta}{\int_0^\infty \int_{-\pi}^{\pi} G(\omega,\theta)d\omega\, d\theta} \tag{5.2.13}$$

For later reference, the components of S_{ij} are written explicity:

$$S_{11} = E(\overline{\overline{n\cos^2\theta}} + \overline{\overline{n}} - \tfrac{1}{2}) \quad , \tag{5.2.14}$$

$$S_{22} = E(\overline{\overline{n\sin^2\theta}} + \overline{\overline{n}} - \tfrac{1}{2}) \quad , \tag{5.2.15}$$

and

$$S_{12} = S_{21} = E(\overline{\overline{n\sin\theta\cos\theta}}) \quad . \tag{5.2.16}$$

5.2.2 Effects of short-crestedness on the radiation stresses

Prior to the development of suitable statistical theories for the description of wind-generated waves it was customary to deal with these waves on the basis of a periodic, unidirectional wave train which was, or was assumed to be, equivalent to the irregular ones with respect to a few mean properties, such as the mean energy, period and direction of propagation. Needless to say, the elementary substitute-waves differ from the more complicated ones in other respects. The errors incurred by the use of a so-called equivalent wave may be acceptable for certain purposes. However, usually no explicit justification is given for applying this approximation. The fact that this method in one form or another has persisted up to the present time is reason to inquire into the errors which may arise from its use for the calculation of S_{ij}. Particular attention will thereby be given to the

effects of short-crestedness, for the following reason [105]. The radiation stresses are proportional to the mean wave energy per unit area, E. In unidirectional waves, the coefficients of proportionality depend on $\bar{n}$ only, which in deep water and in shallow water is the same for periodic waves as it is for waves with a continuous frequency spectrum. Lumping the energy in one frequency therefore does not affect the radiation stresses in these cases. The situation is quite different with respect to the directional spectrum, which we will therefore consider in more detail.

We shall initially deal with the principal values of the radiation stress tensor S_{ij}. The x_1- and x_2-axes can without loss of generality be chosen to be the principal axes of S_{ij}, in which case S_{11} and S_{22}, given by (5.2.14) and (5.2.15), are the principal stresses. If the directional spectrum is symmetric about a mean direction which is common to all the frequencies then this direction defines one of the principal axes of S_{ij}, say the x_1-axis. S_{11} will then be the largest principal stress, for typical forms of the energy spectrum.

The effect of the short-crestedness of the waves on the magnitudes of the radiation stresses will be examined by comparing the values of S_{11} and S_{22} in the given, short-crested wave system, with energy spectrum $G(\omega,\theta) = S(\omega)D(\theta;\omega)$, to the values in a unidirectional wave system with the same frequency spectrum $S(\omega)$ and with a direction of propagation perpendicular to the plane across which the largest principal radiation stress acts in the short-crested waves. The energy spectrum of this second system, written as $G^*(\omega,\theta)$, is therefore given by

$$G^*(\omega,\theta) = S(\omega)\delta(\theta) \quad . \tag{5.2.17}$$

Since the two wave systems considered differ only in the directional distribution of the energy, they have the same value of the mean square modulus of the horizontal particle velocity at each depth. The mean square horizontal velocity components in the direction of the x_1- and x_2-axes are $(\overline{q_1^2}, \overline{q_2^2})$ and $(\overline{q^2},0)$ for the short-crested and

the long-crested waves, respectively, in which $\overline{q^2} = \overline{q_1^2} + \overline{q_2^2}$. Thus, the principal radiation stresses in the substitute wave system are given by

$$S_{11}^{*} = \int_{-d}^{0} \rho(\overline{q^2} - \overline{w^2})dz + \tfrac{1}{2}\rho g\overline{\zeta^2} = E(2\bar{\bar{n}} - \tfrac{1}{2}) \qquad (5.2.18)$$

and

$$S_{22}^{*} = \int_{-d}^{0} \rho(-\overline{w^2})dz + \tfrac{1}{2}\rho g\overline{\zeta^2} = E(\bar{\bar{n}} - \tfrac{1}{2}), \qquad (5.2.19)$$

as compared to

$$S_{11} = \int_{-d}^{0} \rho(\overline{q_1^2} - \overline{w^2})dz + \tfrac{1}{2}\rho g\overline{\zeta^2} = E(\overline{\overline{n\cos^2\theta}} + \bar{\bar{n}} - \tfrac{1}{2}) \qquad (5.2.20)$$

and

$$S_{22} = \int_{-d}^{0} \rho(\overline{q_2^2} - \overline{w^2})dz + \tfrac{1}{2}\rho g\overline{\zeta^2} = E(\overline{\overline{n\sin^2\theta}} + \bar{\bar{n}} - \tfrac{1}{2}) \qquad (5.2.21)$$

in the short-crested waves. The absolute value of the differences is

$$\Delta = S_{11}^{*} - S_{11} = S_{22} - S_{22}^{*} = \int_{-d}^{0} \rho\overline{q_2^2}\, dz = E(\overline{\overline{n\sin^2\theta}}) \quad . \qquad (5.2.22)$$

The relative error in the horizontal velocity-square term in S_{11} is

$$\delta = \frac{\int_{-d}^{0} \overline{q_2^2}\, dz}{\int_{-d}^{0} \overline{q_1^2}\, dz} = \frac{\overline{\overline{n\sin^2\theta}}}{\overline{\overline{n\cos^2\theta}}} \quad , \qquad (5.2.23)$$

which in deep water reduces to

$$\delta' = \frac{\overline{\overline{\sin^2\theta}}}{\overline{\overline{\cos^2\theta}}} = \frac{\overline{\overline{\sin^2\theta}}}{1 - \overline{\overline{\sin^2\theta}}} \quad . \qquad (5.2.24)$$

The relative error in S_{11} itself is

$$\delta_1 = \frac{S_{11}^* - S_{11}}{S_{11}} = \frac{\Delta}{S_{11}} = \frac{\overline{\overline{n \sin^2\theta}}}{\overline{\overline{n \cos^2\theta}} + \overline{n} - \frac{1}{2}} \quad , \qquad (5.2.25)$$

which in deep water reduces to $\delta_1' = \delta'$. The relative error in the smallest principal stress is

$$\delta_2 = \frac{S_{22}^* - S_{22}}{S_{22}} = -\frac{\Delta}{S_{22}} = -\frac{\overline{\overline{n \sin^2\theta}}}{\overline{\overline{n \sin^2\theta}} + \overline{n} - \frac{1}{2}} \quad , \qquad (5.2.26)$$

which in deep water reduces to

$$\delta_2' = -1 \quad . \qquad (5.2.27)$$

The radiation shear stress across a vertical plane inclined at an angle α to the x_1-axis is given by

$$\tau_\alpha = \tfrac{1}{2}(S_{11} - S_{22}) \sin 2\alpha \quad , \qquad (5.2.28)$$

which is proportional to the difference between the largest and the smallest principal stress. It follows that an overestimation of S_{11} and an underestimation of S_{22} will give rise to relatively large errors in the calculated value of τ_α. The shear stress in the substitute waves is

$$\tau_\alpha^* = \tfrac{1}{2}(S_{11}^* - S_{22}^*) \sin 2\alpha \quad , \qquad (5.2.29)$$

which has a relative error

$$\delta_\tau = \frac{\tau_\alpha^* - \tau_\alpha}{\tau_\alpha} = \frac{2\,\overline{\overline{n \sin^2\theta}}}{\overline{n} - 2\,\overline{\overline{n \sin^2\theta}}} \quad . \qquad (5.2.30)$$

In deep water this reduces to

$$\delta_\tau' = \frac{2\,\overline{\overline{\sin^2\theta}}}{1 - 2\,\overline{\overline{\sin^2\theta}}} = \frac{2\delta'}{1 - \delta'} \quad . \qquad (5.2.31)$$

Numerical evaluation. - It appears from the preceding equations that the relative effects of the short-crestedness on the radiation stresses in deep water are wholly determined by $\overline{\sin^2\theta}$. We shall calculate this value for a few typical spectra of wind-driven waves.

The definition of $\overline{\sin^2\theta}$ can be written as

$$\overline{\sin^2\theta} = \frac{\int_0^\infty \left[\int_{-\pi}^{\pi} \sin^2\theta \; D(\theta;\omega) d\theta \right] S(\omega) d\omega}{\int_0^\infty S(\omega) d\omega} \quad . \tag{5.2.32}$$

The factor in the brackets is the average of $\sin^2\theta$ over the directions of propagation at a fixed frequency; if the directional distribution of energy is independent of the frequency then it also represents $\overline{\sin^2\theta}$. It will be calculated first, for the directional spectra described by (4.5.2), (4.5.4) and 4.5.10).

For the spectra given by (4.5.4) we have

$$\int_{-\pi}^{\pi} \sin^2\theta \; D_2(\theta;\omega) d\theta = \{I(m)\}^{-1} \int_{-\frac{\pi}{2}}^{\frac{\pi}{2}} (1 - \cos^2\theta) \cos^m\theta \; d\theta = \tag{5.2.33}$$

$$= 1 - \frac{I(m+2)}{I(m)} = (m+2)^{-1} \quad .$$

in which I(m) is defined by (4.5.6). If m is independent of ω then

$$\overline{\sin^2\theta} = (m+2)^{-1} \quad . \tag{5.2.34}$$

Putting m = 2, as in (4.5.2), we find $\overline{\sin^2\theta} = 0.25$. If m is variable, as in (4.5.15), then the average value of $\{m(\omega) + 2\}^{-1}$ has to be determined, weighted with $S(\omega)$. This average has been calculated numerically for a spectrum of the Pierson-Moskowitz type (eq. 4.5.21), with the result $\overline{\sin^2\theta} = 0.30$. Using the SWOP spectrum (4.5.10) gives

$$\int_{-\pi}^{\pi} \sin^2\theta \; D_3(\theta;\omega) d\theta = 1 - \tfrac{1}{2}A_0 - \frac{3}{8} A_2 - \frac{5}{16} A_4 \quad , \tag{5.2.35}$$

which becomes, upon substitution of (4.5.11) and (4.5.12),

$$\int_{-\pi}^{\pi} \sin^2\theta \; D_3(\theta;\omega)d\theta = 0.375 - 0.205 \exp\{-\tfrac{1}{2}(\tfrac{\omega W}{g})^4\} . \quad (5.2.36)$$

The average of this quantity over the frequencies, using the Pierson-Moskowitz spectrum (4.5.17) as a weighting function, equals

$$\overline{\overline{\sin^2\theta}} = 0.375 - 0.205 \sqrt{2\beta_2}\, K_1(\sqrt{2\beta_2}) \approx 0.27 \quad (5.2.37)$$

in which K_1 is the modified Bessel function of the third kind of order zero.

The three values of $\overline{\overline{\sin^2\theta}}$ calculated from the above-mentioned spectra for wind-driven waves are in fair agreement. Substituting the lowest and the highest calculated values, 0.25 and 0.30, in (5.2.24) and (5.2.31), we find $\delta' = \delta_1' \approx 0.33$ to 0.43 and $\delta_\tau' = 1.0$ to 1.5, which means that the radiation shear stress in wind-driven deep-water waves can be overestimated by 100% to 150% if the waves are assumed to be long-crested. This is noteworthy particularly in view of the importance of this shear stress to the generation of longshore currents in the surfzone.

The preceding equations for the radiation stresses in deep-water are illustrated by means of Mohr circles in fig. 5.1 for an assumed value of $\overline{\overline{\sin^2\theta}} = 0.25$ ($\delta_1' = 1/3$, $\delta_\tau' = 1$).

Comparison with measurements. - The preceding calculations were based on theoretical relations between the fluctuating velocity field and the surface motion, applied to idealised empirical spectra. It would be interesting to have a direct check on the order of magnitude of the results. To this end measurements of horizontal particle velocities at various depths in wind-driven deep-water waves would be required, from which the vertically-integrated horizontal convection of horizontal momentum could be calculated. Such measurements are not known to the author. The situation is slightly better if we relax the conditions on the empirical data and are satisfied with measurements at one or two

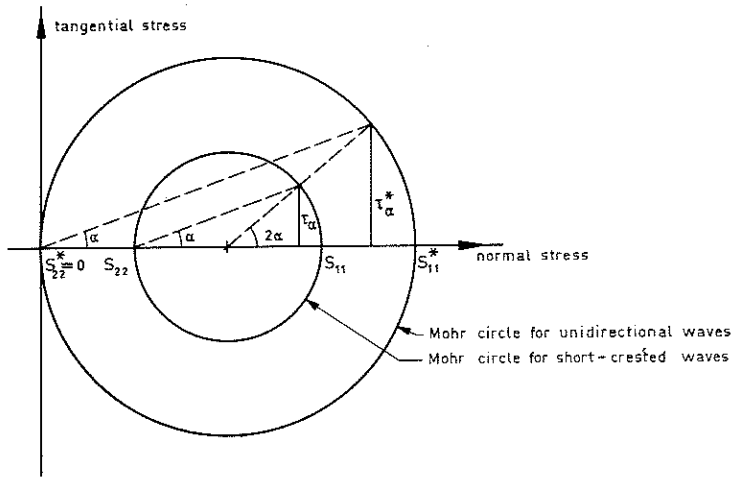

Fig. 5.1 - Mohr circles for the radiation stresses in long-crested and short-crested waves, for an assumed value $\overline{\sin^2\theta} = 0.25$ $(S_{11}/S^*_{11} = 0.75)$.

points in a vertical, not necessarily in deep water. Nagata [106] has presented some results obtained near the bottom in fairly shallow water subject to incident waves from deep water. Velocity data were collected successively at various points, with mean depths ranging from only 2m to approximately 10m. The mean period was about 7s while the mean wave height varied from 0.4m to 0.8m. The effects of refraction were considerable. These generally tend to narrow the angular distribution of energy as the waves move into shallower water with more or less parallel depth contours. However, because of the somewhat irregular topography the angular width of the spectrum was found to increase shoreward in a number of areas. These will not be considered further. Three of the measuring locations were in an area with nearly straight and parallel depth contours. It is useful to consider the results in these points in more detail since they should give a lower bound to the deep-water values of the short-crestedness

which occurred.

Simultaneous values of horizontal particle velocities in two mutually perpendicular directions were obtained by Nagata; these will be denoted by $u_1(t)$ and $u_2(t)$. The principal values of the tensor $\overline{u_i u_j}$ (i.e., $\overline{u^2}\big|_{max}$ and $\overline{u^2}\big|_{min}$, considering $\overline{u^2}$ as a function of its azimuth) can be calculated from these data according to

$$\overline{u^2}\Big|_{max},\ \overline{u^2}\Big|_{min} = \tfrac{1}{2}\left[\overline{u_1^2} + \overline{u_2^2}\right] \pm \tfrac{1}{2}\left[(\overline{u_1^2} - \overline{u_2^2})^2 + 4\,\overline{u_1 u_2}^2\right]^{\frac{1}{2}} . \tag{5.2.38}$$

The parameter Γ defined by

$$\Gamma^2 = \frac{\overline{u^2}\Big|_{min}}{\overline{u^2}\Big|_{max}} \tag{5.2.39}$$

is a quantitative measure of the short-crestedness. It can range from 0 in a unidirectional wave train to 1 in waves which are horizontally isotropic.

The value of Γ^2 is closely related to the relative error (δ) in the velocity contributions to the largest principal stress, which would result from assuming the waves to be unidirectional. This error has been defined in (5.2.23). The velocity components q_1 and q_2 appearing in this equation were referred to the principal axes of S_{ij}, which implies that (5.2.23) can be written as

$$\delta = \frac{\left[\int_{-d}^{0} \overline{u^2}\,dz\right]_{min}}{\left[\int_{-d}^{0} \overline{u^2}\,dz\right]_{max}} . \tag{5.2.40}$$

The resemblance of Γ^2 and δ is evident from the eqs. (5.2.39) and (5.2.40), but so is their difference. The parameter δ is defined in terms of a vertically integrated quantity, whereas Γ^2 is defined as

a function of the vertical coordinate z. They are equal only, for arbitrary values of z, if Γ^2 is independent of z. This cannot be expected to be the case, for the rate of attenuation of the wave motion with distance below the surface increases with increasing frequency, and higher-frequency spectral components have a broader angular distribution of energy than lower-frequency components. The net effect is that the directional spectrum narrows with depth below the surface. It is therefore expected that Γ^2 will be larger than δ near the surface and less than δ near the bottom.

The preceding arguments are based on an assumed velocity field which is fully coherent with the surface motion. In measurements at sea, turbulence can also contribute to the variances of the velocity. This will in general decrease the relative differences between $\overline{u^2}\Big|_{max}$ and $\overline{u^2}\Big|_{min}$, because the turbulence is more nearly isotropic than the waves.

With the above-mentioned reservations in mind we can compare the measured values of Γ^2 with the calculated values of δ. The measurements reported by Nagata were performed in waves wich had been generated in deep water by a local storm, but the observations were made "after the storm had almost subsided". On the day following the storm, values of Γ of 0.58 and 0.41 were measured at two points with depths of 10.1 m and 5.7 m respectively. The next day a value of 0.34 was measured at the 5.2 m contour. The decrease of the angular width of the energy spectrum is ascribed by Nagata to the greater distance of the storm from the measuring site. The three values of Γ^2, 0.34, 0.17 and 0.12, can be compared with the calculated values of δ', which ranged from 0.33 to 0.43. It is to be remembered that the measurements should give a lower bound on δ', because the calculations were done for wind-driven waves in deep water, while the measurements were made in waves which had at least partly transformed into swell, and which moreover had refracted considerably. It would therefore appear that the calculated value of δ' of 0.33 is not unrealistically high. A similar conclusion can be derived from more recent measurements by Yefimov and Khristoforov [107] in deep water in the Black Sea. The

results presented by them which are of use for our present purpose are given in the first six columns of Table 5.1. Values of $\overline{u^2}\big|_{max}$ and $\overline{u^2}\big|_{min}$ were calculated from these data using eq. (5.2.38). The results as well as their ratios are given in the last three columns of the Table. With the same reservations as mentioned above , the

z	$\hat{\omega}$	$\overline{\zeta^2}$	$\overline{u_1^2}$	$\overline{u_1 u_2}$	$\overline{u_2^2}$	$\overline{u^2}\big\|_{max}$	$\overline{u^2}\big\|_{min}$	Γ^2
(m)	(rad s^{-1})	(cm^2)	($cm^2 s^{-2}$)	($cm^2 s^{-2}$)	($cm^2 s^{-2}$)	($cm^2 s^{-2}$)	($cm^2 s^{-2}$)	-
-1.25	1.51	515	340	39	150	348	142	0.41
-1.25	1.92	315	290	39	200	285	205	0.72
-2.50	1.92	315	160	17	70	162	68	0.42

Table 5.1

measured values of Γ^2 can be compared with the calculated values of δ'. The second of the measured values is quite high. It cannot be explained on the basis of known directional properties of single wind-driven wave systems. The paper by Yefimov and Khristoforov suggests that such waves in fact prevailed during the measurements. The first and the third value of Γ^2 are in the upper calculated range of δ'. On the whole the data indicate that the computed values of $\overline{u^2}\big|_{min}/\overline{u^2}\big|_{max}$ are not too high. This in turn means that the relative errors in the radiation stresses in wind-driven deep-water waves, due to the use of "equivalent" unidirectional waves, would be at least as large as indicated by the calculations.

5.3 Radiation stresses in the surf zone

5.3.1 Introduction

The aim of this section is to establish a procedure with which the radiation stresses can be calculated in the surf zone of wind-

generated waves. The approximations which will have to be made for this purpose are necessarily cruder than those employed in the preceding section, which dealt with the waves outside the surf zone. Needless to say, the approximations should be such that those features of the physical phenomena are incorporated in the computational model which are deemed essential for the purpose at hand. In making such approximations we are guided by a general, qualitative knowledge of the problem, by a theoretical and empirical quantitative knowledge of statistical properties of non-breaking waves, by some empirical knowledge concerning the breaking of periodic waves, and by the knowledge that the breaking of an individual wave in a random wave field is qualitatively similar to the breaking of individual waves in a periodic-wave train. This similarity pertains both to the mode of breaking (plunging, spilling) and to the order of magnitude of the height-depth ratio. However, there is an essential difference between the surf zones of random waves and of periodic waves as a whole. In the latter case there is a reasonably well defined seaward limit, the breaker line, at which there is an abrupt change in flow regime and a discontinuity in the computational model. In random waves no point can be defined inshore of which all the waves are breaking while offshore from it no waves would break. Instead, at each point only a certain percentage of the waves passing it is breaking or broken, while this percentage in general varies gradually with the distance offshore. Associated herewith is a gradual variation of average values of other wave parameters, such as energy density, energy flux, momentum flux, etc. It is considered essential to represent this gradual variation in the computational model. This precludes the possibility of replacing the given, irregular wave train by an "equivalent" periodic wave train, on quite different grounds than those mentioned in the preceding paragraph, which dealt with the effects of short-crestedness. The problem then centres on a suitable description of the waves in the surf zone, one which does justice both to the random character of the waves and to the effects of wave breaking, in particular the dissipation of wave energy and the attendant decrease in radiation stress.

Regarding the applicability of the spectral approach there are two distinct problems: prediction of the spectrum as a function of location in the surf zone, and calculation of the local radiation stresses from the given (computed or measured) local energy spectrum. Concerning the latter of these problems, we derive a clue from the analogous situation with periodic waves, for which Bowen et al [6] found empirical confirmation of theoretical predictions based on the assumption that the principal radiation stress S_{11} could be expressed in terms of the local wave height by the second-order equation (3.4.2), despite the fact that the wave profile is far from sinusoidal. On this basis it seems reasonable to assume that (5.2.11) is adequate for the calculation of the radiation stresses from the local spectrum in irregular waves, even in the surf zone. If this is accepted, at least as a first approximation, then "only" the problem of spectrum prediction remains. Ideally, the effects of wave breaking should be expressed as a contribution to the spectral source function $Q(\vec{k};\vec{x},t)$, defined in paragraph 4.3.3. However, present knowledge is insufficient for this purpose. In numerical spectral schemes for the prediction of wind-driven deep-water waves, it is usually assumed that the effects of wave breaking can be accounted for by using Phillips' equilibrium spectral density (eq. 4.5.19) as a ceiling, and by making some assumption regarding the rate of approach to this ceiling. Collins [65] applies this method even in shallow water, although Phillips' equilibrium spectrum was not derived for such conditions. A calculation of an equilibrium spectral density in water of arbitrary depth is given by Ijima et al [108]. This will be considered in paragraph 5.3.2, where it is concluded that the assumptions used by Ijima et al are too arbitrary, and that the result is not as generally valid as is suggested. An alternative approach to the problem of calculating energies and radiation stresses in the surf zone of random waves will be given in paragraph 5.3.3.

5.3.2 The equilibrium range of shallow-water wave spectra proposed by Ijima, Matsuo and Koga

We shall first summarize the derivation given by Ijima et al, and make some comments afterwards.

The authors consider the maximum height of a wave as a function of its period, the local mean depth and the local bottom slope. They use the following empirical adaptation of Miche's theoretical breaking criterion (2.3.16):

$$H_{max} = C_1 \, L \tanh \{f(\alpha)\frac{2\pi D}{L}\} \quad , \tag{5.3.1}$$

in which

$$f(\alpha) = \cosh \, (3.5\alpha^{2/3}) \quad . \tag{5.3.2}$$

C_1 is a coefficient of proportionality which is left undetermined by the authors, and L is a wavelength calculated from T and D using the classical dispersion relation for linear gravity waves. The factor $f(\alpha)$ expresses the tendency for H_{max} to increase with slope angle α, at least in shallow water.

In order to establish the equilibrium spectrum $S_e(\omega)$, the authors consider an arbitrary frequency band extending from $\omega-\frac{1}{2}\Delta\omega$ to $\omega+\frac{1}{2}\Delta\omega$, and assume that there are N discrete spectral components in this band. These components are assumed to have a common wave height, H_T, proportional to H_{max}. The reason for this proportionality is that "the limiting wave height H_{max} is interpreted as the result that all the phases of component waves whose periods are within narrow range of period band between $T-\frac{1}{2}\Delta T$ and $T+\frac{1}{2}\Delta T$ centered at period T happened to coincide and their spectral wave heights were summed up to attain the limiting height H_{max}." The total energy in the band can then be written as

$$S_e(\omega)\Delta\omega = C_2 \, N \, H_T^2 = C_3 \, N \, H_{max}^2 . \tag{5.3.3}$$

The number of spectral components in the band "is considered to become large when the period band ΔT becomes wide, but to become small when the period T becomes large for limited length of wave record". On this basis the authors assume that N is proportional to $\Delta T/T$, or to $\Delta\omega/\omega$, so that

$$S_e(\omega) = C_4\, \omega^{-1}\, H_{max}^2 \tag{5.3.4}$$

or

$$S_e(\omega) = C_5\, \omega^{-1}\, L^2\, \tanh^2 \{f(\alpha)\tfrac{2\pi D}{L}\}. \tag{5.3.5}$$

In deep water this reduces to

$$S_e(\omega) = C_5\, \omega^{-1}\, L_0^2 = C_5\, 4\pi^2\, g^2\, \omega^{-5}, \tag{5.3.6}$$

which is identical in form to Phillips' equilibrium range (eq. 4.5.19). Equating the coefficients gives

$$C_5 = \beta/4\pi^2. \tag{5.3.7}$$

In shallow water (5.3.5) reduces to

$$S_e(\omega) = C_5\, \omega^{-1}\, \{f(\alpha)\ 2\pi D\}^2 \tag{5.3.8}$$

or

$$S_e(\omega) = \beta f^2(\alpha)\ D^2\, \omega^{-1}. \tag{5.3.9}$$

In order to estimate the actual shallow-water spectrum from a given deep-water spectrum $S_0(\omega)$, Ijima et al simply equate the local spectral density to $S_0(\omega)$ or to $S_e(\omega)$, whichever is smaller. Effects of shoaling and refraction are not considered. Examples are given for a wind-driven wave spectrum and a (narrow) swell spectrum.

This concludes our summary of the approach and the results given by Ijima et al. The following remarks can be made.

The authors use a discrete spectrum in order to derive a result concerning a continuous spectrum. This procedure is used more often. It gives valid results if it can be shown that the particular discretization adopted has no effect on the final result regarding the continuous spectrum. It is on this point that the arguments presented by Ijima et al are believed to be inadequate. In fact, they do not even mention it.

The number of components in the period band $(T-\frac{1}{2}\Delta T,\ T+\frac{1}{2}\Delta T)$ is assumed by the authors to be proportional to $\Delta T/T$. The inverse proportionality of N with T is argued with reference to the limited length of the record. This does not seem to be a particularly relevant parameter in the present context, since the value of a possible equilibrium range is quite independent of sampling procedures which are used.

The preceding objections were raised against the derivation given by the authors; we shall in the following consider the result itself, apart from its derivation.

An important point in the discussion of the result given by Ijima et al is the interpretation of the "equilibrium" spectral density, represented in eq. 5.3.5. It appears from the authors' statements and examples that they consider $S_e(\omega)$ as a saturation value which cannot be exceeded, regardless of the fact whether one deals with wind-driven waves (as Phillips does) or with swell, or, emphasizing an important difference between these categories, regardless of the width of the energy spectrum. If this were indeed correct then the maximum energy (per unit area) which can be present in water of a given mean depth D would have an upper limit which diminishes with the width of the spectrum. The calculated maximum possible r.m.s. wave height would then be only a minute fraction of the depth or the wavelength if the spectrum were narrow, so that virtually no waves would break. This is not consistent with the assumption of saturation. It is believed that a more realistic estimate of the saturation conditions can be obtained by relating the actually occurring wave heights to the

maximum value possible without breaking, rather than the so-called spectral wave heights. The actual wave heights are representative of the total energy per unit area of the wave system. In this manner we are led to an upper limit of the total energy in shallow water, determined by the depth D, independent of the width of the spectrum. (In deep water such limit would be determined by the wavelengths which are present in the spectrum.) In order words, according to this view, it is the integral of the spectrum which has an upper bound in shallow water, rather than the spectral density itself. This alternative approach will be elaborated in the following paragraph.

5.3.3 Radiation stresses in irregular, breaking waves

In the preceding discussion an approach was suggested for the determination of the saturation conditions in shallow water. By a slight extension the same method can be used for the estimation of the local energy in water of intermediate depth, where the saturation conditions are not yet attained. The basic assumption is that at each depth a limiting wave height H_b can be defined (which may also depend on the wave period), which cannot be exceeded by the individual waves of the random wave field, and that those wave heights which in the absence of breaking would exceed H_b are reduced by breaking to the value H_b. In other words, the energy corresponding to the height in excess of the local breaker height is assumed to be dissipated. The breaker height decreases gradually with decreasing depth. Thus, the calculated percentage of broken or breaking waves passing each point gradually increases with decreasing depth (excluding waves on very gentle slopes, on which the energy is dissipated without breaking). In this manner the calculated energy varies gradually from deep water to shallow water, partly because of the effects of shoaling, refraction and bottom friction, partly because of the increasing number of breaking waves. There is no well-defined seaward boundary of the surf zone in this approach. The calculations can proceed without change from deep water to shallow

water. For this reason shallow-water relations such as $n=1$, $c=(gD)^{\frac{1}{2}}$ etc. are not assumed a priori, although it is realized that it is only in the shallow-water zone that the effects being calculated, i.e. the spatial variations of the radiation stresses and the resultant set-up and longshore currents, become pronounced. The shallow-water conditions should therefore receive relatively much weight when approximations have to be introduced which are not uniformly valid in water of arbitrary depth.

Collins [109] has previously considered the probabilities of breaking-wave characteristics in order to arrive at estimates of the energy, energy flux, etc. There is an essential difference between his approach and the one just described. Collins treats the irregular-wave situation entirely as an ensemble of periodic-wave situations, each with a constant wave height (H_0), length (L_0) and direction of propagation (Θ_0) in deep water. Dependent variables such as energy, energy flux and longshore current velocities are expressed, or are assumed to be expressible, in terms of (H_0,L_0,Θ_0) using periodic-wave relations. The mathematical expectations of the dependent variables can then be calculated, assuming that the joint p.d.f. of $\underline{H}_0$, $\underline{L}_0$ and $\underline{\Theta}_0$ is known. Our approach is based on the two-dimensional random phase model, or another spectral model similar to this, according to which in any one realization the incident waves consist of a large number of independent spectral components of different amplitudes, frequencies, directions of propagation, and phases. A realization in this model has the properties of irregularity which are characteristic of wind waves. This is in contrast with Collins' model, in which individual realizations represent periodic, unidirectional waves. This model is of course not intended to be a realistic simulation of wind waves. It is used only as a means to and end, apparently on the implied assumption that ensemble averages determined from it give results equivalent to those obtainable from models in which the different waves are present more or less simultaneously. But there are various nonlinearities in the equations governing the mean motion which invalidate this assumption. We can cite as

examples the nonlinear interactions between the waves and the mean motion (e.g., the waves give rise to a set-up which in turn affects the waves), the inclusion of the set-up in the mean depth in the differential equation for the set-up (eq. 3.3.49), and a nonlinear relation between the bottom shear stress and the longshore current velocity. In consequence of each of these causes the contribution of a wave of certain characteristics to the set-up and the longshore current velocity is affected by the presence of waves of different characteristics. In other words, with regard to the mean motion it is not indifferent whether a wave is part of a periodic, long-crested wave train or whether it is part of a random wave field. Thus, instead of calculating expected values (ensemble averages) of time--mean responses to periodic waves, it is preferred to calculate the responses to the (time-mean) radiation stresses in the random waves, taking the afore-mentioned interactions into account.

The approach outlined above will be worked out in the following. For clarity of presentation we shall at first restrict ourselves to a narrow frequency spectrum and a narrow directional spectrum, so that only the variability of the wave heights need be taken into account. The effects of variable period and direction of propagation will be considered afterwards.

The breaking criterion which has been adopted for use is based on Miche's formula for the limiting steepness of stable periodic waves in water of constant depth, eq. (2.3.16):

$$H_b = 0.14\ L \tanh \frac{2\pi D}{L} = \{0.88\ \frac{\tanh kD}{kD}\}\ D, \qquad (5.3.10)$$

which in shallow water approximates to

$$H_b = 0.88\ D. \qquad (5.3.11)$$

Since we are here dealing with deforming waves in water of variable depth, Miche's formula cannot be expected to apply exactly, even if

the waves were periodic. The data presented in fig. 2.6 illustrate that the breaker height-to-depth ratio (γ) in shallow water varies mildly with the beach slope and the wave steepness. Thus, instead of (5.3.10), which a priori assigns the constant value of 0.88 to γ, we prefer a form which in shallow water reduces to

$$H_b = \gamma D. \tag{5.3.12}$$

The coefficient γ is in principle a variable, though its actual value is expected to deviate but little from 0.8 in the case of spilling breakers, with which alone we are concerned.

It was noted above that we want to use expressions which are not restricted to shallow water. For this reason we should include the effect of the depth-length ratio on the wave breaking in the formulation. We are guided in this by Miche's formula. A simple choice would be

$$H_b = \{\gamma \frac{\tanh kD}{kD}\} D = \frac{\gamma}{2\pi} L \tanh \frac{2\pi D}{L} \quad . \tag{5.3.13}$$

However, this would imply that the bottom slope could affect the wave breaking even in deep water. The following expression is therefore preferred:

$$H_b = 0.14 L \tanh \left(\frac{\gamma}{0.88} \frac{2\pi D}{L}\right) \quad . \tag{5.3.14}$$

Actually, whether we use (5.3.13) or (5.3.14) is of little influence on the results of the final calculations since the two expressions can differ significantly in deep water only, where ordinarily the waves break very infrequently. Even the use of (5.3.12) throughout the region from deep water to shallow water may give a good approximation, particularly for waves of low initial steepness, for which the depth--length ratio is very small where they begin to break in significant numbers. Steeper waves begin to break in water of greater relative depth. The use of (5.3.12) for such waves would therefore underestimate the width of the surf zone.

Equation (5.3.14) will be applied as a breaking criterion for individual waves in an irregular wave train. The wavelength L will be calculated from the depth D and the zero-crossing period T, using (3.2.14); it can at first be treated as a constant in view of the restriction to a narrow spectrum.

Having adopted a breaking criterion, we now need to estimate the fraction of the waves which would actually be breaking, and the mean energy which would remain. Even if breaking did not occur then the energy per unit area would vary as the waves enter shallow water, because of shoaling, refraction and bottom friction. These effects can be calculated by conventional means referred to in paragraph 4.3.3. (As long as the frequency spectrum and the directional spectrum are assumed to be narrow we can even use the methods derived for monochromatic, unidirectional waves described in chapter 3.) This results in a local energy per unit area, denoted as E_f, which is a fictitious quantity because wave breaking is not yet accounted for. Corresponding to E_f we define fictitious wave heights $\underline{H}_f$. Their mean square value $\overline{H_f^2}$ is by definition related to E_f according to

$$E_f = \frac{1}{8} \rho g \overline{H_f^2} \quad . \tag{5.3.15}$$

The fictitious wave heights are assumed to be Rayleigh-distributed; their distribution function can be written as

$$\begin{aligned} F_f(H) \triangleq \Pr\{\underline{H}_f \leq H\} &= 0 && \text{for } H<0 \\ &= 1 - \exp(-H^2/\overline{H_f^2}) && \text{for } H \geq 0 \quad . \end{aligned} \tag{5.3.16}$$

In accordance with the assumption that the height of a breaking wave equals the local breaker height H_b, we shall clip the fictitious wave height distribution at $H=H_b$ in order to obtain an approximation to the actual wave height distribution:

$$F(H) \equiv \Pr\{\underline{H} \leq H\} = 0 \qquad \text{for } H<0$$
$$= 1 - \exp(-H^2/\overline{H_f^2}) \qquad \text{for } 0 \leq H < H_b \qquad (5.3.17)$$
$$= 1 \qquad \text{for } H \geq H_b.$$

This distribution function is discontinuous at $H=H_b$. This is a result of the assumption that a finite fraction of all the wave heights would be equal to H_b.

The mean energy per unit area at a fixed point, taking account of breaking, is calculated from

$$E = \frac{1}{8} \rho g \overline{H^2}, \qquad (5.3.18)$$

in which

$$\overline{H^2} = E\{\underline{H}^2\} = \int_{-\infty}^{\infty} H^2 \, dF(H) \quad . \qquad (5.3.19)$$

Substitution of (5.3.17) and integration gives

$$\overline{H^2} = \int_0^{H_b} H^2 \, d\{1 - \exp(-H^2/\overline{H_f^2})\} + H_b^2 \exp(-H_b^2/\overline{H_f^2})$$

$$= -H^2 \exp(-H^2/\overline{H_f^2}) \Big|_0^{H_b} + \int_0^{H_b} \exp(-H^2/\overline{H_f^2}) dH^2 +$$

$$+ H_b^2 \exp(-H_b^2/\overline{H_f^2})$$

$$= \{1 - \exp(-H_b^2/\overline{H_f^2})\} \, \overline{H_f^2} \qquad (5.3.20)$$

or

$$\overline{H^2} = F_f(H_b) \, \overline{H_f^2} \quad . \qquad (5.3.21)$$

If we introduce the probability of exceedance for the fictitious wave heights,

$$Q_f(H) \equiv \Pr\{\underline{H}_f > H\} = \exp(-H^2/\overline{H_f^2}) \quad \text{for } H \geq 0, \qquad (5.3.22)$$

then (5.3.21) can be written as

$$\overline{H^2} = \{1 - Q_f(H_b)\}\ \overline{H_f^2} \tag{5.3.23}$$

or as

$$\frac{\overline{H_f^2} - \overline{H^2}}{\overline{H_f^2}} = Q_f(H_b)\ , \tag{5.3.24}$$

which may be stated in words as follows: clipping the upper fraction $Q_f(H_b)$ of the fictitious wave height distribution reduces the mean square wave height by a relative amount equal to $Q_f(H_b)$. (It may be shown that only the Rayleigh distribution has this property.) Stated more briefly, the relative reduction in energy due to breaking equals the fraction of the waves that break.

So far we have only dealt with the case of a narrow frequency spectrum and a narrow directional spectrum. We shall now consider how the preceding calculations should be modified in order to include the effects of variability in period and direction. The fictitious two-dimensional spectrum $G_f(\omega,\theta)$ and, therefore, the fictitious energy E_f can be calculated in a straightforward manner using the transformation rules for the spectrum, referred to in par. 4.3.3. The next step is to estimate the effects of the variability of wave period and direction on the breaker heights. The latter effect is very weak, particularly in shallow water, where the waves are propagating nearly perpendicular to the shore as a result of refraction. As noted previously, the conditions in the shallow-water zone should be emphasized in formulating our assumptions, since it is there that most of the waves begin to break. This is an additional reason for neglecting the effects of the variability of wave direction on the breaking process. The effects of the period variability could be taken into account by calculating for each depth a range of breaker heights corresponding to the range of periods. However, it does not seem

worthwhile to do this inasmuch as it is (again) precisely in the important shallow-water zone that the period vanishes from the breaking criterion, which there reduces to a constant height-to-depth ratio. And in order to estimate the period-effect on the breaker heights in deeper water, it is considered sufficient to use only the mean period and to neglect the effects of the period variability, since the wave breaking in deeper water is of minor importance anyhow.

The preceding approximations refer to the calculated breaker heights only. They should not be interpreted to imply that in the proposed approach the variability of wave period and direction would have no effect on the wave breaking at all. For the complete two--dimensional spectrum is used in the calculations of the fictitious wave heights, and so the differences in shoaling and refraction of different component-waves are taken into account.

The following remarks can be made regarding the computational model outlined above.

1) It can happen that in very shallow water $H_b^2/\overline{H_f^2} \ll 1$. In that case eq. (5.3.20) reduces to

$$\overline{H^2} = H_b^2 \quad . \tag{5.3.25}$$

It may be seen that $\overline{H^2}$ in this limiting case equals the value which it would have for periodic waves with height H_b. This is to be expected because the approximation involved in effect consists of considering almost all the wave heights to be equal to H_b, while neglecting the contributions to $\overline{H^2}$ from wave heights less than H_b. It follows that (5.3.25) represents the saturation condition already referred to in qualitative terms at the end of the previous paragraph. It should be noted that this condition does not necessarily occur whenever the waves travel into very shallow water, for on very gentle slopes the dissipation in the bottom boundary layer may become of such importance that the inequality $H_b^2/\overline{H_f^2} \ll 1$ does not hold anywhere. These cases are rather exceptional, however.

2) The condition $H_b^2/\overline{H_f^2} \ll 1$ usually implies $D/L \ll 1$, in which case (5.3.12) is a valid approximation of (5.3.14). With this substitution (5.3.25) becomes

$$\overline{H^2} = \gamma^2 D^2 \quad , \tag{5.3.26}$$

so that the energy in irregular waves according to this model approaches that which is usually assumed for regular waves, as the relative depth decreases. It follows that under these circumstances the calculated local set-up gradient is equal to the value given in section 3.4 for regular waves.

3) The wave height distribution is assumed to be discontinuous at $H = H_b$. The actual distribution is naturally smoother, because of various causes which have not been taken into account, such as the effects of preceding larger or smaller waves, the variability of the wave period, and the changes in depth (averaged over a time interval of the order of a few wave periods) due to surf beat. Some waves with a height larger than the calculated H_b will therefore pass a point unbroken, while others with a smaller height do break. However, this does not necessarily mean that the mean square wave height calculated from (5.3.17) would be seriously in error. And it is only this result which is used in subsequent calculations of the radiation stresses and their effects.

4) The calculation of the fictitious wave heights may include dissipation of wave energy due to the generation of turbulence in the bottom boundary layer, which is a nonlinear damping process. If wave breaking decreases the wave heights then the rate of damping due to bottom friction is less than it would be in the absence of breaking. In such cases the calculation of the resultant wave energy at each point cannot be carried out by going only once through the two-step process in which E_f is calculated first (with shoaling, refraction and bottom friction), and in which breaking is taken into account afterwards by putting $E=(1-Q_b)E_f$. It becomes necessary to go through this loop repeatedly, and so to find E by iteration.

5) In the computational model given above, the wave heights are related to the local breaker height in such a manner that they not only decrease with decreasing breaker height, which occurs in shoaling water, but they also increase with increasing breaker height, which occurs after passage of an offshore bar. In other words, the process of "dissipation" of energy in breaking, which consists mainly of the transformation of organized wave motion into disorganized turbulent motion, would be reversible in the computational model. This violation of the second law of thermodynamics must be excluded, which can be achieved by giving the calculated losses due to breaking a lower limit equal to zero. This limit is not quite realistic, since the random nature of the waves gives rise to occasional breaking, even if the depth is constant or increasing in the propagation direction.The corresponding energy losses have in effect been neglected in comparison with those occurring in shoaling water.

We have so far in this paragraph considered the wave energy only, while our actual aim was to calculate radiation stresses. As stated in the introduction to this section (par. 5.3.1), the radiation stresses can be calculated to second order, as weighted integrals of the two-dimensional spectral density $G(\omega,\theta)$. Now the procedure described above leads to a fictitious spectral density $G_f(\omega,\theta)$ -from which fictitious radiation stresses S_{ij_f} can be determined according to eq. 5.2.11, to its integral E_f and to the reduction of this integral due to breaking, but it does not lead directly to the reduced spectrum $G(\omega,\theta)$. Breaking does not necessarily affect the spectral components equally, so that it may not be correct to reduce the spectral density in the same proportion (E/E_f) for all (ω,θ). In particular the shape of the frequency spectrum may be altered by the breaking process. But the only frequency-dependent weight factor in the calculation of S_{ij} from $G(\omega,\theta)$ is n, which in shallow water is in effect independent of ω, and approximately equal to one. It seems reasonable therefore

to assume that the radiation stresses are reduced by breaking in the same proportion as the total energy:

$$S_{ij} = \frac{E}{E_f} S_{ij_f} = \{1 - \exp(-H_b^2/\overline{H_f^2})\} S_{ij_f} \quad . \qquad (5.3.27)$$

Needless to say, the validity of this approximation increases with decreasing width of the frequency spectrum and of the directional spectrum.

6 SET-UP AND LONGSHORE CURRENTS

6.1 Introduction

In the preceding chapter an outline has been given of a method to calculate radiation stresses in random waves. This method will now be applied in the computation of the set-up and the longshore current velocity profile in a few typical cases. To this end, supplementary equations will be given in section 6.2. Results of numerical computations are presented and discussed in section 6.3, while a comparison with experimental data on wave height decay and set-up in the surf zone is given in section 6.4.

The same situation is considered as in paragraph 3.3.6, fig. 3.1, viz. an infinitely long beach with straight and parallel depth contours, and incident waves which are statistically stationary, and homogeneous in the x_2-direction. This implies that time-averaged flow parameters vary with x_1 at most. The waterdepth is assumed to decrease monotonically in the shoreward direction.

6.2 Supplementary equations

6.2.1 Shoaling and refraction

The transformation of the incident waves propagating towards the shore will be calculated with neglect of local generation, and of dissipation other than through wave breaking, in which case the fictitious spectral density obeys the differential equation (4.3.19). In the situation of no x_2-dependence, this becomes simply

$$\frac{\partial}{\partial x_1} \{ c \, c_g \, G_f(\omega,\theta) \} = 0 \quad , \tag{6.2.1}$$

provided the auxiliary relations

$$\frac{\partial \omega}{\partial x_1} = 0 \tag{6.2.2}$$

and

$$\frac{\partial}{\partial x_1}\left(\frac{\sin\theta}{c}\right) = 0 \quad \text{or} \quad \frac{\partial}{\partial x_1}(k \sin\theta) = 0 \tag{6.2.3}$$

hold. The boundary condition to be used in conjunction with (6.2.1) is a spectral density function at some point offshore. In subsequent calculations we use a deep-water spectrum for this purpose, written as $G_0(\omega,\theta_0)$. Corresponding to this spectrum we have a r.m.s. wave height

$$H_0 = (8\, m_0)^{\frac{1}{2}} \tag{6.2.4}$$

and a characteristic (angular) frequency

$$\Omega = (m_2/m_0)^{\frac{1}{2}} = 2\pi/T_0 \quad , \tag{6.2.5}$$

in which T_0 is the mean zero-crossing period in deep water, and m_0 and m_2 are the zeroth- and second-order moment of the deep water frequency spectrum defined by

$$S_0(\omega) = \int_{-\pi}^{\pi} G_0(\omega,\theta_0)\, d\theta_0 \quad . \tag{6.2.6}$$

The local fictitious spectral density can be expressed in terms of $G_0(\omega,\theta_0)$ by means of (6.2.1) through (6.2.3), which gives

$$G_f(\omega,\theta) = \frac{c_0\, c_{g_0}}{c\, c_g}\, G_0(\omega,\theta_0) \quad . \tag{6.2.7}$$

The fictitious mean square wave height can then be found from

$$\frac{1}{8}\overline{H_f^2} = \int_0^{\infty}\int_{-\pi}^{\pi} G_f(\omega,\theta)\, d\omega\, d\theta \quad . \tag{6.2.8}$$

Substitution of (6.2.7) into (6.2.8) and changing the angular variable of integration from θ to θ_0 gives

$$\frac{1}{8}\overline{H_f^2} = \int_0^{\infty}\int_{-\pi}^{\pi} \frac{c_0\, c_{g0}}{c c_g}\left|\frac{\partial\theta}{\partial\theta_0}\right| G_0(\omega,\theta_0)\, d\omega\, d\theta_0 \quad , \qquad (6.2.9)$$

or, using (6.2.3),

$$\frac{1}{8}\overline{H_f^2} = \int_0^{\infty}\int_{-\pi}^{\pi}\left[\frac{c_{g_0}}{c_g}\frac{\cos\theta_0}{\cos\theta}\right] G_0(\omega,\theta_0)\, d\omega\, d\theta_0 \quad . \qquad (6.2.10)$$

The factor in the brackets is the square of the product of the shoaling coefficient and the refraction coefficient, referred to in paragraph 3.2.3.

It can be seen that the determination of $\overline{H_f^2}$ in general requires a double integration over the spectrum. However, the calculations are reduced considerably if the spectrum is narrow, with mean frequency $\bar{\omega}$ and mean direction of propagation $\bar{\theta}_0$, say. Eq. (6.2.10) then approximates to

$$\frac{1}{8}\overline{H_f^2} \approx \left[\frac{c_{g_0}}{c_g}\frac{\cos\theta_0}{\cos\theta}\right]_{\substack{\omega=\bar{\omega}\\ \theta_0=\bar{\theta}_0}} \int_0^{\infty}\int_{-\pi}^{\pi} G_0(\omega,\theta_0)\, d\omega\, d\theta_0 \quad , \qquad (6.2.11)$$

which is equivalent to

$$\overline{H_f^2} \approx \left[\frac{c_{g_0}}{c_g}\frac{\cos\theta_0}{\cos\theta}\right]^{\sim\sim\sim\sim\sim\sim\sim\sim\sim\sim\sim\sim} H_0^2 \quad , \qquad (6.2.12)$$

in which the designation $\overset{\sim\sim\sim\sim\sim\sim\sim\sim\sim\sim\sim\sim}{}$ indicates the value of the term ..... for $\omega = \bar{\omega}$ and $\theta_0 = \bar{\theta}_0$. Eq. (6.2.12) is here given as a special

case of the more general eq. (6.2.8); it could as well have been written down at once, from the known results for monochromatic waves (eq. 3.2.40).

The radiation stresses S_{ij} are calculated from $G_f(\omega,\theta)$ according to

$$S_{ij} = (1 - Q_b)\, S_{ij_f} \quad , \tag{6.2.13}$$

in which

$$S_{ij_f} = \rho g \int_0^\infty \int_{-\pi}^{\pi} \{ne_i e_j + (n-\tfrac{1}{2})\, \delta_{ij}\}\, G_f(\omega,\theta)\, d\omega\, d\theta \quad , \tag{6.2.14}$$

and Q_b equals $Q_f(H_b)$, the fraction of breaking waves, calculated from $\overline{H_f^2}$ and H_b using (5.3.22). In principle, the radiation shear stress S_{12_f} need not be calculated at each step (i.e., each value of x_1), because it is independent of x_1. It was nevertheless determined at each step from the local values of G_f, in order to obtain a check on the numerical integration procedures. It varied by less than by 0.5% in all of the calculations.

If the spectrum is narrow then the radiation stresses can be *expressed directly in terms of* $\overline{H^2}$:

$$S_{ij} = \overline{\{ne_i e_j + (n-\tfrac{1}{2})\delta_{ij}\}}.\ \frac{1}{8}\rho g\, \overline{H^2} \quad . \tag{6.2.15}$$

6.2.2 Set-up

The differential equation for the set-up reads

$$\frac{dS_{11}}{dx_1} + \rho g(d+\bar{\zeta})\, \frac{d\bar{\zeta}}{dx_1} = 0 \quad . \tag{6.2.16}$$

This equation is integrated numerically with the boundary condition $\bar{\zeta} = 0$ in deep water. The radiation stress S_{11} depends on the mean depth $D = d + \bar{\zeta}$, and therefore on $\bar{\zeta}$. Eq. (6.2.16) must therefore in general be integrated iteratively, in which S_{11} has to be re-calculated in each iteration. This requires two double integrations over the spectrum in each iteration: one for S_{11_f} and one for $\overline{H_f^2}$ (to be used for the calculation of $Q_f(H_b)$). However, if $\frac{dD}{dx_1} \neq 0$ for all x_1, which is the case if the depth decreases monotonically towards the shore, then (6.2.16) can be rewritten as

$$\frac{dS_{11}}{dD} + \rho g D \frac{d\bar{\zeta}}{dD} = 0 \quad . \tag{6.2.17}$$

This equation can be integrated with D as the independent variable, without having to iterate with respect to S_{11} at each step. The result is $\bar{\zeta}$ as a function of D, from which $\bar{\zeta}$ can be found as a function of d ($= D - \bar{\zeta}$) simply by subtraction.

A partial check on the results is provided by the known behaviour of $\bar{\zeta}$ in shallow water. If $D \to 0$ we have $\cos\theta \to 1$ and $n \to 1$ for all of the spectral components, so that $S_{11} \to \frac{3}{2}E$. Furthermore, $H_{rms} \to H_b \to \gamma D$ (eqs. 5.3.25 and 5.3.26), so that $E \to \frac{1}{8}\rho g \gamma^2 D^2$. It follows that

$$\frac{d\bar{\zeta}}{dd} \to -\frac{\frac{3}{8}\gamma^2}{1 + \frac{3}{8}\gamma^2} \qquad \text{for } D \to 0 \tag{6.2.18}$$

(compare with eq. 3.4.4).

6.2.3 Longshore current velocity

Two equations for the longshore current velocity which are not affected by the randomness of the waves are

$$\frac{dS_{12}}{dx_1} + \bar{\tau}_2 = 0 \tag{6.2.19}$$

and

$$\bar{\tau}_2 = C_f \rho \overline{q_2 |\vec{q}|} \quad . \tag{6.2.20}$$

In (6.2.20), the value of $\vec{q}$ near the bottom should be used. The average longshore bottom shear stress $\bar{\tau}_2$ will be expressed in terms of the local velocity field by the same approximation as is generally used for periodic waves, referred to in chapter 3. That is to say, the mean current velocity is supposed to be small compared with the wave-induced fluctuations, and to be directed approximately perpendicular to them. Eq. (6.2.20) then becomes

$$\bar{\tau}_2 \approx C_f \rho V \overline{|\vec{q}'|} \quad . \tag{6.2.21}$$

For the calculation of $\overline{|\vec{q}'|}$ we consider first a random wave train with a narrow spectrum, with mean frequency $\bar{\omega} = \Omega = 2\pi/T_0$. For these waves we have, to first order,

$$\overline{|\vec{q}'|} = \left[\frac{\omega}{\sinh \tilde{k}D}\right]_{\omega=\Omega} \times \overline{|\zeta'|} = \frac{\Omega}{\sinh \tilde{k}D} \frac{\bar{H}}{\pi} \tag{6.2.22}$$

(see eq. 3.2.16), in which $\tilde{k}$ is a wavenumber calculated from $\Omega^2 = g\tilde{k} \tanh \tilde{k}D$. Eq. (6.2.22) will in what follows be used for an arbitrary spectrum, even if this is not narrow. This implies a

neglect of the effects of the period variability. This is considered permissible because the effects of the wave period on $\overline{|\vec{q}'|}$ vanish in the important shallow-water region:

$$\overline{|\vec{q}'|} \to \frac{\bar{H}}{\pi}\left[\frac{\omega}{kD}\right]_{\omega = \Omega} = \frac{\bar{H}}{\pi}\left[\frac{c}{D}\right]_{\omega = \Omega} \to \frac{\bar{H}}{\pi}\left(\frac{g}{D}\right)^{\frac{1}{2}} \text{ for } kD \to 0. \qquad (6.2.23)$$

The mean wave height $\bar{H}$ appearing in (6.2.22) and (6.2.23) can be expressed in terms of the local breaker height H_b and the local fictitious wave heights by means of the clipped Rayleigh distribution given by (5.3.17):

$$\bar{H} = E\{\underset{\sim}{H}\} = \int_0^{H_b} H \, d\{1 - \exp(-H^2/\overline{H_f^2})\} + H_b \exp(-H_b^2/\overline{H_f^2})$$

$$= \frac{\sqrt{\pi}}{2} H_{f_{rms}} \operatorname{erf}(H_b/H_{f_{rms}}) \quad , \qquad (6.2.24)$$

in which

$$H_{f_{rms}} = (\overline{H_f^2})^{\frac{1}{2}} \qquad (6.2.25)$$

and erf is the error function defined by

$$\operatorname{erf}(x) = \frac{2}{\sqrt{\pi}} \int_0^x e^{-u^2} \, du \quad . \qquad (6.2.26)$$

It follows from the behaviour of erf(x) for small or large values of x that

$$\bar{H} \to H_b \quad \text{for } H_b/H_{f_{rms}} \to 0 \quad , \qquad (6.2.27)$$

which occurs in very shallow water, where the clipped Rayleigh probability density becomes narrowly concentrated near $H = H_b$, and

$$\bar{H} \to \frac{\sqrt{\pi}}{2} H_{f_{rms}} \quad \text{for} \quad H_b/H_{f_{rms}} \to \infty \quad , \tag{6.2.28}$$

which is the deep-water result for the (unclipped) Rayleigh p.d.f. For general values of $H_b/H_{f_{rms}}$, a rational approximation to the error function can be employed in numerical computations [90].

It can be seen from the preceding equations that, strictly speaking, $\bar{H}$ should be calculated at each point where V is to be determined, in addition to H_{rms}, which is needed for the radiation stresses. However, only relatively small errors are made if H_{rms} is used in (6.2.22) instead of $\bar{H}$, because the ratio between them varies theoretically (i.e., based on the clipped Rayleigh distribution) from $\bar{H}/H_{rms} = \frac{\sqrt{\pi}}{2} \approx 0.89$ in deep water, to $\bar{H}/H_{rms} = 1$ in shallow water.

Substitution of (6.2.21) and (6.2.22) into (6.2.19) and solving for V gives

$$V = - \frac{T_0}{2\rho\, C_f\, \bar{H}} \sinh \tilde{k}D \, \frac{dS_{12}}{dx_1} \quad . \tag{6.2.29}$$

Using the preceding equations, V can be calculated as a function of x_1, the distance offshore. However, it is considered more meaningful to determine a dimensionless velocity as a function of the dimensionless mean depth D/H_0. We have

$$\frac{dS_{12}}{dx_1} = \frac{dS_{12}}{dD} \cdot \frac{dD}{dx_1} = - \frac{dS_{12}}{dD} m_D \quad . \tag{6.2.30}$$

The mean-depth gradient (m_D) is not known a priori from the bottom profile since it also depends on the set-up. It can however be expressed in terms of the bottom slope m_d (= $-dd/dx_1$) by means of (6.2.16), which gives

$$m_D = -\frac{dD}{dx_1} = -\frac{d}{dx_1}(d+\bar{\zeta}) = m_d + \frac{1}{\rho g D}\frac{dS_{11}}{dx_1} = m_d - \frac{1}{\rho g D}\frac{dS_{11}}{dD} m_D, \quad (6.2.31)$$

so that

$$m_D = m_d\left(1 + \frac{1}{\rho g D}\frac{dS_{11}}{dD}\right)^{-1} . \quad (6.2.32)$$

Eq. (6.2.29) then becomes

$$V = \frac{m_d T_0}{2\rho C_f \bar{H}} \sinh \tilde{k}D \frac{dS_{12}}{dD}\left(1 + \frac{1}{\rho g D}\frac{dS_{11}}{dD}\right)^{-1} . \quad (6.2.33)$$

A normalized current velocity V^* will now be defined as

$$V^* = \frac{C_f}{m_d}\frac{T_0}{\pi H_0} V . \quad (6.2.34)$$

Substitution of (6.2.33) yields

$$V^* = \frac{1}{2\pi\rho}\frac{T_0^2}{H_0\bar{H}} \sinh \tilde{k}D \frac{dS_{12}}{dD}\left(1 + \frac{1}{\rho g D}\frac{dS_{11}}{dD}\right)^{-1} , \quad (6.2.35)$$

which can also be written as

$$V^* = \frac{\tilde{L}_0}{H_0}\frac{D}{\bar{H}} \sinh \tilde{k}D \frac{dS_{12}}{dD}\left(\rho g D + \frac{dS_{11}}{dD}\right)^{-1} . \quad (6.2.36)$$

This is the equation which will be used in numerical calculations. A partial check on the results is provided by the known behaviour of V (or V^*) in shallow water. The following approximations hold for $D \to 0$, in addition to those mentioned in the previous paragraph:

$$\sinh \hat{k}D \to \hat{k}D \to \Omega \left(\frac{D}{g}\right)^{\frac{1}{2}} \quad , \tag{6.2.37}$$

and, if the incident wave spectrum is narrow,

$$S_{12} \to nE \sin \bar{\theta} \cos \bar{\theta} \to E \sin \bar{\theta} \approx E \sin \bar{\theta}_0 \frac{\sqrt{gD}}{\tilde{c}_0} \tag{6.2.38}$$

in which $\tilde{c}_0 = g/\Omega$. Substitution of these approximations and of those presented in paragraph 6.2.2 gives

$$V \to \frac{5\pi}{16} \frac{m_d}{c_f} \gamma \left(1 + \frac{3}{8}\gamma^2\right)^{-1} \sin \bar{\theta}_0 \frac{gD}{\tilde{c}_0} \qquad \text{for } \frac{D}{H_0} \to 0 \quad , \tag{6.2.39}$$

which agrees with eq. 3.4.16 (if the difference between m_D and m_d is taken into account), and

$$V^* \to \frac{5\pi}{8} \gamma \left(1 + \frac{3}{8}\gamma^2\right)^{-1} (\sin \bar{\theta}_0) \frac{D}{H_0} \qquad \text{for } \frac{D}{H_0} \to 0 \quad . \tag{6.2.40}$$

Thus, a plot of V^* vs. D/H_0 should approach a straight line through the origin for small values of D/H_0, with a gradient which is independent of the incident wave steepness, and proportional to $\sin \bar{\theta}_0$. If the directional spectrum of the incident waves is not narrow then V is expected to be less than the value indicated by (6.2.39), as has been pointed out in chapter 5.

6.3 Numerical evaluation

6.3.1 Boundary conditions

In this paragraph the boundary conditions will be stated which have been chosen for some sample calculations based on the equations presented in section 6.2 and in chapter 5.

The two-dimensional spectral density function in deep water is factorized as follows:

$$G_0(\omega,\theta_0) = S_0(\omega)D_0(\theta_0;\omega) \quad . \tag{6.3.1}$$

If it is narrow then only the total energy (E), the mean frequency ($\bar{\omega}$) and the mean direction of propagation ($\bar{\theta}_0$) need be given, or, in terms of dimensionless quantities, only the wave steepness ($H_0/\hat{L}_0$) and $\bar{\theta}_0$. Two series of calculations were made with a narrow spectrum. In series I the wave steepness was kept constant ($H_0/\hat{L}_0 = 0.02$) and $\bar{\theta}_0$ was varied: $\bar{\theta}_0 = 0^o$, 15^o, 30^o, 45^o, 60^o, 75^o and 85^o. In series II, $\bar{\theta}_0$ was kept constant at 15^o, and the wave steepness was varied: $H_0/\hat{L}_0 = 0.005$, 0.01, 0.02, 0.03 and 0.04. A third calculation (III) was performed with $H_0/\tilde{L}_0 = 0.04$ and $\bar{\theta}_0 = 15^o$, but with a wide spectrum, more representative of wind-driven waves. $S_0(\omega)$ was chosen similar to a Pierson-Moskowitz spectrum. Expressed in terms of H_0 and Ω, which have been defined in (6.2.4) and (6.2.5), it can be written as

$$S_0(\omega) = \frac{1}{2\pi} H_0^{\,2}\, \Omega^4\, \omega^{-5} \exp\{-\frac{(\Omega/\omega)^4}{\pi}\} \quad . \tag{6.3.2}$$

The directional spectrum was chosen to be of the $\cos^2$-type:

$$D_0(\theta_0) = \frac{2}{\pi}\cos^2(\theta_0 - \bar{\theta}_0) \quad \text{for } |\theta_0 - \bar{\theta}_0| \leq \frac{\pi}{2} \tag{6.3.3}$$
$$= 0 \qquad\qquad \text{otherwise.}$$

$\bar{\theta}_0$ is the mean angle of incidence of the wave system in deep water with respect to the x_1-direction. For $\bar{\theta}_0 \neq 0$ the directional spectrum (6.3.3) includes non-zero components for which $|\theta_0| > \frac{\pi}{2}$, and which therefore propagate offshore. These were excluded in the calculations.

6.3.2 Presentation and discussion of results

The equations summarized in section 6.2, supplemented with the above-mentioned boundary conditions, have been programmed in Fortran IV for computation on an IBM 360-65. The results are shown in the figures 6.1 through 6.4, in which $\bar{\zeta}/H_0$ has been plotted vs. d/H_0, and V^* vs. D/H_0. A value $\gamma = 0.8$ has been used.

The set-up curves display the characteristic slowly-varying negative values in deep water and a fairly steep rise in shallow water, with a gradual transition. In very shallow water the set-up gradient approaches a constant value; it can be verified that the value of this constant agrees with (6.2.18). The points of maximum set-up correspond to $D = 0$, or, in other words, to $d + \bar{\zeta} = 0$. The locus of these points is therefore given by a straight line through the origin in the $(\bar{\zeta},d)$ plane (the dashed line in the figures 6.1 and 6.3), corresponding to the beach elevation. It appears from fig. 6.1 that the value of $\bar{\zeta}_{max}/H_0$ decreases with increasing $\bar{\theta}_0$. This can be expected in view of the increasing effect of refraction, which tends to reduce the wave heights occurring at a certain depth (for a given deep-water wave steepness), thereby narrowing the surf zone. Fig. 6.3 shows that $\bar{\zeta}_{max}/H_0$ decreases with increasing wave steepness, although not nearly as fast as in inverse proportion. Thus, increasing the wave height at constant wave length results in an almost proportionate increase in maximum set-up. Conversely, an increase in wave length at constant wave height gives rise to a moderate increase of $\bar{\zeta}_{max}$ only.

The longshore current profiles in the figures 6.2 and 6.4 show a smooth variation from a zero value in deep water to a maximum in an intermediate depth, from where it falls off gradually to zero in the point of maximum set-up ($D = 0$). It should be noted that the profiles for series II, shown in fig. 6.4, have a common tangent at the point $D = 0$, which agrees with (6.2.40). Those in fig. 6.2 have a gradient at $D = 0$ proportional to $\sin \bar{\theta}_0$. Furthermore, fig. 6.2

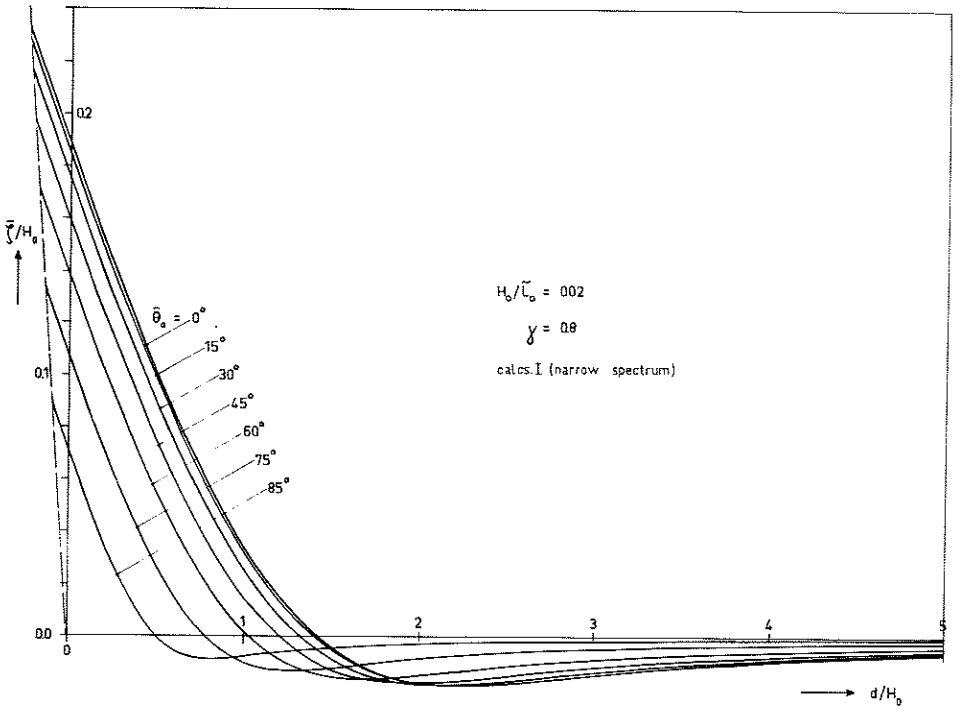

Fig. 6.1. Calculated set-up curves for various mean angles of incidence.

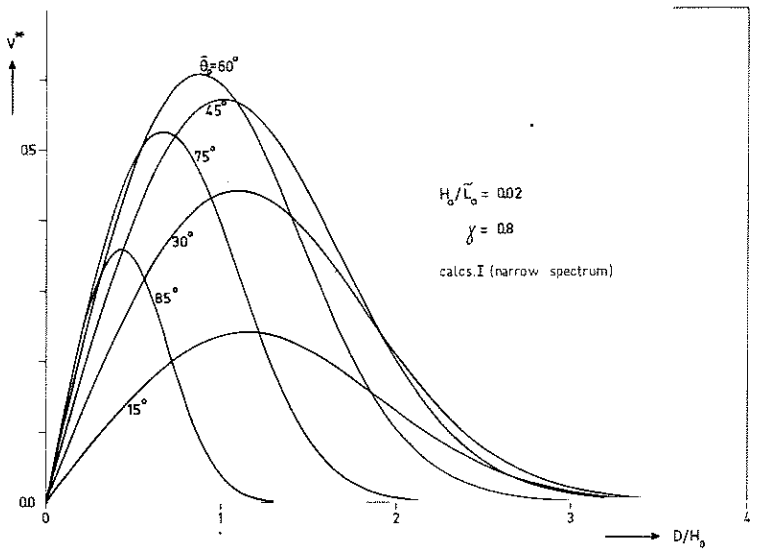

Fig. 6.2. Calculated longshore current velocity profiles for various mean angles of incidence.

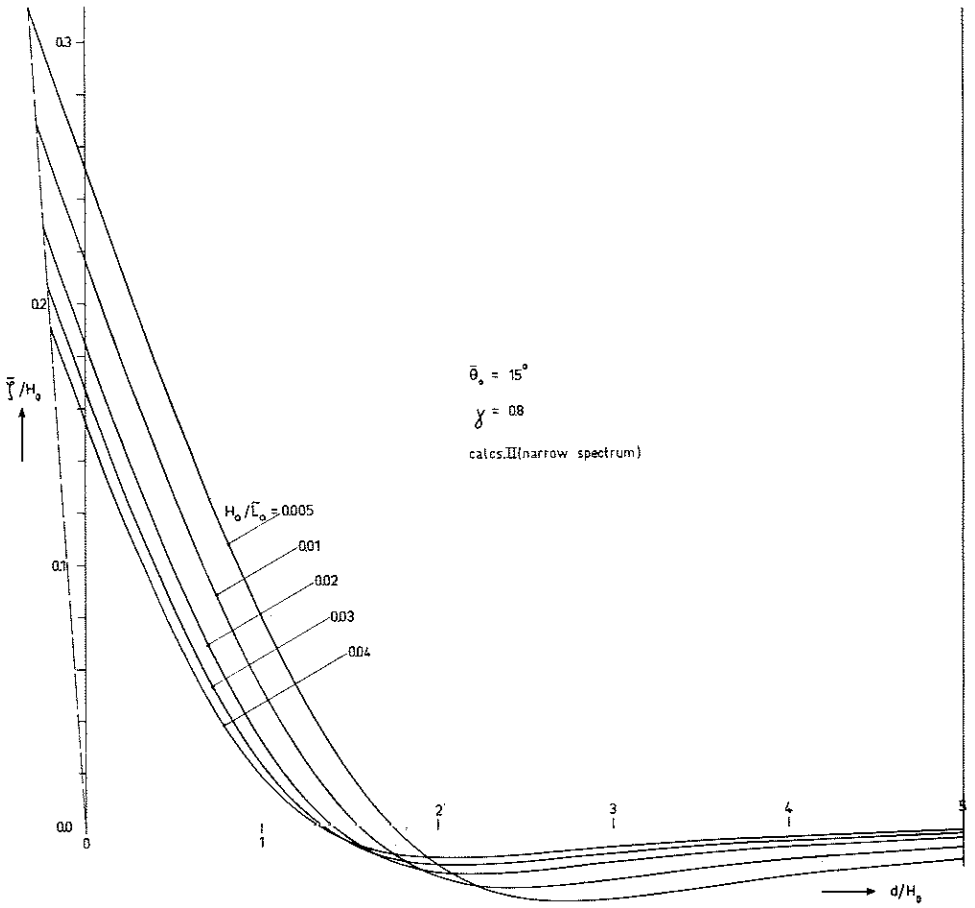

Fig. 6.3. Calculated set-up curves for various wave steepnesses.

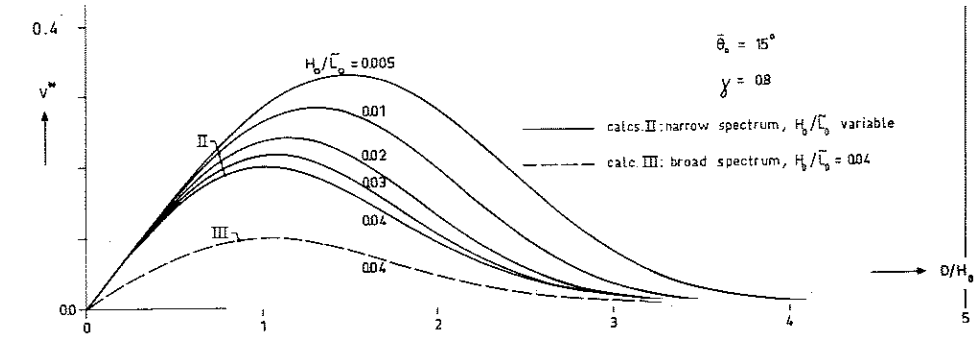

Fig. 6.4. Calculated longshore current velocity profiles for various wave steepnesses.

shows clearly how the angle of incidence affects not only the value of the maximum longshore current velocity in a profile (which is greatest for $\bar{\theta}_0 \tilde{\approx} 60^\circ$), but the whole profile as well, which narrows with increasing obliqueness of the waves. This is due to refraction, which causes the waves to break nearer to the shore. Although the location of the maximum of the calculated profiles varies considerably, depending on the values of the parameters $\bar{\theta}_0$ and $H_0/\tilde{L}_0$, it was found from inspection of the original calculated data that in all cases this maximum occurs very near to the point where dQ_b/dx_1 reaches its maximum. This can be expected in view of the fact that at the latter point the driving force $|dS_{12}/dx_1|$ obtains its maximum value (because $S_{12}=(1-Q_b)S_{12_f}$ and $dS_{12_f}/dx_1=0$), while V^* is proportional to this driving force, apart from the relatively slowly varying factor $\overline{|q'|}$. The value of Q_b at the point of maximum V^* was found to vary within rather narrow limits, from 0.55 to 0.58 approximately. An illustration of the preceding observations is given in fig. 6.5,

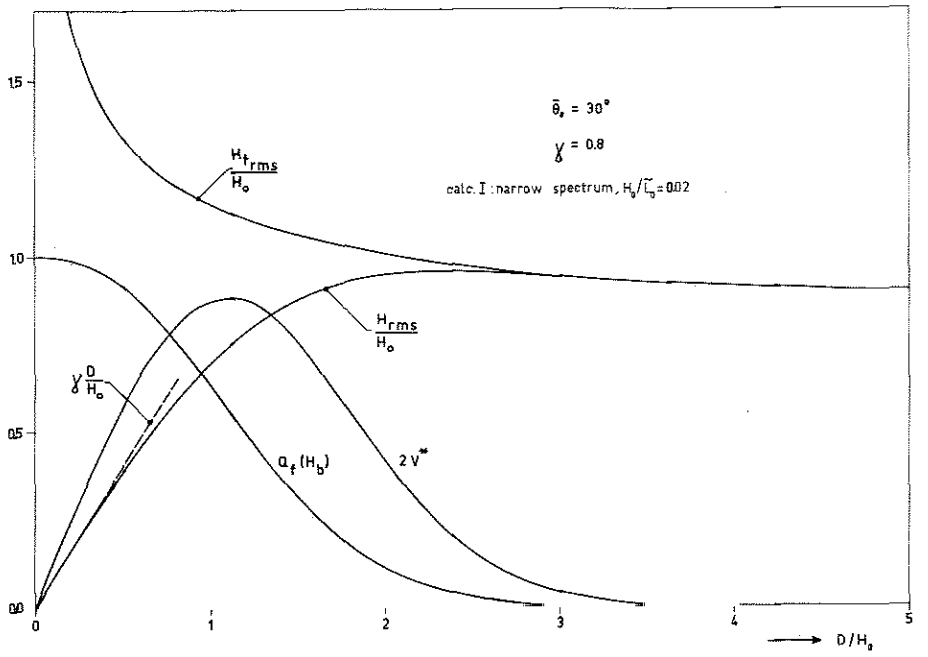

Figure 6.5.

in which Q_b and V^* are plotted vs. D/H_0 for one of the calculations of series I. The values of $H_{f_{rms}}/H_0$ and H_{rms}/H_0 are also shown.

It is of interest to compare the velocity profile in calculation III (broad spectrum) with the result in series II (narrow spectrum) at the same values of $\bar{\theta}_0$ (15^o) and $H_0/\tilde{L}_0$ (0.04). Both profiles are given in fig. 6.4. The longshore current velocities were calculated as $\bar{\tau}_2/\{\rho C_f|\vec{q}'|\}$. It has been pointed out in paragraph 5.2.2 that the total longshore thrust exerted on the surf zone is reduced by a factor $\frac{1}{2}$ if the waves are short-crested, with a directional spectrum proportional to $\cos^2(\theta_0-\bar{\theta}_0)$, instead of being long-crested. This is equivalent to saying that the laterally integrated longshore bottom shear stress ($\int\bar{\tau}_2\,dx_1$) is reduced by a factor $\frac{1}{2}$, but it does not imply that the local shear stresses $\bar{\tau}_2(x_1)$ are reduced in the same proportion, because the lateral distribution of these stresses may be different in the two cases of a broad spectrum and a narrow spectrum. The same applies to $\overline{|\vec{q}'|}$, and, therefore, also to the velocity V itself. Thus, although it may be expected that in calculation III the velocities are less than those in series II by a factor which is of the order of one half (for the same $\bar{\theta}_0$ and $H_0/\tilde{L}_0$), there is no a priori reason to expect the profiles in the two cases to be exactly similar. In order to check whether such similarity did nevertheless exist, V_{II} and $2V_{III}$ (in an obvious notation) were plotted vs. D/H_0 in a single graph. The result is not shown here because the differences between the two curves would not even be visible in a graph of the size which is used here. It would appear, then, that for the purpose of longshore current calculations based on the method presented in this thesis, and in cases such as considered above, the wave energy can be lumped into a very narrow frequency-and-direction interval, thereby obviating the need to carry out a number of numerical integrations over the two-dimensional spectrum at each step, provided the velocities so obtained are afterwards reduced by a factor equal to the ratio of the deep-water radiation shear stresses corresponding to the actual spectrum and the lumped, narrow spectrum. In terms of the notation used in paragraph 5.2.2, this ratio can be written as S_{12}/S_{12}^*, or as $2\sin^2\theta_0$.

6.4 Comparison with empirical data

6.4.1 Purpose and scope

The computational model put forward in chapter 5 and section 6.2 needs empirical verification. This requires measurements in the field and/or in the laboratory. Dorrestein [36] has made measurements of set-up on a natural beach; his results will be dealt with in paragraph 6.4.2. For the purpose of the present study, measurements have been made of the set-up due to random waves in a laboratory flume. The aim of these experiments was restricted to the verification of those aspects of the theory which relate to the two-dimensional situation of a unidirectional wave train of perpendicular incidence, in particular the prediction of the wave height decay in the shoreward direction and the associated set-up.

6.4.2 Field data

Dorrestein [36] has made field measurements of the set-up induced by wind-generated waves; he compared the results to the set-up calculated from an equation equivalent to (3.3.46), and arrived at the conclusion "... it can be stated that the theory presented to relate the wave set-up on a beach to the wave properties in relatively deep water is in fair agreement with the observations but that the accuracy of both the theory and the observations can be improved." Actually, this conclusion is not quite warranted, since the theory presented by Dorrestein deals with the relation between set-up and local wave properties, which in the calculations of the set-up were known from direct measurements. The relation between the wave properties in the surf zone and the wave properties in relatively deep water are not considered in [36]. This is precisely the relation considered in this thesis, particularly in chapter 5, the results of which were used in the computations presented in the preceding paragraph. For this reason it is of interest to compare these computations with Dorrestein's measurements. Five such measurements

are presented in [36], with different combinations of water level (tide) and incident waves. In three cases, a considerable fraction of the waves was breaking on an offshore bar, so that the calculated relationships between set-up on the beach and the deep-water wave properties, presented in section 6.3, are not applicable. The data pertaining to the other two cases are presented in Table 6.1*). The first column gives the characteristics of the incident waves. The period $\hat{T}$ equals $2\pi/\hat{\omega}$, in which $\hat{\omega}$ is the frequency at which $S(\omega)$ reaches its maximum. The second and third column give the depths at the locations of the measurements, and the values of $\bar{\zeta}$. Due to inaccuracies in leveling and reading the various gauges, the measured values of $\bar{\zeta}$ have a probable unsystematic error of about 0.5 cm to 0.8 cm, and a possible constant error of about 0.5 cm. In addition, there is a sampling error of at least 1 cm to 2 cm, due to the rather short averaging interval which was used (72 s), so that the given values may be in error by at least $\pm$ 2 cm, as indicated in the table.

In the calculations of $\bar{\zeta}$, no refraction effects were taken into account because the waves were of almost perpendicular incidence. The mean zero-crossing period in deep water was taken to be equal to $\hat{T}$ at the most seaward measurement location; this is considered permissible because the set-up is not very sensitive to variations in T_0. The values of γ which have been used are indicated in the table. The results are given in the fourth column. (Those for γ=0.75 can be obtained approximately from the curves in fig. 6.3.) The difference $\bar{\zeta}_{meas} - \bar{\zeta}_{calc}$ is listed in the last column of Table 6.1. Its average value is - 0.5 cm for the first case, and - 0.7 cm for the second case. The maximum deviation from this average is about 1.6 cm. These values are of the same order as the possible constant and unsystematic errors in $\bar{\zeta}_{meas}$, which are mentioned above. It is concluded that these field measurements lend support to the computational model used for the calculation of $\bar{\zeta}$ from the incident wave properties.

*) The author is indebted to Dr. Dorrestein for providing the original data.

inc. waves	d (cm)	$\bar{\zeta}_{meas}$ (cm) ($\pm$ 2 cm)	$\bar{\zeta}_{calc}$ (cm)	$\bar{\zeta}_{meas}-\bar{\zeta}_{calc}$ (cm)
$\sqrt{m_0}$=21 cm,	254	0.5	0.0	+ 0.5
$\hat{T}$=6.6 s	35.0	6.5	6.9	- 0.4
at d=4.55 m.	22.7	7.0	9.1	- 2.1
$H_0/\hat{L}_0$=0.009	12.5	8.8	10.7	- 1.9
Assumed:	3.7	11.7	12.3	- 0.6
γ=0.75	- 2.9	13.8	13.4	+ 0.4
	- 7.3	14.7	14.2	+ 0.5
$\sqrt{m_0}$=15 cm,	27.6	0.7	2.5	- 1.8
$\hat{T}$=2.8 s	22.5	2.1	2.9	- 0.8
at d=6.00 m.	16.2	3.7	3.6	+ 0.1
$H_0/\hat{L}_0$=0.035.	7.0	4.4	4.6	- 0.2
Assumed:				
γ=0.65				

Table 6.1

6.4.3 Laboratory measurements

Measurements of wave set-up were carried out in a random-wave flume of the Delft Hydraulics Laboratory. The flume which was used is 100 m long and 2 m wide; the water in the constant-depth portion of the flume was about 0.55 m deep. A hydraulically driven wave board capable of generating irregular waves is located at one end of the flume. At the other end a 1:20 plywood slope was installed. For measurements of the change in mean water level, particularly the set-up in the surfzone, 7 pressure taps (inner diameter 4 mm) were provided, flush with the slope. The taps were connected by plastic tubes (inner diameter 16 mm) to 15 cm inner diameter stilling wells, where a vibrating-point gauge sensed the water surface elevation to an accuracy of approximately 0.1 mm.

Four resistance type, temperature-corrected surface elevation sensors were installed. The gauges in a mean depth less than 20 cm were inserted through the plywood slope in order to maintain the minimum submergence necessary for a linear gauge response. As a consequence of this arrangement, these gauges could not easily be moved. The signal from each gauge was fed into analog equipment for the on-line determination of wave height histograms (based on 1000 wave heights between zero crossings) and energy spectra. The signals could also be recorded.

A r.m.s. incident wave height H_0 of 7 cm to 8 cm was used in all runs. It was kept more or less constant so that the pressure taps and the shallow-water wave gauges would be in the zone of breaking waves without being moved between runs. The mean period T_0 was approximately 1.2 s or 2.0 s. Each combination of H_0 and T_0 was used in conjunction with three different spectral widths. It appeared from the measurements that the applied variation of the width of the energy spectrum hardly affected the wave energy decay and the set-up. Its influence will not be further discussed.

A comparison of measured and calculated r.m.s. wave heights is given in table 6.2. The calculations are based on a value γ=0.8 for T_0=1.2 s and γ=0.9 for T_0=2.0 s. The value of H_{rms} in the constant-depth portion of the flume (d=55 cm) was taken as a boundary condition. This is indicated by arrows in the table.

It appears that the calculated value of H_{rms} at d=36 cm is consistently approximately 10% too high. This value is not affected by the choice of γ (within reasonable limits) because at the depth of 36 cm virtually no waves were breaking. At the remaining measurement points with smaller depths, where breaking did occur, the differences between computed and measured values are generally considerably smaller; the average absolute value of the deviation in these points is 4%. This is considered to be satisfactory.

Two examples of measured and computed set-up are given in fig. 6.6, one for T_0=1.2 s and one for T_0=2.0 s.

d (cm)	T_0=1.2 s						T_0=2.0 s					
	H_{rms} (cm)						H_{rms} (cm)					
	meas	calc	meas	calc	meas	calc	meas	calc	meas	calc	meas	calc
∞		7.85		8.22		8.11		7.70		8.48		7.95
55.0	7.25→7.25		7.60→7.60		7.50→7.50		7.26→7.26		7.99→7.99		7.49→7.49	
36.0	-	7.15	6.75	7.50	6.81	7.40	-	7.70	7.66	8.48	7.17	7.95
15.9	6.88	7.21	6.50	7.45	6.90	7.42	8.41	8.46	8.81	9.05	9.29	8.67
8.8	5.71	5.70	5.64	5.85	6.02	5.82	6.53	6.70	6.98	6.95	6.87	6.84
4.1	3.54	3.43	-	3.58	-	3.54	4.50	4.15	-	4,49	-	4.45

Table 6.2

The data which are not shown are in essence similar to those in fig. 6.6. The above-mentioned values of γ (0.8 and 0.9 respectively) were used in the calculations, while the value of $\bar{\zeta}$ at the toe of the slope was taken to be zero.

Inspection of fig. 6.6 shows that the set-down at the most seaward measuring point is fairly well predicted by the theory; this point is located outside the surf zone. Shoreward from this point, from $d \tilde{\sim} 15$ cm to $d \tilde{\sim} 8$ cm, the computed values show a much stronger rise towards the shore than the measurements. In smaller depths the computed values have very nearly the same trend as the data points.

The disagreement between theory and experiment was systematically present in all the laboratory data. It is therefore necessary to inquire into its possible causes. The theory was found to describe the r.m.s. wave height variation fairly well, particularly in the region $d < 16$ cm, which contains the area where the calculated set-up differs essentially from the measured set-up. In order to eliminate any uncertainties which nevertheless might be present in the theoretically calculated wave heights, the set-up between the wave gauges was computed using measured rather than calculated wave heights. As expected, the disagreement hardly diminished.

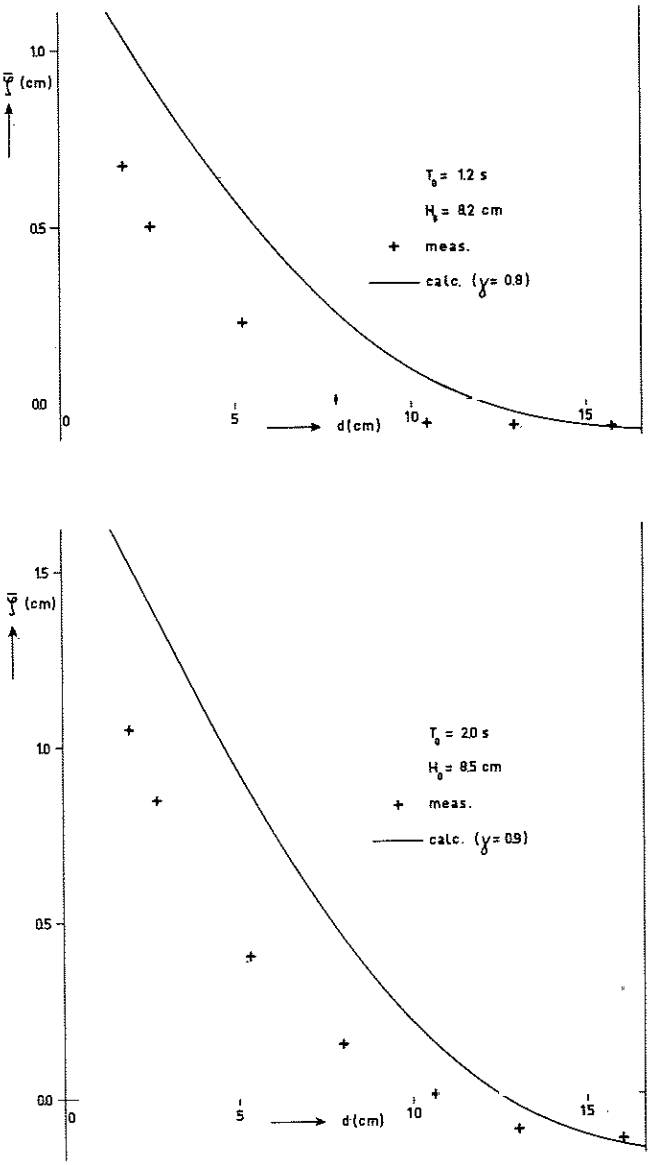

Fig. 6.6. Comparison of computed and measured set-up.

There is a region in which the mean square wave heights decrease considerably in the shoreward direction, which leads one to expect a proportionate decrease in the radiation stress S_{11} and a corresponding rise of the mean water level, while the measurements show a much smaller rise. The conclusion is that the measurements are in error, and/or that the theory used in relating wave characteristics and set-up is in error. The following remarks can be made regarding the measurements.

The wave height gauges are considered reliable. Calibrations were carried out frequently; they showed good linearity and no measurable drift.

The measurements of the mean water level were made indirectly, by means of bottom-mounted pressure taps. It has been shown by Dorrestein [31] and Longuet-Higgins and Stewart [33] that the mean pressure head at the bottom equals the mean depth, if the waves are statistically stationary in time and homogeneous in the horizontal coordinates (see eq. 3.3.9). The latter condition is not exactly met in the present tests but an analysis such as given by Dorrestein shows that errors arising from the horizontal inhomogeneities which occurred in the experiments cannot account for the observed discrepancy. In an interim report dealing with these measurements [110] the author conjectured that air entrainment in the water, due to breaking waves, might give a systematic error which could possibly explain the discrepancy. The reasoning behind this was as follows.

If wave breaking causes air entrainment then this occurs in the water of the flume only, not in the stilling well. It follows that the wave-induced rise in mean water level in the flume ($\bar{\zeta}$) is greater than the rise measured in the stilling well (denoted by $\bar{\zeta}_s$). The difference can be found by equating the mean bottom pressures:

$$\int_{-d}^{\bar{\zeta}} \rho\, g\, dz = \int_{-d}^{\bar{\zeta}_s} \rho g\, dz, \qquad (6.4.1)$$

in which $\overline{\rho'}$ is the mean density of the air-water mixture in the flume, which is roughly equal to $\rho(1-C)$, if C denotes the time-averaged volume concentration of air in water. It follows from (6.3.1) that the mean water level in the flume is underestimated by an amount equal to

$$\bar{\zeta} - \bar{\zeta}_s \approx \int_{-d}^{\bar{\zeta}} C(z)\, dz = \tilde{C}(d+\bar{\zeta}) = \tilde{C}D, \qquad (6.4.2)$$

in which $\tilde{C}$ is the air concentration averaged with respect to time and depth. The difference $(\bar{\zeta}-\bar{\zeta}_s)$ vanishes outside the surf zone, where $\tilde{C}\to 0$, and in very shallow water, where $D\to 0$. For small values of $\tilde{C}$, the absolute error is small compared with the total depth D, but not necessarily with respect to the set-up $\bar{\zeta}$. In order to check whether the air entrainment which does occur is sufficient to cause the observed differences, additional measurements were made with periodic waves (the experimental arrangement in the random-wave flume had already been dismantled). In these tests the change in mean water level was measured with a bottom-mounted pressure-gauge and with a surface elevation sensor; the measurement errors were of the order of 0.2 mm. No significant differences were found; if they occurred then they were totally inadequate to explain the discrepancy between measured and computed set-up in the random-wave experiments, which amounted to several mm (see fig. 6.6).

In summary, it can be said that for the conditions in these experiments, the mean pressure head at the bottom may be equated with the local mean depth. The problem then centres on the measurement of the mean bottom pressure, which was done by means of pressure taps connected by tubes to stilling wells. In an evaluation of this procedure, distinction should be made between the hydrodynamic and the electronic aspects of the system, i.e. between the water in the connection tubes and the stilling well, and its response to the varying pressure at the bottom of the flume on the one hand, and the electronic measurement of this response on the other hand.

The electronic part was frequently calibrated and is not suspect. Therefore, only the hydrodynamic aspects of the system are considered further. If this system were linear, as had been assumed initially, then the mean water level inside the stilling well would correspond to the mean bottom pressure in the flume. However, the connection tubes had several sudden profile contractions and enlargements; some of these were brought about by clamps on the plastic tubes. Such profile changes give rise to a quadratic flow resistance, which implies that the mean water level in the well is not necessarily the same as that in the flume. The difference varies with the asymmetry in the back--and-forth motions. For steep waves in shallow water, with narrow crests and elongated troughs, the mean level in the stilling well would be lower than that in the flume. Unfortunately, the geometrical characteristics of the profile changes are not known sufficiently for a quantitative analysis, so that it remains uncertain whether this effect can account for the observed discrepancies between theory and experiments. The measurements should be repeated with a better system for measuring the bottom pressure, e.g. with electronic pressure gauges mounted in the bottom.

Apart from the possibility of errors in the measurements, one should consider the question at which points the theory is most likely to be in error. The differential equation for the set-up (eq. 3.3.46) is obtained from eq. 3.3.44, which is exact in the problem under consideration, by neglecting the mean bottom shear stress in the onshore direction ($\bar{\tau}_1$). Although good estimates of this term are not available, it is difficult to see how it could account for the effects being investigated. It is therefore considered very unlikely that (3.3.46) would be seriously in error. Needless to say, in this statement it is assumed that S_{11} represents the total contribution of the unsteady motion to the mean horizontal flow of horizontal momentum; its definition involves an integral over the depth of terms involving the pressure and the horizontal velocity fluctuations. These have not been measured; they have instead been expressed in terms of the wave

heights. This is achieved by neglecting the contributions of the turbulence, and by using two essentially different approximations relating to the wave motion. The first of these is the neglect of the influence of inhomogeneities of average wave properties on the magnitude of the local radiation stress; the second is the use of a linear theory. It has been assumed so far that these approximations would give reasonable results. It is however quite conceivable that application to breaking waves gives erroneous results. For instance, in shallow water the following approximation is used for S_{11}:

$$S_{11} \approx \int_{-d}^{\bar{\zeta}} \rho \, \overline{q_1'^2} dz + \tfrac{1}{2}\rho g \, \overline{\zeta'^2} \approx 2E_k + E_p \approx \frac{3}{2} E. \qquad (6.4.3)$$

It can be seen that this implies that the kinetic energy of the waves equals the potential energy. However, in higher-order approximations, such as Stokes' third order, the kinetic energy exceeds the potential energy [111]. Furthermore, the ratio of kinetic energy to potential energy may depend on the rate of deformation of the waves. If these effects are significant at all then this is expected to be the case for relatively high waves in shallow water, particularly where many waves start breaking. A decrease in potential energy (wave heights) in such an area would then be accompanied by a less than proportionate decrease in kinetic energy. In addition to this, the intensity of the turbulence is relatively high in this region. As a result of these effects, S_{11} will decrease not as fast as calculated on the basis of the decrease in wave heights, and the set-up gradient is therefore overestimated in the area where the waves begin breaking in significant numbers.

It should be emphasized that the preceding arguments are of a hypothetical nature, in the sense that the effects which are mentioned are not known quantitatively. Additional measurements are needed to investigate this matter. The internal velocity field should be considered explicitly therein.

A question which arises in the present context is whether the hypothesis which has been advanced with respect to the magnitude of S_{11} is compatible with the conclusions arrived at by Bowen et al [6], whose experimental results are generally considered as confirmation of the "set-up theory". It is believed that such compatibility does exist. Bowen et al, using periodic waves, found agreement between theory and experiment with respect to the set-down (eq. 3.3.33) "in the region well outside the breakpoint", which is not significantly affected by the hypothesis given above, and with respect to the gradient of the set-up (eq. 3.4.4) "further inshore, where the bore was well formed" (thus, inshore of the area of most rapid wave deformation). The absolute value of the set-up in the surf zone is not considered in the comparison of theory and experiment given by Bowen et al, because they omitted the area near the breakpoint of the waves from the calculations. Because of this, no boundary condition was available for the integration of the set-up gradient shoreward of the breakpoint. The measured mean water level was found to be practically constant in the area from the breakpoint (where the crest of the wave begins to curl over) to the point where the wave form collapses, although the measured wave heights there decreased considerably. This is the same phenomenon as was observed in the experiments reported here.

Let us summarize the comparison of the theory with field data and laboratory data. The field data give support to the theory. The laboratory data give support to the theoretical prediction of the wave height decay in the surf zone, while systematic differences appeared to exist between measured and calculated set-up. However, the system which was used for the set-up measurements represents to some degree an uncertain element due to nonlinearities which are unknown in a quantitative sense. In conclusion, it must be said that the comparison of the theory with the field data and the laboratory data has been promising, but ultimately inconclusive. Additional investigations are required for more definitive answers to the questions which have been raised.

7 RUN-UP

7.1 Introduction

The preceding chapters dealt with waves on beaches, for which the similarity parameter ξ was sufficiently small for the occurrence of spilling breakers. In this and the following chapter we shall be concerned with waves breaking on steeper slopes, typical of sea dikes. The similarity parameter ξ is supposed to be of order one, which implies plunging breakers and a significant up-and-down motion of the water along the slope. We shall in particular consider the run-up height $\underline{R}$, i.e. the maximum height above S.W.L. reached by a wave rushing up the slope. This is a frequently used parameter in considerations of the required height of a dike. It will for brevity be called the run-up if no confusion is possible with the process of run-up. The run-up $\underline{R}$ associated with random waves is a random variable. Its distribution function will be considered extensively.

Most studies of run-up which have been made in the past were based on periodic waves. The approach has been predominantly empirical, particularly for the conditions of breaking waves envisaged in this chapter. The run-up for such waves varies non-linearly with the incident wave height, so that it is not possible to simulate the stochastic run-up process by linear superposition of periodic-wave solutions. In this respect we face the same situation as in the calculation of the set-up and the longshore current due to irregular, spilling breakers on a beach. There is an important difference, however. In the latter case the calculations were aimed at the time-mean value of a continuous variable to which all of the different waves in a random wave field contribute. In the case of the run-up height $\underline{R}$ we deal with discrete occurrences which can be attributed to individual waves breaking on the slope. For this reason run-up relationships for individual waves will play a key role in the computations.

Distribution functions of the run-up $\underline{R}$ were first calculated by Saville [112], who assigned to each individual wave of a random wave train the run-up value of a periodic wave train of corresponding height

and period. The hypothesis that this gives valid results will be referred to as the hypothesis of equivalency. A similar hypothesis has been widely and successfully used to compute distributions of non-linear wave forces on piles [113].

It should be noted that the hypothesis of equivalency does not necessarily imply that each individual wave causes a run-up equal to the run-up of the corresponding uniform wave train. The assumption is weaker, as it pertains to the distribution of wave height and period on the one hand, and of run-up on the other hand. In other words, it pertains to averages of many values, rather than to individual values. Empirical evidence supporting the hypothesis of equivalency has been given by van Oorschot and d'Angremond [114].

The run-up R of periodic waves of perpendicular incidence on a plane slope is determined mainly by the height H and the period T of the incident waves, by the gravitational acceleration g, and by the slope angle α: $R = R(H,T,g,\alpha)$. Therefore, in order to calculate the distribution function of the run-up $\underline{R}$ of random waves of perpendicular incidence on a plane slope by means of the hypothesis of equivalency, the function $R(H,T,g,\alpha)$ should be known, as well as the joint distribution function of $\underline{H}$ and $\underline{T}$. Saville uses the empirical run-up data published previously by him [115], and the joint distribution of $\underline{H}$ and $\underline{T}$ proposed by Bretschneider [83] for the case where these are stochastically independent, referred to in paragraph 4.5.4. The resulting distributions of the normalized run-up $\underline{R}/H_{1/3}$ have to be calculated numerically for each combination of structure slope and wave steepness.

The approach used herein is similar to the one used by Saville, as far as the hypothesis of equivalency is concerned. However, this hypothesis is elaborated differently in various respects. By considering only waves which break on the slope, Hunt's formula (eq. 2.3.22) can be used for the run-up of periodic waves. An analysis is made of existing laboratory data in order to check the validity of this approach. The use of Hunt's analytical expression enables us to normalize the run-up in such a way that it becomes independent of the slope angle and the wave steepness, obviating the need to

compute the run-up distribution anew for each combination of these parameters. It also permits the transformation of the joint distribution of $\underline{H}$ and $\underline{T}$ into the distribution of $\underline{R}$ to be carried out graphically or analytically. The analytical transformation is carried out first for an arbitrary joint distribution of $\underline{H}$ and $\underline{T}$, and subsequently for waves with a bivariate Rayleigh distribution of $\underline{H}$ and $\underline{T}^2$ and arbitrary degree of correlation. Results are given in closed form. They are compared to empirical data.

7.2 Run-up of periodic waves breaking on a slope

Hunt [1] has given the following empirical equation for the run-up of periodic waves of perpendicular incidence breaking on a plane slope:

$$R = 2.3T\sqrt{H}\,\tan\alpha \quad . \tag{7.2.1}$$

Eq. (7.2.1) is stated in the ft-sec system. Restoring dimensional homogeneity by substitution of $g = 32.2\ ft/s^2$, (7.2.1) may be written as

$$R = 0.4T\sqrt{gH}\,\tan\alpha \quad , \tag{7.2.2}$$

or, in view of (2.1.3), as

$$R = \sqrt{HL_0}\,\tan\alpha \quad , \tag{7.2.3}$$

which is equivalent to (2.3.22).

Eq. 7.2.1 is based on measurements made at the Waterways Experiment Station in Vicksburg, Mississippi, and at the Beach Erosion Board in Washington, D.C. According to Hunt, the breaking criterion of Iribarren and Nogales (eq. 2.3.5) is adequate to describe the transition from breaking to no breaking.

The author has previously given the following physical interpretation of Hunt's empirical equation [116]. The formula applies to

waves breaking on the slope. The initial horizontal velocity of the water particles in the mass of water which runs up the slope must be of the same order of magnitude as the particle velocities in the breaking wave, i.e., $O(\sqrt{gH})$. The motion is periodic, with period T, and the run-up time is $O(T)$. If it is assumed that the shape of the velocity-time curve of the advancing wave front does not significantly depend on the slope angle and the wave steepness, then the displacements along the slope are expected to be $O(T\sqrt{gH})$, and the vertical displacements, including the run-up height, are expected to be of order $T\sqrt{gH}\tan\alpha$. This agrees with (7.2.2).

The interpretation given suggests certain similarities in the run-up process. In order to investigate this a series of experiments was carried out in which the details of the run-up and run-down above S.W.L. were considered [19]. Slopes of 1:3, 1:5 and 1:7 were used, with wave steepnesses H/L_0 from 0.02 to 0.09. The parameter ξ ranged from 0.5 to 1.9. It was found that the interpretation given above needs some adjustment. The time of run-up from S.W.L. to the maximum height (t_r), and the mean velocity of the run-up front above S.W.L. ($\bar{c}_r$), normalized with T and $\sqrt{gH}$ respectively, were not in fact independent of α and H/L_0. They were found to vary with ξ:

$$\frac{t_r}{T} = 0.7\ \xi^{-\frac{1}{2}} \qquad (7.2.4)$$

and

$$\frac{\bar{c}_r}{\sqrt{gH}} = 0.6\ \xi^{\frac{1}{2}} \quad . \qquad (7.2.5)$$

The run-up height R which can be calculated from these equations deviates less than 4% from the value according to Hunt's formula.

The empirical data referred to above were obtained with waves of perpendicular incidence. The run-up of waves of oblique incidence is usually assumed to be proportional to the cosine of the angle of incidence [3]. This proportionality has been argued by noting that

the run-up of breaking waves of perpendicular incidence is proportional to tan α, i.e. to the component of the slope in the direction of propagation. This component reduces to (cos θ)(tan α) if θ is the angle of incidence. Empirical data presented by Hosoi and Shuto [117] are in reasonable agreement with this reduction, at least for breaking waves and $|\theta| < 50^{o}$. (For non-breaking waves the reduction is less than it is for breaking waves.)

7.3 A check of the applicability of Hunt's formula to irregular waves

It has been mentioned in the introduction to this chapter that run-up distributions will be calculated by applying Hunt's formula to individual waves. Before proceeding to elaborate deductions which can be made from this premiss we will in this paragraph present some laboratory data which can be used for a partial check of the validity of the approach. The check can be no more than partial because of the restricted variation in the available data. These data were obtained in the Delft Hydraulics Laboratory in a study of run-up carried out on behalf of the Department of Zuiderzee Works [3]. The results have partly been published by Wassing [118]. Additional information has been gathered by the author from the original, unpublished data.

In the experiments the run-ups of irregular waves on various plane slopes were measured. The waves were generated by a combination of wind and a bulkhead with a periodic motion. As a result, the model waves were not natural wind waves on a small scale. The measured wave height distribution was much narrower than the Rayleigh distribution. The deviation from natural conditions was even greater for the wave periods, which in the model varied but very little. They will be considered to be constant.

Two series of measurements were made, with a nominal wave height of 0.10 m and 0.07 m, respectively. It is not clear from the original report how the wave heights had been defined. For this reason they are called the nominal wave heights, H_{nom}. The waterdepth (0.35 m), the mean wave period (1s), and the mean wavelength (1.40 m) were the same in both series.

We have to check to what extent the application of Hunt's formula ($R = 0.4\ T\sqrt{gH}\ \tan\alpha$) to individual waves yields a run-up distribution in agreement with the measured distribution. The proportionality of the run-up with T cannot be investigated because T was not varied. Only the proportionality with $\sqrt{H}\ \tan\alpha$ can be checked. This will be done in two stages. First, the magnitude of the median run-up (R_{50}) is considered, and after that the shape of the run-up distribution, as given by R_n/R_{50}, in which n is the probability of exceedance, expressed as a percentage [$n = 100\ (1 - F)$].

The raw experimental data regarding R_{50} are given in the first three columns of Table 7.1. The last two columns represent the experimental values of the dimensionless parameter R^*_{50} defined by

$$R^*_{50} = \frac{R_{50}}{0.4\ T\ \sqrt{gH_{nom}}\ \tan\alpha} \quad , \qquad (7.3.1)$$

which should be a constant according to the hypothesis to be tested. The value of the constant cannot be predicted because of the uncertainty with respect to H_{nom}. The agreement between R^*_{50} values for the same

tan α	R_{50}		R^*_{50}	
	H_{nom} = 10 cm	H_{nom} = 7 cm	H_{nom} = 10 cm	H_{nom} = 7 cm
0.1	4.7	3.7	1.17	1.11
0.15	6.9	5.7	1.15	1.14
0.2	9.3	8.1	1.16	1.21
0.25	11.8	9.3	1.18	1.12
0.286	15.4	13.4	1.35	1.40
0.333	15.8	13.2	1.19	1.19
0.4	17.5	15.4	1.09	1.15

Table 7.1

value of tan α is good within 5%, and confirms the proportionality of R and $\sqrt{H}$. The agreement between R^*_{50} values within one column is

fairly good; this confirms the proportionality of R and tan α. Only the two points for tan α = 0.286 (1 : 3½) deviate considerably from the others, for unknown reasons. Apart from these two, all measured values of R^*_{50} are grouped closely around the mean value of 1.15, with a maximum deviation of approximately 5% only. This means that for these experiments the variation of the median run-up with wave height and slope angle is adequately expressed by Hunt's equation. Whether or not this is also the case for run-up values with a different probability of exceedance can be investigated by comparing R_n/R_{50} to $(H_n/H_{50})^{\frac{1}{2}}$. According to the hypothesis to be tested, these parameters should be equal to each other for all n, because T was assumed to be constant. Such a comparison has been given in Table 7.2 for values of n from 50 to 2. The values of R_n/R_{50} and H_n/H_{50} have been obtained by averaging over the different slope angles

n(%)	R_n/R_{50}	H_n/H_{50}	$(R_n/R_{50})/\sqrt{H_n/H_{50}}$
	(a) H_{nom} = 7 cm		
50	1.00	1.00	1.00
40	1.04	1.09	1.00
30	1.08	1.18	1.00
20	1.13	1.30	0.99
10	1.20	1.46	0.99
5	1.27	1.60	1.00
2	1.33	1.71	1.02
	(b) H_{nom} = 10 cm		
50	1.00	1.00	1.00
40	1.06	1.11	1.01
30	1.12	1.26	1.00
20	1.19	1.41	1.00
10	1.29	1.58	1.03
5	1.37	1.77	1.03
2	1.46	1.96	1.04

Table 7.2

in each of the two series. It can be seen that the ratio between R_n/R_{50} and $(H_n/H_{50})^{\frac{1}{2}}$ deviates at most a few percent from one. This lends strong support to the approach which has been adopted, and which will be elaborated in the following sections of this chapter.

7.4 Run-up distributions of breaking waves with arbitrary joint distribution of $\underline{H}$ and $\underline{L}_0$

7.4.1 Analytical solution

In this section run-up distributions for waves of perpendicular incidence will be determined by assigning to each wave a run-up height according to Hunt's formula. It is assumed that effects of oblique incidence on the run-up can be accounted for by multiplying the calculated run-ups for perpendicular incidence with a constant factor, tentatively taken to be the cosine of the mean angle of incidence. The fact that this factor is common to all the waves in a given wave train implies that the influence of the variability of the direction of propagation on the run-up is neglected.

It is convenient to use Hunt's formula as given by (7.2.3), rather than (7.2.2), since (7.2.3) is symmetric in H and L_0. On the basis of the hypothesis of equivalency a similar equation is assumed to hold for random waves:

$$\underline{R} = \sqrt{\underline{H}\,\underline{L}_0}\,\tan\alpha \quad . \tag{7.4.1}$$

The quantity $\underline{L}_0$ is defined as $g\underline{T}^2/2\pi$, in which $\underline{T}$ is the zero-crossing period. $\underline{L}_0$ will for brevity be called the deep-water wave-length even though this interpretation is valid for periodic waves only.

It is to be noted that in (7.4.1) $\underline{H}$, $\underline{L}_0$ and tan α appear in a product of powers. This has the advantage that the run-up can be so normalized as to make its distribution independent of slope angle and mean wave steepness. The variables will be normalized as follows:

$$\underline{h} = \underline{H}/\overline{H} \quad , \tag{7.4.2}$$

$$\underline{\ell} = \underline{L}_0/\overline{L}_0 \quad , \tag{7.4.3}$$

and

$$\underline{r} = \underline{R}/(\sqrt{\overline{H}\,\overline{L}_0}\,\tan\alpha) \quad . \tag{7.4.4}$$

Substitution of (7.4.1), (7.4.2) and (7.4.3) into (7.4.4) gives

$$\underline{r} = \sqrt{\underline{h}\,\underline{\ell}} \quad . \tag{7.4.5}$$

Thus, the distribution of the normalized run-up equals the distribution of $\sqrt{\underline{h}\underline{\ell}}$. Denoting the distribution function of $\underline{r}$ by F(r), we have

$$F(r) = \Pr\{\underline{r} \leq r\} = \Pr\{\sqrt{\underline{h}\,\underline{\ell}} \leq r\} \quad . \tag{7.4.6}$$

It should be determined from the joint p.d.f. of $\underline{h}$ and $\underline{\ell}$, which is assumed to be known in the present context; it is written as $f(h,\ell)$ and defined by

$$\Pr\{h < \underline{h} \leq h + dh \quad \text{and} \quad \ell < \underline{\ell} \leq \ell + d\ell\} = f(h,\ell)dh\,d\ell \quad . \tag{7.4.7}$$

The right-hand side of (7.4.7) is called a probability element. The probability that $\underline{h}$ and $\underline{\ell}$ simultaneously assume values in a certain interval of the (h,ℓ) plane is determined by summing the corresponding probability elements, i.e. by integrating $f(h,\ell)$ over the area of the (h,ℓ) plane under consideration. Thus, F(r) is found by integration of (h,ℓ) with respect to h and ℓ for all values thereof which fulfil the inequality $\sqrt{h\ell} \leq r$:

$$F(r) = \iint_{\substack{\text{all } h,\ell \text{ for} \\ \text{which } \sqrt{h\ell} \leq r}} f(h,\ell)dh\,d\ell \quad . \tag{7.4.8}$$

Only positive values of h, ℓ and r need be considered. The interval of integration is indicated in fig. 7.1 by the hatched area of the (h,ℓ) plane. It is bordered by the hyperbola $h\ell = r^2$ and by the straight lines h = 0 and ℓ = 0. The integral can be written as

$$F(r) = \int_0^{\infty} dh \int_0^{r^2/h} f(h,\ell)\,d\ell \quad . \tag{7.4.9}$$

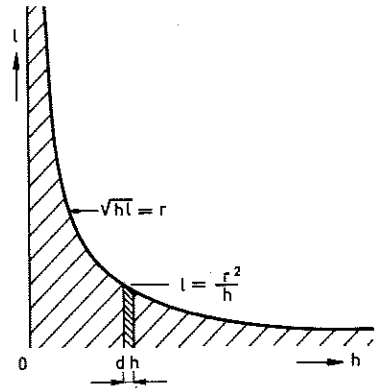

Fig. 7.1 - Area of integration in the (h,ℓ) plane.

Differentiation of this expression with respect to r yields the probability density of $\underline{r}$:

$$f(r) = \frac{dF(r)}{dr} = 2r \int_0^{\infty} \frac{1}{h} f\left(h, \frac{r^2}{h}\right) dh \quad . \tag{7.4.10}$$

A more formal derivation of this result can be given by using the rules for the transformation of one multi-dimensional p.d.f. into another one of the same number of dimensions [51]. If (h,ℓ) and (p,q) are single-valued functions of each other then

$$f(p,q) = f(h,\ell)\,|J| \quad , \tag{7.4.11}$$

in which

$$J = \frac{\partial(h,\ell)}{\partial(p,q)} = \begin{vmatrix} \frac{\partial h}{\partial p} & \frac{\partial h}{\partial q} \\ \frac{\partial \ell}{\partial p} & \frac{\partial \ell}{\partial q} \end{vmatrix} \tag{7.4.12}$$

is the Jacobian of the transformation, which is assumed to be non-zero. We choose one of the variables p and q to be equal to $\sqrt{h\ell}$ (=r); the other, say p, is a dummy variable which can be chosen for convenience. The p.d.f. of r can then be found as a marginal p.d.f. of f(p,r) by integration with respect to the dummy variable p. Choosing p = h gives

$$J = \frac{\partial(h,\ell)}{\partial(h,\sqrt{h\ell})} = 2\sqrt{\frac{\ell}{h}} \quad , \tag{7.4.13}$$

so that

$$f(h,\sqrt{h\ell}) = 2\sqrt{\frac{\ell}{h}}\, f(h,\ell) \tag{7.4.14}$$

or

$$f(h,r) = \frac{2r}{h}\, f(h, \frac{r^2}{h}) \quad , \tag{7.4.15}$$

from which (7.4.10) follows by integration with respect to h.

The equations 7.4.9 and 7.4.10 represent the formal solution to the problem of determining the run-up distribution from a known joint distribution of wave height and period, if Hunt's equation is applied to individual waves. These expressions are valid for arbitrary f(h,ℓ), as long as the waves are breaking on the slope. Before substituting specific functions for f(h,ℓ) a graphical method of estimating F(r) from discrete data on wave heights and periods is presented.

7.4.2 Graphical solution for discrete data

In this paragraph it will be assumed that a scatter diagram is available of wave height versus period, in which each realization of ($\underline{H}$,$\underline{T}$) is represented by a dot. The problem is to compute an estimate of the associated run-up distribution, if for individual waves the run-up is given by Hunt's equation.

A practical solution to this problem is suggested by the analytical derivation in the preceding paragraph. On a transparent sheet of

paper a family of curves is drawn along each of which $T\sqrt{H}$ is constant. (On double-log paper such curves will be straight lines). This sheet is used as an overlay over the given scatter diagram. By simply counting the number of dots of the scatter diagram between consecutive pairs of curves $T\sqrt{H}$ = constant, the number of anticipated run-ups in certain classes can be determined. The cumulative probability can next be found by summation.

7.5 Run-up distributions of waves with a bivariate Rayleigh distribution of $\underline{H}$ and $\underline{L}_0$

7.5.1 Probability density and distribution function

The expressions for the run-up distribution obtained in paragraph 7.4.1 can be used for waves with an arbitrary joint p.d.f. of $\underline{H}$ and $\underline{L}_0$. In order to obtain more specific results we shall now confine ourselves to winddriven waves for which $\underline{H}$ and $\underline{L}_0$ are tentatively assumed to be jointly Rayleigh-distributed. Referring to Appendix 1, the p.d.f. of the normalized wave height and length can then be written as

$$f(h,\ell;\kappa) = \frac{\pi^2}{4} \frac{h\ell}{1-\kappa^2} \exp\left(-\frac{\pi}{4}\frac{h^2+\ell^2}{1-\kappa^2}\right) I_0\left(\frac{\pi}{2}\frac{\kappa}{1-\kappa^2} h\ell\right), \quad (7.5.1)$$

in which

$$0 \leq \kappa \leq 1 \quad . \quad (7.5.2)$$

The dependence on the parameter κ is indicated explicitly for later reference.

Eq. 7.5.1 can be substituted into (7.4.10) with the result

$$f(r;\kappa) = \frac{\pi^2}{2} \frac{r^3}{1-\kappa^2} I_0\left(\frac{\pi}{2}\frac{\kappa}{1-\kappa^2} r^2\right) \int_0^\infty \frac{1}{h} \exp\left(-\frac{\pi}{4}\frac{h^2 + r^4 h^{-2}}{1-\kappa^2}\right) dh \quad (7.5.3)$$

By substituting

$$t = \frac{\pi}{4} \frac{h^2}{1 - \kappa^2} \tag{7.5.4}$$

and

$$x = \frac{\pi}{2} \frac{r^2}{1 - \kappa^2} \tag{7.5.5}$$

the integral in (7.5.3) can be written as

$$\int_0^\infty e^{-t} \left(\frac{1}{2t} e^{-\frac{x^2}{4t}}\right) dt \quad . \tag{7.5.6}$$

It is equal to $K_0(x)$, the modified Bessel function of the third kind of order zero [90, eq. 29.3.120]. Substitution into (7.5.3) gives

$$f(r;\kappa) = \frac{\pi^2}{2} \frac{r^3}{1 - \kappa^2} I_0\left(\frac{\pi}{2} \frac{\kappa}{1 - \kappa^2} r^2\right) K_0 \left(\frac{\pi}{2} \frac{r^2}{1 - \kappa^2}\right) \quad . \tag{7.5.7}$$

This function is shown graphically in fig. 7.2 for six values of κ which have been so selected as to give equal increments of λ, the coefficient of linear correlation between $\underline{h}$ and $\underline{\ell}$ (see Appendix 1).

The distribution function may be found by integration of f(r):

$$F(r) = \int_0^r f(r^*)\, dr^* \quad . \tag{7.5.8}$$

In order to carry out this integration, it is convenient to transform to the variable x defined by (7.5.5). Because x is a single-valued function of r, and vice versa (for $r \geq 0$), we have

$$f(x) = f(r) \frac{dr}{dx} \quad . \tag{7.5.9}$$

Substitution of (7.5.5) and (7.5.7) into (7.5.9) gives

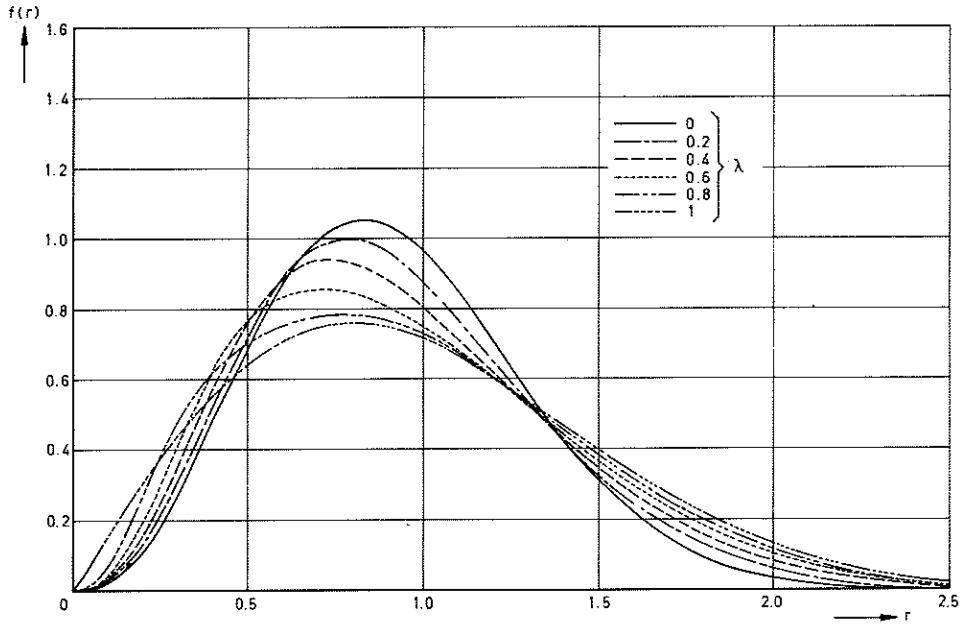

Fig. 7.2 - Probability density of normalized run-up.

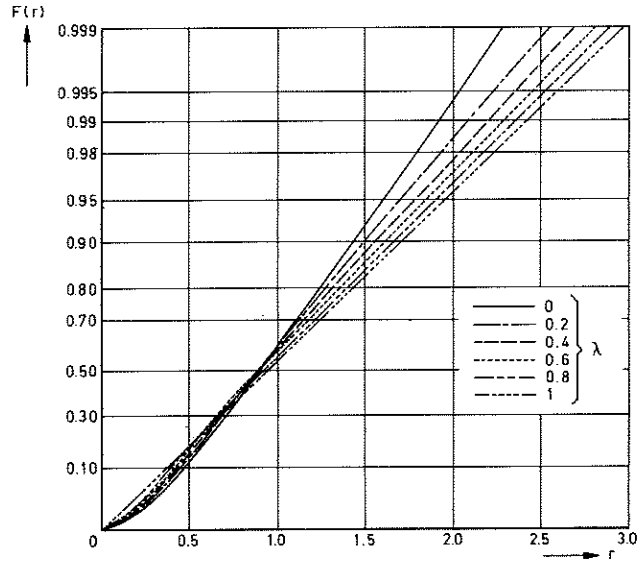

Fig. 7.3 - Distribution function of normalized run-up.

$$f(x;\kappa) = (1 - \kappa^2)\ x\ I_0(\kappa x)\ K_0(x) \quad . \qquad (7.5.10)$$

The distribution function is

$$F(x;\kappa) = (1 - \kappa^2) \int_0^x x^* I_0(\kappa x^*)\ K_0(x^*)\ dx^* \quad . (7.5.11)$$

The following relations hold between I_0, I_1, K_0 and K_1 and their derivatives:

$$I_0'(z) = I_1(z) \quad , \qquad (7.5.12)$$

$$\{z\ I_1(z)\}' = z\ I_0(z) \quad , \qquad (7.5.13)$$

$$K_0'(z) = -\ K_1(z) \quad , \qquad (7.5.14)$$

and

$$\{z\ K_1(z)\}' = -\ z\ K_0(z) \quad , \qquad (7.5.15)$$

in which a prime denotes a differentiation with respect to z [90]. With these relationships (7.5.11) can be evaluated by repeated integration by parts:

$$\int x\ I_0(\kappa x)\ K_0(x)\ dx = -\int I_0(\kappa x)\ d\ \{x\ K_1(x)\}$$

$$= -\ I_0(\kappa x)\ x\ K_1(x) + \int x\ K_1(x)\ d\ I_0(\kappa x)$$

$$= -\ x\ I_0(\kappa x)\ K_1(x) + \int x\ K_1(x)\ \kappa\ I_1(\kappa x)\ dx$$

$$= -\ x\ I_0(\kappa x)\ K_1(x) - \int \kappa x\ I_1(\kappa x)\ d\ K_0(x)$$

$$= -\ x\ I_0(\kappa x)\ K_1(x) - \kappa x\ I_1(\kappa x)\ K_0(x) + \int K_0(x)\ d\ \{\kappa x\ I_1(\kappa x)\}$$

$$= - x\, I_0(\kappa x)\, K_1(x) - \kappa x\, I_1(\kappa x)\, K_0(x) + \kappa^2 \int K_0(x)\, x\, I_0(\kappa x)\, dx \quad , \tag{7.5.16}$$

so that

$$(1 - \kappa^2) \int x\, I_0(\kappa x)\, K_0(x)\, dx = - x\, I_0(\kappa x)\, K_1(x) - \kappa x\, I_1(\kappa x)\, K_0(x) \quad . \tag{7.5.17}$$

The Bessel functions in (7.5.17) behave as follows for small values of their argument:

$$I_0(z) \to 1 \quad ,$$

$$I_1(z) \to \tfrac{1}{2} z \quad ,$$

$$K_0(z) \to - \ell n\, z \quad ,$$

and

$$K_1(z) \to z^{-1} \qquad \text{for } z \to 0 \quad , \tag{7.5.18}$$

so that

$$\lim_{x \to 0} x\, I_0(\kappa x)\, K_1(x) = 1 \tag{7.5.19}$$

and

$$\lim_{x \to 0} \kappa x\, I_1(\kappa x)\, K_0(x) = 0 \quad . \tag{7.5.20}$$

It follows from (7.5.11), (7.5.17), (7.5.19) and (7.5.20) that

$$F(x;\kappa) = 1 - x\, I_0(\kappa x)\, K_1(x) - \kappa x\, I_1(\kappa x)\, K_0(x) \quad . \tag{7.5.21}$$

Substitution of (7.5.5) in the right-hand side of (7.5.21) gives $F(r;\kappa)$, which has been plotted in fig. 7.3 for selected values of κ.

7.5.2 Special values

Eq. 7.5.21 reduces to simpler forms in the two special cases of zero correlation and 100% correlation between $\underline{h}$ and $\underline{\ell}$. In the first case we have $\kappa = 0$, so that

$$x = \frac{\pi}{2} r^2 \quad , \tag{7.5.22}$$

as follows from (7.5.5), and

$$F(r;0) = 1 - \frac{\pi}{2} r^2 K_1(\frac{\pi}{2} r^2) \quad . \tag{7.5.23}$$

In the second case, $\kappa = 1$, so that x is unbounded if $r \neq 0$. The asymptotic behaviour of the Bessel functions in (7.5.21) for large values of their argument is given by

$$I_m(z) \to \frac{e^z}{\sqrt{2\pi z}} \qquad \text{for } z \to \infty \tag{7.5.24}$$

and

$$K_m(z) \to \sqrt{\frac{\pi}{2z}}\, e^{-z} \qquad \text{for } z \to \infty \tag{7.5.25}$$

for m = 0, 1, etc. Substitution of (7.5.5), (7.5.24) and (7.5.25) into (7.5.21) gives after some manipulation

$$F(r;\kappa) \to 1 - \frac{1 + \kappa}{2\sqrt{\kappa}} \exp(-\frac{\pi}{2} \frac{r^2}{1 + \kappa}) \quad \text{for } \kappa \to 1 \tag{7.5.26}$$

so that

$$F(r;1) = 1 - \exp(-\frac{\pi}{4} r^2) \quad , \tag{7.5.27}$$

which is the (univariate) Rayleigh distribution function. This is to be be expected, since $\kappa = 1$ implies that $\underline{h} = \underline{\ell}$ with 100% probability (see Appendix 1). This in turn means that

$$\underline{r} = \sqrt{\underline{h}\,\underline{\ell}} = \underline{h} = \underline{\ell} \quad , \tag{7.5.28}$$

so that the distribution function of $\underline{r}$ for $\kappa \to 1$ converges to that of $\underline{h}$ or $\underline{\ell}$, i.e. to the Rayleigh distribution function. Indeed, the preceding investigation of the behaviour of $F(r;\kappa)$ for $\kappa = 1$ is given more as a check on the general formula (7.5.21) than because of its practical importance, for the case $\kappa = 1$ is not expected to occur in actual wind waves. However, it is interesting to note that (7.5.26) represents not only the asymptotic behaviour of $F(r;\kappa)$ for $\kappa \to 1$ but also that of $F(r;\kappa)$ for $r \to \infty$ at a constant value of $\kappa \neq 0$, since in both cases $x \to \infty$ and $\kappa x \to \infty$, as follows from (7.5.5). This implies that for large r and arbitrary $\kappa > 0$ a plot of $F(r;\kappa)$ on Rayleigh - probability-paper approaches a straight line through the origin, as can indeed be seen in fig. 7.3. This may be shown by noting that in the Rayleigh-probability-paper of fig. 7.3 the scale of r along the abscissa is linear, while the scale of F is chosen so that the plot of $F(r;1)$ gives a straight line; this can be achieved by plotting the inverse function of $F(r;1)$ linearly along the ordinate. This inverse function is, from (7.5.27),

$$\frac{2}{\sqrt{\pi}} \{ - \ell n(1 - F)\}^{\frac{1}{2}} \quad . \tag{7.5.29}$$

Substitution of (7.5.26) into (7.5.29) gives

$$\frac{2}{\sqrt{\pi}} \{\frac{\pi}{2} \frac{r^2}{1 + \kappa} - \ell n \frac{1 + \kappa}{2\sqrt{\kappa}} \}^{\frac{1}{2}} \quad , \tag{7.5.30}$$

which approximates to

$$(\frac{2}{1 + \kappa})^{\frac{1}{2}} r \tag{7.5.31}$$

for sufficiently large r. If $\kappa = 0$ then we must start from (7.5.23). Using (7.5.25) it can be shown that

$$F(r;0) \to 1 - \frac{\pi}{2} r \exp(-\frac{\pi}{2} r^2) \qquad \text{for } r \to \infty \tag{7.5.32}$$

Substitution of this equation into (7.5.29) leads to the same result

as (7.5.31) for $\kappa = 0$, since $\frac{\pi}{2} r^2 - \ln(\frac{\pi}{2} r) \underset{\sim}{>} \frac{\pi}{2} r^2$ for large r.

The mean of the normalized run-up can be found as a moment of the joint p.d.f. of $\underline{h}$ and $\underline{\ell}$, a general expression for which has been given in Appendix 1. Substituting (A1.19) gives

$$\overline{r} = E\{\underline{h}^{\frac{1}{2}} \underline{\ell}^{\frac{1}{2}}\} = M_{\frac{1}{2}\frac{1}{2}} = \frac{2}{\sqrt{\pi}} \{\Gamma(\tfrac{5}{4})\}^2 \, {}_2F_1(-\tfrac{1}{4}, -\tfrac{1}{4}; 1; \kappa^2). \tag{7.5.33}$$

This expression reduces to

$$\overline{r} = \frac{2}{\sqrt{\pi}} \{\Gamma(\tfrac{5}{4})\}^2 \underset{\sim}{>} 0.93 \quad \text{if} \quad \kappa = 0 \tag{7.5.34}$$

and to

$$\overline{r} = 1 \quad \text{if} \quad \kappa = 1 \quad . \tag{7.5.35}$$

The associated cumulative probabilities are 0.535 and 0.544 respectively, i.e. approximately 0.54 in both cases. From the monotonic behaviour of the functions involved it may be inferred that this value will also hold for other values of κ.

The mean square normalized run-up can also be calculated as a moment of $f(h,\ell)$. Using (A1.23) and (A1.27) we find

$$\overline{r^2} = E\{\underline{h}\underline{\ell}\} = {}_2F_1(-\tfrac{1}{2}, -\tfrac{1}{2}; 1; \kappa^2) = (\frac{4}{\pi} - 1)\lambda + 1 \quad . \tag{7.5.36}$$

It may be useful to revert briefly to non-normalized variables. Using (2.1.3), eq. 7.4.4 can be written as

$$\underline{R} = \underline{r} \sqrt{\overline{H}\, \overline{L}_0} \tan\alpha = 0.4 \, \underline{r} \sqrt{g\overline{H}\, \overline{T^2}} \tan\alpha \tag{7.5.37}$$

This equation can be expressed in terms of the commonly used parameters $\overline{T}$ and $H_{1/3}$ by utilizing the following relationships, which

hold if $\underline{H}$ and $\underline{T}^2$ are Rayleigh-distributed:

$$\overline{T} = (\tfrac{4}{\pi})^{\frac{1}{4}}\, \Gamma(\tfrac{5}{4})\, \sqrt{\overline{T^2}} \underset{\sim}{\approx} 0.96\, \sqrt{\overline{T^2}} \qquad (7.5.38)$$

and

$$\overline{H} \underset{\sim}{\approx} 0.625\, H_{1/3} \quad . \qquad (7.5.39)$$

This yields

$$\underline{R} = 0.33\, \underline{r}\, \overline{T}\, \sqrt{gH_{1/3}}\, \tan\alpha \ , \qquad (7.5.40)$$

or, using the wave steepness $\overset{\sim}{\delta}$ defined by (4.5.24),

$$\underline{R} = 0.83\, \underline{r}\, \overset{\sim}{\delta}^{-\frac{1}{2}}\, H_{1/3}\, \tan\alpha \quad . \qquad (7.5.41)$$

As an example, the value exceeded by 2% of the run-ups will be considered for the limiting cases $\kappa = 0$ and $\kappa = 1$. The 2%-value is chosen in view of a comparison with empirical data in section 7.7. Entering fig. 7.3 with the value $F = 0.98$ and reading the corresponding values of r gives

$$r_2 = 1.78 \quad \text{if} \quad \kappa = 0 \qquad (7.5.42)$$

and

$$r_2 = 2.23 \quad \text{if} \quad \kappa = 1 \ , \qquad (7.5.43)$$

in which the subscript refers to the exceedance percentage. Substituting these into (7.5.40) and (7.5.41) we find

$$R_2 = 0.59\, \overline{T}\, \sqrt{gH_{1/3}}\, \tan\alpha = 1.47\, \overset{\sim}{\delta}^{-\frac{1}{2}}\, H_{1/3}\, \tan\alpha \quad \text{if } \kappa = 0 \qquad (7.5.44)$$

and

$$R_2 = 0.74\ \overline{T}\ \sqrt{gH_{1/3}}\ \tan\alpha = 1.84\ \delta^{\gamma-\frac{1}{2}}\ H_{1/3}\ \tan\alpha \quad \text{if } \kappa = 1 \quad . \tag{7.5.45}$$

These formulae are compared to empirical data in section 7.7.

7.5.3 Maximum run-up

Consider the maximum normalized run-up height ($\underline{r}_{max}$) in a series of N run-ups. Its distribution function $F_N(r)$ can be derived by the reasoning already referred to in paragraph 4.4.8 with respect to $\underline{H}_{max}$. Thus,

$$F_N(r) = \Pr\{\underline{r}_{max} \leq r\} = \{F(r)\}^N \quad . \tag{7.5.46}$$

As in paragraph 4.4.8, we consider large values of N (greater than 100, say), in which case only large values of r are of interest. Eq. (7.5.46) then approximates to

$$F_N(r) = e^{-NQ(r)} \quad , \tag{7.5.47}$$

in which

$$Q(r) = 1 - F(r) \quad . \tag{7.5.48}$$

The expected value of $\underline{r}_{max}$ can be calculated from this distribution function as

$$E\{\underline{r}_{max}\} = \int_0^\infty r\ dF_N(r) = -\int_0^\infty r\ dQ_N(r) = \int_0^\infty Q_N(r)\ dr \tag{7.5.49}$$

in which

$$Q_N(r) = 1 - F_N(r) \tag{7.5.50}$$

Substitution of (7.5.21) and (7.5.5) and numerical integration has given the result shown in fig. 7.4.

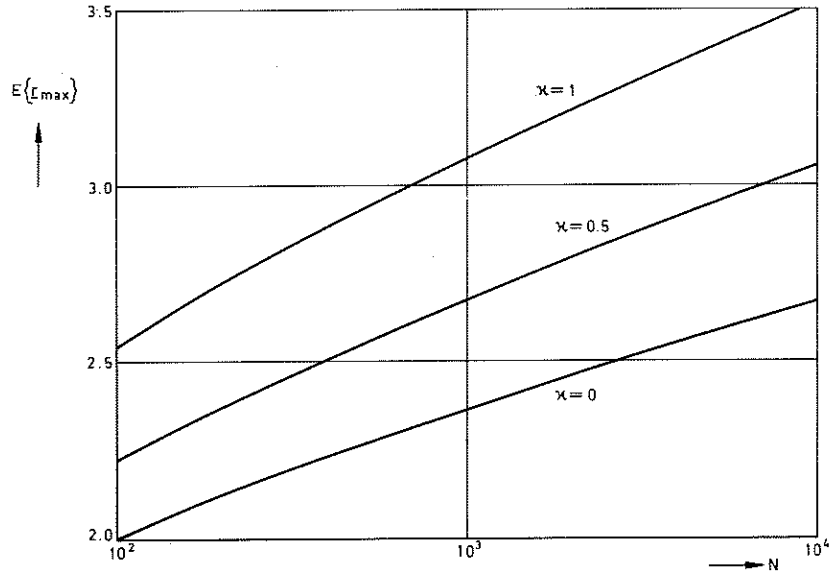

Fig. 7.4 - Expected value of normalized maximum run-up.

An approximate expression in closed form for $E\{r_{max}\}$ can be found by using the approximation to $F(r;\kappa)$ given by (7.5.26), which can be written as

$$F(r;\kappa) \approx F^*(r;\kappa) = 1 - \frac{1+\kappa}{2\sqrt{\kappa}} \exp\left(-\frac{\pi}{2}\frac{r^2}{1+\kappa}\right) \quad , \tag{7.5.51}$$

and which is valid for large $\frac{\kappa r^2}{1-\kappa^2}$. This gives

$$F_N(r) \approx F_N^*(r) = e^{-N\{1-F^*(r)\}} = e^{-N\frac{1+\kappa}{2\sqrt{\kappa}} e^{-\frac{\pi}{2}\frac{r^2}{1+\kappa}}} \tag{7.5.52}$$

It then follows from analogy with (4.4.29) and (4.4.30) that

$$E\{r_{max}\} \approx \{\frac{2}{\pi}(1+\kappa)\}^{\frac{1}{2}}\{(\ell n\, N)^{\frac{1}{2}} + 0.29\,(\ell n\, N)^{-\frac{1}{2}}\} \quad , \tag{7.5.53}$$

in which

$$\hat{N} = \frac{1 + \kappa}{2\sqrt{\kappa}} N \quad . \tag{7.5.54}$$

As noted previously, the approximation (7.5.51) is not valid for $\kappa \to 0$. However, a comparison of (7.5.53) with the result calculated numerically from the exact distribution function $F(r;\kappa)$ has shown that for $N > 100$ the relative error is less than 1% for $\kappa > 0.1$ and less than 5% for $\kappa > 0.01$, so that the lower limit of κ, for which (7.5.53) is still a useful approximation, is quite small.

7.6 Steepness distribution

It has been pointed out that Hunt's equation is not applicable to waves for which the steepness $S = H/L_0$ is less than the critical value given by Iribarren and Nogales' breaking criterion. Like $\underline{H}$ and $\underline{L}_0$, $\underline{S}$ is a stochastic variable. Its distribution function will be determined in order to be able to estimate for a given random wave train the fraction of the waves that will break on the slope.

The steepness will be normalized as follows:

$$\underline{s} = \frac{\underline{S}}{\overline{H/L_0}} = \frac{\underline{H/L_0}}{\overline{H/L_0}} \quad , \tag{7.6.1}$$

or, using (7.4.1) and (7.4.2),

$$\underline{s} = \underline{h}/\underline{\ell} \quad . \tag{7.6.2}$$

The distribution function and the probability density of $\underline{s}$ can be obtained from $f(h,\ell)$ by exactly the same procedures as were used in paragraph 7.4.1 for $\underline{r}$. The results are

$$F(s) = \int_0^\infty d\ell \int_0^{s\ell} f(h,\ell)\, dh \tag{7.6.3}$$

and

$$f(s) = \int_0^\infty \ell \, f(s\ell,\ell) \, d\ell \quad . \tag{7.6.4}$$

Only positive values of s need be considered.

Substitution of the bivariate Rayleigh probability density for $f(h,\ell)$ into (7.6.4) gives

$$f(s;\kappa) = \frac{\pi^2}{4} \frac{s}{1-\kappa^2} \int_0^\infty \ell^3 \exp(-\frac{\pi}{4} \frac{1+s^2}{1-\kappa^2} \ell^2) I_0(\frac{\pi}{2} \frac{\kappa s}{1-\kappa^2} \ell^2) \, d\ell \quad . \tag{7.6.5}$$

By substituting

$$y = \frac{\pi}{2} \frac{\kappa s}{1-\kappa^2} \ell^2 \tag{7.6.6}$$

and

$$p = \frac{1+s^2}{2\kappa s} \quad , \tag{7.6.7}$$

(7.6.5) becomes

$$f(s;\kappa) = \frac{1-\kappa^2}{2\kappa^2 s} \int_0^\infty y \, e^{-py} \, I_0(y) \, dy \quad . \tag{7.6.8}$$

The integral in (7.6.8) converges if and only if $p > 1$ [119]. This can be seen from the asymptotic behaviour of $I_0(y)$ for large y, given by (7.5.24). The condition $p > 1$ can also be written as

$$\frac{\frac{1}{2}(s^{-1} + s)}{\kappa} \geq 1 \quad . \tag{7.6.9}$$

The numerator is greater than 1 except for $s = 1$, in which case it equals 1. The denominator is at most 1. Thus, only if $\kappa = 1$ *and* $s = 1$ does the integral fail to converge. This is to be expected inasmuch as $\kappa = 1$ implies that $\underline{h} = \underline{\ell}$, or $\underline{s} = 1$, with a probability of 100%. The corresponding probability density is zero for all $s \neq 1$ and it is unbounded for $s = 1$. It is described by Dirac's unit impulse function:

$$f(s;1) = \delta(s - 1) \quad . \tag{7.6.10}$$

The distribution in this case is the unit step function centred at $s = 1$.

If $\kappa < 1$, which will always be the case for actual waves, then $p > 1$ for all s, and the integral in (7.6.8) is bounded. It has been evaluated using section 13.2 from Watson [119], with the result

$$\int_0^\infty y\, e^{-py}\, I_0(y)\, dy = \frac{p}{(p^2 - 1)^{3/2}} \quad . \tag{7.6.11}$$

Substitution of (7.6.7) and (7.6.11) into (7.6.8) gives for the p.d.f. of $\underline{s}$

$$f(s;\kappa) = 2(1 - \kappa^2) \frac{s(1 + s^2)}{\{s^4 + (2 - 4\kappa^2)s^2 + 1\}^{3/2}} \quad . \tag{7.6.12}$$

This equation has been plotted in fig. 7.5 for selected values of κ; for $\kappa = 0$ it reduces to

$$f(s;0) = \frac{2s}{(1 + s^2)^2} \quad . \tag{7.6.13}$$

The distribution function $F(s;\kappa)$ can be found by integration of (7.6.12). It is convenient to transform to a variable q defined by

$$q = s^2 \quad . \tag{7.6.14}$$

The transformed p.d.f. is

$$f(q;\kappa) = (1 - \kappa^2) \frac{1 + q}{\{q^2 + (2 - 4\kappa^2)q + 1\}^{3/2}} \quad , \tag{7.6.15}$$

which can readily be integrated. The result, transformed back in terms of s, is

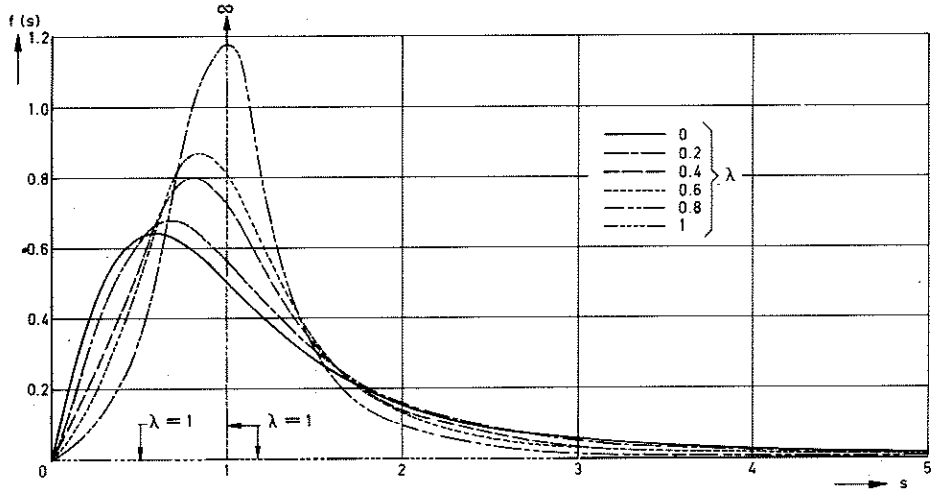

Fig. 7.5 - Probability density of normalized steepness.

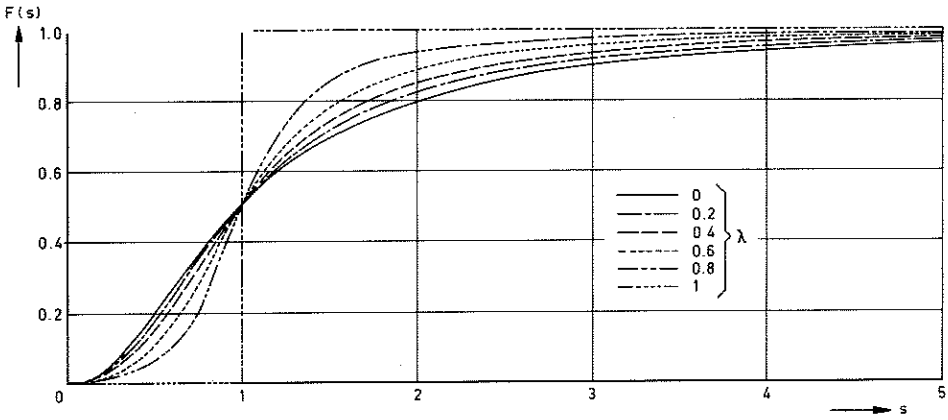

Fig. 7.6 - Distribution function of normalized steepness.

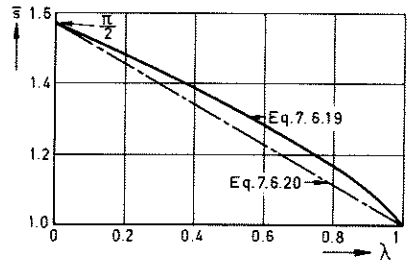

Fig. 7.7 - Mean normalized steepness vs. correlation coefficient of $\underline{H}$ and $\underline{L_0}$.

$$F(s;\kappa) = \tfrac{1}{2} + \frac{s^2 - 1}{2\{s^4 + (2 - 4\kappa^2)s^2 + 1\}^{\frac{1}{2}}} \quad . \qquad (7.6.16)$$

For $\kappa = 0$ it reduces to

$$F(s;0) = \frac{s^2}{1 + s^2} = \frac{1}{1 + s^{-2}} \quad . \qquad (7.6.17)$$

Graphs of $F(s;\kappa)$ are given in fig. 7.6.
It is evident from this figure as well as from (7.6.16) that the median of the normalized steepness does not depend on κ; it is always 1.

The mean steepness has been evaluated as a moment of $f(h,\ell)$:

$$\bar{s} = E\{\underline{s}\} = \int_0^\infty \int_0^\infty (h/\ell)\, f(h,\ell)\, dh\, d\ell \quad . \qquad (7.6.18)$$

Substitution of (A1.19) and (A1.29) gives

$$\bar{s} = E(\kappa) \quad , \qquad (7.6.19)$$

the complete elliptic integral of the second kind of modulus κ. Utilizing the relationship between κ and λ given in Appendix 1, $\bar{s}$ is plotted as a function of λ in fig. 7.7. Eq. (7.6.19) may be compared to a result given by Bretschneider [83], who in his work on wave variability referred to in paragraph 4.5.4 considered not only the wave heights and periods but the steepness as well. He did not determine its distribution function but only the mean value, with the result

$$\bar{s} = \frac{\pi}{2} - \lambda\,(\frac{\pi}{2} - 1) \quad , \qquad (7.6.20)$$

which is shown in fig. 7.7. Only for $\lambda = 0$ and $\lambda = 1$ do (7.6.19) and (7.6.20) give the same result. Bretschneider's derivation is based on knowledge of the marginal distributions of $\underline{H}$ and $\underline{L}_0$ alone (Rayleigh), and on the assumption that the mutual regressions of $\underline{H}$ and $\underline{L}_0$ would

be linear, while (7.6.19) is based on a bivariate Rayleigh distribution of $\underline{H}$ and $\underline{L}_0$. It has been shown in Appendix 1 that the assumption of linear regression is incompatible with the assumption of a bivariate Rayleigh distribution, except in the limiting cases $\lambda = 0$ and $\lambda = 1$. Therefore, only in these limiting cases is exact agreement between (7.6.19) and (7.6.20) to be expected. For intermediate values of λ the difference between the two is at most 5%.

The distribution function $F(s;\kappa)$ may be used to estimate the fraction of the waves for which Hunt's formula would (not) be applicable. As an example, consider a case in which $\tan\alpha = 1 : 5$, $\bar{H}/\bar{L}_0 = 0.03$, and $\underline{H}$ and $\underline{L}_0$ are uncorrelated. The critical steepness for the occurrence of breaking is given by Iribarren and Nogales' criterion, eq. 2.3.5, as

$$S_c = (H/L_0)_c \approx (\frac{\tan\alpha}{2.3})^2 \approx 0.19 \tan^2\alpha \quad , \qquad (7.6.21)$$

which gives $S_c = 0.19\ (0.2)^2 = 0.0076$. The corresponding normalized critical steepness is $s_c = 0.0076/0.03 \approx 0.25$. From fig. 7.6 or from (7.6.17) it can be seen that $F(0.25;0) \approx 0.06$. This means that, in the example given, Hunt's formula would be applicable to 94% of the waves in the wave train.

7.7 Comparison with empirical data

The derivations in section 7.5 were based on the following premisses:

P1 The distribution function of the run-up of waves of perpendicular incidence on a plane slope can be determined by assigning to each individual wave, characterized by a pair of values of height and period, a run-up according to Hunt's formula.

P2 $\underline{H}$ and $\underline{L}_0$ have a bivariate Rayleigh distribution.

The first of these premisses has been partly verified in section 7.3, using laboratory data. The waves in the laboratory had been

generated mainly with a wave board with a periodic motion, and modified by wind. The statistical properties of the waves were not similar to those in nature: the variability of the wave heights was much less than for a Rayleigh-distributed variable, while the period was approximately constant. It is therefore useful to make additional checks on the validity of P1 for more natural wave conditions.

Van Oorschot and d'Angremond [114] have carried out run-up experiments in the laboratory with irregular waves generated with a programmed wave board. In addition, a wind with a mean velocity of up to 3m/s was blown over the water surface. The resulting waves were a much more realistic simulation of natural wind waves than the laboratory waves used previously. This was checked with respect to the energy spectra, some of which were in fact modelled on measured North Sea spectra, and with respect to the wave height distributions. However, no data are given with respect to the wave period distribution. While the experimental results therefore cannot be used for a detailed check of the validity of P1 or P2, it is nevertheless deemed useful to use them for comparison with the deductions made from (P1 + P2) in order to obtain an indication of whether or not the calculated results are realistic.

The main object of the study by van Oorschot and d'Angremond was the effect of the spectral shape on the wave run-up, in particular the effect of the spectral width. The parameter ε introduced by Cartwright and Longuet-Higgins (see eqs. 4.4.10 and 4.4.11) was used as a quantitative measure of the spectral width. (It can be shown [63] that ε, if small, represents the relative root-mean-square width of the spectral density function.) The values of ε were computed after cutting off the high-frequency tail of each spectrum at the frequency at which the spectral density was 5% of the maximum value. As a result, the actual ε-values are considerably underestimated (by about 40% for a Pierson-Moskowitz or a Neumann-spectrum). This is of no concern, however, as in this application there is no compelling reason to use just ε as a measure of the spectral width.

A spectrum which was roughly similar to that given by Pierson-Moskowitz was used as a reference spectrum; its ε-value was 0.45. This

spectrum was considered to be of medium width. The values of ε in the other spectra ranged from 0.34 for a narrow spectrum to 0.59 for a wide spectrum (excluding a case of $\varepsilon = 0.22$ in one run in which the waves were generated entirely by wind, and in which the wave height distribution was quite different from the Rayleigh distribution, in contrast to the other runs).

In addition to ε , the following parameters were varied: $\hat{T}$, the period of the spectral component with maximum energy density (0.71s to 1.64s); $H_{1/3}$, the significant wave height (3.7 cm to 13.6 cm); $H_{1/3}/g\hat{T}^2$ (4.0×10^{-3} to 12.2×10^{-3}); $d/g\hat{T}^2$, a relative waterdepth (1.7×10^{-2} to 8.1×10^{-2}); and tan α (1 : 4 and 1 : 6).

The effects of wave height, wave period and slope angle on the run-up were found to be adequately expressed by a Hunt-type formula with a proportionality factor which is given as a function of n, the exceedance percentage, and of ε:

$$R_n = C_n(\varepsilon)\ \hat{T}\ \sqrt{gH_{1/3}}\ \tan\alpha \quad . \tag{7.7.1}$$

This implies that the shape of the run-up distribution is significantly affected by ε only, not by the wave steepness, the relative water depth or the slope angle. It is in agreement with PI if the additional assumption is made that the shape of the distribution of $\underline{H}$ and $\underline{T}$ is determined by the spectral shape, as is indeed the case in the linear approximation.

For a comparison of (7.5.40) with (7.7.1), it is necessary that both equations be expressed in terms of the same parameters. The characteristic wave period in (7.5.40) is $\overline{T}$, while that in (7.7.1) is $\hat{T}$. The ratio $\hat{T}/\overline{T}$ in the laboratory experiments was roughly 1.05, so that (7.7.1) can be written as

$$R_n \approx 1.05\ C_n(\varepsilon)\ \overline{T}\ \sqrt{gH_{1/3}}\ \tan\alpha \quad . \tag{7.7.2}$$

(It is not known which of the equations (7.7.1) and (7.7.2) should be preferred if $\hat{T}/\overline{T} \neq 1.05$.) However, the relationship between ε and λ is

not known, so that (7.5.40) and (7.7.2) cannot be compared for specific values of these parameters. For an overall comparison, the measured range and the calculated range will be considered. Van Oorschot and d'Angremond give the values of the coefficient $C_n(\varepsilon)$ for n = 2%. It ranges from 0.57 to 0.73 for $0.34 \leq \varepsilon \leq 0.59$. This gives a range of 1.05 C_2 from 0.60 to 0.77 approximately, as compared to the calculated range of the coefficients in (7.5.44) and (7.5.45) from 0.59 to 0.74. It appears that the calculated range is realistic.

In a discussion of empirical run-up data reference should be made to the following formula, which is well known and widely used in the Netherlands:

$$R_2 = 8\, H_{1/3} \tan \alpha \quad . \tag{7.7.3}$$

This equation is nominally valid for a steepness of 0.05 [118]. It is based partly on the laboratory data already referred to in section 7.3, and partly on unpublished visual observations during storms in the Yssel Lake and the Wadden Sea [3]. Wassing [118] gives the following formulae, based on the laboratory data alone:

$$R_2 = 7.5\, H \tan \alpha \qquad \text{for} \quad H/L = 0.05 \tag{7.7.4}$$

and

$$R_2 = 7\, H \tan \alpha \qquad \text{for} \quad H/L = 0.07 \quad . \tag{7.7.5}$$

H is referred to by Wassing as "the average height of the .... waves in the model which did not vary very much". Regarding the transformation of the latter equations into (7.7.3), Wassing observes:

> "Since the waves in the model were proportionally too steep (resulting in too small values of R_2), the difficulty arose how to transfer the model results to the prototype. After considering all the factors involved, it was decided to increase

the factor 7.5 in the model to 8 in the prototype, for the 2% run-up on a dike with a stone revetment and waves of a steepness of 0.05. The run-up is thereby expressed in the "significant wave height" $H_{1/3}$. In this way the following formula was obtained:

$$R_2/H_{1/3} = 8 \tan \alpha \qquad \text{(for } H/L = 0.05\text{)}$$

This formula ..... proved to be in good agreement with the prototype observations carried out in the Netherlands for slopes not steeper than 16 degrees".

The author has elsewhere [3] given a detailed re-analysis of the laboratory data; it was concluded that these give more support to a proportionality of the run-up with $T\sqrt{H} \tan \alpha$ than to a proportionality with $H \tan \alpha$. Reference is made to paragraph 7.3. Furthermore, the laboratory results cannot unambiguously be transferred to prototype conditions, even for the same wave steepness, because the statistical properties of the laboratory waves were very different from those in nature. Also, the prototype data referred to by Wassing were only few in number, and they were obtained visually, so that their quantitative value is doubtful. (Wave recorders did not yet exist at the time of the observations.) In summary, it appears that the factual basis of (7.7.3) is rather weak. The formula is to be regarded as giving an indication only. (It was not intended to be more when it was first formulated [3]. But this fact is at present not as well known as the formula itself.) For this reason it will not be used as a standard of reference for checking the validity of the calculated results. At most a rough comparison is appropriate. Eq. (7.7.3) is nominally valid for a steepness of 0.05. Substituting this value for $\hat{\delta}$ into (7.5.44) and (7.5.45) we find

$$R_2 = (6.6 \text{ to } 8.2)\, H_{1/3} \tan \alpha \quad \text{for } 0 \leq \lambda \leq 1 \quad . \tag{7.7.6}$$

It can be seen that (7.7.3) and (7.7.6) are not mutually exclusive.

8 OVERTOPPING

8.1 Introduction

The considerations in the preceding chapter concerning the run-up of waves were based on the tacit assumption that the crest of the dike was of sufficient height to prevent overtopping. Situations in which overtopping does occur can also be of major interest; they will be dealt with in this chapter. The overtopping volumes of water will first be related to the run-up heights of periodic waves. The result will be applied in the calculation of the distribution function and the expected value of the overtopping volumes in random waves.

8.2 Overtopping due to periodic waves breaking on a slope

8.2.1 Relation between run-up and overtopping

In chapter 7 reference has been made to a study by Battjes and Roos [19] concerning certain details of the process of run-up of periodic, breaking waves. Information was obtained about the variation of the profile of the water in the uprush and in the downrush on the slope above S.W.L. as a function of time. The results have been used in relation to overtopping, although this phenomenon did not actually occur in the experiments. A certain hypothetical relation has been formulated. Before this is given here we need to define a number of parameters.

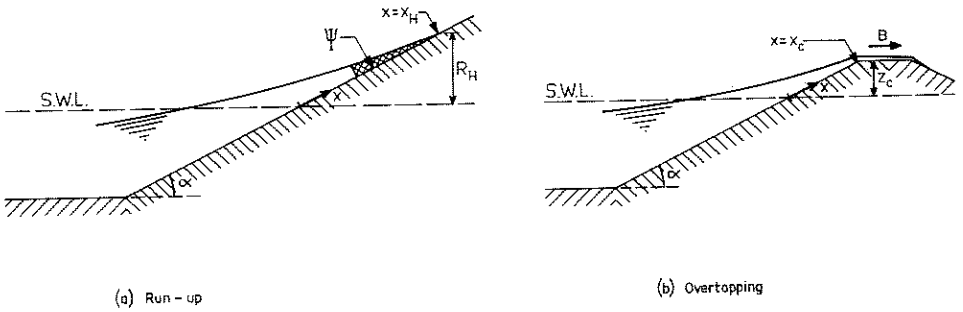

Fig. 8.1 - Definition sketch

A coordinate axis (x) is chosen, directed upward along the slope, with the origin at the still-water line (see fig. 8.1). Let $\Psi(x,t)$ represent the instantaneaous volume of water on the slope above a point at a distance x from the still-water line, as measured in the run-up experiments (without overtopping). This function is periodic in t for periodic waves; its local maximum value is denoted as $\Psi_m(x)$. Furthermore, let $B(x_c)$ represent the volume of water which would overtop the dike during one wave period if the crest were located at $x = x_c$, other conditions being the same. In the following we use volumes per unit width, so that Ψ and B actually represent areas.

In order to express overtopping quantities (such as B) in terms of run-up parameters (such as Ψ) it was tentatively assumed that

$$B(x_c) = \Psi_m\Big|_{x = x_c} \quad . \tag{8.2.1}$$

The values of Ψ_m should be expressed in terms of the incident wave parameters. In this regard it is convenient to use the run-up height according to Hunt's formula as a scaling parameter. It is written as R_H:

$$R_H \equiv \sqrt{HL_0}\,\tan\alpha \quad . \tag{8.2.2}$$

The corresponding run-up length along the slope is given by

$$x_H \equiv \frac{R_H}{\sin\alpha} = \frac{\sqrt{HL_0}}{\cos\alpha} \quad , \tag{8.2.3}$$

which on gentle slopes is nearly equal to $\sqrt{HL_0}$. The layer thicknesses on the slope were experimentally found to be proportional to $\sqrt{HL_0}$. This led to the expectation that Ψ_m would be proportional to HL_0. An analysis of the data confirmed this. However, the ratio Ψ_m/HL_0 was found to increase with α, approximately in proportion to $\sqrt{\tan\alpha}$, at a constant value of the fractional distance along the slope defined by

$$\eta \equiv \frac{x}{x_H} \quad . \tag{8.2.4}$$

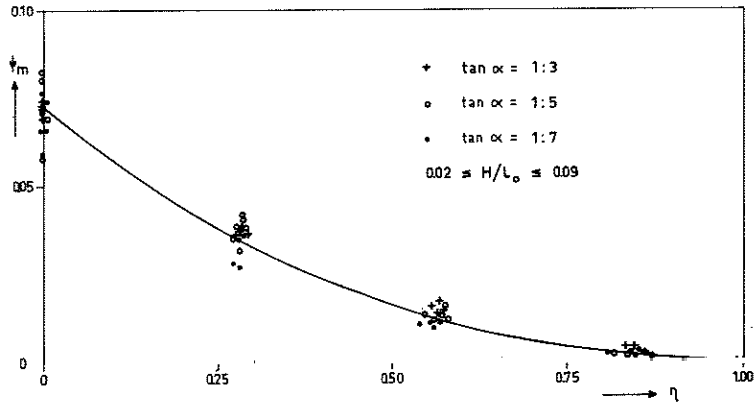

Fig. 8.2 - Normalized volume of uprush.

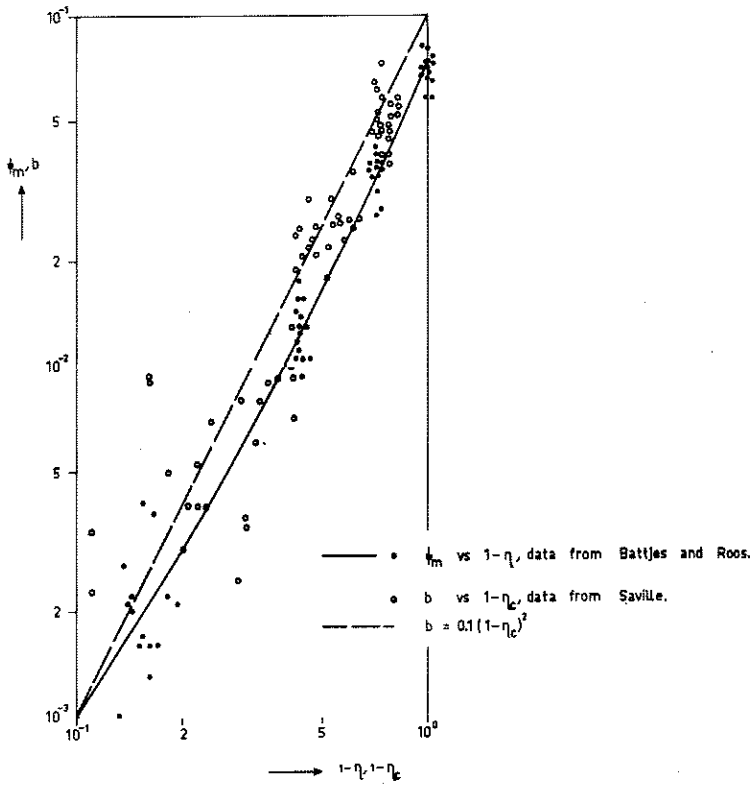

Fig. 8.3 - Normalized volume of uprush and of overtopping.

In other words, the normalized volume ψ_m, defined by

$$\psi_m \equiv \frac{\Psi_m}{HL_0 \sqrt{\tan \alpha}} \quad , \tag{8.2.5}$$

is approximately a function of η only. The experimental results are shown in fig. 8.2. A smooth curve has been drawn through the data points to indicate the trend more clearly. The data have been replotted as ψ_m versus $(1 - \eta)$ in fig. 8.3 on double-logarithmic paper (solid circles). The parameter $(1 - \eta)$ has been chosen instead of η itself because $(1 - \eta)$ represents a relative excess of run-up length past the location on the slope under consideration; it may be surmised that the normalized volume above this location is more simply related to $(1 - \eta)$ than to η itself. Inspection of fig. 8.3 shows that ψ_m is roughly proportional to $(1 - \eta)^2$.

The volume which is overtopped in one wave period will be normalized as follows:

$$b \equiv \frac{B}{HL_0 \sqrt{\tan \alpha}} \quad . \tag{8.2.6}$$

According to the hypothesis expressed by (8.2.1) we have

$$b(\eta_c) = \psi_m \Big|_{\eta = \eta_c} \tag{8.2.7}$$

in which

$$\eta_c = \frac{x_c}{x_H} \quad . \tag{8.2.8}$$

If we denote the crest height of the dike above S.W.L. by z_c (see fig. 8.1b) then (8.2.8) is equivalent to

$$\eta_c = \frac{z_c}{R_H} \quad , \tag{8.2.9}$$

and $(1 - \eta_c)$ then represents a relative excess of run-up height above crest height.

It should be pointed out that the parameter Ψ_m in (8.2.4) depends on the incident waves through the product HL_0 only. This is significant because the steepness H/L_0 was varied considerably in the experiments (from 0.02 to 0.09 approximately). In view of (8.2.2) it implies that Ψ_m can be expressed as a function of the run-up height R_H, for a given slope angle. The same then holds for the volume which overtops per wave (B), provided (8.2.1) is true. It should be said that B is expected to be somewhat underestimated by (8.2.1), because the uprush in each wave is to a certain extent impeded by the water which is still on the slope due to the preceding wave, and this is less if overtopping occurs than in the absence of overtopping. The effect of this has to be checked empirically. Even if the hypothesis adopted would not lead to quantitatively correct results, then it may still serve a purpose in suggesting suitable normalization factors, i.e. by suggesting that

$$b = f(\eta_c) \quad , \tag{8.2.10}$$

in which f is an unspecified function to be determined empirically.

8.2.2 Empirical data

Experimental results concerning overtopping of periodic waves breaking on sloping structures have been presented by Saville [115]. Only the tabulated values for plane slopes will be used here. The results are given as a mean discharge per unit width, $\overline{q}$. It follows from the definitions of B, $\overline{q}$ and T that

$$B = \overline{q}\, T \quad . \tag{8.2.11}$$

Values of the normalized volume b were calculated according to (8.2.6). They have been plotted in fig. 8.3 (open circles). It can be seen that the normalization which has been adopted does serve to bring the data in a common range for all the wave steepnesses used in the study and

for both slope angles (1 : 3 and 1 : 6). However, it also shows that there is considerable scatter. This is a common fact in measurements of overtopping, which are very sensitive to variations in the input parameters, particularly for relatively small rates of overtopping. The mean value of the normalized overtopped volume is roughly given by the following equation,

$$\begin{aligned} b &= A(1 - \eta_c)^2 \qquad \text{for } \eta_c \leq 1 \\ &= 0 \qquad\qquad\quad \text{for } \eta_c \geq 1 \quad , \end{aligned} \tag{8.2.12}$$

in which A is a coefficient which is of order 10^{-1}.

Inspection of fig. 8.3 shows that the curve indicating the average ψ_m-values is more or less a lower bound for b in the upper range, while it represents more nearly a mean value in the lower range. However, the relation between ψ_m and η will not be used in the calculations to be given in the following section, which are based on (8.2.12) with A = 0.1. This equation is represented in fig. 8.3 by the dashed line.

8.3 Overtopping due to random waves breaking on a slope

8.3.1 Distribution of overtopped volume

In this paragraph we shall consider the probability distribution of the amount of water passing the crest of a dike due to overtopping by random waves. We denote the instantaneous discharge per unit width as $\underline{q}(t)$. This is a stochastic process which is defined for continuous time. However, for most cases of practical interest the dike crest is of such height that $\underline{q}(t) = 0$ most of the time, even in storm conditions, so that it is possible to define the occurrences of uninterrupted flow over the crest ($\underline{q} > 0$) as individual overtopping events. These can usually be ascribed to single waves running up the slope. In each of the overtopping events a certain total volume of water is discharged per unit width, written as $\underline{B}$. The probability

distribution of $\underline{B}$ will be dealt with in the following. It is assumed that this distribution can be found by assigning to each wave of the random wave train an overtopped volume as if it were part of a periodic wave train. This procedure has been applied by Tsuruta and Goda [120] for the calculation of the mean rate of overtopping over vertical sea walls, taking wave height variability into account. It has previously been discussed by Paape [121], who rejects it on the grounds that it was observed that not just the highest waves in a random wave train cause overtopping. But, as noted in a similar context in the introduction to chapter 7, such a condition is not necessary for the validity of the hypothesis, which refers to the distribution of the overtopping quantities, rather than to individual values. Needless to say, the validity of the hypothesis must be checked empirically. A preliminary attempt at such verification is given in paragraph 8.3.3.

It has been shown in the preceding section that for periodic waves, and for a given slope angle and crest height, there is a relation between the volume of water overtopping per wave period, and the height to which the wave would have run up if the slope would have extended to higher elevations. This relation will be used in the calculation of the p.d.f. of $\underline{B}$. However, equation (8.2.12) as it stands is not suitable for this purpose, inasmuch as its variables have been normalized with factors containing the product HL_0, which is a random variable in random waves. For this reason (8.2.12) is first put into dimensional form, using (8.2.2), (8.2.6) and (8.2.9):

$$\begin{aligned} B &= 0.1 \cot^{3/2}\alpha \, (R_H - z_c)^2 && \text{for } R_H \geq z_c \\ &= 0 && \text{for } R_H \leq z_c \ . \end{aligned} \tag{8.3.1}$$

On the basis of (8.3.1) and the above-mentioned hypothesis, the following relation is stated for the overtopped volume in random waves:

$$\begin{aligned} \underline{B} &= 0.1 \cot^{3/2}\alpha \, (\underline{R}_H - z_c)^2 && \text{for } \underline{R}_H \geq z_c \\ &= 0 && \text{for } \underline{R}_H \leq z_c \ . \end{aligned} \tag{8.3.2}$$

The variables in this equation will now be normalized using non-random parameters:

$$\underline{\beta} \equiv \frac{\underline{B}}{0.1\ \overline{H}\ \overline{L}_0\ \sqrt{\tan\alpha}} \quad , \tag{8.3.3}$$

$$\underline{r} \equiv \frac{\underline{R}_H}{\sqrt{\overline{H}\ \overline{L}_0}\ \tan\alpha} \quad , \tag{8.3.4}$$

and

$$\zeta_c \equiv \frac{z_c}{\sqrt{\overline{H}\ \overline{L}_0}\ \tan\alpha} \quad . \tag{8.3.5}$$

This gives

$$\begin{aligned} \underline{\beta} &= (\underline{r} - \zeta_c)^2 \qquad \text{for } \underline{r} \geq \zeta_c \\ &= 0 \qquad\qquad\ \ \text{for } \underline{r} \leq \zeta_c \quad . \end{aligned} \tag{8.3.6}$$

The probability distribution of $\underline{\beta}$ can therefore be expressed in terms of the probability distribution of the normalized run-up $\underline{r}$:

$$\begin{aligned} \Pr\{\underline{\beta} \leq \beta\} &= \Pr\{\underline{r} \leq \zeta_c + \sqrt{\beta}\} \quad \text{for } \beta \geq 0 \\ &= 0 \qquad\qquad\qquad\qquad\ \ \text{for } \beta < 0 \quad . \end{aligned} \tag{8.3.7}$$

This relationship permits the calculation of $F(\beta)$ from $F(r)$ by simply substituting $r = \zeta_c + \sqrt{\beta}$. The distribution function of the normalized maximum overtopped volume in a series of N waves ($\underline{\beta}_{max}$) can be obtained from that of $\underline{r}_{max}$ in the same manner:

$$\begin{aligned} \Pr\{\underline{\beta}_{max} \leq \beta\} &= \Pr\{\underline{r}_{max} \leq \zeta_c + \sqrt{\beta}\} \quad \text{for } \beta \geq 0 \\ &= 0 \qquad\qquad\qquad\qquad\ \ \text{for } \beta < 0 \, . \end{aligned} \tag{8.3.8}$$

The preceding derivations are based on the assignment of a certain value to $\underline{\beta}$ for each value of the run-up $\underline{r}$. This implies that the cumulative probability of $\underline{\beta}$ must be thought of as the expected ratio of the number of run-ups resulting in an overtopped volume not exceeding β, to the total number of run-ups. An alternative would have been to consider the expected ratio between the number of overtopping events for which the overtopped volume does not exceed a certain value, to the total number of overtopping events. The probability of exceedance of the overtopped volume in this case could be obtained by dividing the probability of exceedance of $\underline{\beta}$, as defined above, by the fraction of the run-up heights exceeding the crest height. This operation will not be carried out because the formulation given is more convenient in the applications envisaged, such as the calculation of the mean discharge and of the expected maximum overtopped volume per wave during a given time interval.

8.3.2 Mean discharge

The mean discharge over a dike due to overtopping by random waves will be considered in this paragraph. It is defined as

$$\overline{q} = \frac{\int_{t_1}^{t_2} q(t)\, dt}{t_2 - t_1} \quad , \tag{8.3.9}$$

in which (t_1, t_2) is a time interval which is long compared with a characteristic period of the waves, but sufficiently short for the flow to be quasi-stationary. The denominator in the right-hand side of (8.3.9) can be written as $N\overline{T}_r$, in which N is the number of run-ups in the total time interval (t_1, t_2) and $\overline{T}_r$ is the average time interval between run-ups. The overtopped volume which results from the i^{th} run-up ($i = 1,2,.....N$) is denoted as B_i. (Most of the B_i-values will be zero in practical cases,) We then obtain the following expression for the mean discharge from (8.3.9):

$$\overline{q} = \frac{\sum_{i=1}^{N} B_i}{N\, \overline{T}_r} = \frac{\overline{B}}{\overline{T}_r} \quad , \tag{8.3.10}$$

in which $\overline{B}$ is the average overtopped volume per run-up. (Note that $\overline{q}$ is not equal to the average of the time-mean discharge per run-up, which would be equal to $\overline{B/T_r}$.) The average value of B will next be calculated in normalized form as $E\{\underline{\beta}\}$.

It follows from (8.3.6) or (8.3.7) that

$$E\{\underline{\beta}\} = \int_{\zeta_c}^{\infty} (r - \zeta_c)^2 \, dF(r) \qquad (8.3.11)$$

or

$$E\{\underline{\beta}\} = M_2(\zeta_c) - 2\,\zeta_c\, M_1(\zeta_c) + \zeta_c^{\,2}\, M_0(\zeta_c) \quad , \qquad (8.3.12)$$

in which

$$M_n(\zeta_c) = \int_{\zeta_c}^{\infty} r^n \, dF(r) \quad . \qquad (8.3.13)$$

In order to obtain quantitative estimates for $E\{\underline{\beta}\}$ we will use the run-up distributions derived in chapter 7. The general expression for $F(r)$ based on the bivariate Rayleigh distribution for $\underline{H}$ and $\underline{L}_0$ is given by (7.5.21). Substitution of this equation into (8.3.11) and numerical integration has given the results shown in fig. 8.4 for $\kappa = 0$, $\kappa = 0.5$ and $\kappa = 1$. These appear to be very sensitive to variations in κ, particularly for low values of the overtopped volume. This statement can probably be generalized in the sense that the expected quantity of overtopping is sensitive to the statistical properties of the incident waves. It also varies strongly with small changes in the relative crest height, ζ_c.

It is possible to obtain approximate analytical expressions for $E\{\underline{\beta}\}$. Small values of ζ_c are not of practical interest, as far as overtopping of earth dikes is concerned, because for small ζ_c the dike would be overtopped quite frequently (with the given NWL and sea state), a situation for which dikes are not (yet) designed. This means that we can use the approximations to $F(r;\kappa)$ given by (7.5.26) and (7.5.32),

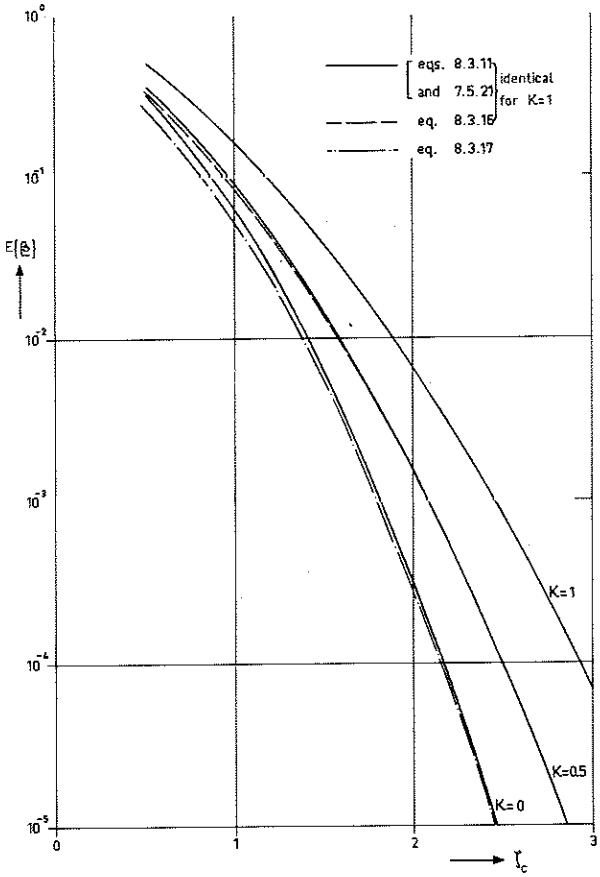

Fig. 8.4 - Calculated mean volume of overtopping per run-up.

provided κ is not nearly zero. Substitution of (7.5.26) into (8.3.13) and integration by parts gives

$$M_n(\zeta_c) \approx - \frac{1 + \kappa}{2\sqrt{\kappa}} \int_{\zeta_c}^{\infty} r^n \, de^{- \frac{\pi}{2} \frac{r^2}{1 + \kappa}} \tag{8.3.14}$$

$$= \frac{1 + \kappa}{2\sqrt{\kappa}} \left\{ \zeta_c^n \, e^{- \frac{\pi}{2} \frac{\zeta_c^2}{1 + \kappa}} + \int_{\zeta_c}^{\infty} e^{- \frac{\pi}{2} \frac{r^2}{1 + \kappa}} \, dr^n \right\} .$$

For n = 0 the last integral in (8.3.14) need not be evaluated; for n = 2 it can be evaluated in closed form; for n = 1 it can be transformed to the complementary error function defined by

$$\mathrm{erfc}(x) = \frac{2}{\sqrt{\pi}} \int_{x}^{\infty} e^{-u^2}\, du \quad , \tag{8.3.15}$$

which is extensively tabulated [90]. Substitution of the results in (8.3.12) gives

$$E\{\underset{\sim}{\beta}\} \underset{\sim}{\approx} \frac{(1+\kappa)^{3/2}}{\sqrt{\kappa}} \quad \frac{\sqrt{1+\kappa}}{\pi} e^{-\frac{\pi}{2}\frac{\zeta_c^2}{1+\kappa}} - \frac{1}{\sqrt{2}} \zeta_c \, \mathrm{erfc}\{\sqrt{\frac{\pi}{2+2\kappa}}\, \zeta_c\}$$

$$\text{for } 0 < \kappa_1 \leq \kappa \leq 1 \quad , \tag{8.3.16}$$

in which κ_1 is a limit value of κ below which the result no longer holds with sufficient accuracy (the value of κ_1 depends of course on the error permitted as well as on ζ_c). For $\kappa = 1$ the "approximation" (7.5.26) is identical with the exact expression (7.5.21). It follows that in this case (8.3.16) is identical with the result obtained by substituting the original expression (7.5.21) into (8.3.11).

In a similar way we obtain from (7.5.32) and (8.3.12)

$$E\{\underset{\sim}{\beta}\} \underset{\sim}{\approx} \frac{1}{\sqrt{2}} \mathrm{erfc}\{\sqrt{\frac{\pi}{2}}\, \xi_c\} \qquad \text{for} \quad \kappa = 0 \quad . \tag{8.3.17}$$

The approximations (8.3.16) and (8.3.17) can, in fig. 8.4, be compared with the numerical results based on the exact expression for $F(r;\kappa)$.

8.3.3 Comparison with empirical data

The derivations in the preceding paragraphs were based on the application of the expression (8.2.12), for the overtopping volume in periodic waves, to individual waves in a random wave train; they were evaluated on the assumption of a bivariate Rayleigh distribution of $\underline{H}$ and $\underline{L}_0$. The only empirical data known to the author with

which the results can be compared are those given by Paape [121], who presents the results of an extensive laboratory investigation of the overtopping of dikes with plane slopes by irregular waves. The waves were generated entirely by wind, over a fetch of 50m. The mean wind velocity and the mean depth were 8m/s and 0,3m in most runs. The wave height distribution in the upper range deviated somewhat from the Rayleigh distribution in the sense that relatively high waves occurred less frequently. No results are given regarding the period distributions. Thus, just as in the chapter on run-up distributions, the validity of the hypothesis of equivalency cannot be checked with these data; the calculated results will be compared to the measurements only to obtain an indication whether they are somewhat realistic. Such a comparison is given in fig. 8.5. The experimental data are for dike

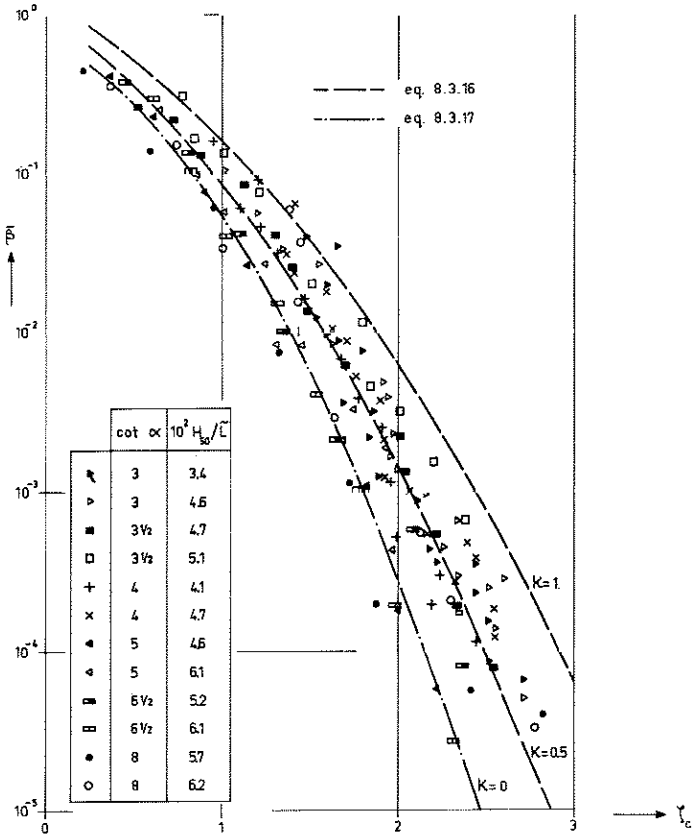

Fig. 8.5 - Measured mean volume of overtopping per wave, compared with eqs. 8.3.16 and 8.3.17.

slopes from 1 : 3 to 1 : 8 and for wave steepnesses $H_{50}/\tilde{L}_0$ from 0.034 to 0.062. The calculated curves are based on eqs. (8.3.16) and (8.3.17). They show the same trend as the experimental data. The curve for $\kappa = 0.5$ corresponds approximately to the mid-range of measurements, while that for $\kappa = 0$ serves more or less as a lower bound. It is concluded that the approach which has been developed has the potential of yielding realistic results.

9 SUMMARY AND CONCLUSIONS

The main problem dealt with in this thesis is the calculation of certain effects caused by random waves breaking on a slope.

The solution to this problem is greatly complicated by the fact that wave breaking is a highly nonlinear process. The flow field is further complicated by far stronger inhomogeneities than those occurring outside the breaker zone, by air entrainment and by generation of turbulence. No realistic deductive treatment of it has been developed so far. Even for the simpler case of periodic waves, empirical knowledge of certain macroscopic properties of the breakers is still an integral part of calculations relating to the surf zone. An attempt has been made in this thesis to apply this knowledge in a formulation incorporating the stochastic nature of wind-generated waves.

The computations are of two distinct categories, those relating to comparatively gentle slopes and those relating to comparatively steep slopes. A summary of the results will be given in the following.

The computations of the first category, pertaining to gentle slopes on which the waves break by spilling, are aimed at the estimation of the variation of the energy of the waves as they propagate towards the shore, of the radiation stresses, and of the resultant longshore current velocities and change in mean water level.

The energy variation is calculated in chapter 5 by clipping a fictitious wave height distribution, which theoretically would be present if breaking did not occur, at an upper limit which is determined from an adapted breaking criterion for periodic waves. The computed results are in fair agreement with measurements carried out on a plane slope.

Knowledge of the energy variation permits the radiation stresses to be evaluated, which in turn are necessary for the calculation of the set-up and the longshore current velocity profiles. In chapter 6, examples are given for incident waves with a narrow spectrum and with a wide spectrum (wide in frequency and direction). If turns out that

the longshore current velocity is sensitive to the width of the directional energy distribution in deep water. A spreading proportional to $\cos^2 \theta$, typical for wind-driven waves, gives a reduction of 50%, compared to a unidirectional wave train with the same mean direction of propagation and the same frequency spectrum.

A comparison of the calculated set-up profiles with empirical data has not given conclusive results. Good agreement has been found with field data, but not with laboratory data, which locally showed a systematically smaller rise towards the shore than would be expected on the basis of the measured or calculated wave height variations. However, there is some uncertainty with respect to the system used for measuring the set-up in the laboratory, so that is not known to which extent the differences are real or apparent.

The second category of computations pertains to plunging breakers, which occur on relatively steep slopes or for relatively small wave steepnesses, compared to spilling breakers. Furthermore, breaking by plunging takes place relatively close to the water line (in terms of wavelengths), which results in a pronounced up-and-down motion of the water along the slope.

The largest height above still water level reached by each wave which runs up the slope is the so-called run-up height. Its distribution function is calculated in chapter 7 by assigning to each wave of the random wave train a run-up according to Hunt's formula for periodic waves breaking on the slope. This formula contains the slope gradient and the height H and the period T of the incident waves in a product of powers, so that the run-up can be normalized in such a manner that its distribution function depends on the shape of the joint distribution of $\underline{H}$ and $\underline{T}$ only. The run-up distribution is derived as a functional of this joint distribution. The potential validity of this approach is demonstrated by a comparison with laboratory data, which showed a very good agreement. However, the wave height variability in this case was less than for natural wind waves, while the wave period was practically constant. Calculations have also been made for the case where

$\underline{H}$ and $\underline{T}^2$ are jointly Rayleigh-distributed, which is a better approximation for wind-driven waves. The available experimental data do not permit an exact comparison with the theoretical results, but they do at least indicate that the results are realistic.

A similar statement can be made with respect to the mean rate of overtopping of a dike by random waves, which is determined in chapter 8 from the calculated distribution function of the volume overtopped per wave. These calculations are based on a relationship between overtopping and run-up derived from measurements with periodic waves.

On the whole, the comparison of the calculated results with empirical data has not been conclusive in every respect, although generally speaking the results appear to be promising. The ideas proposed and elaborated in this thesis can be a useful guide in interpreting new experimental data or in setting up new experiments.

Viewing the subject of this thesis in a long-term perspective, the following remark can be made. Methods of dealing with breaking waves on a macroscopic level, such as have been used here, should ultimately be replaced by more fundamental descriptions of the breaking process, including the aspects of flow separation at the crest, the entrainment of air and water by the re-entrant flow, and the generation, transport and dissipation of turbulence. These problems have been totally neglected up to very recently [122, 123]. The establishment of knowledge in this area should be one of the long-range goals in the research pertaining to the problems of waves on beaches or dikes.

ACKNOWLEDGEMENTS

This thesis was prepared while the author was employed at the Civil Engineering Department of the Delft University of Technology. The encouragement received through the years from the late Prof.ir. W.C. Bischoff van Heemskerck is gratefully acknowledged. Mr. K. Popp of the Fluid Mechanics group wrote the programs for the numerical computations; his accurate and speedy work is very much appreciated. Thanks are also due to Mr. R. van der Klis and to Mr. H. Remeyn for making the drawings, and to Mrs. J.L. van 't Hof and to Miss D.H. van Riel for typing the manuscript.

APPENDIX I - THE BIVARIATE RAYLEIGH DISTRIBUTION

The purpose of this Appendix is to give some details concerning the bivariate Rayleigh distribution, which has been mentioned in paragraph 4.5 and which has been used in the chapters 7 and 8. It should be noted that we deal here solely with properties of a theoretical distribution without regard to the question of its applicability to wind waves.

The probability density function. The bivariate Rayleigh p.d.f. seems to have been derived independently by Uhlenbeck [103] and Rice [55] in studies of the statistical properties of the envelope of a narrow-band Gaussian process. Consider the complex process

$$\underline{z}(t) = \sum_{j=1}^{n} a_j \, e^{i(\omega_j t - \underline{\psi}_j)} \quad . \tag{A1.1}$$

The random phases are distributed as usual in the Rice representation. The spectral density of $\underline{z}(t)$ in the limit for $n \to \infty$ and $\max |\omega_{j+1} - \omega_j| \to 0$ will be denoted by $S(\omega)$. Rice considers the case in which $S(\omega)$ is narrow, with a representative midband frequency ω_m. Eq. A1.1 can then be rewritten as

$$\underline{z}(t) = \underline{Z}(t) e^{i\omega_m t} \quad , \tag{A1.2}$$

in which

$$\underline{Z}(t) = \sum_{j=1}^{n} a_j e^{i\{(\omega_j - \omega_m)t - \underline{\psi}_j\}} \tag{A1.3}$$

is a slowly varying function which modulates the much more rapidly varying carrier wave $e^{i\omega_m t}$. $|\underline{Z}(t)|$ represents the envelope of the process *Re* $\underline{z}(t)$. The values of this envelope at times (t) and (t + τ) are considered, denoted for brevity by $\underline{Z}_1 = |\underline{Z}(t)|$ and $\underline{Z}_2 = |\underline{Z}(t + \tau)|$. Their joint p.d.f. can be found from the joint distribution of *Re* $\underline{Z}(t)$, *Im* $\underline{Z}(t)$, *Re* $\underline{Z}(t + \tau)$ and *Im* $\underline{Z}(t + \tau)$, which is Gaussian in four dimen-

sions with a covariance matrix which is known in terms of $S(\omega)$ and τ. The result is

$$f(Z_1,Z_2) = \frac{Z_1 Z_2}{m_0^2(1-\kappa^2)} \exp\left\{-\frac{Z_1^2+Z_2^2}{2m_0(1-\kappa^2)}\right\} I_0\left\{\frac{\kappa Z_1 Z_2}{m_0(1-\kappa^2)}\right\} \qquad \text{(A1.4)}$$

$$\text{for} \quad Z_1 \geq 0, \quad Z_2 \geq 0$$

$$= 0 \qquad \text{otherwise} \ ,$$

in which the parameter κ^2 is determined from

$$m_0^2\kappa^2 = \left[\int_0^\infty S(\omega)\cos(\omega-\omega_m)\tau\, d\omega\right]^2 + \left[\int_0^\infty S(\omega)\sin(\omega-\omega_m)\tau\, d\omega\right]^2 . \qquad \text{(A1.5)}$$

Although Rice in his derivation assumes the spectrum to be narrow, so that the realizations of the process *Re* $\underline{z}(t)$ have a well-defined envelope, it should be pointed out that this assumption is not actually needed in the derivation of (A1.4). This can be seen immediately from the fact that $|\underline{Z}(t)| = |\underline{z}(t)|$. If the spectrum is not narrow then neither ω_m nor the envelope of the process *Re* $\underline{z}(t)$ is defined, so that $|\underline{Z}(t)|$ loses its meaning, but (A1.4) still represents the joint p.d.f. of $|\underline{z}(t)|$ and $|\underline{z}(t+\tau)|$. The fact that ω_m appears in the definition of the parameter κ is more apparent than real, since (A1.5) can be rewritten as

$$m_0^2\kappa^2 = \int_0^\infty\int_0^\infty S(\omega_1)S(\omega_2)\cos(\omega_1-\omega_m)\tau\cos(\omega_2-\omega_m)\tau\, d\omega_1 d\omega_2 +$$

$$+ \int_0^\infty\int_0^\infty S(\omega_1)S(\omega_2)\sin(\omega_1-\omega_m)\tau\sin(\omega_2-\omega_m)\tau\, d\omega_1 d\omega_2$$

$$= \int_0^\infty\int_0^\infty S(\omega_1)S(\omega_2)\cos(\omega_1-\omega_2)\tau\, d\omega_1 d\omega_2 \ , \qquad \text{(A1.6)}$$

which does not depend on ω_m. These broader definitions are given here because they widen the field of potential applications. One can go even further away from the model of a narrow-band stationary Gaussian process and consider the joint p.d.f. of $\underline{X} = (\underline{X}_1^2 + \underline{X}_2^2)^{\frac{1}{2}}$ and $\underline{Y} = (\underline{Y}_1^2 + \underline{Y}_2^2)^{\frac{1}{2}}$, in which $\underline{X}_1$, $\underline{X}_2$, $\underline{Y}_1$ and $\underline{Y}_2$ are jointly Gaussian in four dimensions, each with zero expectation, while $E\{\underline{X}_1\underline{X}_2\} = 0$, $E\{\underline{Y}_1\underline{Y}_2\} = 0$, $E\{\underline{X}_1^2\} = E\{\underline{X}_2^2\}$, and $E\{\underline{Y}_1^2\} = E\{\underline{Y}_2^2\}$. The variables $\underline{X}$ and $\underline{Y}$ taken separately then have a one-dimensional Rayleigh distribution, while their joint p.d.f. defines the general two-dimensional Rayleigh p.d., given by

$$f(X,Y) = \frac{\pi^2}{4} \frac{XY}{\mu_X^2 \mu_Y^2 (1-\kappa^2)} \exp\{ - \frac{\pi}{4} \frac{(X/\mu_X)^2 + (Y/\mu_Y)^2}{1 - \kappa^2} \} \; I_0\{ \frac{\pi}{2} \frac{\kappa}{1-\kappa^2} \frac{XY}{\mu_X \mu_Y} \} \tag{A1.7}$$

for $X \geq 0$ and $Y \geq 0$, and $f(X,Y) = 0$ otherwise, in which

$$\mu_X = E\{\underline{X}\} \quad , \quad \mu_Y = E\{\underline{Y}\} \quad . \tag{A1.8}$$

κ^2 is the coefficient of linear correlation of $\underline{X}^2$ and $\underline{Y}^2$, as will be shown; therefore, $0 \leq \kappa^2 \leq 1$. We can without loss of generality assume that

$$0 \leq \kappa \leq 1 \tag{A1.9}$$

since (A1.7) is even in κ.

Transformation to the normalized variables

$$\underline{x} = \underline{X}/\mu_X \quad \text{and} \quad \underline{y} = \underline{Y}/\mu_Y \tag{A1.10}$$

gives

$$f(x,y) = \frac{\pi^2}{4} \frac{xy}{1-\kappa^2} \exp\{ - \frac{\pi}{4} \frac{x^2 + y^2}{1-\kappa^2} \} \; I_0\{ \frac{\pi}{2} \frac{\kappa \, xy}{1-\kappa^2} \} \quad \text{for} \quad \begin{matrix} x \geq 0 \\ y \geq 0 \end{matrix}$$

$$= 0 \qquad \text{otherwise,} \tag{A1.11}$$

which is symmetric in x and y. We shall in the following deal exclusively with (A1.11). The explicit expression of the fact that $f(x,y) = 0$ for $x < 0$ and/or $y < 0$ will be omitted.

The marginal p.d. functions should of course be given by the one-dimensional Rayleigh p.d.f.:

$$f(x) = \frac{\pi}{2} x \exp\left(-\frac{\pi}{4} x^2\right) \tag{A1.12}$$

and

$$f(y) = \frac{\pi}{2} y \exp\left(-\frac{\pi}{4} y^2\right) \quad . \tag{A1.13}$$

This can be proved from (A1.11) and the definition of a marginal p.d.f. by using the series representation of $I_0(.)$ [90, eq. 9.6.10]:

$$I_0(t) = \sum_{j=0}^{\infty} \frac{(\frac{1}{4} t^2)^j}{(j!)^2} \quad , \tag{A1.14}$$

and by integrating termwise.

The moments, defined by

$$M_{k\ell} = E\{\underline{x}^k \underline{y}^{\ell}\} \quad , \tag{A1.15}$$

can be evaluated by substitution of (A1.14) and by termwise integration, which gives [53]

$$M_{k\ell} = \left(\frac{4}{\pi}\right)^{\frac{k+\ell}{2}} (1 - \kappa^2)^{\frac{k+\ell}{2} + 1} \sum_{j=0}^{\infty} \frac{\Gamma(j + 1 + \frac{k}{2})\, \Gamma(j + 1 + \frac{\ell}{2}) \kappa^{2j}}{(j!)^2} \quad . \tag{A1.16}$$

Apart from a constant factor, the series in (A1.16) is the expression for the Gauss hypergeometric series [90, eq. 15.1.1], so that (A1.16) can be written as

$$M_{k\ell} = \left(\frac{4}{\pi}\right)^{\frac{k+\ell}{2}} (1 - \kappa^2)^{\frac{k+\ell}{2} + 1} \Gamma\left(\frac{k}{2} + 1\right) \Gamma\left(\frac{\ell}{2} + 1\right) {}_2F_1 \left(\frac{k}{2} + 1, \frac{\ell}{2} + 1; 1; \kappa^2\right) \quad , \tag{A1.17}$$

or, using the transformation [90, eq. 15.3.3]

$${}_2F_1 (a,b; c; z) = (1 - z)^{c - a - b} {}_2F_1 (c - a, c - b; c; z) \quad , \tag{A1.18}$$

as

$$M_{k\ell} = \left(\frac{4}{\pi}\right)^{\frac{k+\ell}{2}} \Gamma\left(\frac{k}{2} + 1\right) \Gamma\left(\frac{\ell}{2} + 1\right) {}_2F_1 \left(-\frac{k}{2}, -\frac{\ell}{2}; 1; \kappa^2\right) \quad . \tag{A1.19}$$

Expressions similar to (A1.17) and (A1.19) are presented by Middleton [53], but his eq. 9.22, corresponding to (A1.17), contains a misprint in the exponent of $(1 - \kappa^2)$.

The even moments can be expressed as a finite series by utilizing the fact that the hypergeometric function ${}_2F_1 (a,b; c; z)$ reduces to a polynomial of degree m when a or b is equal to -m (m = 0, 1, 2, ...) [90, eq. 15.4.1]:

$${}_2F_1 (-m, b; c; z) = \sum_{n=0}^{m} \frac{(-m)_n (b)_n}{(c)_n} \frac{z^n}{n!} \tag{A1.20}$$

in which

$$\begin{aligned} (a)_0 &= 1 \\ (a)_n &= a(a + 1)(a + 2) \ldots (a + n - 1) \end{aligned} \tag{A1.21}$$

It follows from the definitions and normalizations adopted that the zero- and first-order moments are equal to 1. The second-order moments are given by

$$E\{\underline{x}^2\} = E\{\underline{y}^2\} = M_{20} = M_{02} = \frac{4}{\pi} \tag{A1.22}$$

and

$$E\{\underline{x}\,\underline{y}\} = M_{11} = {}_2F_1\left(-\tfrac{1}{2}, -\tfrac{1}{2}; 1; \kappa^2\right) \quad . \tag{A1.23}$$

The even fourth-order moments are

$$E\{\underline{x}^4\} = E\{\underline{y}^4\} = M_{40} = M_{04} = \frac{32}{\pi^2} \tag{A1.24}$$

and

$$E\{\underline{x}^2\underline{y}^2\} = M_{22} = \left(\frac{4}{\pi}\right)^2 (1 + \kappa^2) \quad . \tag{A1.25}$$

It can be verified with (A1.22), (A1.24) and (A1.25) that κ^2 is indeed the coefficient of linear correlation of $\underline{x}^2$ and $\underline{y}^2$, as was stated above.

The correlation coefficient of $\underline{x}$ and $\underline{y}$ will be considered in some detail in view of the applications in the chapters 7 and 8. It is defined by

$$\lambda = \frac{M_{11} - M_{10}\,M_{01}}{(M_{20} - M_{10}^2)^{\frac{1}{2}}(M_{02} - M_{01}^2)^{\frac{1}{2}}} \quad , \tag{A1.26}$$

which gives

$$\lambda = \frac{{}_2F_1\left(-\tfrac{1}{2}, -\tfrac{1}{2}; 1; \kappa^2\right) - 1}{\frac{4}{\pi} - 1} \quad . \tag{A1.27}$$

The hypergeometric function appearing in (A1.27) can be expressed in terms of the complete elliptic integrals of the first and second kind, which have been tabulated, and for which the following equalities hold:

$$K(\kappa) = \frac{\pi}{2}\,{}_2F_1\left(\tfrac{1}{2}, \tfrac{1}{2}; 1; \kappa^2\right) \tag{A1.28}$$

and

$$E(\kappa) = \frac{\pi}{2}\,{}_2F_1\left(-\tfrac{1}{2}, \tfrac{1}{2}; 1; \kappa^2\right) \quad . \tag{A1.29}$$

By using a recursive relation between contiguous hypergeometric functions [90, eq. 15.2.15],

$$(c - a - b)\, {}_2F_1(a, b; c; z) + a(1 - z)\, {}_2F_1(a + 1, b; c; z) - (c - b)\, {}_2F_1(a, b - 1; c; z) = 0 \quad , \tag{A1.30}$$

it follows that

$${}_2F_1(-\tfrac{1}{2}, -\tfrac{1}{2}; 1; \kappa^2) = \frac{4}{\pi} E(\kappa) - \frac{2}{\pi}(1 - \kappa^2) K(\kappa) \quad , \tag{A1.31}$$

so that

$$\lambda = \frac{E(\kappa) - \tfrac{1}{2}(1 - \kappa^2) K(\kappa) - \frac{\pi}{4}}{1 - \frac{\pi}{4}} \quad . \tag{A1.32}$$

This equation seems to have been first given by Uhlenbeck [103], quoted in [53]. A plot of $\lambda(\kappa)$ based on (A1.32) is given in fig. A1.1.

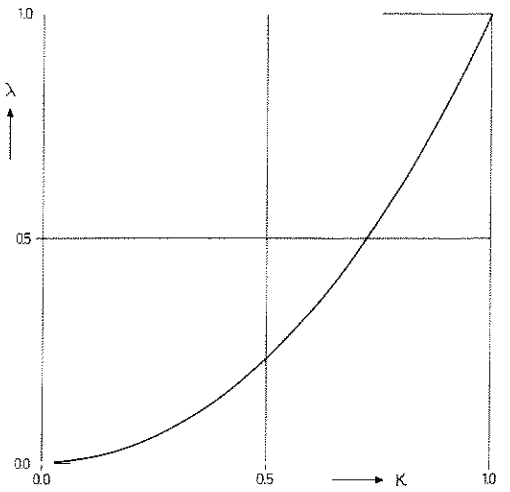

Fig. A1.1 - Coefficient of linear correlation of $\underline{x}$ and $\underline{y}$, as a function of κ.

Two special cases occur when κ assumes its limiting values of 0 or 1. For $\kappa = 0$ we have $E(0) = K(0) = \frac{\pi}{2}$, so

$$\lambda = 0 \quad \text{if} \quad \kappa = 0 \quad . \tag{A1.33}$$

For $\kappa \to 1$ we have $E(1) = 1$ and $\lim_{\kappa \to 1} (1 - \kappa^2)\, K(\kappa) = 0$, so

$$\lambda = 1 \quad \text{if} \quad \kappa = 1 \quad . \tag{A1.34}$$

These limiting values could be expected from the interpretation of $f(x,y)$ as the joint p.d.f. of two values of the envelope of a narrow-band random process, since $\kappa = 0$ corresponds to $\tau \to \infty$, and $\kappa = 1$ to $\tau = 0$ (see eq. A1.5), which implies that values of the envelope are considered with an infinitely long time interval between them, or with an interval of zero duration, respectively.

An approximate expression for $\lambda(\kappa)$ which is more easily handled than (A1.32) can be obtained by using the series representations for $E(\kappa)$ and $K(\kappa)$ [90, eqs. 17.3.11-12]:

$$K(\kappa) = \frac{\pi}{2} \left[1 + \sum_{j=1}^{\infty} \left\{ \frac{1.3.5.....(2j-1)}{2.4.6.....(2j)} \right\}^2 \kappa^{2j} \right] \tag{A1.35}$$

$$E(\kappa) = \frac{\pi}{2} \left[1 - \sum_{j=1}^{\infty} \left\{ \frac{1.3.5.....(2j-1)}{2.4.6.....(2j)} \right\}^2 \frac{\kappa^{2j}}{2j-1} \right] . \tag{A1.36}$$

This gives after some manipulations

$$\lambda = \frac{\pi}{16 - 4\pi} \left[\kappa^2 + \sum_{j=2}^{\infty} \left\{ \frac{1.3.5.....(2j-3)}{4.6.8.....(2j)} \right\}^2 \kappa^{2j} \right] . \tag{A1.37}$$

It can be seen that λ is a non-negative function of κ. Thus, two stochastic variables with a joint Rayleigh distribution cannot be negatively correlated.

The series in (A1.37) is rapidly converging for $\kappa^2 \leq 1$. Truncating it after two terms gives

$$\lambda \approx \frac{\pi}{16 - 4\pi} \{\kappa^2 + \frac{\kappa^4}{16} + \frac{\kappa^6}{64}\}. \qquad \text{(A1.38)}$$

In order to obtain an explicit expression for κ as a function of λ, the series (A1.38) has been inverted, with the result

$$\kappa^2 \approx \lambda^* - \frac{\lambda^{*2}}{16} - \frac{\lambda^{*3}}{128} \quad , \qquad \text{(A1.39)}$$

in which

$$\lambda^* = \frac{16 - 4\pi}{\pi} \lambda. \qquad \text{(A1.40)}$$

The truncation errors involved in the approximations (A1.38) and (A1.39) are less than 0.1% for $0 \leq \kappa < 0.7$ and less than 1% for $0 \leq \kappa < 0.95$.

Case of zero correlation. For $\lambda = 0$, which implies $\kappa = 0$, (A1.11) reduces to

$$f(x,y) = \frac{\pi^2}{4} xy \exp\{-\frac{\pi}{4}(x^2 + y^2)\} \quad , \qquad \text{(A1.41)}$$

which is the product of the marginal p.d. functions f(x) and f(y) given by (A1.12-13). Thus, two stochastic variables with a joint Rayleigh p.d. are stochastically independent if they are uncorrelated.

Case of 100% correlation. If 100% correlation occurs then the two variables $\underline{x}$ and $\underline{y}$ are linearly dependent. Moreover, $\underline{x}$ and $\underline{y}$ are identically distributed. Therefore, $\underline{x} = \underline{y}$ with probability 1 if $\lambda = 1$. The two-dimensional p.d. must then be zero for all $x \neq y$ and be infinite for $x = y$. This may be shown formally by investigating the behaviour of $f(x,y)$ as $\kappa \to 1$. To this end, the following asymptotic expression for $I_0(.)$ is substituted in (A1.11) [90, eq. 9.7.1]:

$$I_0(t) = \frac{e^t}{(2\pi t)^{\frac{1}{2}}} \{1 + O(t^{-1})\}. \qquad \text{(A1.42)}$$

After some algebraic manipulations, the result can be written as

$$f(x,y) \to \frac{\pi}{2}\left(\frac{xy}{\kappa}\right)^{\frac{1}{2}} \exp\left(-\frac{\pi}{2}\frac{xy}{1+\kappa}\right)\left[\frac{\exp\{-(x-y)^2/(2\sigma^2)\}}{(2\pi)^{\frac{1}{2}}\sigma}\right] \text{ as } \kappa \to 1 \quad (A1.43)$$

in which

$$\sigma^2 = \frac{2}{\pi}(1-\kappa^2) \quad . \quad (A1.44)$$

The expression in brackets is formally equal to a Gaussian p.d.f. with independent variable (x-y), zero mean and variance σ^2. In the limit for $\kappa \to 1$, which implies $\sigma \to 0$, the Gaussian function defines Dirac's unit impulse function $\delta(x-y)$ [54]. Thus,

$$f(x,y) = \frac{\pi}{2}(xy)^{\frac{1}{2}} \exp(-\frac{\pi}{4}xy)\,\delta(x-y) \quad \text{for } \kappa = 1 \quad , \quad (A1.45)$$

which is equivalent to

$$f(x,y) = f(x)\,\delta(x-y) \quad \text{for } \kappa = 1 \quad (A1.46)$$

and to

$$f(x,y) = f(y)\,\delta(x-y) \quad \text{for } \kappa = 1 \quad . \quad (A1.47)$$

Regression lines. The regression of $\underline{x}$ on $\underline{y}$ is given by

$$x_y = E\{\underline{x} \mid \underline{y} = y\} = \frac{\int_0^\infty x\, f(x,y)dx}{f(y)} \quad . \quad (A1.48)$$

The integral which results upon substitution of (A1.11) can be expressed in known functions by means of [90, eq. 11.4.28]

$$\int_0^\infty e^{-a^2t^2}\, t^{\mu-1}\, J_\nu(bt)dt = \frac{\Gamma(\frac{\nu+\mu}{2})(\frac{b}{2a})^\nu}{2a^\mu\,\Gamma(\nu+1)} M(\frac{\nu+\mu}{2}, \nu+1, -\frac{b^2}{4a^2}) \quad , (A1.49)$$

in which $J_\nu(.)$ is the Bessel function of the first kind of order ν, and $M(.)$ is the confluent hypergeometric function. For $\nu = 0$ and $b = i = (-1)^{\frac{1}{2}}$ we have

$$J_0(it) = I_0(t) \quad , \tag{A1.50}$$

whereupon (A1.48) becomes

$$x_y = (1 - \kappa^2)^{\frac{1}{2}} \exp(-\frac{\pi}{4} \frac{\kappa^2 y^2}{1 - \kappa^2}) \, M(\tfrac{3}{2}, 1, \frac{\pi}{4} \frac{\kappa^2 y^2}{1 - \kappa^2}) \quad . \tag{A1.51}$$

This expression can be slightly further reduced by applying the following Kummer transformation [90, eq. 13.1.27]:

$$M(a, b, z) = e^z \, M(b - a, b, -z) \quad , \tag{A1.52}$$

which gives

$$x_y = (1 - \kappa^2)^{\frac{1}{2}} \, M(-\tfrac{1}{2}, 1, -\frac{\pi}{4} \frac{\kappa^2 y^2}{1 - \kappa^2}) \quad . \tag{A1.53}$$

The regression of $\underline{x}$ on $\underline{y}$ appears to be nonlinear in general. Thus, the assumptions made by Bretschneider [83] that $\underline{x}$ and $\underline{y}$ would have a bivariate Rayleigh distribution and that their mutual regressions would be linear, are incompatible. An exception must be made for the trivial cases of stochastic independence and linear dependence of $\underline{x}$ and $\underline{y}$. The values of x_y should in these cases be 1 and y, respectively. They will be calculated from (A1.53) in order to provide a check on the calculations.

In the case of stochastic independence we have $\lambda = 0$, $\kappa = 0$, which gives, after substitution in (A1.53),

$$x_y = 1 \quad \text{for} \quad \lambda = 0 \quad , \tag{A1.54}$$

as expected. In the case of linear dependence, $\lambda = 1$, $\kappa = 1$. Using the

following asymptotic expression for the confluent hypergeometric function [90, eq. 13.5.1]

$$M(a, b, z) \to \frac{\Gamma(b)e^{i\pi a}}{\Gamma(b - a)} \; z^{-a} \; \{1 + O|z|^{-1})\} \quad \text{for } |z| \to \infty, \; z \text{ real}, \tag{A1.55}$$

we find

$$M(-\tfrac{1}{2}, 1, -\frac{\pi}{4}\frac{\kappa^2 y^2}{1 - \kappa^2}) \to \frac{\kappa y}{(1 - \kappa^2)^{\frac{1}{2}}} \quad \text{for } \kappa \to 1 \;, \tag{A1.56}$$

so that

$$x_y = y \quad \text{if} \quad \kappa = 1 \;, \tag{A1.57}$$

as expected.

The regression of $\underline{y}$ on $\underline{x}$ is obtained by interchanging x and y in the preceding expressions, because the joint p.d.f. (A1.11) is symmetric in x and y.

APPENDIX 2 - LIST OF SYMBOLS

The most important symbols used in the text are listed below. Variables which have been used only locally are not listed, nor are those used in Appendix 1. Some symbols have more than one meaning; it should be clear from the context which meaning is intended. Vector quantities have in the text either been indicated by an arrow, or they have been written in the Cartesian tensor index notation, whichever was most convenient. In the following list, the arrow symbol is used exclusively for vectors.

A_i	coefficients in the SWOP spectrum (eq. 4.5.10)
a	amplitude of $\zeta'(t)$ in harmonic motion
B	overtopped volume per unit width due to one wave
b	normalized value of B in periodic waves (eq. 8.2.6)
C	covariance
C	in ch. 6: time-mean volume concentration of air in water
$\tilde{C}$	in ch. 6: depth-averaged value of C
C_f	coefficient for bottom shear stress in turbulent boundary layer
C_n	normalized value of R_n (eq. 7.7.1)
c	phase velocity
c_g	group velocity
$\vec{c}_r$	average velocity of run-up front from SWL to point of maximum run-up
D	mean depth
$D(\omega;\theta)$	normalized directional spectral density
$\vec{e}$	unit vector in the direction of propagation
E	mean energy per unit area
E_p	mean potential energy per unit area
E_k	mean kinetic energy per unit area
$E\{\underline{x}\}$	expected value of $\underline{x}$
$F(x)$	distribution function of $\underline{x}$
$F^*(r)$	approximation to F(r) given by eq. 7.5.51

F	in ch. 4: fetch
F^*	in ch. 4: dimensionless fetch (gF/W^2)
$f(x)$	probability density function of $\underline{x}$
$G(\omega,\theta)$	spectral density in frequency-direction space
$G'(\vec{k})$	spectral density in wave number space
g	gravitational acceleration
H	wave height (height of highest maximum of $\zeta'(t)$ above lowest minimum between successive zero-upcrossings)
$H_{1/3}$	mean value of the highest one-third of the wave heights
H_{max}	for periodic waves: largest height possible for non--breaking, stable wave
H_{max}	for random waves: largest value of H in a sample
H_{nom}	in ch. 7: nominal wave height of random wave train
H_0	rms wave height in deep water
$\bar{h}$	normalized wave height ($H/\bar{H}$)
$I(.)$	function defined by eq. 4.5.6
Im x	imaginary part of x
$\vec{k}$	wave number vector
k	$\lvert\vec{k}\rvert$
$\tilde{k}$	theoretical value of k for wave with period T_0 in depth D
L	wave length
L_0	$gT^2/2\pi$
$\tilde{L}_0$	$gT_0^2/2\pi$
$\hat{L}_0$	$g\hat{T}^2/2\pi$
ℓ	normalized value of L_0 ($\ell=L_0/\bar{L}_0$)
$\vec{M}$	mean horizontal mass flux per unit width
$\vec{M}^c$	contribution of mean current to $\vec{M}$
$\vec{M}^w$	contribution of waves to $\vec{M}$
m	exponent of cos θ in directional spectrum (eq. 4.5.4)
m_D	absolute value of mean-depth gradient ($\lvert\nabla D\rvert$)
m_d	bottom slope ($\lvert\nabla d\rvert$)
m_j	j-th moment of $S(\omega)$ about $\omega=0$
N	number of zero-upcrossings of $\zeta'(t)$ in a given time interval
N_m	number of maxima of $\zeta'(t)$ in a given time interval
n	c_g/c

$\vec{n}$	normal unit vector
$\vec{P}$	mean horizontal energy flux per unit width
P	$\lvert\vec{P}\rvert$
Pr	probability
p	pressure
$Q(\vec{k})$	source function in spectral energy balance (eq. 4.3.20)
$Q(x)$	probability of exceedance ($Q(x) = 1 - F(x)$)
Q_b	calculated fraction of breaking waves at a fixed point
$\vec{q}$	horizontal particle velocity
q	$\lvert\vec{q}\rvert$
R	run-up height (maximum height above SWL reached by a wave which runs up a slope)
R_H	value of R according to Hunt (eq. 7.2.3): $\sqrt{HL_0}\tan\alpha$
R_{max}	largest value of R in a sample
R^*_{50}	normalized median run-up (eq. 7.3.1)
Re	Reynolds number
Re x	real part of x
r	normalized value of R (eq. 7.4.4)
r	in ch. 2: reflection coefficient
$\vec{r}$	horizontal displacement
S	in ch. 7: wave steepness (H/L_0)
$\tilde{S}(\omega)$	two-sided spectral density of $\zeta'(t)$
$S(\omega)$	one-sided spectral density of $\zeta'(t)$
$S_e(\omega)$	equilibrium value of $S(\omega)$
$S_0(\omega)$	value of $S(\omega)$ in deep water
S_{ij}	contribution of unsteady motion to mean flux in x_i-direction of x_j-momentum (i=1,2; j=1,2)
S^*_{ij}	value of S_{ij} in random, long-crested wave train with same $S(\omega)$ as given random, short-crested wave system
s	coordinate along a wave ray
s	in ch. 7: normalized wave steepness (h/ℓ)
T	wave period (time interval between successive zero-upcrossings of $\zeta'(t)$
T_0	mean value of T in deep water

$\hat{T}$	$2\pi/\hat{\omega}$
T_m	time interval between successive maxima of $\zeta'(t)$
t	time
t_r	travel time of run-up front along dike slope, from SWL to point of maximum run-up
$\vec{U}$	$\vec{M}/\rho D$
$\vec{\hat{U}}$	vertically-averaged mean current velocity ($\vec{M}^c/\rho D$)
$\vec{u}$	particle velocity
u	x-component of $\vec{u}$
V	component of $\vec{\tilde{U}}$ parallel to the shore (longshore current velocity)
V^*	normalized value of V (eq. 6.2.34)
v	y-component of $\vec{u}$
W	mean wind velocity at a fixed point
w	z-component of $\vec{u}$
$\vec{x}$	coordinate vector
x	horizontal coordinate
x	in ch. 8: coordinate along dike slope, measured positive upward from SWL
x_H	in ch. 8: $R_H/\sin\alpha$, or: $\sqrt{HL_0}/\cos\alpha$
x_c	in ch. 8: $z_c/\sin\alpha$
y	horizontal coordinate (parallel to the shore, if applicable)
z	vertical coordinate, measured positive upward from SWL
z_c	in ch. 8: height of dike crest above SWL
α	slope angle with respect to the horizontal
β	in ch. 4 and 5: proportionality coeff. in equilibrium spectrum
β	in ch. 8: normalized value of B in random waves (eq. 8.3.3)
β_1, β_2	coefficients in Pierson-Moskowitz spectrum (eq. 4.5.17)
Γ	measure of short-crestedness of waves (eq. 5.2.39)
γ	height-depth ratio of breaking wave in shallow water
Δ	absolute error
δ	relative error
$\tilde{\gamma}$	$H_{1/3}/\tilde{L}_0$

$\delta(.)$	Dirac distribution
δ_{ij}	Kronecker delta (eq. 3.3.11)
ε	$(1-m_2^2/m_0m_4)^{\frac{1}{2}}$
ε_t	total rate of energy dissipation per unit area
ε_f	rate of energy dissipation per unit area in turbulent boundary layer at the bottom
ζ	elevation of free surface above SWL
ζ_m	value of $\zeta'(t)$ at a maximum
$\tilde{\zeta}_m$	largest value of ζ_m on an interval between a zero-upcrossing of $\zeta'(t)$ and the next zero-downcrossing
$\bar{\zeta}_{max}$	maximum value of $\bar{\zeta}$ on a beach
$\bar{\zeta}_s$	height of MWL in stilling well above SWL
ζ_c	in ch. 8: normalized height of dike crest above SWL (eq. 8.3.5)
η	in ch. 8: x/x_H
θ	direction of wave propagation with respect to x-axis
θ_0	value of θ in deep water
κ	parameter of bivariate Rayleigh distribution (eq. A1.5)
λ	coefficient of linear correlation of $\underline{H}$ and $\underline{L}_0$
λ	in ch. 2: scale ratio
μ	dynamic viscosity of water
ν	$m_2/\sqrt{m_0m_4}$
ξ	$\tan\alpha/\sqrt{H/L_0}$
$\xi(t)$	$\zeta'(t)/\sqrt{m_0}$
ξ_m	$\zeta_m/\sqrt{m_0}$
$\tilde{\xi}_m$	$\tilde{\zeta}_m/\sqrt{m_0}$
ρ	mass density of water
σ	standard deviation
σ	in ch. 3: small parameter, of the order of the wave slope
$\vec{\tau}$	bottom shear stress
τ	time lag
τ_η	time interval between successive crossings of a level η by $\zeta'(t)$
ϕ	scalar velocity potential
χ	phase

Ψ	in ch. 8: volume per unit width stored above a certain point on the dike slope, during run-up of periodic waves
Ψ_m	maximum value of Ψ at a fixed point
ψ_m	normalized value of Ψ_m (eq. 8.2.5)
ψ	in ch. 4: random phase
Ω	$2\pi/T_0$
ω	angular frequency
$\hat{\omega}$	value of ω for which $S(\omega)$ reaches its maximum

Abbreviations

MWL	mean water level
SWL	still water level
p.d.f.	probability density function
r.m.s.	or rms: root-mean-square

Subscripts

B	refers to bottom
b	refers to breakpoint
c	refers to condition of incipient breaking
c	refers to crest of dike (in ch. 8)
f	refers to fictitious quantity, calculated without taking account of wave breaking
n	refers to value exceeded with probability of n%

Other symbols

$\bar{x}$	average value of x, in most cases a time average or an arithmetic average
$\overline{\overline{x(\omega,\theta)}}$	average of $x(\omega,\theta)$ with respect to (ω,θ), weighted with $G(\omega,\theta)$
$\underset{\sim}{x}(\omega,\theta)$	value of $x(\omega,\theta)$ for $\omega=\bar{\omega}$ and $\theta=\bar{\theta}$
$\langle x \rangle$	ensemble average of x

$x'(t)$	fluctuation of x about its mean value
$\underline{x}$	stochastic variable

APPENDIX 3 - REFERENCES

1. Hunt, I.A., Design of seawalls and breakwaters, Proc. ASCE, 85, WW3, Sept. 1959, p. 123-152.

2. LeMéhauté, B., Koh, R.C.Y. and Hwang, Li-San, A synthesis on wave run-up, Proc. ASCE, 94, WW1, Feb. 1968, p. 77-92.

3. Technical Advisory Committee on Sea Defences, Golfoploop en golfoverslag (Wave run-up and wave overtopping), The Hague, 1972, 184 pages. (English translation in press).

4. Longuet-Higgins, M.S. and Stewart, R.W., Changes in the form of short gravity waves on long waves and tidal currents, J. Fluid Mech., 8, pt. 4, 1960, p. 565-583.

5. Iribarren, C.R. and Nogales, C., Protection des Ports, Section II, Comm. 4, XVIIth Int. Nav. Congress, Lisbon, 1949, p. 31-80.

6. Bowen, A.J., Inman, D.L. and Simmons, V.P., Wave "set-down" and set-up, J. Geoph. Res., 73, 8, 1968, p. 2569-2577.

7. Miche, R., Le pouvoir réfléchissant des ouvrages maritimes exposés à l'action de la houle, Ann. des Ponts et Chaussées, 121è Année, 1951, p. 285-319.

8. Munk, W.H. and Wimbush, M., A rule of thumb for wave breaking, Oceanology, 9, 1969, p. 56-69.

9. Miche, R., Mouvements ondulatoires de la mer en profondeur constante ou décroissante, Ann. des Ponts et Chaussées, 114è Année, 1944.

10. McCowan, J., On the solitary wave, London, Edinburgh, Dublin Phil. Mag. J. Sci., 32, 5, 1891, p. 45-58.

11. Ippen, A.T. and Kulin, G., The shoaling and breaking of the solitary wave, Proc. 5th Conf. Coastal Eng., Berkeley, Calif. 1955, p. 27-49.

12. Iversen, H.W., Laboratory Study of Breakers, Nat. Bur. of Standards, Circular 521, Washington, D.C., 1952, p. 9-32.

13. Patrick, D.A. and Wiegel, R.L., Amphibian tractors in the surf, Conf. Ships and Waves, 1, 1954, p. 397.

14. Galvin, C.J. Jr., Breaker Type Classification on Three Laboratory Beaches, J. Geoph. Res., 73, 12, June 1968, p. 3651-3659.

15. Galvin, C.J. Jr., Wave Breaking in Shallow Water, in Waves on Beaches, Ed. R.E. Meyer, Academic Press, New York, 1972, p. 413-456.

16. Kemp, P.H., The relationship between wave action and beach profile characteristics, Proc. 7th Conf. Coastal Eng., The Hague, 1960, Vol. I, p. 262-277.

17. Goda, Y., A synthesis of breaker indices, Trans. Jap. Soc. Civ. Eng., 2, 2, 1970, p. 227-230.

18. Longuet-Higgins, M.S. and Stewart, R.W., A note on wave set-up, J. Mar. Res., 21, 1963, p. 4-10.

19. Battjes, J.A. and Roos, A., Characteristics of flow in periodic wave run-up, in press, 1974.

20. Moraes, Carlos de Campos, Experiments of Wave Reflexion on Impermeable slopes, Proc. 12th Conf. Coastal Eng., Washington, D.C., 1970, Vol. I, p. 509-521.

21. Yalin, M.S., Theory of Hydraulic Models, MacMillan Press, 1971.

22. Longuet-Higgins, M.S., Recent Progress in the Study of Longshore Currents, in Waves on Beaches, Ed. R.E. Meyer, Academic Press, New York, 1972, p. 203-248.

23. Longuet-Higgins, M.S., Mass transport in water waves, Phil. Trans. Roy. Soc. London, A, 245, 903, 1953, p. 535-581.

24. Batchelor, G.K., An introduction to fluid dynamics, Cambridge University Press, 1967.

25. Stokes, G.G., On the theory of oscillatory waves, Mathematical and Physical Papers, I, Cambridge University Press, 1880.

26. Biesel, F., Equations approchées de la refraction de la houle, Proc. 11th Conf. Coastal Eng., Lisbon, 1964, p. 55-69.

27. Battjes, J.A., Refraction of water waves, Proc. ASCE, 94, WW 4, 1968, p. 437-451.

28. Webster, A.G., Partial differential equations of mathematical physics, Dover Inc., New York, 1966.

29. Bretschneider, C.L. and Reid, R.O., Changes in wave height due to bottom friction, percolation and refraction, U.S. Army Corps of Engineers, B.E.B., Tech. Mem. 45, 1954.

30. Phillips, O.M., The Dynamics of the Upper Ocean, Cambridge Univ. Press, 1966.

31. Dorrestein, R., On the deviation of the average pressure at a fixed point in a moving fluid from its "hydrostatic" value, Appl. Sci. Res., A, 10, 1961, p. 384-392.

32. Longuet-Higgins, M.S. and Stewart, R.W., The changes in amplitude of short gravity waves on steady non-uniform currents, J. Fluid. Mech., 10, 1961, p. 529-549.

33. Longuet-Higgins, M.S. and Stewart, R.W., Radiation stress and mass transport in gravity waves, with applications to "surf-beats", J. Fluid Mech., 13, 1962, p. 481-504.

34. Longuet-Higgins, M.S. and Stewart, R.W., Radiation stresses in water waves; a physical discussion, with applications, Deep-Sea Res., 11, 1964, p. 529-562.

35. Longuet-Higgins, M.S., On the Wave-induced Difference in Mean Sea Level Between the Two Sides of a Submerged Breakwater, J. Mar. Res., 25, 2, 1967, p. 148-153.

36. Dorrestein, R., Wave set-up on a beach, Proc. Second Techn. Conf. on Hurricanes, June 1961, Miami Beach; Washington, D.C., 1962, p. 230-241.

37. Lundgren, H. Wave thrust and wave energy level, Proc. IAHR Congress, London, 1963, p. 147-151.

38. Bowen, A.J., Rip Currents, 1. Theoretical Investigations, J. Geoph. Res., 74, 23, 1969, p. 5467-5478.

39. Longuet-Higgins, M.S., Longshore currents generated by obliquely incident sea waves, J. Geoph. Res., 75, 1970, p. 6778-6801.

40. Galvin, C.J., Longshore current velocity: A review of theory and data, Rev. Geoph., 5,3, 1967, p. 287-304.

41. Bowen, A,J., The generation of longshore currents on a plane beach, J. Mar. Res., 27, 1969, p. 206-215.

42. Thornton, E.B., Longshore current and sediment transport, Tech. Rep. 5, Dept. of Coastal and Ocean. Eng., Un. of Florida, Gainesville, Florida, 1969 (see also Proc. 12th. Conf. Coastal Eng., Washington D.C., 1970, vol. I, p. 291-308).

43. Bakker, W.T., Littoral drift in the surf zone, Report WWK 70-16, Rijkswaterstaat, Directorate for Hydraulic Research, Department for Coastal Research, 1970.

44. Jonsson, I.G., Wave boundary layers and friction factors, Proc. 10th Conf. Coastal Eng., Tokyo, 1966, p. 127-148.

45. Bijker, E.W., Some considerations about scales for coastal models with movable bed, Delft Hydraulics Lab. Publ. 50, 1967.

46. Bakker, W.T., Bottom friction and velocity distribution in an oscillatory flow, Memo 72-23b, Rijkswaterstaat, Directorate for water management and hydraulic research, Dept. for coastal research, The Hague, Jan. 1973.

47. Mazure, J.P., De berekening van getijden en stormvloeden op benedenrivieren (Computation of tides and storm surges in estuaries), The Hague, 1937.

48. Bowden, K.F., Note on wind drift in a channel in the presence of tidal currents, Proc. Roy. Soc., A, 219, 1953, p. 426-446.

49. Weenink, M.P.H., A theory and method of calculation of wind effects on sea levels in a partly-enclosed sea, with special application to the southern coast of the North Sea, K.N.M.I., Med. en Verh., 73, 1958.

50. Doob, J.L., Stochastic Processes, John Wiley & Sons, Inc., New York, 1953.

51. Cramér, H., Random variables and probability distributions, Cambridge Univ. Press, 3d ed., 1970.

52. Bendat, J.S., Principles and Applications of Random Noise Theory, John Wiley & Sons, Inc., New York, 1958.

53. Middleton, D., An Introduction to Statistical Communication Theory, McGraw-Hill Book Comp. Inc., N.Y., 1960.

54. Lighthill, M.J., Fourier Analysis and Generalised Functions, Cambridge Univ. Press, 1959.

55. Rice, S.O., Mathematical Analysis of Random Noise, Bell System Tech. Journ., 23, 1944, p. 282-332 and 24, 1945, p. 46-156.

56. Cramér, H., Mathematical Methods of Statistics, Princeton Univ. Press, 1946.

57. Longuet-Higgins, M.S., On the statistical distribution of the heights of sea waves, J. Mar. Res. XI, 3, 1952, p. 245-266.

58. Cartwright, D.E. and Longuet-Higgins, M.S., The statistical distribution of the maxima of a random function, Proc. Roy. Soc. London, A, 237, 1956, p. 212-232.

59. Cartwright, D.E., On estimating the mean energy of sea waves from the highest waves in a record, Proc. Roy. Soc. London, A, 247, 1958, p. 22-48.

60. Longuet-Higgins, M.S., The statistical analysis of a random, moving surface, Phil. Trans. Roy. Soc. London, A, 249, 966, Feb. 1957, p. 321-387.

61. Rayleigh, Lord, On the resultant of a large number of vibrations of the same pitch and of arbitrary phase, Phil. Mag., X, 1880, p. 73-78, (also in: Scientific Papers, Vol. I, p. 491-496).

62. Pierson, W.J., Wind-generated gravity waves, in Advances in Geophysics, 2, 1955, p. 93-178.

63. Cartwright, D.E., Analysis and Statistics, in The Sea, Ed. M.N. Hill, Vol. I, 1962, Interscience Publishers, p. 567-589.

64. Longuet-Higgins, M.S., On the transformation of a continuous spectrum by refraction, Proc. Cambridge Phil. Soc., 53, 1957, p. 226-229.

65. Collins, J.I., Prediction of shallow-water spectra, J. Geoph. Res., 77, 11, 1972, p. 2693-2707.

66. Putz, R.R., Statistical analysis of wave records, Proc. 4th Conf. Coastal Eng., Berkeley, Calif., 1954, p. 13-24.

67. MacKay, J.H., On the Gaussian nature of ocean waves, Eng. Exp. Sta., Georgia Inst. Tech., Atlanta, Ga., Internal Tech. Note 8, 1959 (quoted in Kinsman, [68]).

68. Kinsman, B., Wind Waves, their Generation and Propagation on the Ocean Surface, Prentice-Hall, Inc., Englewood Cliffs, N.J., 1965.

69. Koelé, L.A. and de Bruyn, P.A., Statistical Distribution of Wave Heights in Correlation with Energy Spectrum and Water Depth, Proc. 11th Conf. Coastal Eng., Lisbon, 1964, p. 123-139.

70. Collins, J., Wave statistics from hurricane Dora at Panama City, Florida Proc. Specialty Conf. on Coastal Eng., Santa Barbara, Calif., 1965, p. 461-485.

71. Longuet-Higgins, M.S., The effect of non-linearities on statistical distributions in the theory of sea waves, J. Fluid Mech., 17, 3, Nov. 1963, p. 459-480.

72. Longuet-Higgins, M.S., Modified Gaussian distributions for slightly nonlinear variables, Radio Science, 68D, 9, Sept. 1964, p. 1049-1062.

73. Vugts, J.H., Wave spectra: measured samples and their representation for theoretical predictions, Report EP-42516, Shell Exploration and production, May 1971, 22 p.

74. McFadden, J.A., The axis-crossing intervals of random functions, Trans. Inst. Rad. Engrs., IT-2, 1956, p. 146-150.

75. McFadden, J.A., The axis-crossing intervals of random functions II, Trans. Inst. Rad. Engrs., IT-4, 1958, p. 14-24.

76. Ehrenfeld, S. et al, Theoretical and observed results for the zero and ordinate crossing problems of stationary Gaussian noise with application to pressure records of sea waves, N.Y. Univ., Coll. Eng., Tech. Rep. 1, Dec. 1958.

77. Longuet-Higgins, M.S., On the intervals between successive zeros of a random function, Proc. Roy. Soc. London, A, 246, 1958, p. 99-118.

78. Longuet-Higgins, M.S., The distribution of intervals between zeros of a stationary random function, Phil. Trans. Roy, Soc. London, 1047, 254, May 1962, p. 557-599.

79. Longuet-Higgins, M.S., Bounding Approximations to the Distribution of Intervals between Zeros of a Stationary Gaussian Process, in Time Series Analysis, Wiley & Sons Inc., 1963, p. 63-88.

80. Goda, Y., Numerical Experiments on Wave Statistics with Spectral Simulation, Rep. Port and Harbour Res. Inst. 9, 3, Sept. 1970, p. 3-57.

81. Taylor, G.I., Diffusion by continuous movements, Proc. London Math. Soc., Ser. 2, 20, 1921, p. 196-211.

82. Barber, N.F., Ocean waves and swell, Lecture publised by the Inst. of Civil Engrs., London, 1950.

83. Bretschneider, C.L., Wave Variability and Wave Spectra for Wind Generated Gravity Waves, U.S. Army Corps of Engineers, B.E.B., Tech. Mem. 118, 1959.

84. Goodknight, R.C. and Russell, T.L., Investigation of the statistics of wave heights, Proc. ASCE, 89, WW2, May 1963, p. 29-54.

85. Hess, G.D., Hidy, G.M. and Plate, E.J., Comparison Between Wind Waves at Sea and in the Laboratory, J. Mar. Res., 27, 2, 1969, p. 216-225.

86. Svasek, J.N., Statistical Evaluation of Wave Conditions in a Deltaic Area, Symp. Res. on Wave Action, Delft Hydraulics Lab., 1969, Vol. I, paper 1.

87. Titov, L.F., Wind-Driven Waves, Israel Program for Scientific Translations, Jerusalem, 1971.

88. Jahns, H.O. and Wheeler, J.D., Long-Term Wave Probabilities Based on Hindcasting of Severe Storms, Fourth Annual Offshore Techn. Conf., Houston, Texas, May 1972, paper 1590.

89. St. Denis, M. and Pierson, W.J., Jr., On the motions of ships in confused seas, Trans. Soc. Naval Arch. and Mar. Eng., 61, 1953, p. 280-357.

90. Abramowitz, M. and Stegun, I.A., Handbook of Mathematical Functions, Dover Publications, Inc., N.Y., 1965.

91. 4th Int. Ship Structures Congress, Tokyo, 1970, Report Committee 1, Environmental Conditions.

92. Barber, N.F., Finding the direction of travel of sea waves, Nature, 174, 1954, p. 1048-1050.

93. Cote, L.J. et al, The directional spectrum of a wind generated sea as determined from data obtained by the Stereo Wave Observation Project, New York, Univ., Coll. Eng., Meteor. Papers, 2, 6, June 1960.

94. Longuet-Higgins, M.S., Cartwright, D.E. and Smith, N.D., Observations of the directional spectrum of sea waves using the motions of a floating buoy, in Ocean wave spectra, Proc. of a Conf., Prentice-Hall, Inc., Englewood Cliffs, N.J., 1963, p. 111-136.

95. Krylov, Yu. M., Strekalov, S.S. and Tsyplukhin, V.F., Investigation of the two-dimensional energy spectrum and of the wavelength of wind-induced waves, Izvestia, Atm. and Ocean Phys., 4, 6, 1968, p. 660-670 (English transl. p. 376-381).

96. St. Denis, M., On wind generated waves, in Topics in Ocean Engineering, Gulf Publ. Comp., Texas, 1969, p. 3-41.

97. Nemann, G., On ocean wave spectra and a new method of forecasting wind-generated sea, U.S. Army Corps of Engineers, B.E.B., Tech. Mem. 43, 1953.

98. Strekalov, S.S., Determination of the analytic form of the energy spectrum of a fully arisen sea, Okeanologiya, 1, 3, 1961 (quoted in Titov [87]).

99. Pierson, W.J., Jr. and Moskowitz, L., A Proposed Spectral Form for Fully Developed Wind Seas Based on the Similarity Theory of S.A. Kitaigorodskii, J. Geoph. Res., 69, 24, Dec. 1964, p. 5181-5190.

100. Davidan, I.N., The dependence of the probability characteristics of waves on wind, in Sbornik "Teoreticheskie i prakticheskie voprosy

morekhodnosti sudov." Izdatel'stvo "Transport", 1967 (quoted in Titov [87]).

101. Phillips, O.M., The equilibrium range in the spectrum of wind-generated waves, J. Fluid Mech., 4 1958, p. 426-434.

102. Strekalov, S.S., Tsyploukhin, V.Ph. and Massel, S.T., Structure of sea wave frequency spectrum, Proc. 13th Conf. Coastal Eng., Vancouver, B.C., 1972, p. 307-314.

103. Uhlenbeck, G.E., Theory of random process, MIT Radiation Lab. Rep. 454, 1943 (quoted in Rice [55]).

104. Fréchet, M., Sur les tableaux de corrélation dont les marges sont données, Comptes Rendus de l'Acad. des Sciences, Tome 242, 1956, p. 2426-2428.

105. Battjes, J.A., Radiation stresses in short-crested waves, J. Mar. Res. 30, 1, 1972, p. 56-64.

106. Nagata, Y., The Statistical properties of orbital wave motion and their application for the measurement of directional wave spectra, J. Ocean Soc. Japan, 19, 1964, p. 169-181.

107. Yefimov, V.V. and Khristoforov, G.N., Spectra and statistical relations between the velocity fluctuations in the upper layer of the sea and surface waves, Izv., Atmospheric and Oceanic Physics, 7, 12, 1971, p. 1290-1310 (English translation p. 841-851).

108. Ijima, T., Matsuo, T. and Koga, K., Equilibrium Range Spectra in Shoaling Water, Proc. 12th Conf. Coastal Eng., Washington, D.C., 1973, Vol. I., p. 137-149.

109. Collins, J.I., Probabilities of Breaking Wave Characteristics, Proc. 12th Conf. Coastal Eng., Washington, D.C., 1970, Vol. I, p. 399-414.

110. Battjes, J.A., Set-up due to irregular waves, Proc. 13th. Conf. Coastal Eng., Vancouver, B.C., 1972, Vol. III, p. 1993-2004.

111. Skjelbreia, L., Gravity waves-Stokes'third order approximation- Tables of functions, Council on Wave Research, California, 1959.

112. Saville, T., An approximation of the wave run-up frequency distribution, Proc. 8th Conf. Coastal Eng., Mexico, 1962, p. 48-59.

113. Pierson, W.J., Jr. and Holmes, P., Irregular Wave Forces on a Pile, Proc. ASCE, 91, WW4, Nov. 1965, p. 1-10.

114. van Oorschot, J.H. and d'Angremond, K., The effect of wave energy spectra on wave run-up, Proc. 11th Conf. Coastal Eng., London, 1968, Vol. II, p. 888-900.

115. Saville, T., Laboratory data on wave run-up and overtopping on shore structures, U.S. Army Corps of Engineers, B.E.B., Tech. Mem. 64, 1955.

116. Battjes, J.A., Run-up distributions of waves breaking on slopes, Proc. ASCE, 97, WW1, Feb. 1971, p. 91-114.

117. Hosoi, M. and Shuto, N., Run-up height on a single slope dike due to waves coming obliquely, Coastal Eng. in Japan, 7, 1964, p. 95.

118. Wassing, F., Model investigations of wave run-up on dikes carried out in the Netherlands during the past twenty years, Proc. 6th Conf. Coastal Eng., Gainesville, 1957, p. 700-714.

119. Watson, G.N., A Treatise on the Theory of Bessel Functions, Cambridge University Press, 1966.

120. Tsuruta, S. and Goda, Y., Expected overtopping discharge of irregular waves over sea wall, Proc. 11th Conf. Coastal Eng., London, 1968, Vol. II, p. 833-852.

121. Paape, A., Experimental data on the overtopping of seawalls by waves, Proc. 7th. Conf. Coastal Eng., The Hague, 1960, vol. 2, p. 674-681.

122. Longuet-Higgins, M.S., A model of flow separation at a free surface, J. Fluid Mech., 57, 1973, p. 129.

123. Banner, M.L. and Phillips, O.M., On small scale breaking waves, Chesapeake Bay Institute, Tech. Rep. 82, July 1973.

SAMENVATTING

Het probleem dat in dit proefschrift wordt behandeld is de berekening van een aantal effecten, teweeggebracht door windgolven die breken op een hellende oever. Tot deze effecten behoren de verhoging van de gemiddelde waterstand (opstuwing) en de opwekking van een brandingsstroom door golven bij stranden, en de oploop en overslag van golven bij dijken.

Het proefschrift bestaat uit twee delen. Het eerste deel bevat een samenvatting van basiskennis die nodig is voor de in het tweede deel omschreven berekeningen.

Het eerste deel begint in hoofdstuk 2 met een overzicht van een aantal kenmerkende eigenschappen van golven op hellingen, gezien als functies van de golfsteilheid en de taludhelling. Het doel hiervan is een geïntegreerde visie te geven op het onderwerp in zijn totaliteit, zodat de delen ervan in één kader kunnen worden gezien. Vervolgens wordt in de hoofdstukken 3 en 4 een résumé gegeven van een aantal begrippen en resultaten betreffende hydrodynamische en stochastische aspecten van zeegolven.

Het tweede deel is gewijd aan de berekeningen van de in de aanhef genoemde effecten. Het feit dat het gaat om *brekende* onregelmatige golven bemoeilijkt de berekeningen in hoge mate. Het breken van golven is een sterk niet-lineair proces, dat bovendien vergezeld gaat van luchtopname en turbulentie. Een enigszins realistisch deductief model is er tot op heden niet voor ontwikkeld. Zelfs in het geval van periodieke golven zijn de berekeningen betreffende de brekerzône tot nu toe voor een belangrijk deel gebaseerd geweest op empirische kennis van macroscopische eigenschappen van de brekers. In het proefschrift worden rekenmodellen gegeven waarin deze kennis is geïncorporeerd, en waarin tevens recht wordt gedaan aan het stochastische karakter van windgolven. De problemen aangaande golven op relatief flauwe taluds (stranden) en op relatief steile taluds (dijken) worden apart behandeld.

In hoofdstuk 5 wordt ingegaan op de energie dissipatie in onregelmatige golven die zich voortplanten in water van langzaam afnemende diepte. In de berekeningen wordt een fictieve golfhoogteverdeling, die theoretisch aanwezig zou zijn indien breken niet optrad, afgekapt bij een bovengrens die is ontleend aan een brekingscriterium voor regelmatige golven. Met afnemende diepte neemt deze bovengrens af, en neemt het percentage brekende golven toe. Op deze wijze wordt een continue variatie gevonden van de golfenergie met de diepte. De berekende resultaten stemmen behoorlijk goed overeen met metingen die zijn verricht op een flauw hellend, vlak talud.

Als de golfenergie eenmaal bekend is kan de hoeveelheid beweging worden berekend die door het golfveld op de gemiddelde stroming wordt overgedragen. Deze is op zijn beurt bepalend voor de opstuwing van de gemiddelde waterstand en voor de aandrijving van de brandingsstroom.

In hoofdstuk 6 worden hiervoor rekenresultaten gegeven, bij invallende golven met een smal energie spectrum en bij invallende golven met een breed energie spectrum (in frekwentie en richting). De snelheid van de brandingsstroom is gevoelig voor de verdeling van de golfenergie over de richtingen. Bij een verdeling die kenmerkend is voor zeegang op diep water is de brandingsstroomsnelheid ongeveer de helft van wat hij zou zijn indien de energie in de gemiddelde richting was geconcentreerd.

Een vergelijking van de berekende opstuwing met empirische gegevens heeft niet tot een eenduidige conclusie geleid. Weliswaar was er een goede overeenstemming met metingen in de natuur, maar de resultaten van metingen in het laboratorium gaven plaatselijk een systematisch kleinere opstuwing te zien dan zou mogen worden verwacht op grond van de berekende of gemeten golfhoogten. Er is echter enige onzekerheid aangaande het systeem waarmee in het laboratorium de opstuwing is gemeten, zodat het niet bekend is in hoeverre de afwijkingen reëel zijn.

De hoofdstukken 7 en 8 hebben betrekking op relatief steile taluds, die kenmerkend zijn voor dijken. Op dergelijke taluds breken de

golven dicht bij de gemiddelde waterlijn, hetgeen resulteert in een aanzienlijke op- en neergaande beweging van het water langs de helling.

De grootste hoogte boven het stil-water niveau, bereikt door een golf die tegen het talud oploopt, heet de oploophoogte, of kortheidshalve de oploop. De verdelingsfunctie ervan is in hoofdstuk 7 berekend door aan elke golf van de onregelmatige golftrein, gekenmerkt door een combinatie van hoogte H en periode T, een oploop toe te kennen overeenkomstig de formule van Hunt, die geldt voor periodieke golven die breken op het talud. De oploop verdeling wordt gegeven als een functionaal van de simultane kansdichtheidsfunctie van $\underline{H}$ en $\underline{T}$. Dat dit tot geldige resultaten kan leiden blijkt uit een vergelijking met enige laboratorium metingen, waarmee een zeer goede overeenstemming werd gevonden. In de proeven vertoonden de golfhoogten echter veel minder spreiding dan in de natuur, terwijl de periode vrijwel constant was. Er zijn ook berekeningen gemaakt voor het geval dat $\underline{H}$ en $\underline{T}^2$ een samengestelde Rayleigh-verdeling hebben, hetwelk voor zeegang een betere benadering is. De beschikbare empirische gegevens zijn niet geschikt voor een exacte vergelijking met de berekende resultaten, maar zij geven wel een duidelijke indicatie dat deze resultaten realistisch zijn.

In hoofdstuk 8 wordt de overslag van onregelmatige golven over een dijk behandeld. Eerst wordt uit metingen met periodieke golven een betrekking afgeleid tussen oploop en hoeveelheid overslag. Door deze betrekking toe te passen op een onregelmatige golftrein kan de verdelingsfunctie van het per golf overslaand volume worden uitgedrukt in die van de oploop. Hieruit kan het gemiddelde overslagdebiet worden bepaald. Voor het geval dat $\underline{H}$ en $\underline{T}^2$ een samengestelde Rayleigh-verdeling hebben worden expliciete resultaten gegeven. Een vergelijking hiervan met meetgegevens is in beperkte mate mogelijk; hieruit kan worden geconcludeerd dat de gevonden uitkomsten een behoorlijk realiteitsgehalte hebben.